Rheological and Chemical Evaluation of Aging Resistant Binder Technologies

by

Faustina Keuliyan Rodriguez

A thesis submitted to the Graduate Faculty of
Auburn University
in partial fulfillment of the
requirements for the Degree of
Master of Science

Auburn, Alabama
May 7, 2022

Keywords: Asphalt aging, asphalt binder rheology, asphalt modification

Approved by

Nam Hoai Tran, Chair, PhD, Civil and Environmental Engineering
Raquel Moraes Puchalski, PhD, Co-Chair, Civil and Environmental Engineering
Randy West, PhD, Civil and Environmental Engineering
Fan Yin, PhD, Civil and Environmental Engineering

Abstract

Asphalt binder is a dark-colored cementitious hydrocarbon material, with a complex chemical composition that is heavily dependent on crude oil source and manufacturing process. Binder chemistry has been modelled as a colloidal system with four main chemical fractions (i.e., SARA fractions) that directly impact binder rheological properties.

Binders are subjected to aging mechanisms that cause irreversible changes in their chemical composition throughout the pavement service life. Aging increases the concentration of polar functional groups of asphalt, leading to more molecular association and less molecular mobility. As a result, binders become stiffer and less flexible, making them more brittle. Ultimately, binders become more susceptible to fatigue and thermal cracking, affecting the long-term performance of flexible pavements.

This study evaluated aging resistant technologies that can reduce the aging susceptibility of asphalt binders. The evaluated technologies/additives included (1) a blend of biosynthetic oils and petroleum-based oils, (2) a blend of thermosetting epoxy polymer and oil-based flexible modifiers, (3) a sub-epoxidized soybean oil, (4) a hybrid technology composed of a continuous phase styrenic block copolymer with a pine-based chemical additive, and (5) a hybrid system composed of ground tire rubber (GTR) powder and Rheopave®. Each additive was blended with two base binders selected from different crude sources, and their blends with 20 percent reclaimed asphalt pavement (RAP) binder extracted from a RAP source. The aging resistant effectiveness of each technology was evaluated based on their rheological and chemical characteristics before and after multiple aging procedures that included Rolling Thin Film Oven (RTFO), RTFO + 20-hour Pressurized Aging Vessel (PAV) and RTFO + 60-hour PAV. The rheological evaluation included Superpave performance grading, Multiple Stress Creep and Recovery (MSCR) test, Linear Amplitude Sweep (LAS) test, frequency sweep for master curve construction, and extended Bending Beam Rheometer (BBR) test. Chemical testing evaluated the formation of oxidation products through Fourier Transformed Infrared Spectroscopy (FTIR), glass transition and thermal behavior through Differential

Scanning Calorimetry (DSC), binder chemical composition through SARA fractions and molecular size distribution using Gel Permeation Chromatography (GPC).

Rheological and chemical results showed that the binders modified with the candidate technologies were less affected by aging than the control binders. However, the levels of effect were influenced by a combination of technology, base binder and presence of extracted RAP binder. Overall, the technologies can mitigate the effects of aging, reducing the stiffening and embrittlement of binders. The chemical test results help explain the working mechanisms of these technologies, such as decreased formation of oxidation products (i.e., carbonyl and sulfoxides), and supported the findings observed from the rheological test results.

Acknowledgments

I would like to thank my advisors, Dr. Nam Tran and Dr. Raquel Moraes for their support, guidance, and encouragement throughout the course of this project and my entire academic path at Auburn University. Their invaluable advice allowed me to develop skills and characters that have made me a better student, researcher, and engineer. I would also like to thank my committee members, Drs. Fan Yin and Randy West, for their contribution to the success of this project and their efforts in reviewing this Thesis.

My experience at Auburn and NCAT would not have been the same without the people who became my biggest supporters since my arrival at Auburn from Uruguay. I would like to thank my friends Megan Foshee, Tiana Lynn, Mariah Langan and Brooke Earls for sharing this wonderful experience with me from the very beginning, for spending one or two Sundays with me in the binder lab, and for always having my back and encouraging me to succeed.

This work would not have been possible without Ms. Pamela Turner, who trained me in the binder laboratory at NCAT and whose insights and support helped me overcome multiple hurdles throughout this project. I would also like to acknowledge Jason Moore, for creating a workplace where we could strive and do our best work. I would also like to thank the Western Research Institute, Kraton, Lehigh Technologies, and the Blacklidge laboratories for performing some of the chemical testing within this project.

Last but definitely not least, I would like to thank my parents, Elena and Santiago, and my sister Rafaela, for being my role models, and for their love, guidance and understanding throughout this entire process.

Table of Contents

List of Tables

List of Figures

List of Abbreviations

AASHTO	American Association of Transportation and Highway Officials
AD	Alternative Dosage
ASTM	American Society for Testing and Materials
ATR	Attenuated Total Reflectance
BBR	Bending Beam Rheometer
CII	Colloidal Instability Index
CRM	Crumb Rubber Modifiers
DSC	Differential Scanning Calorimetry
DSR	Dynamic Shear Rheometer
FHWA	Federal Highway Administration
FTIR	Fourier Transformed Infrared Spectroscopy
GPC	Gel Permeation Chromatography
LAS	Linear Amplitude Sweep
LMS	Large Molecular Size
LTLG	Low Temperature Limiting Grade
MMS	Medium Molecular Size
MSCR	Multiple Stress Creep and Recovery
MSD	Molecular Size Distribution
NCAT	National Center for Asphalt Technology
OD	Optimum Dosage
PAV	Pressurized Aging Vessel
PG	Performance Grade
RAP	Reclaimed Asphalt Pavement
RHEA	Rheological Analysis

RTFO	Rolling Thin Film Oven
S-VECD	Simplified Viscoelastic Continuum Damage
SARA	Saturates, Aromatics, Resins and Asphaltenes
SBS	Styrene-butadiene-styrene
SHRP	Strategic Highway Research Program
SMS	Small Molecular Size
WRI	Western Research Institute

CHAPTER 1 - INTRODUCTION

1.1. Background

Asphalt binder is a dark-colored cementitious hydrocarbon material with more than 90% of its total weight being carbon and hydrogen (Lesueur, 2009). The chemical composition of asphalt binder is complex and diverse, as it depends on crude oil source and manufacturing process.

Asphalt binder can be separated into four chemical fractions: saturates, aromatics, resins and asphaltenes, referred to as SARA fractions (J.C. Petersen, 2009). These fractions have been used to model asphalt binders as a colloidal system. Within the system, asphaltenes are dispersed in a continuous phase known as maltenes that consist of resins, aromatics and saturates (Lesueur, 2009; J.C. Petersen, 2009). Relative content and molecular weight of these fractions, as well as the degree of asphaltenes dispersion within the binder, govern its physical behavior (J. C. Petersen, Robertson, R.E, Branthaver, J.F., Harnsberger, P.M, Duvall, J.J., Kim, S.S., Anderson, D.A, Christiansen, D.W., Bahia, U.H. , 1994; Weigel & Stephan, 2017). Asphaltenes are highly polar, so they are mostly responsible for binder viscosity. Also, the level of asphaltenes dispersion by resins influences the non-Newtonian flow properties of the binder. In addition, saturates and aromatics act as plasticizers to the resins and asphaltenes, providing fluidity to the asphalt binder (Corbett, 1970). As the colloidal system determines the rheological behavior of binder, any changes in the colloidal system (i.e., binder chemistry) can impact its physical properties.

Aging of asphalt binder during mixture production and throughout the pavement service life can cause changes in asphalt binder's chemical and/or physical properties (Corbett, 1970). The process is usually accompanied by stiffening and embrittlement of the binder, which leads to the deterioration of asphalt pavements (Rad, Elwardany, Castorena, & Kim, 2018). Aging causes an increase in the polar, oxygen-containing functional groups of asphalt, leading to considerable increase in molecular associations (Tauste, Moreno-Navarro, Sol-Sánchez, & Rubio-Gámez, 2018). As polar molecules become associated, they start to lose mobility and cannot flow past one another, which in turn affects the binders' ability to relax when subjected to mechanical or thermal stresses (J.C. Petersen, 2009). With higher stiffness, accompanied by a reduction in their relaxation through viscous flow, asphalt binders become more brittle (Moraes & Bahia, 2018). Ultimately, oxidative aging will make them more susceptible to cracking as well as other surface distresses such as raveling, which considerably reduces their long-term performance (King et al., 2012; Rad et al., 2018).

While several studies (Apostolidis, Liu, Erkens, & Scarpas, 2020; Elkashef, Podolsky, Williams, & Cochran, 2018; Habbouche, Boz, Hajj, & Morian, 2021; Hassan A. Tabatabaee & Kurth, 2017; H. Wang et al., 2020; R. Zhang et al., 2020) have shown that different additives such as polymers or rejuvenators can improve the aging resistance of asphalt binders, there is still a lack of understanding on the working mechanisms of these technologies to enhance aging resistance. Thus, a comprehensive study that includes both chemical and rheological evaluations is needed to determine the effectiveness of candidate additives and their mechanisms for reducing the aging susceptibility of asphalt binders.

1.2. Research Hypothesis

Innovative aging resistant technologies can be used to reduce the asphalt binder's susceptibility to oxidative aging. By various mechanisms, these technologies will lead to changes in the binder's chemical composition and rheological properties to improve their aging resistance, thus enhancing their thermal and fatigue cracking resistance.

1.3. Research Objectives

The objective of this study was to determine if selected additives and modifiers can be used to reduce the aging susceptibility of asphalt binders. The effectiveness of each technology in improving aging resistance of the modified binders was evaluated based on their rheological and chemical characteristics after being subjected to several laboratory aging protocols.

Specifically, this study determined the changes in viscoelastic and chemical properties of modified binders with respect to unmodified materials after extended laboratory aging cycles. Rheological evaluation included (a) Superpave performance grading, (b) elastic recovery and creep compliance, (c) fatigue life, (d) viscoelastic properties of complex modulus and phase angle, and (e) physical hardening effects. Chemical evaluation was conducted to understand working mechanisms of each modifier as well as effects of oxidative aging on the chemical composition of binders and how these related to the observed rheological parameters.

1.1. Research Scope

Five aging resistant technologies were evaluated to determine their effect on reducing aging susceptibility of asphalt binders. Six straight run asphalt binders from different sources were sampled as potential candidates for modification. After a rheological evaluation, two asphalt binders with distinctly different aging characteristics and having no incompatibility issues with each technology were selected as the base binders, which were designated as Binder 1 and Binder 5 in this study. They were evaluated in a neat condition and blended with a recycled binder extracted from a single reclaimed asphalt pavement (RAP) source at a dosage of 20% by total weight of binder. Therefore, the effect of each additive was studied with respect to four control binders: two base binders and two RAP binder blends.

Each additive was blended with Binder 1 and Binder 5 at an optimum dosage (OD) determined by the additive's supplier. Additionally, Additives 2 through 5 were incorporated into RAP blends at the OD and at an alternative dosage (AD), also selected by each supplier. Thus, a total of six modified binder blends were prepared for additives 2 through 5 while four modified binder blends were prepared for Additive 1, as shown in Figure 1.

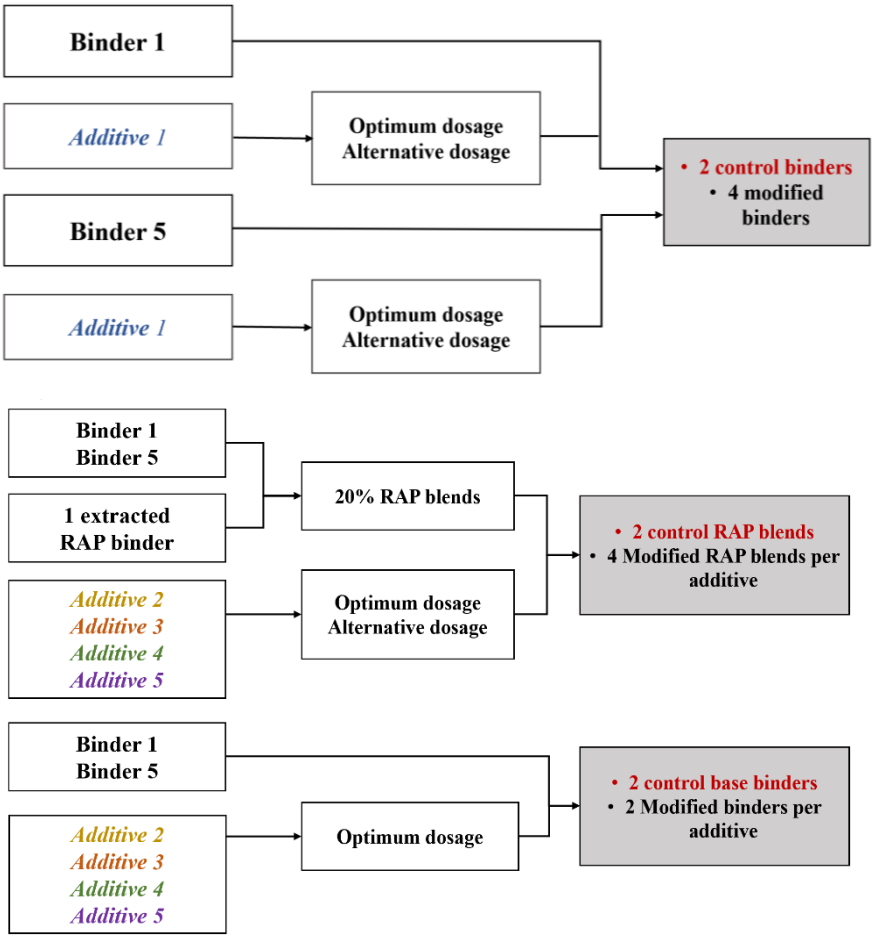

Figure 1. Plan for Preparing Test Binders and Modified Blends

A plan for rheological and chemical testing is briefly discussed in the following paragraphs with more details provided in Section 3. It should be noted that rheological and chemical properties were determined for selected binder blends and selected aging conditions depending on the testing time requirement and equipment availability in this study.

The aging methods selected for rheological evaluation included the Rolling Thin Film Oven (RTFO) procedure for short-term aging and the Pressurized Aging Vessel (PAV) method for long-term aging. Multiple aging conditions were included: unaged, RTFO (short), RTFO + 20-hour PAV (long), and RTFO + 60-hour PAV (extended).

Superpave performance grade (PG) testing was performed per AASHTO M320. High- and intermediate-temperature performance properties were determined based on Dynamic Shear Rheometer (DSR) measurements per AASHTO T315, while low-temperature properties were determined by Bending Bean Rheometer (BBR) testing per AASHTO T313. In addition, PG testing at high, intermediate, and low temperatures was also performed for RTFO + 60-hour PAV aged samples. For some RTFO + 60-hour PAV aged samples that became not workable for preparing BBR specimens, an alternative approach using 4-mm parallel plate DSR testing was conducted to determine their low-temperature properties.

Additionally, the Multiple Stress Creep Recovery (MSCR) test was used to evaluate the impact of the additives on the rutting resistance and elastic response of asphalt binders. The Frequency Sweep test followed by master-curve generation was used for determining the Glover-Rowe (G-R) parameter to

evaluate ductility and block cracking potential. The Linear Amplitude Sweep (LAS) test was used to evaluate fatigue resistance. The BBR was utilized to determine the Superpave low-temperature PG, the physical hardening behavior of the blended binders at the glass transition temperature, and the ΔTc parameter to assess stress relaxation properties.

Fourier Transform Infrared Spectroscopy with Attenuated Total Reflectance (FTIR-ATR) was performed on base and modified binders before and after RTFO + 60-hour PAV aging, to investigate the effects of each technology on the formation of oxidation products (e.g., carboxylic acids, ketones, anhydrides and sulfoxides). Chemical aging indices were calculated by evaluating both carbonyl and sulfoxide areas as the main oxidation products, determining the potential aging resistance of each additive with respect to the base binders.

Additional chemical characterization tests were performed to provide a fundamental understanding of the molecular structure through Gel Permeation Chromatography (GPC), glass transition behavior and thermal responses through Differential Scanning Calorimetry (DSC), and chemical composition (SARA fractions) of asphalt binders after interaction with the aging resistant technologies. Furthermore, this characterization was used to evaluate the level of interaction between the base binders and additives and how the interaction changes the binder properties.

In summary, two base binders and five aging resistant binder technologies were included in the experimental plan of this study. Rheological and chemical properties for the base binders and those modified with each of the technologies were determined before and after multiple laboratory aging conditions to simulate their short-term and long-term (extended) aging in the field. Changes in the properties of the modified binders before and after aging were determined and compared with those of the control binders (i.e., base binders and their blends with 20% RAP binder). Based on the analysis, the effect of each technology on the aging resistance of asphalt binders could be determined.

CHAPTER 2 - LITERATURE REVIEW

2.1 Asphalt Chemical Composition

Asphalt binder is a complex cementitious material that is used in approximately 94% of the 2.8 million miles of paved roads in the United States, according to the Federal Highway Administration (FHWA) (FHWA, 2018). It is defined by the American Society of Testing and Materials (ASTM) as "*a dark brown to black cement-like residuum obtained from the distillation of suitable crude oils […]"* (Materials, 2021).

The chemical composition of asphalt binder is diverse, as it depends on the source of crude oils (Lesueur, 2009). It can be described as a hydrocarbon with hydrogen and carbon atoms making up to 90% by weight of its composition. Other heteroatoms such as sulfur, oxygen and nitrogen, and traces of metals (e.g., vanadium) make up the remaining (Lesueur, 2009). Even though elemental composition appears limited, these components can be arranged into a diverse number of complex organic molecules, making it challenging to characterize (J.C. Petersen, 2009). Several studies have attempted to understand how the chemical composition of asphalt binders affects their physical properties and performance (Corbett, 1970; J.C. Petersen, 2009; J. C. Petersen, Robertson, R.E, Branthaver, J.F., Harnsberger, P.M, Duvall, J.J., Kim, S.S., Anderson, D.A, Christiansen, D.W., Bahia, U.H. , 1994; Tauste et al., 2018).

Models have been developed to explain asphalt chemical composition in terms of molecular types with common polarity, reactivity, and aromaticity (J.C. Petersen, 2009). In this regard, Corbett showed that asphalt can be separated into four fractions: saturates, aromatics, resins and asphaltenes, later known as SARA fractions (Corbett, 1970). Saturates are the least polar fraction in asphalt and make up about 5-15% by total weight. They are liquid at room temperature and impart fluidity to asphalt by plasticizing the asphaltenes and polar aromatics (Corbett, 1970; J.C. Petersen, 2009). Asphaltenes have the highest molecular weight and polarity out of the four fractions and are largely responsible for asphalt viscosity. The presence of resins in asphalt is between 30-45% by weight, and their main role is to peptize asphaltene micelles, making asphalt more stable (Lesueur, 2009; J.C. Petersen, 2009). Finally, aromatics account for 30-45% of total weight. They present a higher glass transition temperature and viscosity than saturates, but they also plasticize the asphaltene fraction and provide fluidity (Lesueur, 2009).

Based on its four SARA fractions, asphalt can be modelled as a colloidal dispersion, as shown in Figure 2. In this model, the asphaltene fraction forms micelles that are dispersed in a continuous or oily phase known as the maltenes, composing of the aromatics, saturates and resins (Lesueur, 2009; J. C. Petersen, Robertson, R.E, Branthaver, J.F., Harnsberger, P.M, Duvall, J.J., Kim, S.S., Anderson, D.A, Christiansen, D.W., Bahia, U.H. , 1994). Asphaltene micelles are formed by the absorption of other resinous components present in the binder onto their surfaces. Resulting micelles will therefore have the highest molecular weight components located in the center, with progressively lower polarity and molecular weight towards the outside, until reaching the continuous oily phase of the maltenes. The relative presence of each fraction will dictate the degree of dispersion of the asphaltene micelles: adequate dispersion will be achieved if enough resins are available within the maltene phase, so that micelles become fully peptized (Pfeiffer & Saal, 1940). Petersen suggested that the degree of molecular interactions between these four fractions and the extent of dispersion of the asphaltene phase affects the rheological properties of asphalts, as discussed in the following section (J.C. Petersen, 2009).

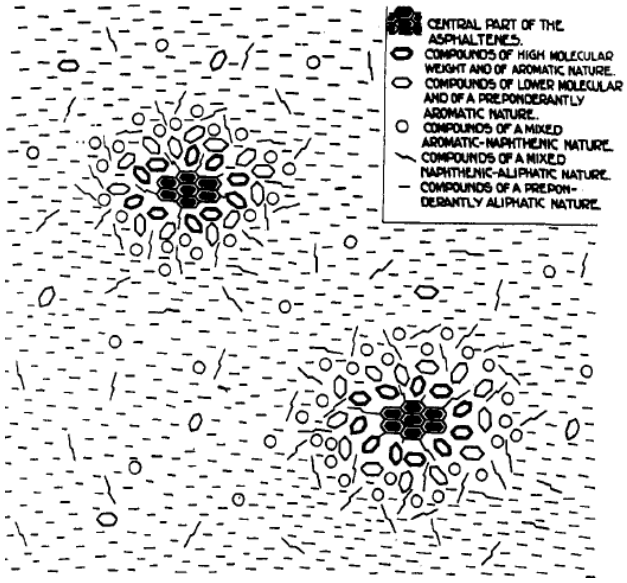

Figure 2 Early representation of binder colloidal system showing asphaltene micelles peptized by resins and dispersed in saturates and aromatics. From (Pfeiffer & Saal, 1940)

2.1.1 Effects of Chemical Composition on Rheological Properties

The colloidal model has been used by researchers to understand the relationships between asphalt chemical composition and its rheological properties. In this regard, two asphalt binders identified as sol and gel binders are shown in Figure 3 (Lesueur, 2009; Pfeiffer & Saal, 1940). The sol binder shows a good degree of dispersion of the asphaltenes within the maltene phase, and thus exhibits Newtonian behavior. The gel binder, on the other hand, shows non-Newtonian behavior (i.e., non-linear viscoelastic properties), which is caused by the inability of the resinous component to keep the asphaltene micelles well dispersed within the oily maltene fraction. In practice, most asphalts exhibit characteristics in between those of the sol and gel binders (Lesueur, 2009; J.C. Petersen, 2009).

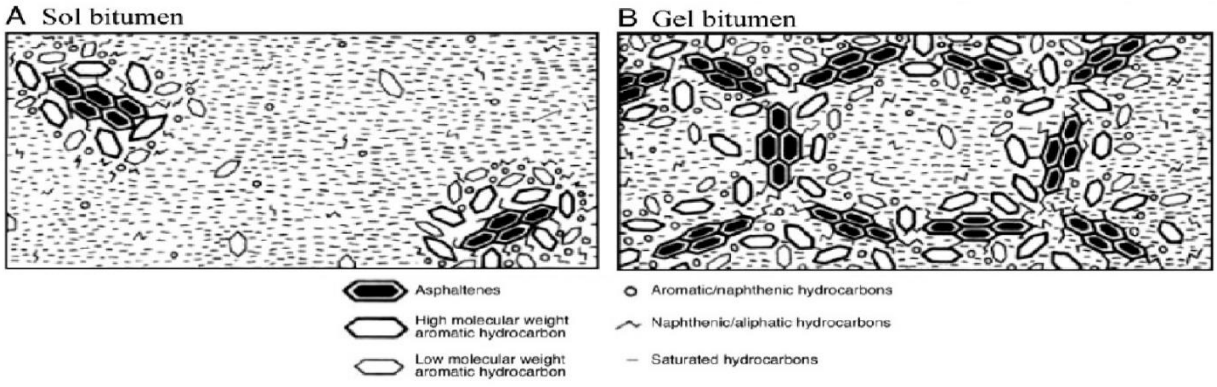

Figure 3. Early representations of sol and gel binders (Lesueur, 2009)

The chemical microstructures of sol and gel binders allowed researchers to explain how a soft grade binder would differ from a harder grade binder from the same crude source with a higher asphaltene content and lower aromatics (Lesueur, 2009; Pfeiffer & Saal, 1940). The inherent characteristics of each fraction, as

well as their relative presence, can dictate asphalt physical properties. When Corbett initially determined the main components of asphalt as saturates, asphaltenes, resins and aromatics, he measured their physical properties based on penetration, softening point, density, and viscosity. He concluded not only that these properties were distinctly different for each fraction, but that the overall properties of asphalt were dictated by their combination. While the saturates and aromatics with lower viscosities and softening points are liquid at room temperatures, asphaltenes and resins having higher viscosities and softening points are largely responsible for overall asphalt viscosity (Corbett, 1970; J.C. Petersen, 2009).

When blending asphaltenes at 35% with each of the remaining fractions (i.e., saturates, aromatics and resins), Corbett found that hardness (as measured by softening point) decreased due to the plasticizing effect of saturates and aromatics but increased with the presence of resins and asphaltenes. In addition, ductility was largely dependent on the presence of resins (i.e., polar aromatics). (Corbett, 1970; Lesueur, 2009).

Relationships between SARA fractions and rheology were also evaluated by the Strategic Highway Research Program (SHRP) researchers tasked with the development of Superpave binder specifications (J. C. Petersen, Robertson, R.E, Branthaver, J.F., Harnsberger, P.M, Duvall, J.J., Kim, S.S., Anderson, D.A, Christiansen, D.W., Bahia, U.H. , 1994). They confirmed the relationship between binder viscosity and asphaltene content and found polar aromatics as predictors for viscosity, though to a lesser extent. In addition, they evaluated the dispersion of the four SARA fractions using the Gaestel index, which is a ratio of asphaltenes plus saturates to aromatics plus resins and found a strong correlation of this index with the binder's relaxation spectrum. Binders with broader relaxation spectra were found to have broader distributions of molecular weights and intermolecular forces and to exhibit delayed elastic responses. SHRP researchers explained binder's relaxation spectrum using the rheological parameter R determined from dynamic shear data and correlated it with molecular dispersion as well as weight (J. C. Petersen, Robertson, R.E, Branthaver, J.F., Harnsberger, P.M, Duvall, J.J., Kim, S.S., Anderson, D.A, Christiansen, D.W., Bahia, U.H. , 1994).

More recently, Weigel and Stephan (2017) attempted to predict binder rheological properties (i.e., complex modulus and phase angle) based on their SARA fractions. They evaluated the relative presence of each fraction by running a Soxhlet extraction using n-heptane and toluene to obtain the asphaltenes and a column chromatography to extract the remaining maltene fractions. Additionally, the molecular weight distribution of the four fractions was determined by size exclusion chromatography. DSR and BBR measurements were used to determine rheological properties at high, intermediate, and low temperatures. They concluded that the rheological properties depended not only on the amount of each fraction within binders but also on their molecular weight, which is consistent with findings by others (Isacsson & Zeng, 1997). In agreement with Corbett's findings, they found that higher contents of saturates and aromatics caused an increase in phase angle, or greater fluidity as shown by traditional consistency tests (i.e., penetration and softening point). The rheological properties measured by DSR (i.e., complex modulus, loss modulus and storage modulus) can be accurately predicted by SARA fractions and their molecular weight at high and intermediate temperatures. However, rheological properties at low temperatures (i.e, from BBR measurements) could not be accurately predicted based on the content of each SARA fraction, as their molecular micro structuring affected binder properties to a greater extent (Weigel & Stephan, 2017).

All in all, saturates, asphaltenes, resins and aromatics can be used to describe the chemical composition of an asphalt binder, which is dependent upon crude source and production method. A colloidal model in which the asphaltenes are dispersed within the three remaining fractions (i.e., maltenes) was developed to explain asphalt structure and its flow properties. Finally, the relative presence of each fraction, as well as their molecular weight, were found to be accurate predictors of rheological properties, including complex modulus, phase angle, loss and storage moduli.

Exposure of asphalt binders to atmospheric oxygen, ultraviolet radiation, and high temperatures causes these molecules (i.e., SARA fractions) to irreversibly evolve through a mechanism called aging. Aging can be understood as a combination of oxidation reactions as well as evaporation of lighter components (Lesueur, 2009). The SARA fractions have varying degrees of polarity and reactivity with oxygen, so their composition in an asphalt binder will affect the binder's susceptibility to aging (J.C. Petersen, 2009). The aging mechanism of asphalt binder and its effects on the binder's chemical composition and rheology are discussed in the following section.

2.2 Mechanisms of Asphalt Aging

The aging phenomenon affects asphalt binders throughout their entire service life within flexible pavements. Due to its detrimental effects on performance, it has been the focus of extensive research(J.C. Petersen, 2009; Qin, Schabron, Boysen, & Farrar, 2014; Tauste et al., 2018). The physicochemical changes caused by aging cause an increase in complex modulus and reduction in phase angle, leading to an overall hardening of the material. For in-service pavements, this means a reduction in fatigue and thermal cracking resistance, which compromises their durability (G. Rowe et al., 2014; Y. Ruan, R. Davison, & C. Glover, 2003a).

Aging of binders follows three different mechanisms: oxidation, volatilization and physical or steric hardening (Tauste et al., 2018). Although all of them change asphalt rheological properties, oxidation and volatilization impact chemical composition and are thus irreversible, while steric hardening can be reversed. Steric or physical hardening causes an increase in complex modulus of binders due to a collapse of free volume following isothermal conditioning above and below the glass transition temperature. Studies showed hardening is caused by molecular reorientation and the formation of crystalline fractions and is dependent on binder source and wax content. However, it can be reversed with the addition of heat or mechanical work (D. A. Anderson & Marasteanu, 1999; Miró, Martínez, Moreno-Navarro, & del Carmen Rubio-Gámez, 2015).

The irreversible aging of binders occurs in two stages represented in Figure 4: an initial, fast rate reaction (i.e. short-term aging) and a long-term slower rate reaction dominated by oxidation (J.C. Petersen, 2009; J Claine Petersen & Glaser, 2011; Tauste et al., 2018). Short-and long-term reaction rates determine the extent of aging on binders. Asphalt chemical composition given by crude source and manufacturing process determines its aging susceptibility; higher susceptibility to aging will result on higher reaction rates. Additionally, temperature is the most significant extrinsic variable to influence aging (Miró et al., 2015), as a 10℃ increase can double oxidation rates (Tauste et al., 2018). As a result, both aging mechanisms cause changes in binder chemical composition which have repercussions on viscoelastic properties, as will be discussed in the following sections.

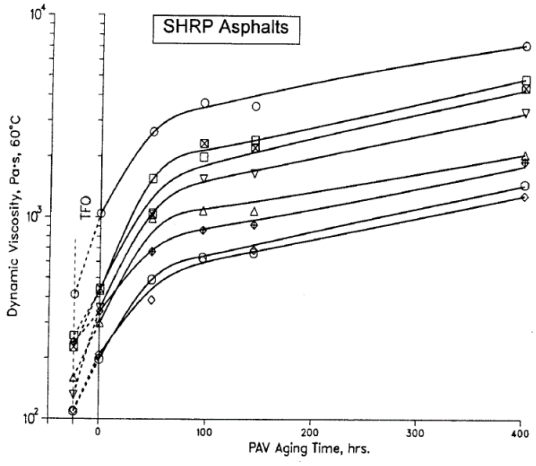

Figure 4. Long and short term aging kinetics shown by hardening of eight SHRP asphalts (J.C. Petersen, 2009)

2.2.1 Effects of Aging on Chemical Composition

Changes in chemical composition of binders are caused by the two irreversible aging mechanisms of volatilization and oxidation (Miró et al., 2015; Tauste et al., 2018). Volatilization is a fast-rate reaction that consists of the evaporation of the lighter components of asphalt and is mostly dependent on temperature. Therefore, it is most significant during the early stages of mixing, placing and compaction of an asphalt pavement (Tauste et al., 2018).

Oxidation occurs at a much slower rate and lasts throughout the entire pavement service life. It causes the most significant hardening effect on asphalts which leads to the deterioration of performance-related properties (J Claine Petersen & Glaser, 2011). Oxidation is a thermal reaction between atmospheric oxygen and asphalt components, driven by temperature and diffusion path (i.e oxygen's ability to access the asphalt component of mixtures through interconnected voids) (Tauste et al., 2018).

The effects of oxidation on binder chemistry are observed in the functional groups that are most reactive with oxygen. These are shown in Figure 5 and include carboxylic acids, anhydrides, ketones, sulfides and sulfoxides and are present in asphalt's polar components or formed as oxidation products (J.C. Petersen, 2009).

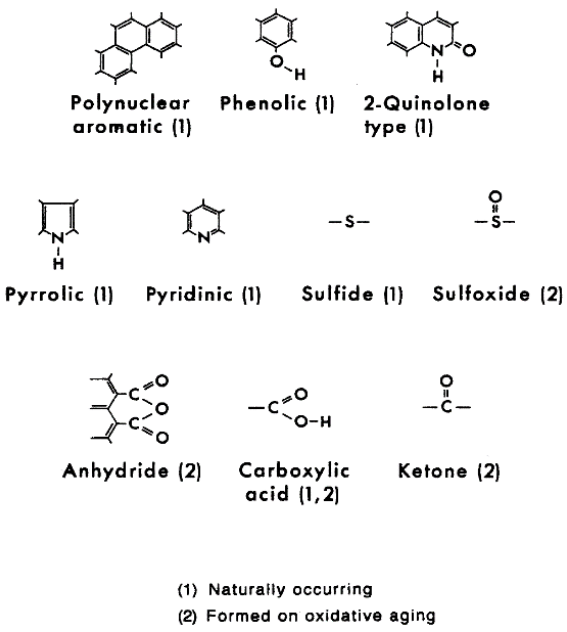

Figure 5. Asphalt functional groups typically present or formed during oxidation (J.C. Petersen, 2009)

The effects of oxidation on these functional groups have been modelled by researchers as a two-stage process (J Claine Petersen & Glaser, 2011). During an initial fast rate reaction, oxygen reactions yield hydroperoxides (Tauste et al., 2018). These functionalities are thermally unstable and can further react one of two ways: first, they can decompose and form free radicals that trigger the second stage of oxidation. During the second stage they would react with benzylic carbon to form carbonyl functions such as ketones. Alternatively, hydroperoxides can further react with sulfides to form sulfoxides (Knotnerus, 1972; J Claine Petersen & Glaser, 2011; Tauste et al., 2018). Thus, a dual aging mechanism was identified, with an initial rapid formation of sulfoxides which progresses at decreasing rates to favor ketone formation, both of which contribute to binder viscosity, as shown in Figure 6 (J.C. Petersen, 2009; J Claine Petersen & Glaser, 2011).

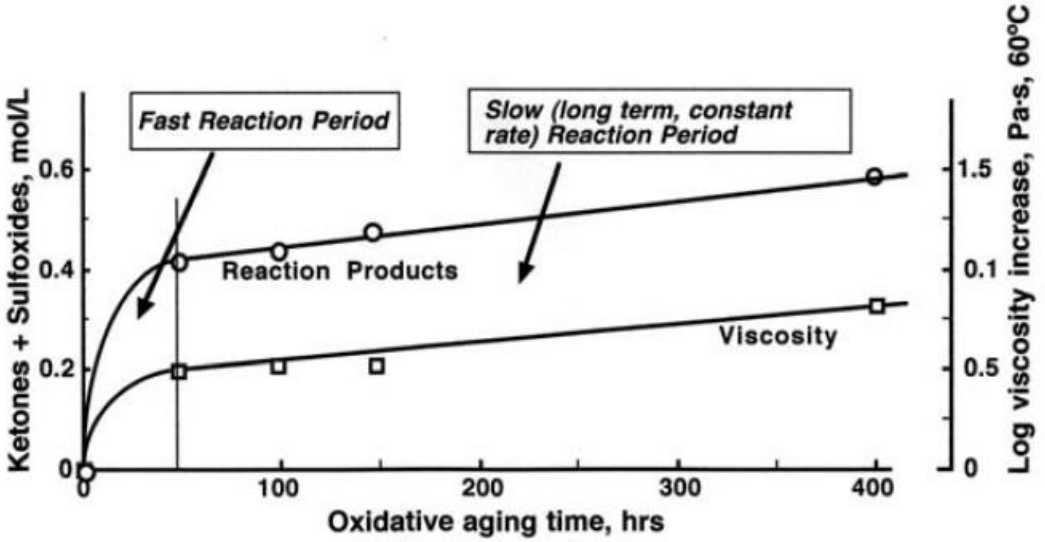

Figure 6. Ketone and sulfoxide formation and viscosity increase during oxidation (J Claine Petersen & Glaser, 2011)

As a result, the major oxidation products are ketones and sulfoxides, although smaller amounts of dicarboxylic anhydrides and carboxylic acids have also been identified. Although oxidation products are consistent across binders from multiple sources, the rate of formation as well as their relative concentrations are highly binder specific (J.C. Petersen, 2009).

Oxidation acts on the less polar molecules, and the formation of oxidation products results in an increase in the more polar components. Oxidation causes a reduction in aromatics, which react with oxygen to form resins. These further react to produce ketones and sulfoxides, which are typically present in the asphaltenes. Saturates are the most inert fraction and therefore show little to no change after aging (Isacsson & Zeng, 1997; Knotnerus, 1972; Mirwald et al., 2020; J.C. Petersen, 2009; Qin et al., 2014; Tauste et al., 2018; Weigel & Stephan, 2017). To illustrate this phenomenon, Mirwald et al. determined SARA fractions of asphalt binders after multiple laboratory aging durations. The low reactivity of saturates fraction was confirmed as its content increased only 1-4% across protocols. The greatest shifts were observed for the more polar fractions: a 17-22% reduction in aromatics, a 10% increase in resins and a 15% increase in asphaltenes. The resins fraction was found to increase due to oxidized aromatics while decreasing as they are oxidized to produce asphaltenes. In addition, Gel Permeation Chromatography (GPC) results of aged binders also indicated aging caused a shift towards longer, heavier molecules, which are typically resins and asphaltenes (Tauste et al., 2018).

Due to the different reactivity of binder fractions during oxidation, the balance between them changes, affecting the dispersion of asphaltenes within the asphalt binders (Mirwald et al., 2020; J.C. Petersen, 2009). To evaluate this effect, Petersen proposed a coefficient of dispersion, which is defined as the ratio of resins plus cyclic aromatics to asphaltenes plus saturates. He found a strong correlation between the coefficient of dispersion and the hardening of asphalts following laboratory aging. A higher coefficient of dispersion resulted on better flow properties (i.e., better Newtonian behavior) with less hardening after aging (J.C. Petersen, 2009). Therefore, both the reactivity and balance of binder fractions influence its aging susceptibility, which has a direct effect on rheological properties.

2.2.2 Effects of Aging on Rheology

As previously explained, aging causes an increase in polar components of asphalt such as ketones and sulfoxides (Lu & Isacsson, 2002; J.C. Petersen, 2009; J Claine Petersen & Glaser, 2011; Tauste et al., 2018). Ketones contain a highly polar C=O bond and therefore tend to attract to each other. An increase in ketones would increase polar-polar interactions and molecular agglomerations, which reduce molecular mobility. The reduction in molecular motion contributes to stiffening of the binder. Similarly, sulfoxides also increase polar-polar interactions and therefore contribute to binder hardening as well (J.C. Petersen, 2009; J Claine Petersen & Glaser, 2011; Qin et al., 2014; Tauste et al., 2018).

Under a more severe aging scenario, molecular interactions would become stronger, and agglomerations become more frequent, causing asphalt molecules to progressively lose mobility and the ability to flow past one another. Therefore, binders will lose the ability to flow under the application of thermal or mechanical stresses, showing a brittle behavior and making them more prone to cracking (Miró et al., 2015; J.C. Petersen, 2009).

In addition to the formation of oxidation products, the extent of hardening of binders will depend on the degree of dispersion exhibited by the four SARA fractions. If the maltene fraction is insufficient to keep the asphaltenes well dispersed, making it easier for asphaltenes to agglomerate, as shown in Figure 7, which would increase hardening even further (J.C. Petersen, 2009).

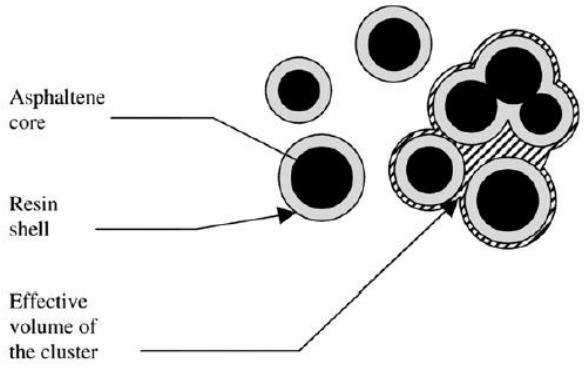

Figure 7. Peptized asphaltene micelles and asphaltene agglomeration into clusters (Lesueur, 2009)

Petersen's viscosity studies on SHRP binders showed binders with higher maltene contents before aging presented lower initial viscosity due to a good degree of dispersion and adequate asphaltene mobility. After aging, viscosity remained lower, meaning oxidation products were still well dispersed. Additionally, a comparison of the viscosity ratios for these binders before and after aging showed that the greatest hardening occurred for those with higher initial asphaltene contents, despite not producing the most oxidation products (J.C. Petersen, 2009).

More recently, researchers have characterized the hardening effect of aging through complex modulus (G^*) and phase angle (δ) obtained from dynamic shear measurements (Al-Khateeb & Ramadan, 2015; Dehouche, Kaci, Khadija, & Mokhtar, 2011; Osmari et al., 2019; Weigel & Stephan, 2017; Wu, Pang, Mo, Chen, & Zhu, 2009). Studies have shown that aging causes an increase in complex modulus and a decrease in molecular mobility that reduces binders' flow properties. In addition, the viscous response of binders shifts towards a more elastic behavior, resulting in a lower phase angle (Tauste et al., 2018). The combined effect of higher complex modulus and lower phase angles causes binders to become stiffer and more brittle, thus becoming more susceptible to cracking (Al-Khateeb & Ramadan, 2015; Miró et al., 2015; Ruan et al., 2003a). Petersen explored the relationship between fatigue performance and chemical composition of binders using a gas chromatographic column and found that binders with more polar components showed the worst cracking performance after 5 years in the field (J.C. Petersen, 2009).

Additionally, a study by Isacsson et al. explored fracture properties of aged binders relative to their SARA fractions. Thin Layer Chromatography tests showed a strong linear correlation between the sum of asphaltenes and resins with fracture temperatures obtained from the Thermal Stress Restrained Specimen Test (Isacsson & Zeng, 1997). Higher resins and asphaltenes were observed for higher aging levels which led to greater hardness and thus lower fracture temperatures.

All in all, asphalt chemical composition provides unique physical and rheological properties that define binder behavior and performance. Saturates, asphaltenes, resins and aromatics define binders' chemical composition, and their relative presence will dictate their rheological properties and aging susceptibility. Oxidation products cause an increase in asphalt polarity and a decrease in molecular mobility, resulting in hardening effects that compromise cracking resistance and binder durability. Understanding these changes will provide important insight into the effect of aging on binder performance properties.

2.3 Proposed Aging Resistant Technologies

2.3.1 Rejuvenators

Use of high reclaimed asphalt pavement (RAP) contents in asphalt mixtures provides environmental and economic benefits, but it can lead to concerns about cracking performance due to the presence of aged, stiff (Kaseer, Martin, & Arámbula-Mercado, 2019). To address these concerns, rejuvenators (i.e., recycling agents) have been used with the goal of restoring the rheological properties of aged binders and thus improve overall mixture performance (Hassan A. Tabatabaee & Kurth, 2017; Yin, Kaseer, Arámbula-Mercado, & Epps Martin, 2017; X. Yu, Zaumanis, Dos Santos, & Poulikakos, 2014). These rejuvenators can be made from petroleum or vegetable feedstocks, and examples include aromatic extracts, waste cooking oil, and soybean oils (Elkashef et al., 2018; Hassan A. Tabatabaee & Kurth, 2017; Yin et al., 2017).

An initial classification of rejuvenators into six grades was developed by ASTM, based on viscosity measurements at 60℃, and this classification was found to be more applicable to petroleum-based products (Kaseer et al., 2019). As more bio-based recycling agents are available in the market, there is a need to develop a classification that can be applicable to both petroleum-based and bio-based products. Thus, an alternative classification was proposed by Tabatabaee et al., which consists of three categories based on the asphalt fraction that is most compatible with the rejuvenator and that would thus be most affected by the rejuvenation mechanism (Hassan A. Tabatabaee & Kurth, 2017). The first category includes *soluble softeners* that lower the viscosity of the maltene phase by acting on the naphthenic aromatic fraction, without reversing asphaltene agglomeration. The second category is for *Compatibilizers* that have affinity for multiple fractions, and they work by disrupting the intermolecular asphaltene associations that are responsible for binder stiffness after aging. The last category was defined as *Incompatible softeners* that lower binder viscosity initially; however, due to poor compatibility with some aromatic and polar fractions, they may cause colloidal instability within the binder, leading to undesirable effects after aging. Regardless of their classification, the effectiveness of recycling agents depends on the degree of dispersion and diffusion as well as compatibility with RAP and virgin binders (Kaseer et al., 2019).

The effects of rejuvenation on asphalt binders may include lower complex modulus and higher phase angles. As shown in Figure 8, a rejuvenator made from soybean oils can improve the low temperature cracking performance by reducing stiffness while increasing m-value and ΔT_c (Elkashef & Williams, 2017; Santos et al., 2021; Hassan A. Tabatabaee & Kurth, 2017; Yin et al., 2017).

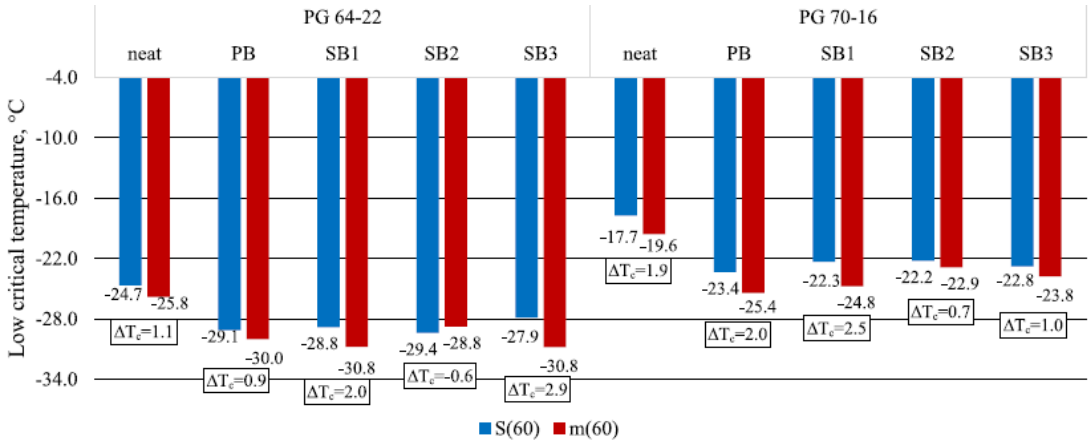

Figure 8. Effects of a soybean-based rejuvenator on low critical temperatures and ΔTc of aged binders (Santos, Faxina, & Soares, 2021)

Furthermore, some rejuvenators can disrupt asphaltene agglomerations in RAP binders, therefore lowering their glass transition temperatures and reducing the embrittlement caused by aging (Elkashef et al., 2020; Hassan A. Tabatabaee & Kurth, 2017). Additionally, Linear Amplitude Sweep tests on rejuvenated binders showed reductions on the B fatigue parameter and greater number of cycles to failure, therefore suggesting improved fatigue resistance (Santos et al., 2021). However, the extent of these rheological improvements depends on binder source and rejuvenator type (Elkashef et al., 2018; X. Yu et al., 2014).

Although rejuvenators can improve the performance properties of aged binders, there are concerns regarding their effects on rutting performance (Elkashef et al., 2018). To address these concerns, some researchers have selected the dosage of recycling agents by controlling the high PG of the rejuvenated binder blends, while trying to maximize the improvement in low and intermediate temperature performance (Santos et al., 2021).

In addition, there are also concerns relating to the long-term rejuvenating effectiveness (Mohammadafzali et al., 2015; Ongel & Hugener, 2015; Yin et al., 2017) as mixed results have been reported for rejuvenated binders after long-term aging in the laboratory. Elkashef et al. studied the aging behavior of a soybean-based rejuvenator using FTIR spectra of unaged and 20-hour PAV aged PG 58-28 and PG 64-28 binders with and without the rejuvenator. They calculated carbonyl and sulfoxide indices to evaluate the aging susceptibility of these binders by normalizing the carbonyl area (between 1753 and 1660 cm^{-1}) and sulfoxide area (between 1047 and 966 cm^{-1}), against that of aliphatic reference groups (at 1525 and 1350 cm^{-1}), which are not expected to change with laboratory aging. The growth rates of carbonyl and sulfoxide indices of the rejuvenated binders were comparable to those of the base PG 58-28 and PG 64-28 binders, suggesting the soybean-based rejuvenator did not affect the aging behavior of virgin binders (Elkashef et al., 2018). Furthermore, Santos et al. calculated similar indices using carbonyl and sulfoxide areas for a PG 70-16 and a PG 64-22 modified with a soybean-based and a petroleum-based rejuvenator. The growth rates of these indices after 20 hours of PAV aging were comparable to or less than the unmodified binders, depending on rejuvenator type and dosage (Santos et al., 2021). However, another study on four rejuvenators (two petroleum-based, one aromatic extract and one bio-based oil) showed that beyond the standard Superpave 20-hour PAV cycle, some rejuvenated binders showed greater aging rates than the base binders, despite showing comparable properties for shorter aging durations (Mohammadafzali et al., 2015). Similarly, in a study on the long-term rejuvenating effectiveness of tall oils and aromatic extracts, Yin et al. reported that both rejuvenators reduced the Glover-Rowe parameter of rejuvenated RAP binders after 20 and 40 hours of PAV aging, restoring some of the embrittlement caused by aging; however, the ratio between the Glover-Rowe parameter of rejuvenated binders to the control decreased with aging duration, indicating a progressively lower rejuvenating effectiveness (Yin et al., 2017).

2.3.2 Polymer Modifiers

Use of polymer modifiers, particularly styrene butadiene styrene (SBS), can improve binder performance properties related to rutting, fatigue cracking, and thermal cracking (Aurilio, Tavassoti, Elwardany, Baaj, & Eng, 2020; Behnood, Shah, McDaniel, Beeson, & Olek, 2016; Habbouche et al., 2020; Zhao, Gu, Xu, & Jin, 2010). When SBS is added to a binder, it absorbs the lighter portion of the maltenes (i.e., saturates and naphthenic aromatics) and becomes dispersed in the continuous binder matrix, resulting in a two-phase system. (Dehouche et al., 2011; Habbouche et al., 2021). As some maltene components are absorbed into SBS, the continuous binder matrix is rich in asphaltenes, becoming stiffer. Greater molecular interactions also occur between SBS and polar molecules of the asphaltenes. As a result, the complex modulus (G^*) of the modified binder increases. In addition, the thermoplastic elastomeric nature of SBS increases the elastic response of the binder, which is reflected by a reduction in phase angle (δ) (Dehouche et al., 2011; Lesueur, 2009; Y. Ruan, R. R. Davison, & C. J. Glover, 2003b). Overall, as compared to base binders, changes in the rheological properties of the respective modified binders will depend on SBS content and its

compatibility with the base binders, with greater compatibility leading to better polymer dispersion and thus greater improvements in binder performance (Dehouche et al., 2011; Habbouche et al., 2021; Hao, Huang, Yuan, Tang, & Xiao, 2017).

An increase in complex modulus in conjunction with a reduction in phase angle help improve the rutting resistance of modified binders and thus increase their high temperature PG grade. An increase of 2℃ in high temperature true grade can be expected for every 1% SBS added (Habbouche et al., 2020; Ruan et al., 2003b). Enhanced high temperature performance is also evidenced in the Multiple Stress Creep and Recovery (MSCR) test results, showing a reduction in non-recoverable creep compliance and an increase in elastic recovery (Behnood et al., 2016; Dehouche et al., 2011; Ruan et al., 2003b).

Improvement in low temperature performance is also reported for polymer modified binders. When comparing the master curves of base and 3% and 5% SBS modified binders, Ruan et al. found a pronounced increase in stiffness (i.e., G^*) at low frequencies (high temperatures) accompanied by a slight reduction in G^* at high frequencies (i.e., low temperatures). Additionally, the lower phase angles of modified binders result in a broader relaxation spectrum. Therefore, lower stiffness and better relaxation properties led to the improved low temperature behavior of SBS modified relative to base binders (Ruan et al., 2003b).

Studies have also shown that SBS improves cracking performance at intermediate temperatures (Ameri et al., 2017; Hasan, Hasan, Bairgi, Mannan, & Tarefder, 2019). Aurilio et al. studied fatigue resistance of modified binders using the Linear Amplitude Sweep (LAS) test and provided two key findings. First, a greater number of cycles to failure (at 50% damage) showed SBS modification increased fatigue life of the base binders (PG 64-28 and PG 52-34). Additionally, progressively higher cycles to failure were observed for higher polymer contents, which is consistent with observed field performance (Aurilio et al., 2020). These findings are in agreement with those observed by Zhang et al. in which modification enhanced fatigue life of modified binders through higher strain tolerance obtained from the LAS test (R. Zhang et al., 2020).

Although oxidation can degrade the SBS polymer, which in turn can diminish its effects, improvement in aged properties of modified binders have still been observed (Dehouche et al., 2011; Hao et al., 2017). Dehouche et al. reported a smaller reduction in penetration and a smaller increase in softening point of polymer modified binders (with 3 to 5% SBS) than the respective virgin binders after RTFO aging. Thus, the hardening effect of aging was less pronounced on modified binders. Additionally, SARA fractions showed that despite having a higher asphaltene content initially, SBS modified binders yielded lower asphaltene contents than the respective virgin binders after aging, confirming their lower stiffening rates (Dehouche et al., 2011). Other studies have used FTIR analysis to show the effects of aging on SBS modified binders (Morian et al., 2015; Zhao et al., 2010). For example, Wu et al. measured carbonyl and sulfoxide areas (around 1700 cm^{-1} and 1030 cm^{-1}, respectively) of neat and SBS modified binders after RTFO and after 600 to 2000 hours of PAV aging (at 60℃). Smaller increases in carbonyl and sulfoxide areas were observed for SBS modified binders, indicating a slower formation of oxidation products, and thus improved aging resistance (Wu et al., 2009). In another study, Morian et al. evaluated the growth in carbonyl area against rheological properties (i.e., low shear viscosity, Glover-Rowe parameter, and crossover modulus) of neat and SBS modified binders after multiple aging durations. Figure 9 shows the correlation between low shear viscosity and carbonyl area growth for a neat PG 64-22 and a 3% SBS modified PG 64-28. The flatter slope of the SBS modified binder indicates less hardening for longer aging durations (Morian et al., 2015).

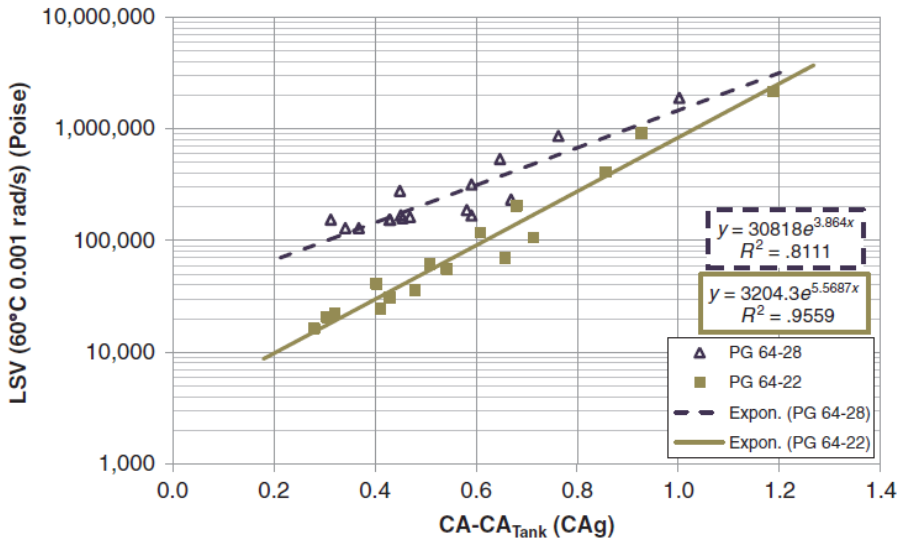

Figure 9. Hardening susceptibility of a neat 64-22 binder and 3% SBS modified 64-28 binder (True Grade 70-31) (Morian, Zhu, & Hajj, 2015)

Finally, highly modified binders (i.e., with SBS contents up to 7.5%) appear to further enhance the aging behavior of binders (Habbouche et al., 2021; Habbouche et al., 2020; Lesueur, 2009). Habbouche et al. conducted low shear viscosity measurements on neat, conventional polymer modified binders (3% SBS) and highly modified binders (8% SBS) after several oven aging protocols. Smaller increases in low shear viscosity were found for conventional polymer modified binders, and even lower for those highly modified, suggesting lower hardening rates with increasing aging durations and polymer contents. Additionally, plots of G^* and δ on a Black Space diagram have shown that the gradual hardening of the neat binder was mitigated by the addition of progressively higher SBS contents. The Black Space diagram in Figure 10 shows lower G^* and higher phase angles for the highly polymer (HP) modified binder than those of the conventional polymer modified asphalts (PMA) after aging, both better than the base binder. Thus, compared to the virgin binder, improvement in aging resistance was observed for PMA, which was further enhanced in the HP binder with a higher SBS content. Finally, the shorter path and steeper slope between G^* and δ for HP and PMA indicates the rheological properties of these binders are less affected by increasing aging durations, further supporting the enhanced aging resistance of HP and PMA with respect to unmodified binders (Habbouche et al., 2021; Habbouche et al., 2020).

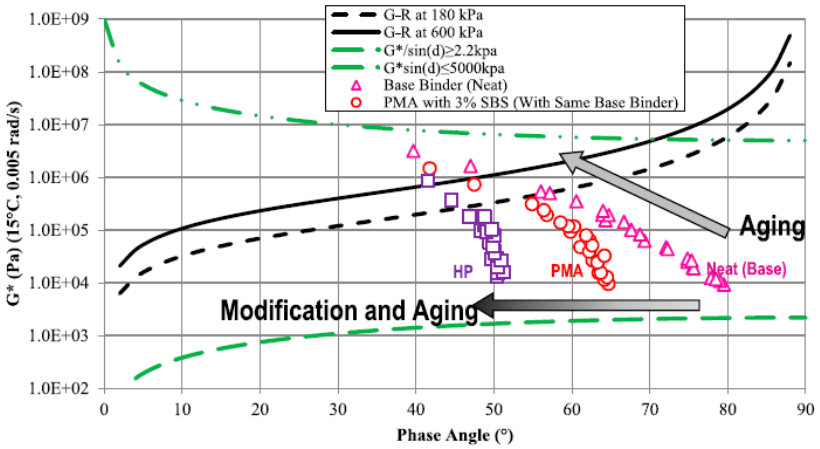

Figure 10. Performance of neat, polymer modified (PMA) and highly polymer modified asphalt (HP) on Black Space diagram (Habbouche, Hajj, Sebaaly, & Piratheepan, 2020)

2.3.3 Crumb Rubber

Crumb rubber modifiers (CRM) are obtained from the micro-milling of scrap tires following a variety of grinding techniques. Each production process yields CRM of different particle sizes, shapes, and surface textures, leading to different properties to modified binders (Heitzman, 1992; Lee, Akisetty, & Amirkhanian, 2008). CRM consists of rubber polymer, carbon black and smaller amounts of antioxidants/antiozonants and processing agents like sulfur (H. Wang et al., 2020).

When CRM is added to an asphalt binder for modification, the rubber particles in CRM absorb the aromatic portion of the maltenes and swell up to 9-10 times its original size at high temperatures. This process is called polymer swell, and depends on time, temperature, size, and texture of rubber particles as well as binder source (Heitzman, 1992; Lee et al., 2008). The loss of part of the oily fraction of binders and the swelling of the rubber polymer result in the formation of a viscous gel that provides greater stiffness and higher viscosity to modified binders (Lee et al., 2008; Xiao, Amirkhanian, & Shen, 2009).

The stiffening caused by the polymer swell reaction leads to higher complex modulus G^* and lower phase angles δ, increasing the high climatic PG of binders (Al-Khateeb & Ramadan, 2015; Heitzman, 1992; Navarro, Partal, Martínez-Boza, Valencia, & Gallegos, 2002; Xiao et al., 2009). Additionally, MSCR measurements have shown CRM modification increases elastic recovery and reduces non-recoverable creep compliance, which increases rutting resistance (Vahidi, Mogawer, & Booshehrian, 2014). Improvement in cracking resistance of CRM modified binders has also been found, given by reductions in the Superpave fatigue parameter $G^* \sin \delta$. Furthermore, when comparing a 10% CRM modified binder against a neat and a SBS modified PG 76-22 binder, Xiao et al. found the CRM binder provided the greatest reduction in $G^* \sin \delta$ after 20 hours of PAV aging (Al-Khateeb & Ramadan, 2015; Xiao et al., 2009). Enhanced cracking resistance of rubber modified binders was also found through LAS testing. For example, Figure 11 presents cycles to failure with respect to the applied strain for neat, SBS and CRM binders. An increase in the A_{35} parameter (i.e. y-intercept) and in the number of cycles to failure (i.e., vertical shift of the curves) can be observed at both 8% and 16% CRM contents, compared to the 85/100 penetration grade base binder (Ameri et al., 2017; Vahidi et al., 2014). Finally, based on BBR testing, CRM binders have lower stiffness and greater m-values than the respective neat binders, thus enhancing their relaxation properties and low

temperature performance (Heitzman, 1992; Navarro et al., 2002; H. Zhang, Xu, Chen, Wang, & Shen, 2019).

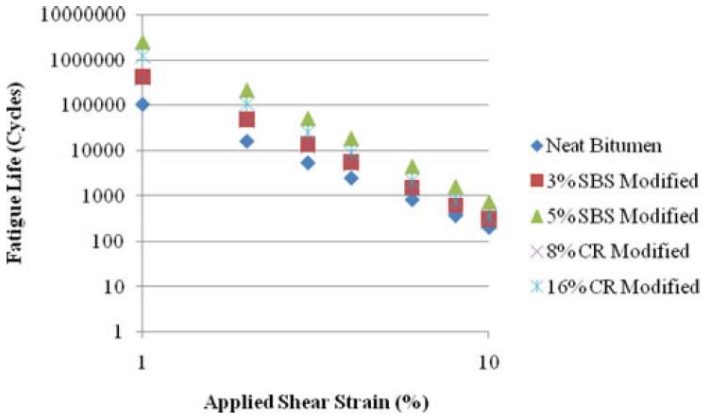

Figure 11. Fatigue models from LAS tests on neat and polymer modified binders (Ameri, Reza Seif, Abbasi, & Khavandi Khiavi, 2017)

The use of rubber modifiers can also improve the aging resistance of asphalt binders. Carbon black and antioxidants within the CRM composition can retard the aging process of asphalt binders (Heitzman, 1992; H. Wang et al., 2020). Additionally, according to Wang et al., as a portion of the oily fraction of the binder is absorbed into rubber particles, a small amount of this fraction is available for oxidation, which would reduce the aging susceptibility of the binder. Finally, polymers present in rubber are more readily attacked by oxygen, thus delaying the oxidation of binder molecules (H. Wang et al., 2020). Such improvement in aging resistance was confirmed by FTIR. A PG 64-22 binder modified with 5-22% CRM contents showed smaller carbonyl and sulfoxide peaks (at 1700 cm-1 and 1030 cm-1, respectively) after 20-hour PAV aging than the neat binder, indicating a slower formation of oxidation products and therefore improved aging susceptibility. The study also showed that creep compliance J_{nr} was the rheological parameter that was better correlated with aging duration (instead of Glover-Rowe, R-value or crossover frequency). Rubber modified binders showed smaller changes in J_{nr} with progressive aging durations than neat binders, suggesting improvement in aging resistance (H. Wang et al., 2020).

2.3.4 Epoxy Resins

Epoxy resins are brittle amorphous thermosetting polymers. They consist of long sequences of covalently linked monomers that can form macromolecules arranged in a three-dimensional network through a curing process. Opposite to thermoplastic polymers, which are linear or radial chains, the three-dimensional structure formed by epoxy resins cannot be melted, therefore the curing process is irreversible (Apostolidis et al., 2020; Kang et al., 2015).

The strong covalent bonds within epoxy resins result in high stiffness and increased thermal stability, improving resistance of asphalt mixtures to rutting, fatigue cracking and moisture damage (Kang et al., 2015; Youtcheff, Gibson, Shenoy, & Al-Khateeb, 2006). However, due to the high cost of epoxy asphalt, it has mainly been used for long span bridge decks or airfields. More recently, the dilution of epoxy resins has led to more interest towards its application in asphalt pavement, showing improved fatigue and rutting performance, as well as resistance to thermal cracking due to higher stiffness and more elastic behavior over wider temperatures (Apostolidis et al., 2020; Kang et al., 2015; Youtcheff et al., 2006).

Kang et al. studied diluted epoxy asphalt at a 2.9:1 ratio of asphalt component to epoxy resin component. Higher stiffness (i.e., G^*) of epoxy binders was confirmed over wider temperature ranges, indicating greater temperature stability than virgin and polymer modified binders (PMBs). Furthermore, creep and recovery measurements (Figure 12) showed that after 100 cycles (1 second load and 9 second recovery), epoxy asphalts presented higher recovery and lower non-recoverable creep compliance, indicating better rutting resistance (Kang et al., 2015). Additionally, master curves developed by Youtcheff et al. showed that epoxy binders retained their $G^*/\sin\delta$ across broader frequencies than a neat PG 70-22, suggesting enhanced rutting resistance and thermal stability (Youtcheff et al., 2006).

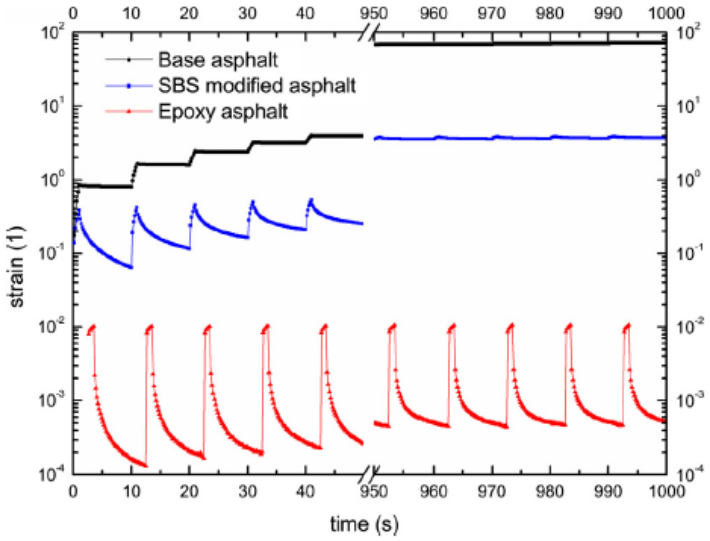

Figure 12. Creep and recovery test results for neat, SBS modified and epoxy asphalts (first and final 5 cycles) (Kang, Song, Pu, & Liu, 2015)

However, there are some challenges in evaluating oxidative aging on epoxy binders, particularly with the use of Superpave aging protocols. The study by Kang et al. discussed above did not include properties of aged binders, and Youtcheff et al. acknowledged these limitations as well. However, they studied the impact of UV aging and found that after the initial curing, both the complex modulus and the phase angle of epoxy binders remain virtually unchanged even after 16 weeks of UV aging durations, suggesting a high aging resistance (Kang et al., 2015; Youtcheff et al., 2006).

Aging of epoxy binders was also evaluated by Apostolidis et al., using a blend of proprietary two-part epoxy resin and base binder at a 20:80 proportion, and instead of following the Superpave protocols, they oven aged the blend at 80℃, 90℃ and 100℃ from 0 to 480 hours. FTIR measurements showed smaller carbonyl areas (between 1753 and 1660 cm^{-1}) for epoxy binders than for neat binders, indicating slower formation of oxidation products and therefore slower aging rates (Apostolidis et al., 2020).

2.4 Laboratory Aging Protocols

The purpose of laboratory aging is to replicate the effects of aging experienced by binders in the field (J. Claine Petersen & Strategic Highway Research, 1994). Both short-term and long-term aging protocols are required to determine binder properties at different stages. The short-term laboratory aging protocol simulates the effects of higher temperatures on asphalt binders during production and construction, where aging is dominated by volatilization of lighter components (Tauste et al., 2018). Long-term protocols simulate the aging of in-service pavements, governed by oxidative aging over an extended period, and

across a range of pavement temperatures experienced in the field. Laboratory aging protocols aim to realistically simulate the aging of asphalt binders in the field efficiently while generating representative binder residue sufficient for further testing (Bonaquist, Adams, & Anderson, 2021; Mirwald et al., 2020).

2.4.1 Short-Term Aging

The Superpave binder specification indicates the Rolling Thin Film Oven Test (RTFOT) as the standard procedure for short-term laboratory aging in AASHTO T240 (Officials, 2021a). During the test, thin films of binder are exposed to the heat and air to simulate the aging during storage, mixing, transportation, and placement of asphalt mixtures. For this procedure, 35 grams of binder are poured into glass bottles, which are then placed in a rotating carrousel, creating a 1.25mm film of asphalt, inside an oven at 163℃ for 85 minutes and are subject to a constant flow of air of 4000 mL/min. Rheological properties of the aged binder can then be determined to evaluate the changes caused by short term aging (Bonaquist et al., 2021; Mirwald et al., 2020; Officials, 2021a; Tauste et al., 2018).

However, RTFO aging has presented some limitations that motivated researchers to propose improvements to the test method (Bonaquist et al., 2021). First, RTFO may not accurately simulate the aging occurring during production. RTFO aging was found to provide a lower content of sulfoxides and greater carbonyl formation and a greater loss of volatiles as compared to field samples (Airey, 2003; Qin et al., 2014; Tauste et al., 2018). Also, binders with higher viscosities such as polymer-modified binders have presented difficulties to form even, thin films for adequate aging (Tauste et al., 2018). In addition, the standard test temperature of 163℃ has been considered too high for binders with warm mix additives (Bonaquist et al., 2021). Finally, other specialty binders such as epoxy asphalts cannot typically be evaluated by this method due to their thermosetting nature (Youtcheff et al., 2006).

2.4.2 Long-Term Aging

The long-term aging procedure included in the Superpave specification is the Pressurized Aging Vessel (PAV) standardized in AASHTO R28 (Officials, 2021b). The PAV aging procedure simulates the physical and chemical changes occurring to binders after presumably 4 to 8 years in service (Bonaquist et al., 2021; Officials, 2021b; J. Claine Petersen & Strategic Highway Research, 1994) and is conducted on RTFO residue. To replicate the oxidation occurred during the extended pavement life in reasonable time, the binder is aged at a high temperature and under a high pressure to accelerate oxygen diffusion (Bonaquist et al., 2021; J. Claine Petersen & Strategic Highway Research, 1994). During the test, a 3.18 mm asphalt film is aged at 90℃, 100℃ or 110℃ based on climatic region for a duration of 20 hours (indicated for AASHTO M320 compliance) and under 2.10 MPa of air pressure.

This procedure has also presented limitations when replicating long-term field aging (Bonaquist et al., 2021; Mirwald et al., 2020; Osmari et al., 2019; Qin et al., 2014). While 20 hours of PAV aging was established to simulate 5- to 10-year-old binders (Bonaquist et al., 2021), researchers were not able to correlate this procedure to the field aging after 8 years in service (Qin et al., 2014). Therefore, this mechanism is highly dependent on local conditions and binder source. Additionally, the aging gradient with pavement depth shows the most severe aging at the top has not been adequately captured through 20 hours of PAV aging, so some researchers have extended the cycle to 40 hours (Bonaquist et al., 2021). PAV aging has also shown some limitations for the characterization of specialty materials such as epoxy asphalt or polymer modified binders (Memon & Chollar, 1997; Youtcheff et al., 2006).

Alternative approaches have been developed based on changes to the current methods rather than actual correlations to field data. Overall, changes to test temperature and duration have been proposed, but the

PAV procedure can be used as an adequate tool to establish differences between binders (Bonaquist et al., 2021).

2.5 Rheological Characterization of Asphalt Binders

2.5.1 Superpave Performance Grading

Superpave Performance Grading (PG) was developed as a result of multiple SHRP projects aimed at providing asphalt performance-related specifications (D. A. Anderson & Kennedy, 1993; J. C. Petersen, Robertson, R.E, Branthaver, J.F., Harnsberger, P.M, Duvall, J.J., Kim, S.S., Anderson, D.A, Christiansen, D.W., Bahia, U.H. , 1994). PG Grading transitioned from traditional grading systems based on physical properties, such as of penetration, viscosity, and ductility, to rheological measurements that captured binder viscoelastic nature.
PG Grading characterizes binder performance in terms of the most critical distresses (i.e., rutting, fatigue and thermal cracking) at high, intermediate, and low temperatures. It incorporates the changes experienced after short- and long-term aging, providing performance-related parameters over the full range of in-service temperatures and throughout the entire service life of binders (J. C. Petersen, Robertson, R.E, Branthaver, J.F., Harnsberger, P.M, Duvall, J.J., Kim, S.S., Anderson, D.A, Christiansen, D.W., Bahia, U.H. , 1994).

2.5.1.1 High-Temperature Evaluation

The most critical distress affecting pavement performance at high temperatures is the accumulation of permanent deformation, or rutting. Although rutting in asphalt mixtures primarily depends on aggregate features, binder properties also have an impact. It was therefore incorporated into the Superpave specification (J. C. Petersen, Robertson, R.E, Branthaver, J.F., Harnsberger, P.M, Duvall, J.J., Kim, S.S., Anderson, D.A, Christiansen, D.W., Bahia, U.H. , 1994).

Binder viscoelastic properties of complex modulus G^* and phase angle δ determine high temperature performance and are measured under oscillatory loading in the Dynamic Shear Rheometer (DSR). The Superpave rutting parameter is the loss compliance $G^*/\sin\delta$ obtained at a frequency of $10\ rad/s$, which replicates the passing of a tire truck at a speed of 50 mph. As binders age, stiffness increases and phase angle is reduced, leading to an improvement in the rutting parameter. For this reason, permanent deformation is more critical at an earlier service life and is therefore evaluated at the unaged condition and after short-term RTFO aging (J. C. Petersen, Robertson, R.E, Branthaver, J.F., Harnsberger, P.M, Duvall, J.J., Kim, S.S., Anderson, D.A, Christiansen, D.W., Bahia, U.H. , 1994; J. Claine Petersen & Strategic Highway Research, 1994).

Softer binders (i.e., with lower values of G^*) may be more susceptible to rutting, while lower phase angles improve the binder's elastic response, having better rutting resistance (Al-Khateeb & Ramadan, 2015). Thus, Superpave specification determined the passing rutting criterion as $G^*/\sin\delta \geq 1.00kPa$ for unaged binders and $2.20\ kPa$ for RTFO-aged binders. DSR measurements of the rutting parameter are conducted using 25-mm parallel plate geometry. Since its incorporation into the Superpave specification the DSR rutting parameter has successfully been used to evaluate rutting resistance of conventional binders as well as epoxy asphalts (Youtcheff et al., 2006), crumb rubber binders (Al-Khateeb & Ramadan, 2015) and even rejuvenated asphalts (Elkashef et al., 2018; Santos et al., 2021).

2.5.1.2 Intermediate-Temperature Evaluation

The Superpave specification at intermediate temperatures addresses fatigue cracking resistance of binders. The development of the fatigue criterion for PG grading was based on dissipated energy per load cycle, given by $G^* \sin\delta$ from DSR measurements at 10 rad/s (J. C. Petersen, Robertson, R.E, Branthaver, J.F., Harnsberger, P.M, Duvall, J.J., Kim, S.S., Anderson, D.A, Christiansen, D.W., Bahia, U.H. , 1994). Fatigue characterization requires the evaluation of samples representative of the long-term properties of binders, when fatigue is likely to occur. Therefore, fatigue is evaluated after RTFO + 20 hours of PAV aging at a temperature equal to the average between the high and low temperature grades plus 4℃ (J. Claine Petersen & Strategic Highway Research, 1994).

For sinusoidal loading, $G^* \sin\delta$ represents the dissipated energy per load cycle. For elastic materials, dissipated energy can be seen as a measure of energy released due to damage propagation. Therefore, higher values of dissipated strain energy (i.e., higher $G^* \sin\delta$) indicate the sample experiences more incremental damage per unit cycle, or greater fatigue (Hajj & Bhasin, 2018). Thus, the Superpave specification limits $G^* \sin\delta$ to a maximum of $5{,}000\ kPa$.

Although the Superpave fatigue parameter was considered an improvement to prior binder specifications, it was based on several assumptions that have limited its ability to accurately predict fatigue performance (D. A. Anderson et al., 2001; Hajj & Bhasin, 2018; G. Rowe et al., 2014). First, it assumes that all dissipated energy is due to incremental damage, and recoverable energy is negligible, which may not be true for some modified binders (Hasan et al., 2019). Additionally, binders are tested at low strain levels within the linear viscoelastic region, so the damaged properties of the material are not fully observed (Hintz et al., 2011). Finally, Rowe suggested the fatigue parameter fails to predict cracking performance of binder after aging. Figure 13 shows the $G^* \sin\delta$ threshold of $5{,}000\ kPa$ would have a negative slope on Black Space. Thus, this parameter would cause harder and more brittle materials to move outside of the Glover-Rowe damage zone, which contradicts observed performance (G. Rowe et al., 2014).

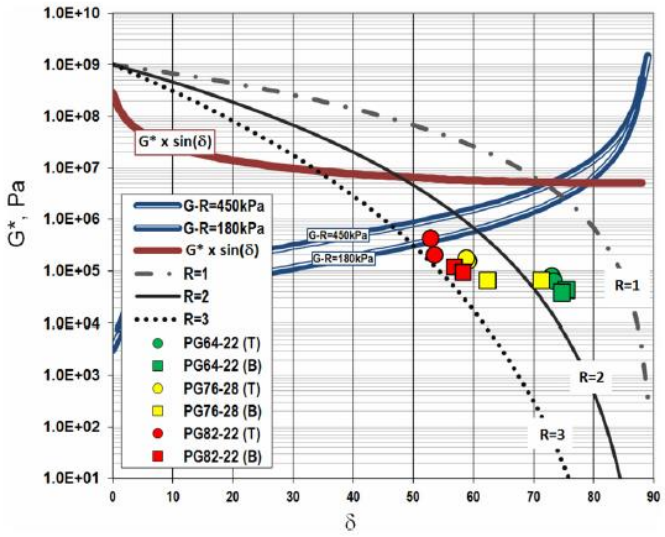

Figure 13. Black Space damage zone predictions using Superpave fatigue parameter and alternative indicators (G. Rowe, King, & Anderson, 2014)

Although it is still in use within the AASHTO M320 specification, and some studies have successfully used to capture pavement performance (Xiao et al., 2009), researchers have chosen alternative approaches to characterize fatigue resistance of neat and modified binders such as the LAS test (D. A. Anderson et al., 2001; Hajj & Bhasin, 2018; Hintz et al., 2011).

2.5.1.3 Low Temperature Evaluation

The buildup of thermal stresses in binders when subject to low temperatures causes transverse cracking. Thermal cracking can occur due to a single cooling event or multiple cooling cycles, leading to shrinkage stresses that cause crack initiation and propagation (D. A. Anderson et al., 1994). Crack initiation due to a single cooling event suggested there might be a critical stiffness temperature beyond which thermal stresses exceed binder strength. Additionally, thermal stress buildup would also be time dependent (J. C. Petersen, Robertson, R.E, Branthaver, J.F., Harnsberger, P.M, Duvall, J.J., Kim, S.S., Anderson, D.A, Christiansen, D.W., Bahia, U.H. , 1994). Thus, the Superpave binder specification for thermal cracking incorporates these two concepts.

Low temperature properties within Superpave PG grading are determined using the Bending Beam Rheometer (BBR). The BBR test measures the low temperature creep response of binders by applying a constant load to a prismatic beam. The midpoint deflection of a binder beam of controlled dimensions is measured, and stiffness is calculated through bending beam theory (D. A. Anderson et al., 1994). SHRP researchers used the concept of limiting stiffness and found that cracking would initiate when binders exceeded 200 MPa, and the temperature at which the limiting stiffness was exceeded after a loading time of 2 hours was the limiting temperature (J. C. Petersen, Robertson, R.E, Branthaver, J.F., Harnsberger, P.M, Duvall, J.J., Kim, S.S., Anderson, D.A, Christiansen, D.W., Bahia, U.H. , 1994). To account for time-dependency, the creep rate was added to the specification and defined as the m-value, which is related to the ability of binders to dissipate thermal stresses experienced upon cooling, regardless of stiffness (Technical Advisory Committee, 2019).

Therefore, the Superpave binder specification indicates 300 MPa as the limiting stiffness and 0.300 as the passing m-value, for low temperature specification. These criteria are used to determine the binder's low critical temperatures $T_{c,S}$ and $T_{c,m}$. SHRP researchers showed that stiffness and m-value at 60-second loading time would be equivalent to those measured at 2-hour loading time if testing was done at the minimum passing temperature +10℃, which simplified the procedure considerably (J. C. Petersen, Robertson, R.E, Branthaver, J.F., Harnsberger, P.M, Duvall, J.J., Kim, S.S., Anderson, D.A, Christiansen, D.W., Bahia, U.H. , 1994; J. Claine Petersen & Strategic Highway Research, 1994).

2.5.1.4 4-mm DSR Approach for Low Temperature Evaluation

The BBR method was adopted in the Superpave specification for low temperature evaluation due to potential errors caused by machine compliance with DSR measurements below 5℃ (Farrar et al., 2015). Although BBR testing is widely used, the amount of material required for specimen fabrication has recently become a challenge when testing extracted binders or emulsion residue (Hajj, Filonzi, Rahman, & Bhasin, 2019; Sui, Farrar, Harnsberger, Tuminello, & Turner, 2011). As a result, researchers at the Western Research Institute (WRI) developed an alternative approach for low-temperature evaluation using DSR measurements (Sui et al., 2011). A considerably smaller sample mass is required (around 25 mg per specimen) and machine compliance errors were solved by changing from an 8-mm diameter to a 4-mm plate with a gap opening of 1.75mm (Büchner et al., 2020; Sui et al., 2011).

The 4-mm DSR approach can evaluate low temperature performance of binders at temperatures between 5 and -40℃. It involves the construction of a frequency sweep and subsequent calculation of the relaxation modulus $G(t)$ and relaxation rate (m_c) (Sui et al., 2011). To obtain the BBR parameters of stiffness and m-value, an interconversion needs to be conducted from the frequency domain of DSR measurements to the time domain where BBR tests are performed (Hajj et al., 2019). Initially, a stiffness of 300 MPa at 60 seconds would correlate with a relaxation modulus of 160 MPa at 7,200 s, and an m-value of 0.300 at 60 seconds would be equivalent to 0.260 at 7,200s for unmodified binders tested at the low PG (Sui et al.,

2011). Later, the test temperature was changed low PG + 10℃, and the correlation was modified and established at 60 seconds, with $G(60s) = 143\ MPa$ and $m_c = 0.275$, as shown in Figure 14 (Farrar et al., 2015).

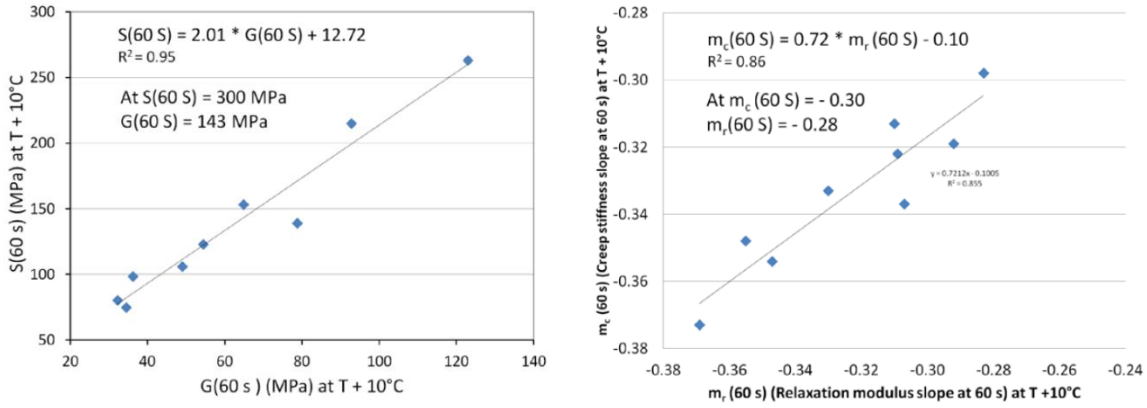

Figure 14. Correlations for low temperature critical values between BBR and DSR measurements, following WRI approach (Farrar, Sui, Salmans, & Qin, 2015)

Studies showed the WRI method yielded more accurate correlations between DSR measurements and Tc_S for unmodified binders, but Tc_m did not show an equally strong correlation. Sample preparation, the effect of wax crystallization or physical hardening due to the different sample sizes could be responsible for these differences (Büchner et al., 2020; Lu, Uhlback, & Soenen, 2017). Although alternative means of conversion have been developed, they resulted in similar findings: the stiffness-based critical temperature can be obtained with a good level of accuracy, while the m-value continuous low grade showed greater dependency on the test method (Hajj et al., 2019).

Despite yielding good correlations for critical temperatures, complex modulus and phase angle, the 4-mm approach still presents certain limitations (Büchner et al., 2020; Lu et al., 2017). First, little research has been conducted to explore these correlations for modified binders. Additionally, interlaboratory findings have indicated the repeatability for the method can be lower than for BBR testing, particularly for stiffness measurements (Büchner et al., 2020).

2.5.1.5 ΔTc Parameter and Correlations with Fatigue Cracking Resistance

The rheological parameter ΔT_C is the difference between the low critical temperatures $T_{C,S}$ and $T_{C,m}$ that result from BBR measurements per AASHTO T313, as shown by Equation 1 (Technical Advisory Committee, 2019).

Equation 1. Calculation of ΔTc

$$\Delta T_C = T_{c,S} - T_{c,m}$$

ΔT_C depends on binder low temperature properties of stiffness and creep rate. Therefore, it is associated with binder relaxation properties. At low temperatures, higher relaxation rates are preferred, so binders can better dissipate stresses without cracking. Therefore, higher m-values (and lower $T_{c,m}$) are indicative of better relaxation properties and therefore result on more positive values of ΔT_C (Christensen et al., 2019).

The concept was developed within a study of block cracking in airfield pavements, using the premise that this distress can be related to the loss in binder ductility when measured at 15℃ (Christensen et al., 2019; Ruan et al., 2003a; Technical Advisory Committee, 2019). Thus, researchers looked for surrogate for binder ductility to predict the occurrence of surface distresses more easily. It was concluded that, for unmodified binders, the Glover parameter (Equation 2) at 15℃ obtained from master curve measurements and ΔT_C could be successfully correlated with binder ductility, as shown in Figure 15.

Equation 2. Glover Parameter

$$Glover\ parameter = \frac{G'}{\left(\eta'/_{G'}\right)}$$

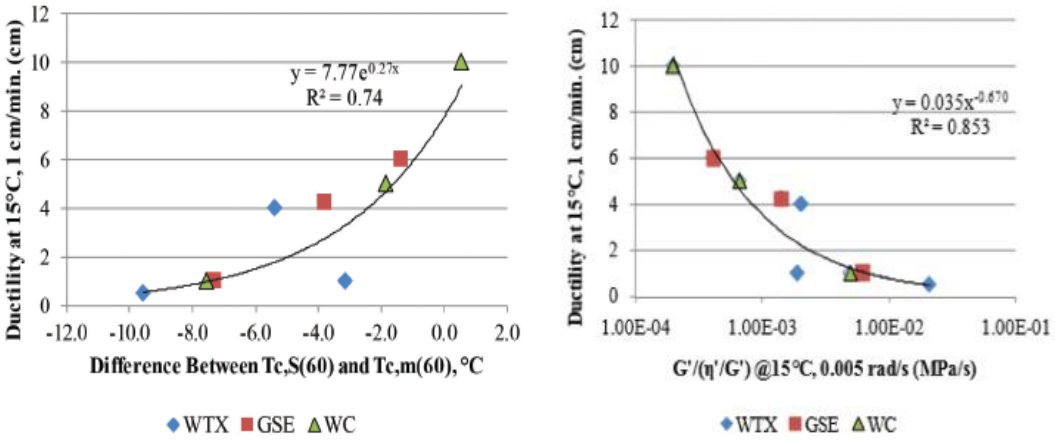

Figure 15. Relationships between Glover parameter and ΔTc with binder ductility (Technical Advisory Committee, 2019)

The relationship between ΔT_C and ductility provided insight into the onset of block cracking in flexible pavements. Additionally, as ΔT_C is inherently linked to relaxation properties of binders, it has also been used to predict fatigue cracking and other age-related distresses (Aurilio et al., 2020; Elwardany, King, et al., 2020; Elwardany, Planche, & King, 2020; Mensching et al., 2015). Aging causes an increase in stiffness and a reduction in m-value, increasing low critical temperatures. Additionally, the rate of change is not equal for both parameters— m-value increases faster than stiffness, causing ΔT_C to become more negative (Aurilio et al., 2020; Zhou, Gu, Dong, Ni, & Jiang, 2020). A more negative value of ΔT_C would be consistent with reduced ductility. As both viscosity and complex modulus increase, the binder becomes a more brittle material and more susceptible to cracking (Ruan et al., 2003a).

The onset of surface cracking occurs when ductility reaches 5 cm, and when ductility is below 3 cm, cracking increases significantly (Christensen et al., 2019; Ruan et al., 2003a). Based on these thresholds, a ΔT_C equal to -5℃ would be indicative of problematic binders with potential early cracking. Such threshold has been adopted by some agencies for improving binder cracking performance (Elwardany, Planche, et al., 2020; Technical Advisory Committee, 2019). When comparing to the LAS test results, Moraes and Bahia found that binders with more negative values of ΔT_C showed lower resistance to damage accumulation (i.e., a higher LAS B parameter) (Moraes & Bahia, 2018). Additionally, Zhang et al. were able to capture field cracking performance and aging gradients by measuring ΔT_C and the Glover-Rowe parameter of binders extracted from field cores (R. Zhang et al., 2020).

However, the ability of ΔT_C to characterize cracking performance of polymer modified asphalts (PMA) has been questioned by researchers (Aurilio et al., 2020; Christensen et al., 2019; Elwardany, Planche, et al., 2020; Habbouche et al., 2021). SBS modification increases the elastic response and therefore reduces phase angle (and m-value) of neat binders, resulting in a more negative ΔT_C, which does not match the enhanced performance observed in the field (Christensen et al., 2019). Kluttz showed that higher polymer contents caused progressively lower values of ΔT_C while resulting in higher fatigue lives measured by LAS, suggesting the R-value from frequency sweeps would be a better indicator for fatigue life of PMAs (Kluttz, 2019). Studies on mixture performance agree with these findings, as shown in Figure 16 from a study by D'Angelo. It can be observed that although similar values of ΔT_C were observed for neat and PMA, the unmodified binder showed significantly lower I-FIT values, indicating poorer cracking performance.

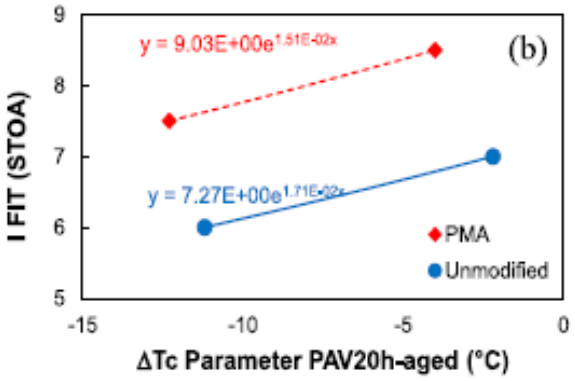

Figure 16. Correlation between ΔTc and mixture I-FIT values (D'Angelo, Baumgardner, Jordan, Daranga, & Hemsley, 2019)

2.5.2 Multiple Stress Creep and Recovery

The Superpave parameter (i.e., $G^*/\sin\delta$) showed some shortcomings when capturing rutting performance of polymer modified binders, particularly the field rutting performance did not correlate well with the high temperature binder properties given by standard PG grading (Behnood et al., 2016). To address the shortcomings, several tests were evaluated to characterize polymer modified binders (Bahia et al., 2016), and the Multiple Stress Creep and Recovery (MSCR) Test (AASHTO T 350) was selected to evaluate the rutting resistance of these materials.

The MSCR is a creep and recovery test, meaning that binders are subjected to a constant load for a fixed period, after which they are allowed to recover. Twenty cycles are run at a 0.1 kPa stress level and ten cycles are run immediately after at a stress level of 3.2 kPa. Compared to the $G^*/\sin\delta$ parameter, MSCR applies higher strain levels that engage the polymer networks, and differences in performance between polymer modified and unmodified binders are observed (Behnood et al., 2016; Salim, Gundla, Underwood, & Kaloush, 2019).

The main output of the test is the non-recoverable creep compliance J_{nr} which indicates the binder strain response to the applied stress levels. Higher values of J_{nr} are indicative of greater susceptibility to plastic deformation and therefore lower rutting resistance. Percent recovery ($\%R$) is also obtained from MSCR and indicates the percent of strain that is recovered at each stress level. Thus, percent recovery can be used to confirm the presence of polymer modifiers (Salim et al., 2019).

The AASHTO M332 binder specification was developed using Results from the MSCR test, which provided an alternative to M320 for high temperature performance grading. The values of J_{nr} define traffic

levels for binder selection. Lower values of J_{nr} indicate higher rutting resistance and more demanding applications. The categories, in order of decreasing J_{nr}, and therefore increasing rutting resistance are "S" for standard traffic, "H" for heavy, "V" for very heavy and "E" for extremely heavy.

2.5.3 Linear Amplitude Sweep Test

An accurate fatigue characterization of asphalt binders is required to adequately predict the cracking performance of flexible pavements (Hajj & Bhasin, 2018; Safaei & Castorena, 2016). Limitations to the current Superpave fatigue parameter led to the development of the LAS test, which progressively induces damage on binder samples (Hajj & Bhasin, 2018; Hintz et al., 2011). The LAS test measures fatigue resistance based on the concept of damage propagation, given by the loss of material integrity under repeated loading. Thus, the LAS test subjects asphalt samples to oscillatory loading in the DSR at progressively increasing amplitudes that lead to the initiation and propagation of microcracks. These microcracks result in binder fatigue failure, which can be seen as a reduction in stress response in Figure 17 (D. A. Anderson et al., 2001; Y. Kim, Lee, & Little, 2006).

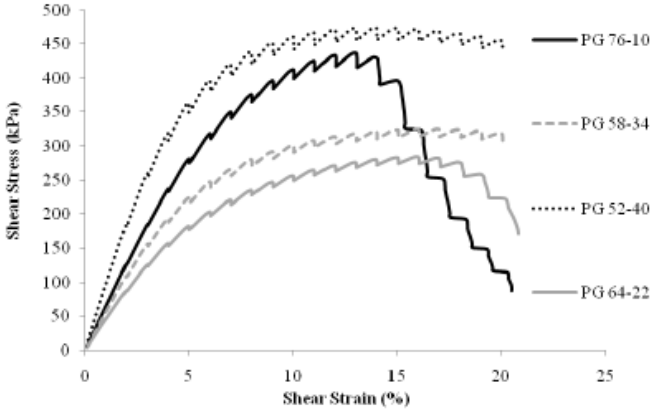

Figure 17. Stress vs. strain output from LAS Test (Hintz, Velasquez, Johnson, & Bahia, 2011)

The LAS test, detailed in AASHTO T391, characterizes binder failure based on Simplified Viscoelastic Continuum Damage (S-VECD) Theory. Following this theory, binder viscoelastic properties G^* and δ are correlated to damage intensity (D) following a linear power law shown in Equation 3 (Hintz et al., 2011).

Equation 3. Damage evolution power law

$$|G^*| \sin \delta = C_0 - C_1(D)^{C_2}$$

The undamaged properties and the model fitting parameters $C_0, C_1,$ and C_2 are obtained from the LAS test output. Failure is defined as the damage intensity to cause a 35% reduction in the initial integrity of the material given by $|G^*| \sin \delta$, which provides a parameter defined as A_{35}. An initial frequency sweep at 0.1% strain levels provides the B parameter which relates to the damage accumulation properties of the binder. This way, A and B define a linear relationship between strain levels and number of cycles to failure (N_f) to represent fatigue life of binders as shown by Figure 18 (Hintz et al., 2011; R. Zhang et al., 2020).

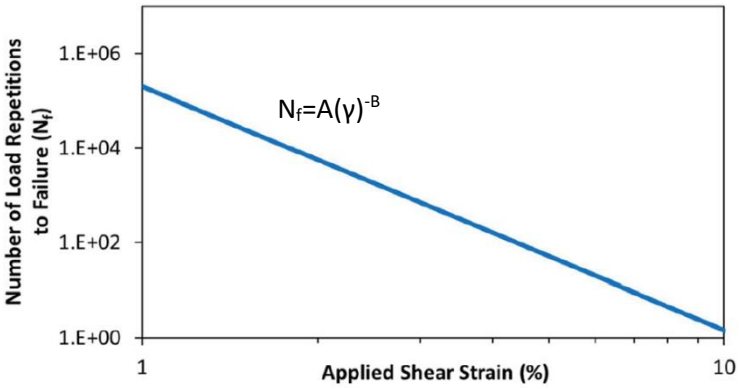

Figure 18. Typical Nf-strain plot from LAS test (R. Zhang, Sias, & Dave, 2020)

The LAS test results have shown good agreement with field cracking performance (Hintz et al., 2011) and good correlations with binder ductility and the Glover-Rowe parameter, also predictors of cracking at intermediate temperatures (Moraes & Bahia, 2018). Additionally, fatigue resistance of polymer modified binders has been successfully captured with this test, with increasing polymer contents leading to higher cycles to failure (Aurilio, Tavassoti, Elwardany, & Baaj, 2021; Aurilio et al., 2020).

However, certain concerns still exist with the use of this test. Test temperature selection can lead to confounding results, as binders may fail due to viscous flow instead of microcracking (from excessive temperatures) or debond from DSR plates if temperatures are too low. Thus, research by Castorena et al. suggested that test temperatures should be such that the linear viscoelastic modulus G^* remained roughly between 12 and 60 MPa (D. A. Anderson et al., 2001; Aurilio et al., 2021; Safaei & Castorena, 2016).

Additionally, the LAS parameters A and B can fail to account for binder aging or the presence of polymer modifiers (García Mainieri, Singhvi, Ozer, Sharma, & Al-Qadi, 2021; C. Wang, Castorena, Zhang, & Richard Kim, 2015; R. Zhang et al., 2020). As a result, alternative failure criteria have been proposed, such as a 50% reduction in initial integrity instead of the current 35% (Aurilio et al., 2020). Kim et al. studied pseudo strain energy as a potential indicator of material failure. As strain levels in LAS increase, materials deviate from the linear viscoelastic behavior, and this difference can be observed through the release of Pseudo Strain Energy. The difference between total Pseudo Strain Energy and what is released is defined as the stored PSE. While released PSE continuously increases, stored PSE presents a peak after which it starts to drop. Thus, the material loses its ability to store energy and has therefore failed. This failure criterion is independent of any non-linearity in materials and can therefore capture the effects of modification, so it is considered a more reliable failure point (C. Wang et al., 2015). Additionally, Zhang et al. defined strain tolerance as the strain level for a 25% reduction in peak stress and Strain Energy tolerance (E_f) (i.e., the area under the curve up to this point) as alternative fatigue parameters. Both parameters improved fatigue characterization with respect to the fatigue parameters *A* and *B*, capturing the effects of aging as well as aging gradients from field cores. As an example, Figure 19 shows inconsistent trends between A and increasing aging levels or pavement depths, while E_f decreases with aging levels, consistently with increasing laboratory aging durations as well as field gradients (R. Zhang et al., 2020).

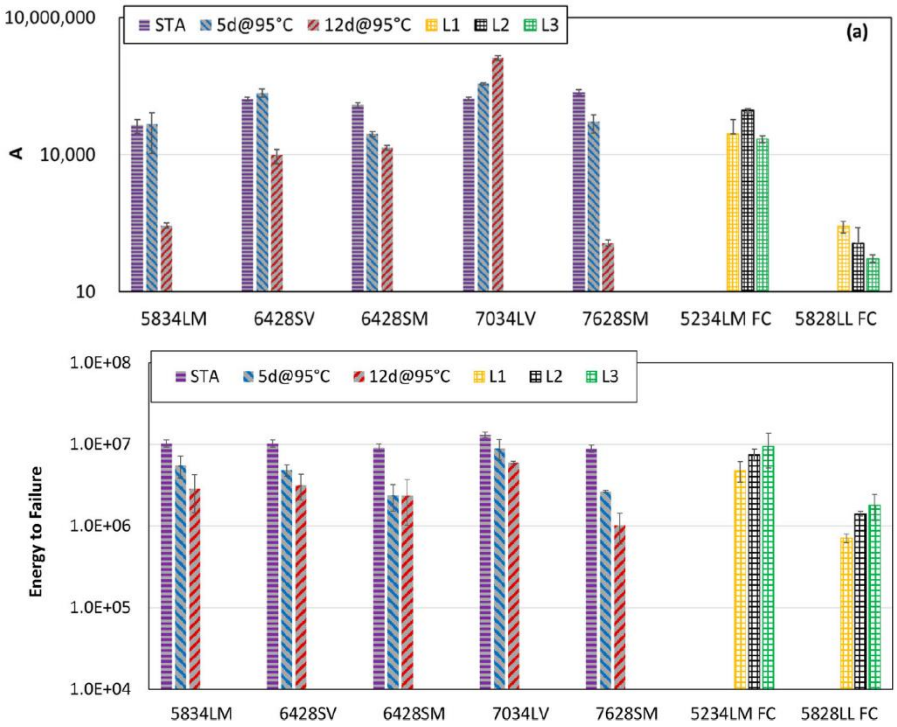

Figure 19. Comparison between current LAS A parameter and alternative Ef (R. Zhang et al., 2020)

Despite the wide acceptance of the LAS test to characterize binder fatigue performance, multiple approaches are still being evaluated to analyze the test output and develop indices that capture the effects of binder type, modification, and aging level on cracking resistance of binders.

2.5.4 Asphalt Master Curve Construction

Another way to evaluate rheological properties of binders is through the use of master curves. The main advantage of this approach is that viscoelastic properties can be studied at a wide range of temperatures that are observable in the field but challenging to replicate through laboratory testing. The governing principle behind master curve analysis is the time-temperature superposition principle (TTSP), which is valid for thermo-rheologically simple materials such as binders at small strain levels (Andriescu & Hesp, 2009; Asgharzadeh, Tabatabaee, Naderi, & Partl, 2015). Based on TTSP, the effects of temperature and time (i.e., frequency) are interchangeable, so stress-strain measurements for a given condition can be shifted to predict the binder behavior in a different scenario.

Master curves are typically developed for viscoelastic parameters, including complex modulus and phase angle. To this end, DSR stress-strain measurements are conducted for a selected range of frequencies and at multiple temperatures (typically in 10℃ increments). Using TTSP, shift functions, such as Arrhenius or Williams-Landel-Ferry, are used to shift data at multiple temperatures to a selected reference temperature. Then, multiple models can be used to fit the measured data and obtain a smooth curve to describe binder properties. A universal model has not been found, and researchers have developed rheological element models such as the Maxwell model or mathematical models like the widely used Christensen-Anderson model (Asgharzadeh et al., 2015; Bahia et al., 2001). Appropriate models can be selected based on binder

type, as some may not accurately fit certain properties of modified binders such as phase angle (Asgharzadeh et al., 2015).

2.5.5 Glover-Rowe Parameter and Black Space Diagram

The Glover-Rowe (G-R) parameter was developed from the Glover parameter that related binder ductility with cracking performance (R. M. Anderson, King, Hanson, & Blankenship, 2011). In his work, Rowe simplified the Glover parameter using the AASHTO M320 specification parameters G^* and δ, as shown in Equation 4.

Equation 4. Glover parameter and Glover-Rowe simplification

$$\frac{G'}{\left(\eta'/_{G'}\right)} = G^* \times \frac{(\cos\delta)^2}{\sin\delta}$$

It was found that binders with ductility values approaching 5 cm would be at risk of cracking, and cracking would be observed for the binders with ductility values close to 3 cm (R. M. Anderson et al., 2011). These thresholds were used to determine a damage zone for cracking in asphalt pavements by Glover and later by Rowe. The onset of cracking would therefore occur for binders with G-R values above 180 kPa, while surface cracking would be visible for binders with G-R values above 450 kPa (King et al., 2012).

Additionally, plots of complex modulus (G^*) in logarithmic scale against phase angle (δ), known as Black Space diagrams, have been used to plot the G-R damage zone and evaluate the cracking resistance of binders (King et al., 2012; G. M. Rowe & Sharrock, 2016). Black Space diagrams and the Glover Rowe parameter have been used as a ranking tool for binder cracking performance, showing good agreement with field observations, as shown for field core data in Figure 20. Reduced cracking performance is shown for RAP mixtures, and the G-R values for the older field cores fall within the damage region, consistent with the observed field cracking performance (Mensching et al., 2015).

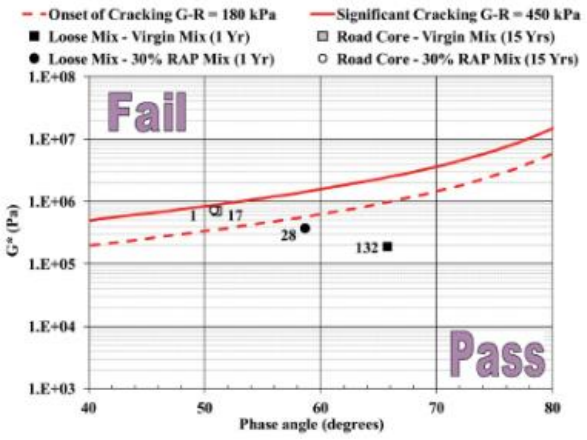

Figure 20. Laboratory and field performance relative to Glover-Rowe damage zone (Mensching, Rowe, Daniel, & Bennert, 2015)

Additionally, plots on Black Space can be used to track the effects of oxidative aging on binders (Elwardany, King, et al., 2020; King et al., 2012; Mensching et al., 2015; G. M. Rowe & Sharrock, 2016). The hardening and embrittlement caused by oxidation can be observed as binders migrate from bottom

right locations to the top left portion of the diagram, due to their higher complex modulus and lower phase angle. Aging susceptibility of binders can also be evaluated based on the length of the path followed in the Black Space Diagram for increasing aging durations. Figure 21, from a study by King, shows the locations in Black Space Diagram for three binders (West Texas, Gulf Southeast and West Canadian) after multiple aging durations. While the Gulf Southeast binder has an equal final location to the West Canadian (i.e., comparable cracking resistance), the West Canadian has a considerably longer path with aging, indicating a greater aging susceptibility. Thus, cracking performance is dictated not only by the aging susceptibility of binders but also by their unaged properties.

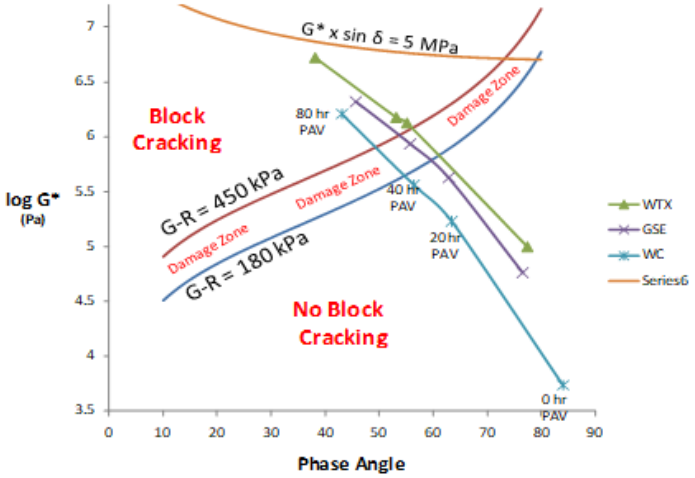

Figure 21. Changes in binder properties with PAV aging on Black Space diagram (King, Anderson, Hanson, & Blankenship, 2012)

Despite its widespread use, the Glover-Rowe parameter and the damage thresholds have certain limitations for the fatigue characterization of polymer modified binders (Aurilio et al., 2021; Morian et al., 2015; G. M. Rowe & Sharrock, 2016). SBS typically results in lower phase angles which may not be accompanied by changes in complex modulus. Their overall location in Black Space may suggest reduced cracking resistance, but this is not the case in the field (Aurilio et al., 2020). Additionally, the damage zone was defined and validated based on ductility for unmodified binders, so it may need to be redefined for polymer modified binders (G. M. Rowe & Sharrock, 2016).

2.5.6 Extended BBR Test

BBR testing for low temperature properties is used to evaluate binders at the expected minimum temperature at the pavement surface (plus 10℃), after subjecting samples to a one-hour conditioning period (Officials, 2016). However, the isothermal conditioning of binders at low temperatures for longer time periods causes a stiffening effect known as physical hardening, which can increase binder thermal cracking susceptibility (D. A. Anderson & Marasteanu, 1999; J. C. Petersen, Robertson, R.E, Branthaver, J.F., Harnsberger, P.M, Duvall, J.J., Kim, S.S., Anderson, D.A, Christiansen, D.W., Bahia, U.H. , 1994).

Field performance of trial sections in Northern Ontario, Canada (Hesp, Genin, Scafe, Shurvell, & Subramani, 2009) showed early cracking distresses despite meeting the low PG requirements established in AASHTO M320. It was hypothesized that during the weeks or months between construction and the occurrence of the coldest temperatures, binders develop molecular structuring that diminishes its ability to relax under thermal stresses, leading to early thermal cracks (Hassan Ali Tabatabaee, 2012). This was

supported by other studies that showed increasing levels of thermal cracking in binders despite little increase in low temperature stiffness over five years of service (Deme, 1987).

As a result, the extended BBR test was developed to study thermal cracking resistance over prolonged conditioning times. This test would replicate service conditions more realistically to evaluate the effects of physical hardening (Hesp et al., 2009). Extended BBR test is standardized in AASHTO TP122 (Officials, 2020), and some local agencies have developed their own methodology following similar principles (Transportation, 2011). The test is conducted on PAV aged binders using similar equipment and beam geometry as the BBR test per AASHTO T 313. Testing is done at the low PG +10℃ and low PG +20℃, after conditioning times of 1, 24 and 72 hours, which provides several physical hardening rates (J. C. Petersen, Robertson, R.E, Branthaver, J.F., Harnsberger, P.M, Duvall, J.J., Kim, S.S., Anderson, D.A, Christiansen, D.W., Bahia, U.H. , 1994). The low temperature limiting grade (LTLG) from extended BBR is determined as the warmest out of every temperature and conditioning time combination. Finally, the grade loss is determined as the difference between the low temperature true grade from BBR testing (per AASHTO T313) and LTLG.

Extended BBR testing has been useful to account for shortcomings on low temperature grading from AASHTO M320, where 1-hour conditioning was found to overestimate thermal cracking resistance of test sections (Bricker & Hesp, 2013; Hesp et al., 2009). Overall, binders with a higher grade loss due to isothermal conditioning showed poorer cracking performance in the field, and this was better captured through AASHTO TP122 testing temperatures and durations.

2.5.6.1 Physical Hardening and Glass Transition Temperature

As previously stated, thermal cracking resistance of binders can diminish due to physical hardening. Isothermal conditioning of binders at low temperatures can cause an increase in stiffness and a loss in relaxation properties which leads to early onset of surface distresses like thermal cracking (D. A. Anderson & Marasteanu, 1999; Bricker & Hesp, 2013; J. C. Petersen, Robertson, R.E, Branthaver, J.F., Harnsberger, P.M, Duvall, J.J., Kim, S.S., Anderson, D.A, Christiansen, D.W., Bahia, U.H. , 1994).

The phenomenon of physical hardening can be explained based on reductions in free volume. As binders cool down, molecular mobility and free volume decrease simultaneously. When cooling occurs at temperatures within the Newtonian flow region, these changes happen almost instantaneously. However, as temperature is further decreased, molecular mobility is so low that volume changes become time dependent. This reduction in free volume progressively increases molecular structuring, which leads to the stiffening effect defined as physical hardening. Additionally, crystallization of waxy fractions present in the binder also contribute to physical hardening. Therefore, this phenomenon is closely related to asphalt chemical composition (D. A. Anderson & Marasteanu, 1999; Bricker & Hesp, 2013; Huynh, Khong, Malhotra, & Blanchard, 1978; J. C. Petersen, Robertson, R.E, Branthaver, J.F., Harnsberger, P.M, Duvall, J.J., Kim, S.S., Anderson, D.A, Christiansen, D.W., Bahia, U.H. , 1994; Hassan Ali Tabatabaee, 2012).

As cooling progresses, a collapse in free volume slows down to negligible rates due to a significant loss of molecular mobility. The temperature at which this occurs has been defined for amorphous materials as Glass Transition Temperature (T_g) (Hassan Ali Tabatabaee, 2012), and it represents the transition from a rubbery to a glassy, brittle state. However, due to the multiple fractions present in the binder, the glass transition results in an overlap of several transitions and occurs over a range of temperatures (D. A. Anderson & Marasteanu, 1999). The collapse in free volume that characterizes the glass transition can be detected as a drop in heat capacity of the material, which is the principle behind some of the testing used to determine glass transition temperatures in binders (Bricker & Hesp, 2013).

Research by Anderson and Marasteanu indicated that, as opposed to amorphous materials such as polymers, physical hardening in asphalts occurs at temperatures above and below T_g. Their findings also showed that, in some cases, glass transition temperatures can be close to low critical temperatures as determined by Superpave PG grading (D. A. Anderson & Marasteanu, 1999). Therefore, the need to measure binder T_g to evaluate the effects of physical hardening becomes significant for a comprehensive characterization of binder durability.

2.6 Chemical characterization of asphalt binders

2.6.1 Fourier Transformed Infrared Spectroscopy

Infrared spectroscopy is based on the incidence of infrared radiation on a sample, which will absorb certain wavelengths that cause vibrations or rotations of atoms at the molecular level. The remaining incident energy will be reflected by the material surface. The different molecular components present in the sample will absorb energy at different frequencies, based on the energy required to cause atom excitation. These frequencies represent peaks in the absorption spectrum of each sample, providing a unique chemical fingerprint of the material (Ren et al., 2019; Zhu, 2015). Therefore, Fourier Transformed Infrared (FTIR) Spectroscopy can be a very powerful tool for chemical characterization of materials.

Although FTIR has been extensively used for chemical analysis of multiple materials, researchers have encountered challenges with this technique for analysis of asphalt due to its dark color and consistency at room temperature which affected sample preparation (Glover, Davison, Ghoreishi, Jemison, & Bullin, 1989). The preferred technique for asphalt analysis using FTIR is Attenuated Total Reflectance (ATR) in which radiation passes through a crystal with a high refractive index, known as diamond, and reflected light is attenuated due to absorption within the sample, which is placed in tight contact with the diamond. The main benefits of using FTIR-ATR for asphalt analysis mainly come from a faster and easier sample preparation as well as high reproducibility across samples (Ren et al., 2019).

FTIR-ATR has been widely used by researchers to study the chemical composition of asphalt across multiple sources and to detect the presence of modifiers such as SBS, PPA or EVA (Ren et al., 2019; Zhu, 2015). Additionally, the chemical changes caused by oxidative aging can be tracked using the FTIR, by looking at the absorbance peaks generated by the main oxidation products of ketones, sulfoxides and carboxylic acids (J.C. Petersen, 2009; Tauste et al., 2018). Typically, aging of asphalt binders is evaluated through the changes in the carbonyl functional group (C=O bond present in ketones, carboxylic and dicarboxylic acids) at a frequency of 1700 cm^{-1} and the sulfoxide functional group (S=O bond) at 1030 cm^{-1} (Lu & Isacsson, 2002; Morian et al., 2015; Qin et al., 2014; Tauste et al., 2018), as shown in Figure 22.

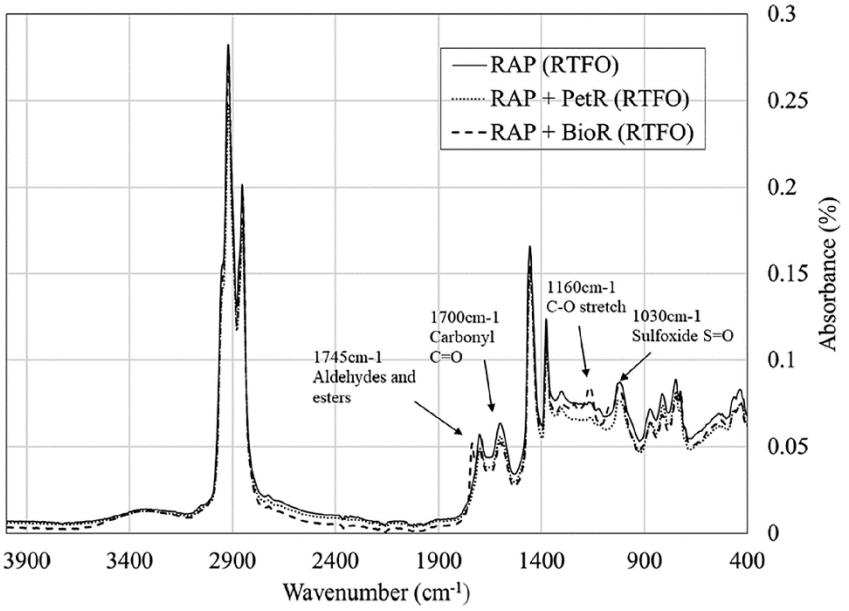

Figure 22. Use of FTIR spectra to evaluate the changes in oxidation products for aged and rejuvenated binders (Elkashef et al., 2020)

Additionally, SBS modifiers would be identified from a peak at 985 cm^{-1} which represents the butadiene double bond (Tauste et al., 2018). By looking at this peak, researchers have studied the effects of aging on SBS modified binders, and have been able to explore polymer degradation as a result of oxidation (Habbouche et al., 2021; Wu et al., 2009). Other modified binders such as epoxy asphalt have also been successfully characterized after aging (Apostolidis et al., 2020). The rejuvenating effects of soybean-based bio-oils and other petroleum-based rejuvenators have also been evaluated by tracking the changes in carbonyl and sulfoxide peaks, either by evaluating the changes in peak intensity or in the areas under a certain region surrounding the peak (Elkashef et al., 2020; Santos et al., 2021; Yin et al., 2017). Finally, the FTIR analysis allows researchers to evaluate the effects of aging on rheological parameters related to binder performance based on the correlations between carbonyl and sulfoxide peaks and master curve parameters such as Glover-Rowe parameter, low shear viscosity or R value (Habbouche et al., 2021; Morian et al., 2015).

2.6.2 SARA Fractionation

Binder composition is based on four fractions defined as saturates (S), asphaltenes (A), resins (R), and aromatics (A), known as SARA (J.C. Petersen, 2009). Each fraction has distinct properties of polarity, solubility, and molecular weight, dictating binder rheological properties. Additionally, the relative content of each fraction determines binder dispersion, affecting its aging susceptibility (Lesueur, 2009; J.C. Petersen, 2009). Typically, saturates make up between 5 and 20% of asphalt composition and are mostly inert (J.C. Petersen, 2009; Weigel & Stephan, 2017). Aromatics make up between 30 and 65% of binder and, with saturates, constitute the lighter fraction of binder, with a molecular weight between 570 and 980 g/mol (Weigel & Stephan, 2017). The resin content ranges between 30 and 45%, with a molecular weight that can vary between 780 and 1400 g/mol (Weigel & Stephan, 2017). Finally, the asphaltene fraction makes up between 5 and 25% of binder, and are large, polar molecules with weights ranging from 400 to 7000 g/mol, depending on the method used (Lesueur, 2009; Weigel & Stephan, 2017).

Separation of the four fractions is based on polarity and solubility with different hydrocarbons. Typically, asphaltenes are the first to be removed using n-heptane (Materials, 2017, 2018). Because asphaltenes are insoluble in n-heptane, when an asphalt sample is diluted in this solvent, asphaltenes will precipitate. After heating under reflux or by filtration techniques, the asphaltene content is determined gravimetrically.

After asphaltenes have been extracted, maltenes, which are soluble in n-heptane (Weigel & Stephan, 2017), are subsequently separated into resins, saturates and aromatics. One technique for separation is the chromatographic column using alumina, with n-heptane, toluene and a methanol:toluene blend as solvents to separate saturates and aromatics right afterwards. Finally, resins can be separated using trichloroethylene (Lesueur, 2009). Another common procedure involves thin layer chromatography using silica gel, followed by an ionization technique, known as Iatroscan, standardized in ASTM D6560 (Lesueur, 2009; Materials, 2018). Separation of saturates aromatics and resins is conducted in that order and several hydrocarbons can be used as solvents. One common setup uses n-heptane for saturates, followed by a blend of n-heptane and methanol for aromatics and finally a methylenedichloride:methanol blend for resins (Lesueur, 2009). It has been reported that the relative content of each fraction may be sensitive to the nature of each solvent used, therefore a detailed description of the experimental setup should be provided before any comparison across binders can be made (Lesueur, 2009).

SARA fractionation has extensively been used to determine how binder chemistry changes due to mechanisms like aging and rejuvenation (Elkashef et al., 2020; J.C. Petersen, 2009; Qin et al., 2014; Hassan A. Tabatabaee & Kurth, 2017; H. Wang et al., 2020). For example, Figure 23 illustrates the typical variation in SARA fractions with aging: an overall increase in asphaltenes with a reduction in aromatics, which convert to resins and then to asphaltenes (Mirwald et al., 2020).

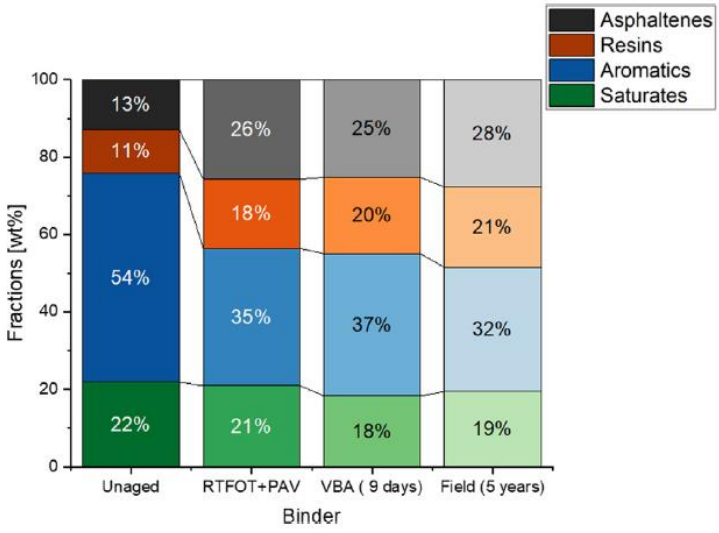

Figure 23. Measured changes in SARA fractions for multiple aging durations (Mirwald et al., 2020)

2.6.3 Differential Scanning Calorimetry

Differential Scanning Calorimetry (DSC) is a chemical analytical tool that subjects materials to linear heating and cooling rates and provides information on binder morphology and thermodynamic properties (Bricker & Hesp, 2013; Lesueur, 2009). As asphalt binders experience consecutive heating and cooling cycles, they undergo both reversible and irreversible thermodynamic processes. The first process is

associated with changes in heat capacity and correspond to glass transition of materials, where they go from a viscous, rubbery state to a glassy state, while the non-reversible events are caused by changes in latent heat and are related to phase transitions (Bricker & Hesp, 2013).

Glass transition of binders is caused by a loss in molecular mobility and a collapse in free volume, and it is typically accompanied by a substantial increase in stiffness and brittleness (Bricker & Hesp, 2013; Memon & Chollar, 1997). It can be identified by changes in heat capacity with respect to temperature obtained as outputs from the DSC test (D. A. Anderson & Marasteanu, 1999; Bricker & Hesp, 2013). However, the multiple phases present in binders cause the glass transition to occur over a range of temperatures corresponding to the overlap of multiple glass transition phenomena (Elkashef et al., 2020; Huynh et al., 1978). Therefore, DSC changes in heat capacity define multiple temperatures that will be of interest, as shown in Figure 24.

The glass transition region is defined by fitting two tangents to the curve, which define the boundaries to the glassy and amorphous phases. Thus, the transition begins at an onset temperature $T_g(Onset)$ as binders start to shift to a more viscous behavior and ends at the end-point temperature $T_g(End)$. The difference between these two temperatures is defined as the glass transition width $T_g(Width)$. Within the glass transition region, the most frequently studied temperatures include (a) the temperature at the inflection point of the reversed heat capacity curve $T_g(I)$, and (b) the temperature calculated at the half-height between the glassy and amorphous phase $T_g(H)$ (Bricker & Hesp, 2013; Elkashef et al., 2020).

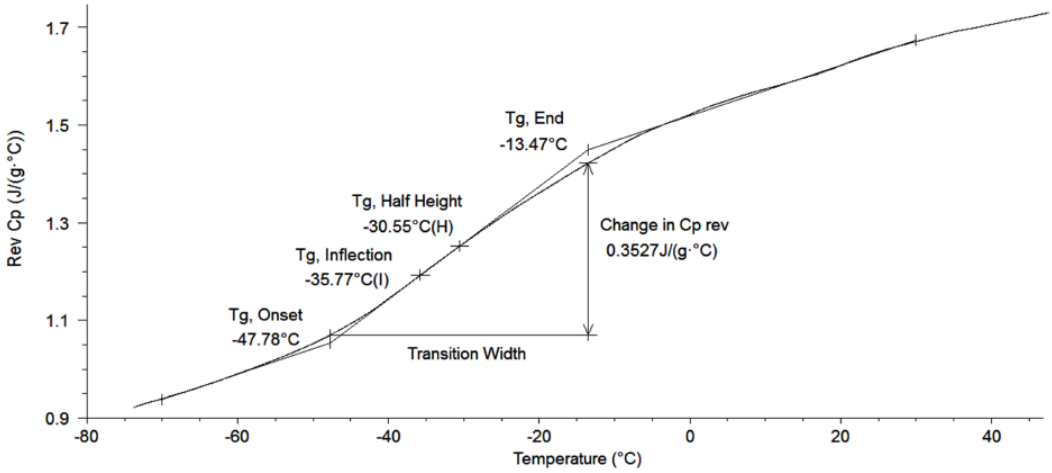

Figure 24. Glass transition region and relevant temperatures from DSC reversed heat capacity output (Bricker & Hesp, 2013)

Glass transition temperatures obtained from DSC have been related to flow properties as well as low temperature performance of binders. For unmodified binders, very strong correlations have been found between $T_g(I)$ and $T_g(H)$ and creep stiffness (S) and m-value (Memon & Chollar, 1997), as well as with Fraas breaking point, where the binder begins to exhibit brittle behavior in a failure test at low temperatures (Elkashef et al., 2020).

Finally, aging of binders will shift T_g to slightly higher values (Hassan A. Tabatabaee & Kurth, 2017; Tauste et al., 2018), caused mostly by higher asphaltene contents and greater molecular structuring, which will contribute to a more brittle, glassy behavior (Huynh et al., 1978). For this reason, changes in glass transition temperatures have been studied after certain rejuvenation processes. Some rejuvenators successfully shift

T_g to lower values, as can be observed in Figure 25, mitigating binder embrittlement and improving low temperature performance after aging (Elkashef et al., 2020; Hassan A. Tabatabaee & Kurth, 2017).

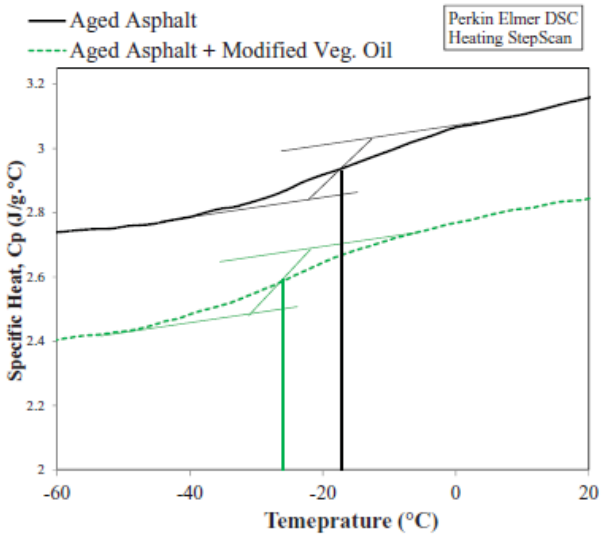

Figure 25. Glass transition temperature from heat capacity plots, for aged and rejuvenated binders (Hassan A. Tabatabaee & Kurth, 2017)

2.6.4 Gel Permeation Chromatography

Gel permeation chromatography (GPC) is a chemical analytical technique used to characterize asphalt molecular composition in terms of molecular size. Asphalt molecules have typically been classified into large molecular size (LMS) components, medium molecular size (MMS) and small molecular size (SMS) components (Noureldin & Wood, 1989; Wahhab et al., 1999), and their relative occurrence can be determined based on the chromatograph resulting from GPC.

More specifically, the technique can be described as a high-pressure liquid chromatography in the gel permeation mode (K. W. Kim & Burati Jr, 1993; Wahhab et al., 1999). An asphalt sample is diluted in a hydrocarbon solvent at a specific concentration. It is filtered for purity and then injected into the GPC system, which consists of multiple silica gel columns through which the sample flows at a controlled rate. As test configurations vary across the literature, multiple flow rates have been used by researchers, 2mL/min (Noureldin & Wood, 1989), 1.0 mL/min (K. W. Kim & Burati Jr, 1993; Lu & Isacsson, 2002), and even 1.0 μL/min (Wahhab et al., 1999), depending on the injected sample size. The porous silica gel medium causes larger molecules to flow first, followed by progressively smaller molecules that are retained in the columns for longer times. The columns are connected to a detector which continuously weighs the amount of passing molecules as a function of time (Noureldin & Wood, 1989). The test output will consist of a chromatogram showing the relative amount of each particle size as a function of time and can be interpreted as the Molecular Size Distribution (MSD) of asphalt.

The total area under the chromatogram represents the relative number of molecules present in the asphalt sample. The analysis of MSD can then be conducted by subdividing the chromatogram into multiple regions (Isacsson & Zeng, 1997; Wahhab et al., 1999). Typically, a division at two elution times is done so that three regions are obtained: 25%, 50% and 75% of total area, which can be related to LMS, MMS and SMS in asphalts as given by Figure 26 (Noureldin & Wood, 1989).

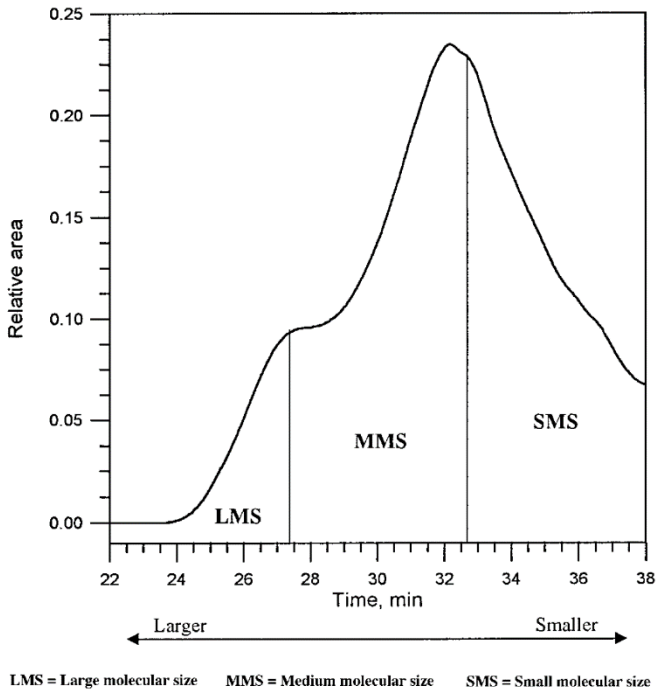

Figure 26. GPC chromatogram showing three elution time distribution and molecular sizes (Wahhab, Asi, Ali, & Al-Dubabi, 1999)

The relative presence of LMS, MMS and SMS can be related to binder source and rheological properties (K. W. Kim & Burati Jr, 1993). By studying GPC and SARA fractions, Isacsson found that LMS components are mostly made up of asphaltenes and resins, which according to Petersen are mostly responsible for asphalt stiffness (Isacsson & Zeng, 1997; J.C. Petersen, 2009). In this regard, Kim et al. found that higher LMS contents would result in higher absolute and kinematic viscosity. Isacsson also found the relationship between binder stiffness and LMS, with higher contents of LMS resulting in higher fracture temperatures and lower cracking resistance (Isacsson & Zeng, 1997).

Given the relationship between molecular size distribution and rheological properties, GPC has been successfully used to track the effect of aging on binders from multiple sources (Isacsson & Zeng, 1997; Lu & Isacsson, 2002; Noureldin & Wood, 1989; Wahhab et al., 1999). During aging, aromatic components are converted to resins and then to asphaltenes, resulting in an increase in LMS content at the expense of MMS and SMS contents (Isacsson & Zeng, 1997; Lu & Isacsson, 2002). In addition to the increased content of asphaltenes, their molecular associations and cluster formation after aging also contributes to the increase in LMS, which progresses with aging duration (K. W. Kim & Burati Jr, 1993; Lu & Isacsson, 2002).

Binder modification can also be identified through GPC. SBS polymer was found to cause an increase in LMS and subsequent reduction in SMS, shifting the chromatogram to the left (Wahhab et al., 1999). The effects of rejuvenation have also been studied by conducting GPC on rejuvenated binders before and after laboratory aging cycles. MSD of unaged and rejuvenated binders showed that although rheological properties were successfully restored to the unaged condition, the particle size distribution did not match that of the original binder, and these offsets were larger for greater aging durations. Although GPC was proposed as an approach for selecting the type and dosage of rejuvenators, it remained unclear whether targeting rheological properties or MSD would yield better pavement performance (K. W. Kim & Burati Jr, 1993).

CHAPTER 3 - MATERIALS AND METHODS

3.1. Selection of Two Base Binders

Six straight run asphalt binders from different crude oil sources were evaluated as potential base binders for the study. TABLE 1 shows the performance grade and origin of each candidate binder, as provided by the respective suppliers. Coming from various sources, these binders presented diverse chemical composition and aging susceptibility. Therefore, two base binders were selected for the study based on (a) adequate compatibility with the proposed modifiers (evaluated by manufacturers) and (b) distinctly different aging susceptibility, shown by rheological properties.

TABLE 1. Performance Grade and Origin of Six Candidate Base Binders

Binder ID	Binder 1	Binder 2	Binder 3	Binder 4	Binder 5	Binder 6
PG	64-16	58-22	67-22	64-22	64-22	64-22
Origin	South Central, US	California Valley, US	Southeast, US	California Coastal, US	West Canadian	Midwest, US

The rheological properties of the six binders were evaluated before and after oxidative aging according to the testing plan presented in TABLE 2. The complete rheological evaluation of the six binders will be detailed in Section 4.1.

TABLE 2. Rheological Testing Plan for Candidate Base Binders

Rheological Evaluation	**Test**	**Standards**	**Research Parameter**	**Aging Level**
High temperature performance	DSR	AASHTO M320 AASHTO T315	$G^*/\sin\delta$	Unaged RTFO RTFO + 20hours PAV RTFO + 60hours PAV
Intermediate temperature performance	DSR	AASHTO M320 AASHTO T315	$G^*\sin\delta$	RTFO + 20hours PAV RTFO + 60hours PAV
Low temperature performance	BBR	AASHTO M320 AASHTO T313	Stiffness, m-value, ΔT_C	RTFO + 20hours PAV RTFO + 60hours PAV

Based on the results to be presented in detail in Section 4.1, Binders 1 and 5 exhibited similar rheological behavior prior to oxidative aging; however, they showed different properties after oxidative aging. Binder 1 was among the most susceptible to aging, while Binder 5 was one of the most resistant to oxidation, which combined represent a broad range of aging effects on binder properties. Based on this distinctly different aging behavior, in addition to the confirmation from the industry partners for this study that there were no incompatibility concerns, Binders 1 and 5 were selected for modification with the proposed aging resistent technologies.

3.2. Reclaimed Asphalt Pavement (RAP)

One source of RAP was sampled from an asphalt plant in Opelika, Alabama for use in this study. The RAP binder was extracted per ASTM D2172 (method A) using toluene as the solvent and then recovered per ASTM D5404 using a rotary evaporator with a nitrogen blanket pumped over the binder to avoid further oxidation. The recovered RAP binder was then graded in accordance with AASHTO M320, and the results are summarized in TABLE *3*. The recovered RAP binder was subsequently blended with Binders 1 and 5 at 20% per weight of the total binder (hereafter referred to as 20% RAP Blends for Binders 1 and 5) to represent the blended binder in an asphalt mixture with 20% RAP binder replacement (assuming 100% RAP binder contribution) for mixture performance evaluation. The mixture performance evaluation is outside the scope of this thesis.

TABLE 3. Performance Grade of RAP Binder

Binder ID	T_{cont} High Original	T_{cont} High RTFO	T_{cont} Intermediate 20 hr PAV	T_{cont} Low, S 20 hr PAV	T_{cont} Low, m-value 20 hr PAV	ΔT_c	PG HT	PG LT
RAP Binder	107.4 ℃	107.7 ℃	40.0 ℃	-17.1 ℃	-8.5 ℃	-8.6 ℃	106	-4

3.3. Aging resistant technologies

Five aging resistant technologies were evaluated, and a brief description of each is provided below.

- Product 1: Proprietary blend of biosynthetic oils, petroleum-based oils, and rheology modifiers.
- Product 2: Mixture of two reactive components that upon mixing and subsequent curing form a two-phase chemical system. At the dosage rates evaluated in this study the discontinuous phase is a three-dimensional low modulus epoxy polymer, and the continuous phase is a proprietary blend of asphalt and oil-based flexible modifiers. Undiluted blends (outside the scope of this work) present a phase inversion resulting in a continuous polymeric phase.
- Product 3: Sub-epoxidized soybean oil.
- Product 4: Hybrid anti-aging technology composed of a continuous phase styrenic block copolymer with a pine-based performance chemical additive.
- Product 5: Hybrid system composed of ground tire rubber (GTR) powder and Rheopave®. Rheopave® consists of three polymeric components: a functional elastomer, a stabilizer, and a dispersant. The elastomer is DuPont™ Elvaloy® Reactive Elastomeric Terpolymer (RET) resin.

For material testing and subsequent data analysis in this document, each product was randomly designated as Additive 1 through Additive 5. For this study, each additive was blended with Binder 1 and Binder 5 at an optimum dosage (OD) that was determined by the respective suppliers. In addition, Additives 2 through 5 were mixed with 20% RAP Blends of Binders 1 and 5 at the OD and at an alternative dosage (AD), which was also selected by the respective suppliers. Thus, a total of six modified binder blends were prepared for Additives 2 through 5, and four modified binder blends were prepared for Additive 1, as detailed in Figure 27.

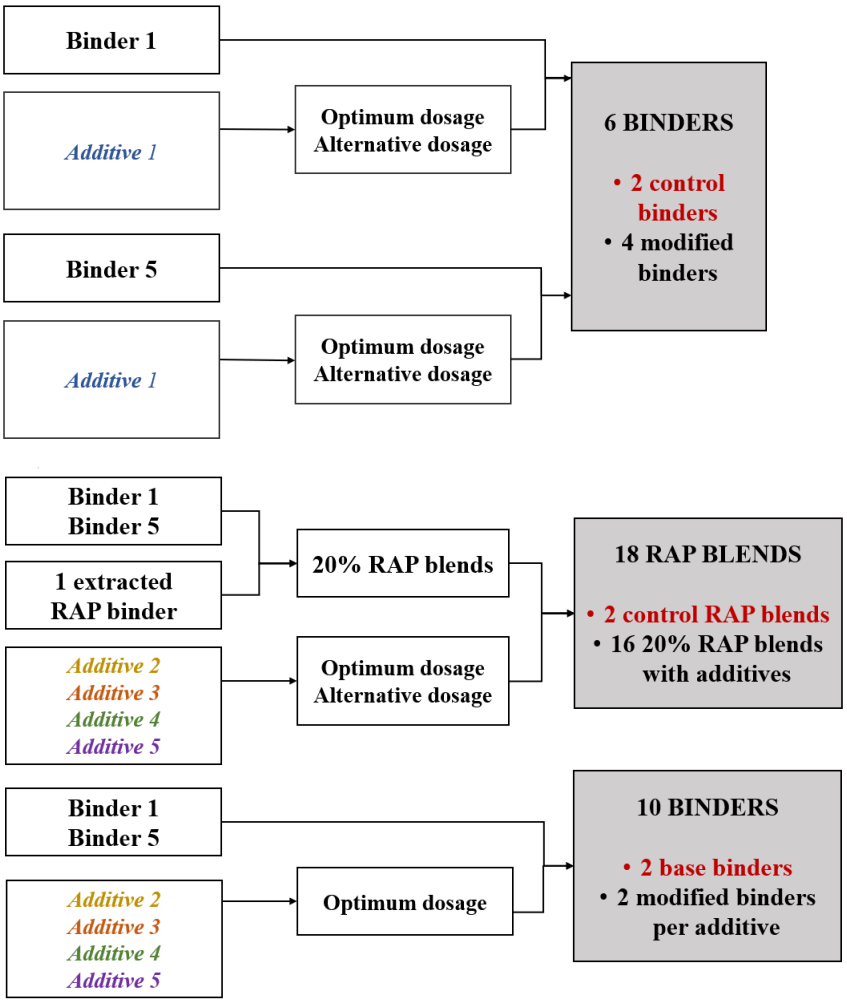

Figure 27. Plan for Preparing Test Binders and Modified Blends

3.3.1. Blending and Curing Binder Blends with Product 2

Product 2 is a two-part blend consisting of a resin (referred to as Part A) and an acid-base curing agent diluted in a soft asphalt binder (referred to as Part B). The dosage of Product 2 can be determined as shown in Equation 5. When mixed at dosages higher than 30%, a blend of Product 2 and a base binder might behave as a thermosetting material (Youtcheff et al., 2006). Since the conventional Superpave binder tests and aging protocols are not applicable to thermosetting materials, dosages of this modifier were selected below 30%. For Binder 1, dosage rates of 10% and 20% were selected while dosage rates of 10% and 15% were selected for Binder 5. At the selected dosages, blends of Product 2 and a base binder behave as conventional thermoplastic asphalt binders and thus, can be aged and tested following the Superpave binder specification.

Equation 5. Dosage Determination for Product 2

$$Dosage\ of\ Product\ 2 = \frac{Epoxy\ Resin + Curing\ Agent}{Epoxy\ Resin + Curing\ Agent + Asphalt\ Binder}$$

The preparation of each binder blend with Product 2 started with preheating the base binder and Part B for two hours at 150°C, and they were then blended in a low shear mixer for 15 minutes. Part A was preheated at the same temperature (i.e., 150°C) for 15 minutes, and manually blended with the blend of base binder and Part B for approximately 30 to 40 seconds using a stirring rod. TABLE 4 presents the blending proportions of the component materials at the two dosage rates (referred to as optimum dosage (OD) and alternative dosage (AD)).

TABLE 4. Blending Proportions of Component Materials for Binders Modified with Additive 1

Binder Identification	Dosage Rate	Proportions (% by weight)		
		Base Binder	Part A	Part B
Binder 1 Blend at OD	10%	75.00	4.84	20.16
Binder 1 Blend at AD	20%	50.00	9.69	40.31
Binder 5 Blend at OD	10%	75.00	4.84	20.16
Binder 5 Blend at AD	15%	62.50	7.26	30.24

The working mechanism of Product 2 is based on a cross-linking reaction, which typically requires an accelerated curing process at elevated temperature. Therefore, once blending was complete, the curing times of modified blends were determined through viscosity measurements following AASHTO T316. Viscosity tests were conducted using a Brookfield DVII+ rotational viscometer, at a selected curing temperature of 150 ℃. Spindle SC27 was used to allow for higher viscosity readings over time without exceeding the torque levels required in AASHTO T316. A binder sample of 10.5 grams was subjected to constant shear, and viscosity readings were taken every 25 minutes. When three consecutive readings were within the single-operator precision detailed in the standard they were considered as stable and the curing process was considered complete, thus defining the curing time for each sample, as shown in Figure 28.

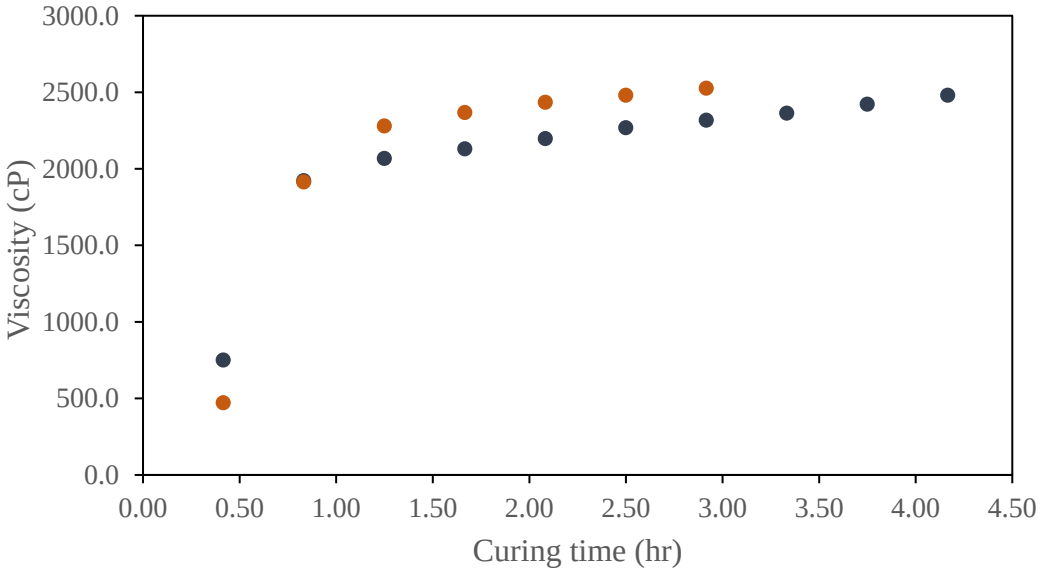

Figure 28. Curing behavior of Binder 5 modified at Optimum Dosage at 150 °C

3.4. Testing Plan

For this study, rheological and chemical testing was conducted on base and modified binders. Rheological properties of base and modified binders were characterized using DSR and BBR testing procedures. The detailed rheological testing plan and aging conditions are presented in TABLE 5.

The DSR was used to conduct the following tests:

- Superpave high- and intermediate-temperature Performance Grading
- Multiple Stress Creep Recovery (MSCR) test to evaluate the impact of the additives on the rutting resistance and elastic response of asphalt binders
- Temperature-Frequency Sweep test followed by master-curve generation, with subsequent calculation of the Glover-Rowe (G-R) parameter to evaluate ductility and block cracking potential
- Linear Amplitude Sweep (LAS) test to evaluate fatigue resistance.

Additionally, BBR was utilized to determine:

- Low-temperature performance grade
- ΔT_c parameter to assess stress relaxation properties
- Physical hardening behavior of the blended binders through Extended BBR at the glass transition temperature.

The chemical characterization provided a fundamental understanding of the effects of aging on binder chemical composition and how changes in chemistry resulted in changes in binder rheology. Chemical testing consisted of:

- Fourier Transformed Infrared Spectroscopy-Attenuated Total Reflection (FTIR-ATR)
- SARA fractions
- Gel Permeation Chromatography (GPC), and
- Differential Scanning Calorimetry (DSC)

The testing was conducted at NCAT and in other laboratories, as shown in TABLE 6. In addition, TABLE 6 provides information about aging conditions and materials included in the chemical testing plan.

TABLE 5. Complete Rheological Testing Plan

Temperature Range	Test	Standard	Aging Level
High Temperature evaluation	**DSR**	AASHTO T 315 AASHTO M 320	Unaged RTFO RTFO+20hPAV RTFO+60hPAV
	MSCR	AASHTO T350 AASHTO M 332	RTFO
Intermediate Temperature evaluation	**DSR**	AASHTO T 315 AASHTO M 320	RTFO+20hPAV RTFO+60hPAV
	LAS	AASHTO T 391	RTFO+60hPAV
	DSR Master curve	AASHTO T 315	Unaged RTFO+60hPAV
Low Temperature evaluation	**BBR**	AASHTO T 313	RTFO+20hPAV RTFO+60hPAV
	DSR	WRI Approach *(AASHTO Draft Specification)*	RTFO+20hPAV RTFO+60hPAV
	BBR	AASHTO TP 122 *(at Tg from DSC)*	RTFO+60hPAV

TABLE 6. Complete Chemical Testing Plan

Property	Test	Testing Laboratory	Aging Level	Analysis parameters	Tested materials
Oxidative Aging Products	FTIR-ATR	NCAT	Unaged RTFO+60h PAV	Carbonyl and Sulfoxide Groups	All binders, modified and unmodified
Molecular Size Distribution	Gel Permeation Chromatography	Kraton	Unaged RTFO+60h PAV	Molecular Weights	Samples without RAP
Thermal Behavior	Differential Scanning Calorimetry	Western Research Institute (WRI)	RTFO+60h PAV	Glass Transition (T_g) Temperature	Selected dosages from rheological findings, without RAP
Chemical Composition	SARA Fractionation	Kraton	Unaged RTFO+60h PAV	Colloidal Index, SARA Fractions	Base binders, Additives 2-5 without RAP

3.4.1. Laboratory aging protocols

For simulation of oxidative aging, the asphalt binders were first short-term aged in the Rolling Thin-Film Oven (RTFO, AASHTO T 240), followed by two separate protocols (i.e., 20 and 60 hours) in the Pressurized Aging Vessel (PAV, AASHTO R 28) for simulation of long-term aging.

a. Short-term aging

Each binder was subjected to RTFO aging conducted per AASHTO T240 to simulate binder properties after the short-term aging condition during mixing and placing operations. For this procedure, a sample of 135 ± 0.5 grams was placed in glass bottles that rotate horizontally on a vertical carriage inside the oven set at 163 ± 1.0°C, while being exposed to heated air at a rate of 4000 ± 100 mL/min for 85 minutes. RTFO residue was then recovered from the glass bottles for further rheological evaluation and subsequent aging procedures.

b. Long-term aging

To simulate the oxidative aging after prolonged periods in service, PAV aging was conducted on the RTFO residue per AASHTO R28. A sample of 50 ± 0.5 grams was placed in 140mm diameter metal pans and aged in the PAV at 100°C and under 2.10 ± 0.1 MPa. The test temperature was 100°C for this study, but it can vary between 90 and 110°C based on climatic regions.

PAV aging was performed following two protocols: standard 20 hours and extended 60 hours. The 20-hour protocol was conducted as it is specified for the Superpave binder performance grading while the 60-hour protocol was selected to simulate an extended aging condition close to the terminal service life of asphalt pavement.

Following PAV aging, a vacuum degassing procedure was conducted to eliminate remaining air bubbles that may compromise subsequent rheological tests using the BBR. For degassing, the metal rack holding the pans was first placed in an oven at temperatures high enough to make the residue fluid. While the oven was typically set at a temperature of 163°C, higher temperatures of 185°C or 195°C were required in some cases, especially for the 60-hour PAV aged samples. After 15 minutes in the oven, the metal pans were scraped, and the residue was placed in a vacuum oven at 170 ± 5°C for 15 minutes, followed by a 0.8MPa vacuum applied for 30 minutes. After that, vacuum was removed, and the residue could be used for subsequent rheological tests.

The degassing procedure was successfully conducted for all blends, except for one blend with Additive 3 that had been PAV aged for 60 hours. It was thought that the high temperature of the vacuum oven caused cross-linking of the polymer in this blend, resulting in a gelled, unworkable sample. For this reason, another sample of this blend was prepared and PAV aged for 60-hours without the degassing procedure.

3.5. Rheological Evaluation

For performance grading, DSR testing was conducted to characterize high and intermediate temperature performance, while BBR testing was used to evaluate low temperature properties, except for binder blends with Additives 1 and 3. The extended aging protocol led to a reduction in flow ability and workability of both base binders blended with these additives (without RAP), which made the molding of BBR beams unfeasible. Therefore, Additives 1 and 3 blended with both base binders without RAP were tested using the DSR 4-mm parallel plate geometry.

In addition to performance grading, extended BBR testing was also conducted on RTFO + 60-hour PAV aged samples to determine the effects of physical hardening at low temperatures. Multiple Stress Creep and Recovery (MSCR) testing was conducted to evaluate the binder rutting performance and formulation. Linear Amplitude Sweep (LAS) testing was performed to determine the binder intermediate temperature cracking resistance. Finally, frequency and temperature sweep tests were conducted on every sample to develop master curves to allow for rheological characterization over a broad range of conditions.

3.5.1. Superpave Performance Grading

Superpave performance grading was performed per AASHTO M320. The high- and intermediate-temperature properties were evaluated using an Anton Paar SmartPave 102 DSR, while low-temperature performance was determined using a Cannon TE BBR. Two replicates were tested for each binder blend.

DSR testing using a 25 mm parallel plate geometry and a 1-mm test gap was conducted on unaged and RTFO aged samples to determine the high temperature performance grade for evaluating the binder rutting resistance. The high temperature PG of unaged binder is defined as the minimum temperature where the rutting parameter $G^*/\sin\delta$ is greater than $1.00\ kPa$ at a frequency of $10\ rad/s$ and a 12% strain level. Additionally, the high temperature PG of RTFO aged sample is determined with a minimum DSR parameter $G^*/\sin\delta$ of $2.20\ kPa$ at the same frequency and a 10% strain level. For both aging conditions, DSR tests were run at passing and failing temperatures, and the high temperature true grade was calculated for each aging condition following ASTM D7643. The high temperature true grade was the lower temperature when comparing the high temperature true grades of the unaged and RTFO aged binders.

Intermediate temperature performance is used to address fatigue cracking resistance. It was evaluated in the DSR using the 8-mm parallel plate geometry. The intermediate temperature true grade was determined based on a minimum fatigue parameter $G^*.\sin\delta$ of $5000\ kPa$ at a strain level of 1% and a frequency of $10\ rad/s$. To guarantee adequate adhesion between the PAV-aged material and DSR plates during testing, each sample was loaded at 45°C and stabilized for five minutes prior to trimming at a 2.1-mm gap opening. Testing was conducted at passing and failing temperatures to determine the intermediate temperature true grade.

Low temperature performance grade was determined by means of BBR testing per AASHTO T313 for evaluating low temperature cracking resistance. It is determined based on creep stiffness (S) and m-value (creep rate). Their respective thresholds are $S \leq 300\ MPa$ and $m\text{-}value \geq 0.300$. BBR testing was conducting in 6℃ increments until passing and failing values of both parameters were obtained. True critical temperatures were calculated by interpolation so that $S = 300\ MPa$ and $m - value = 0.300$. Finally, the continuous low-temperature grade was determined as the maximum of the two critical temperatures determined based on S and m-value (i.e., $T_{c,S}$ and $T_{c,m}$). Two replicates were tested at each temperature and output parameters were reported as the average. In addition to low critical temperatures, the parameter ΔT_c was calculated for all binders, following Equation 6.

Equation 6. Definition of ΔTc parameter

$$\Delta T_c = T_{c,S} - T_{c,m}$$

3.5.1.1. Low-temperature Performance Grading using 4-mm DSR Approach

In the Superpave binder specification, BBR testing is used to determine the low temperature performance grade of binder after RTFO + 20-hour PAV aging. Additionally, an extended aging protocol of RTFO + 60-h PAV aging was also conducted in this study. For base binders modified with Additives 1 and 3 without RAP, the extended aging protocol decreased their flow ability and thus their workability, making the molding of BBR beams unfeasible as illustrated in Figure 29. Therefore, an alternative testing procedure using 4-mm parallel plate DSR was conducted for determining the low-temperature properties of these binders, after both aging protocols. For comparison purposes, base binders 1 and 5 were also tested following this approach. Samples and aging conditions tested under this method are listed in TABLE 7.

Figure 29. Attempted BBR beam with Binder 5 + Additive 3 OD (RTFO + 60-hour PAV)

TABLE 7. Materials and Aging Conditions for 4-mm DSR Approach

Sample ID	Aging conditions tested
Binder 1	RTFO + 20-hour PAV RTFO + 60-hour PAV
Binder 1 + Additive 1 OD	RTFO + 20-hour PAV RTFO + 60-hour PAV
Binder 1 + Additive 1 AD	RTFO + 20-hour PAV RTFO + 60-hour PAV
Binder 1 + Additive 3 OD	RTFO + 20-hour PAV RTFO + 60-hour PAV
Binder 5	RTFO + 20-hour PAV RTFO + 60-hour PAV
Binder 5 + Additive 1 OD	RTFO + 20-hour PAV RTFO + 60-hour PAV
Binder 5 + Additive 1 AD	RTFO + 20-hour PAV RTFO + 60-hour PAV
Binder 5 + Additive 3 OD	RTFO + 20-hour PAV RTFO + 60-hour PAV

Testing was conducted following the proposed draft AASHTO specification proposed by the Western Research Institute (WRI) (Farrar et al., 2015). Samples were annealed at 70℃ and loaded on the plates using a metal spatula. To promote adhesion, plates were heated to 70℃ and stabilized for 5 minutes, and samples were stabilized for 10 minutes at this same temperature prior to trimming. DSR testing is based on two frequency sweeps at low PG + 10℃ and low PG + 20℃, and the test outputs are the binder's relaxation modulus magnitude $G(t)$ and slope m_r at 60 seconds. Strain levels for each frequency sweep followed recommendations provided by the FHWA Asphalt Binder Expert Task Group (Farrar et al., 2015) and are detailed in TABLE 8.

TABLE 8. Strain Levels for 4-mm DSR Frequency Sweeps

Test Temperature (°C)	Strain (%)
-18	0.025%
-12	0.05%
-6	0.05%
0	0.1%
10	0.5%

Testing at -18℃ and -12℃ required a second frequency sweep at 8℃ and 2℃. In these cases, strain levels for 10℃ and 0℃ were selected, respectively. Finally, similar to BBR testing, passing and failing temperatures were required for interpolating the true grade. However, due to equipment limitations, testing below −18℃ was not possible, thus some critical temperatures had to be calculated by extrapolation instead.

Once DSR testing was complete, resulting relaxation modulus $G(t)$ and relaxation rate (m_r) were converted to BBR outputs of creep stiffness (S) and creep stiffness rate $(m - value)$, to subsequently calculate the continuous low-temperature true grades of each material. The correlations developed by WRI were used in the calculation as detailed in TABLE 9.

TABLE 9. WRI Correlation Between DSR and BBR Parameters (Sui et al., 2011)

DSR parameter	Value	BBR parameter	Value
$G(60\ s)$ (MPa) at PG temp +10°C	143 MPa	S(60s)	300 MPa
$m_r(60\ s)$ at PG temp +10°C	-0.275	$m - value$	-0.300

3.5.2. Multiple Stress Creep and Recovery (MSCR) Test

MSCR testing was performed on RTFO aged materials at 64°C, based on the Alabama climate, following AASHTO T350. Testing was conducted using 25-mm parallel plate geometry on the DSR at two stress levels: 0.1 kPa (for twenty cycles) and 3.2 kPa (for ten cycles). Each cycle consisted of 1 second of shear creep, followed by a recovery period of 9 seconds. The MSCR test generated two parameters to characterize high temperature performance: non-recoverable creep compliance (J_{nr}) and percent recovery $(\%R)$. Using MSCR results, base and modified binders were characterized following AASHTO M332, which defines four binder grades based on J_{nr} values at 3.2 kPa.

MSCR grades indicate progressively higher rutting resistance and therefore ability to withstand higher traffic levels (or lower speeds) as follows:

- Standard (S): $J_{nr} \leq 4.5\ kPa^{-1}$ – for traffic levels less than 10 million Equivalent Single Axle Loads (ESALs) or speeds greater than 70 km/h
- Heavy (H): $J_{nr} \leq 2.0\ kPa^{-1}$ – for traffic levels between 10 and 30 million ESALs or speeds between 20 – 70 km/h
- Very Heavy (V): $J_{nr} \leq 1.0\ kPa^{-1}$ – for traffic levels greater than 30 milliion ESALs or speeds lower than 20 km/h
- Extremely Heavy (E): $J_{nr} \leq 0.5\ kPa^{-1}$ – for traffic levels greater than 30 million ESALs or standing traffic (e.g., port facilities)

3.5.3. Linear Amplitude Sweep (LAS) Test

The LAS test was conducted per AASHTO T391 to evaluate the fatigue resistance of the base and modified binders. Testing was performed on RTFO + 60-h PAV-aged samples using 8-mm parallel plate geometry on the DSR. First, a frequency sweep was conducted by running 100 cycles of sinusoidal loading at a 0.1% strain level to determine the undamaged viscoelastic properties. Next, a stepwise loading scheme at 10Hz subjected the binder to strain levels that ranged from 1% to 30% at 1% increments. The high strain levels accelerated damage on binders and therefore captured material failure properties.

Test temperature was selected to accurately capture binder failure, as excessive temperatures would cause plastic flow instead of failure due to microcracking. Additionally, lower temperatures would result in loss of adhesion between the binder sample and the DSR plates. According to studies by Hintz et al., test temperature selection was based on an undamaged $|G^*|$ between 10 and 60 MPa (at $10Hz$) (Safaei & Castorena, 2016). Complex modulus values at 17℃, 18℃, 20℃, 24℃ and 28℃ were obtained from temperature-frequency sweeps, and 20℃ was selected as the test temperature. $|G^*|$ at 20℃ remained within the target interval across all base and modified binders, and undamaged $|G^*|$ from LAS confirm test temperature selection, as shown in Figure 30 through Figure 33.

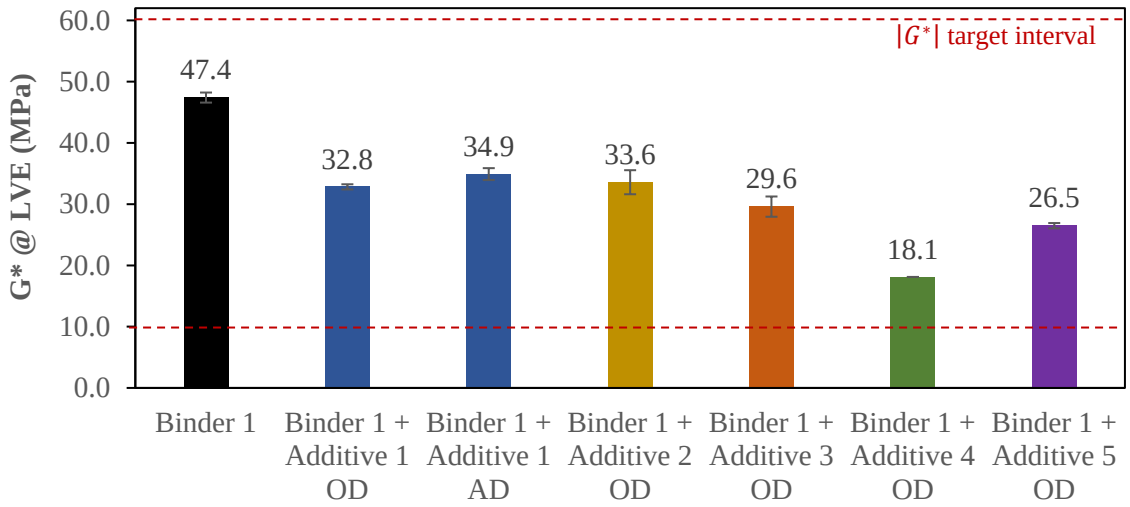

Figure 30. Undamaged G* at 20°C – Binder 1

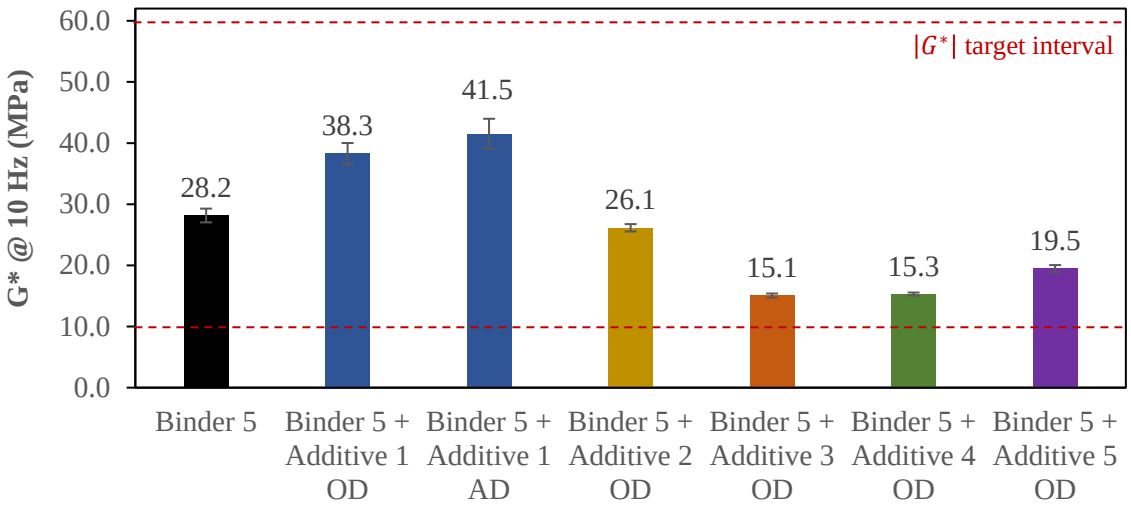

Figure 31. Undamaged G* at 20°C – Binder 5

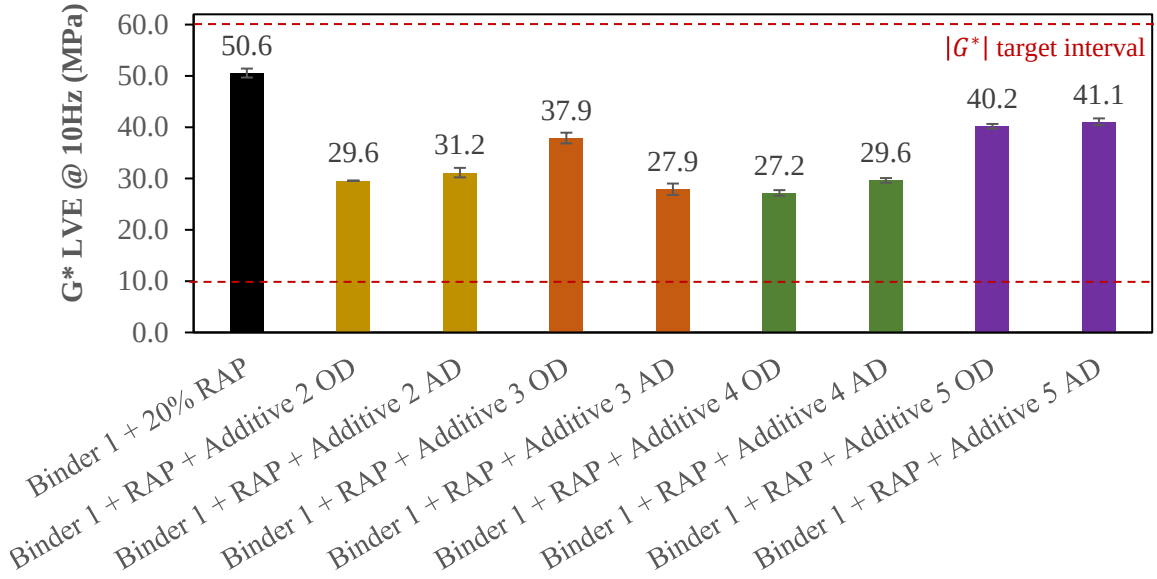

Figure 32. Undamaged G* at 20°C – Binder 1 + RAP

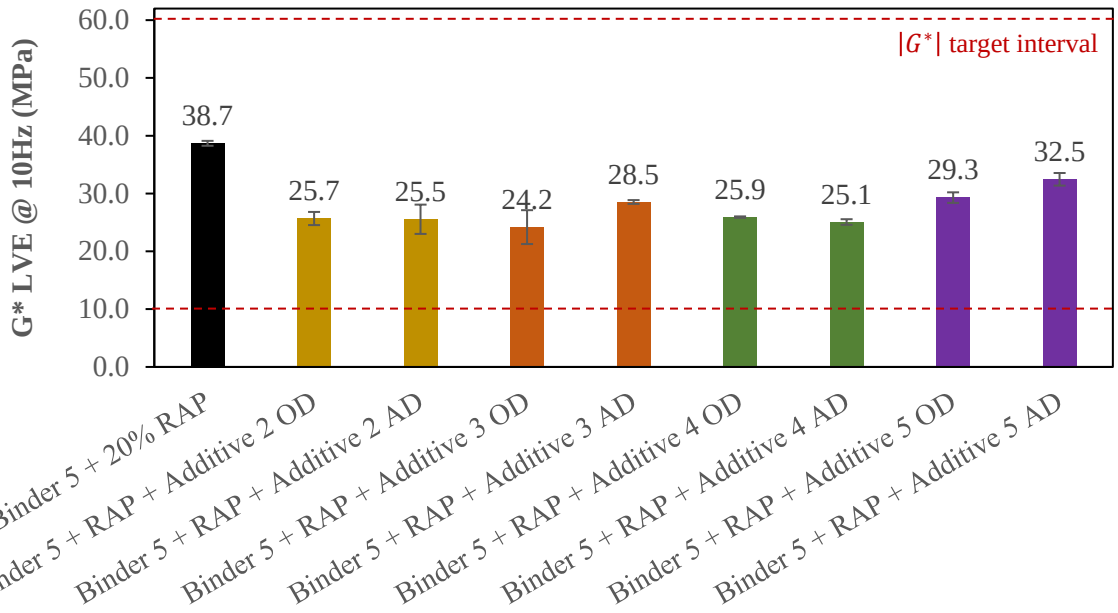

Figure 33. Undamaged G* at 20°C – Binder 5 + RAP

For LAS testing, good adhesion between the binder sample and DSR plates is important for accurate results. After setting the gap to 2 mm and prior to loading the samples, DSR plates were heated to 45℃, 60℃ or 70℃ depending on the stiffness of each material and stabilized for 5 minutes. Once the sample was loaded, it was kept at the selected temperature for 15 minutes, trimmed, and lowered to the required test temperature of 20℃.

LAS data analysis is based on simplified viscoelastic continuum damage (S-VECD). Following this theory, binder viscoelastic properties G^* and δ are related to damage intensity (D) following a linear power law (Hintz et al., 2011). However, in this study, damage is calculated based on reductions in pseudo-stiffness $|G^*|/|G^*|_{initial}$, as damage causes a clear reduction in complex modulus, but the effects on phase angle are not as clear (C. Wang et al., 2015). Thus, the damage power law is given in Equation 7.

Equation 7. Damage evolution power law

$$|G^*|/|G^*|_{initial} = C_0 - C_1(D)^{C_2}$$

$|G^*|_{initial}$ and the model fitting parameters $C_0, C_1,$ and C_2 are obtained from the LAS test output. Then, a relationship between damage accumulation and strain is determined for multiple strain levels (Aurilio et al., 2021). Damage accumulation causes material failure, which, for this study, was taken as a drop of 10% on the peak stress, as opposed to the 35% reduction in $|G^*| \sin \delta$ originally proposed in the specification. This criterion was preferred, as it better reflects ultimate failure and better distinguishes unmodified versus polymer modified binder performance. This material failure criterion provides the LAS parameter A.

Additionally, the initial frequency sweep provides the parameter B which relates to the damage accumulation properties of the binder. The parameters A and B define a linear relationship between number of cycles to failure (N_f) and the applied shear strain, as shown in Equation 8 (Hintz et al., 2011; R. Zhang

et al., 2020). At a certain strain level, asphalt binders with a higher N_f value are expected to have better resistance to fatigue damage.

Equation 8. LAS fatigue life

$$N_f = A(\gamma_{max})^{-B}$$
$$with$$
$$\gamma_{max} = maximum\ expected\ binder\ strain\ for\ a\ given\ pavement\ structure$$
$$A, B = LAS\ fatigue\ model\ parameters$$

Based on LAS output, the fatigue life of base and modified binders was evaluated according to the number of cycles to failure (N_f) at a 5% strain level. Although N_f at 3% strain levels can also be obtained from the test, it was found that a higher strain level may provide more accurate rankings of binder performance at higher levels of aging (Aurilio et al., 2020) and has been more closely related to field performance (Elkashef & Williams, 2017).

The parameter *B* was also studied as an indicator of fatigue resistance of base and modified binders, as it has been related to the rate of binder damage evolution (Y. Kim et al., 2006). Therefore, an increase in the number of cycles to failure or a reduction in the *B* parameter can suggest improvement in the binder fatigue cracking resistance.

3.5.4. Temperature - frequency sweep and master curve construction

Temperature frequency sweeps were conducted using DSR at multiple test temperatures and frequencies on unaged and RTFO + 60-hour PAV aged samples. Testing was performed using 8mm parallel plate geometry with a 2mm gap. The peak-to-peak strain of the binder sample was controlled at 1% to ensure its behavior remained in the linear viscoelastic range. The selected testing temperatures and frequencies were dependent on material type and aging condition, as indicated in TABLE 10.

TABLE 10. Test Conditions for Temperature-Frequency Sweeps

Binder ID	Aging Condition	Temperature range	Frequency range
- Base binders - Additive 1 - Additive 2 - Additive 4 - Additive 5	Unaged	-10 to 70℃	0.1 to 10 rad/s
	RTFO + 60-hour PAV	10 to 70℃	0.1 to 10 rad/s
- Additive 3	Unaged	-10 to 90℃	0.628 to 188 rad/s
	RTFO + 60-hour PAV	10 to 90℃	0.628 to 188 rad/s

DSR outputs were processed using RHEA software version 1.2.32 to develop master curves. RHEA includes several models for curve fitting, including standard and generalized logistic functions, Prony series, or the Christensen-Anderson model (CAM) (Inc, 2011). The software follows the "free shifting" approach, which shifts the data into a smooth master curve without assigning any pre-defined shape – or model. In this study, some of the additives limited the precision of certain models such as the CAM model, which has shown some restrictions for the characterization of polymer modified binders (Asgharzadeh et al., 2015; Habbouche et al., 2021; H. Zhang et al., 2019). Therefore, the discrete spectrum fit was used, converting dynamic moduli measurements $G'(\omega)$ and $G''(\omega)$ to discrete linear relaxation modulus $G(t)$ by adjusting g_i and λ_i, relaxation times and relaxation strengths, respectively.

Master curves were built at a selected reference temperature of 15℃ for base binders and modified blends, at both aging conditions. All dynamic data was processed so that model fitting would yield a root mean square error smaller than 3.5%. To achieve this, certain isotherms were excluded from the analysis due to the presence of viscous flow in the material, which compromised model fitting.

Then, the binder properties $|G^*|$ and δ were determined at 15℃ and 0.005 *rad/s* to subsequently calculate the Glover-Rowe parameter using Equation 9. The Glover-Rowe parameter can be used to evaluate binder cracking performance. Binders, especially unmodified, with G-R values over 180 kPa would be susceptible to the onset of cracking, while those with G-R values above 450 kPa would be susceptible to significant surface cracking (King et al., 2012).

Equation 9. Glover-Rowe parameter

$$G - R\ parameter = |G^*| \times \frac{(\cos\delta)^2}{\sin\delta}$$

where:

$$|G^*| = Binder\ shear\ complex\ modulus\ at\ 15℃\ and\ 0.005\ rad/s$$
$$\delta = Binder\ phase\ angle\ at\ 15℃\ and\ 0.005\ rad/s$$

3.5.5. Extended BBR Test

Extended BBR testing was performed on selected samples after RTFO + 60-h PAV aging to evaluate their physical hardening behavior. The extended BBR procedure in AASHTO TP122 requires two conditioning temperatures and two test temperatures based on the binder low temperature PG. However, the most significant effects of physical hardening occur near the glass transition temperature (T_g) of binders (D. A. Anderson & Marasteanu, 1999). Thus, Differential Scanning Calorimetry (DSC) was performed to determine the glass transition of base and modified binders in this study. Based on the analysis of DSC outputs as later discussed in Section 4.3.3, the T_g at half height of the heat capacity curve was selected as the conditioning and testing temperature for extended BBR testing. In addition, while AASHTO TP122 indicates 1, 24 and 72 hours as conditioning times, only the isothermal conditioning for 24 hours was conducted in this study.

3.6. Chemical characterization

3.6.1. Fourier Transformed Infrared Spectroscopy

Fourier Transformed Infrared Spectroscopy using the Attenuated Total Reflectance technique (FTIR-ATR) was used to track the changes in binder chemical composition due to oxidative aging. Oxidation causes an increase in oxygen-containing functionalities, and carboxylic acids, ketones and sulfoxides have been identified as the main oxidation products (J.C. Petersen, 2009; Rad et al., 2018). Therefore, the aging stability of binders was evaluated through the changes in areas generated around these functional groups.

FTIR testing was performed on all base and modified binders at the unaged condition and after RTFO and 60 hours of PAV aging. Samples were prepared by heating the binders to temperatures ranging from 150°C for unaged materials to 175°C for those heavily aged. Each FTIR spectrum was obtained between wavelengths of 4000 and 650 cm^{-1}, after a total of 64 scans. At least three replicates of each binder were tested, and two were used for data processing. A Bruker ALPHA spectrometer was used, and raw data was retrieved from Opus 7.5 software.

Data analysis was based on the changes in the area around the carbonyl (C=O) functional group and the sulfoxide (S=O) functional group. The carbonyl area was calculated between the wavelengths of 1660 and 1753 cm^{-1}, using the absorption at 1753 cm^{-1} as the baseline. Sulfoxide areas were calculated at the region between 995 and 1047 cm^{-1}, with 1047 cm^{-1} as the baseline. Area calculations follow guidelines from RILEM (Reunion Internationale des Laboratoires et Experts des Materiaux) and derived from a French procedure (Hofko et al., 2018; Marsac et al., 2014). Per this approach, only positive areas were considered around the designated baselines, as shown in the example in Figure 34.

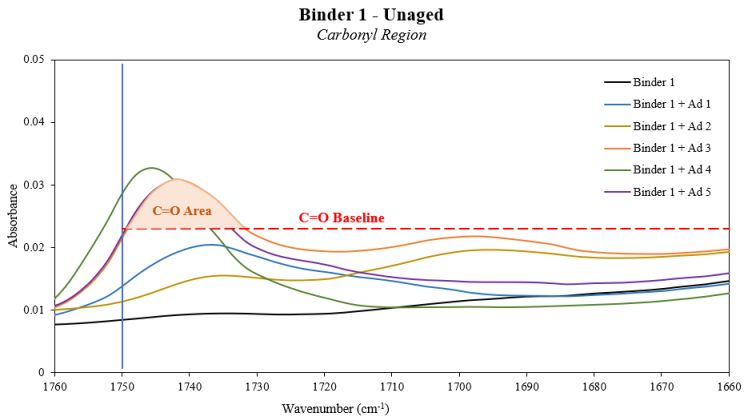

Figure 34. Example of area considered for Carbonyl Area calculations per RILEM guidelines

Both areas were determined for each binder, and aging indices were calculated to evaluate the effect of each additive on the formation of oxidation products. Larger areas would be indicative of a greater presence of oxygen-containing functionalities and thus a greater extent of aging. By comparing the modified binders with the base binders, the effects of additive interactions on oxidation can be evaluated. Aging indices, per this approach, were calculated using Equation 10. Indices lower than 1 would be desirable, meaning modified binders have smaller carbonyl and sulfoxide areas than the respective base binders. Thus, the additives were effective at reducing the rate of formation of oxidation products and improved their aging susceptibility.

Equation 10. Carbonyl and Sulfoxide Aging Index for modified binders – Approach 1

$$(C=O+S=O)Aging\ Index = \frac{(C=O+S=O\ Area)_{RTFO+60hr\ PAV\ Modified}}{(C=O+S=O\ Area)_{RTFO+60hr\ PAV\ Control\ binder}}$$

The FTIR spectrum of some modified binders had a secondary peak within the carbonyl region due to the presence of epoxy or recycling agent within their composition. For example, additives containing bio-oils have fatty acids. These compounds contain two oxygen molecules, one forms an oxygen double bond (C=O), and the other is connected to the carbonyl carbon through a sigma bond. Therefore, the carbonyl group (C=O) will appear shifted and might cause confounding effects when quantifying the carbonyl area. The presence of the carbonyl group for certain additives may lead to an inaccurate quantification of the extent of oxidation, as some of the area within the carbonyl region may be attributed to this secondary peak.

To account for this secondary peak a second approach for FTIR data analysis was followed. The carbonyl region was divided into two areas, designated as Area 1 and Area 2, as illustrated in Figure 35. Area 1 was considered between wavelengths of 1720 and 1753 cm^{-1}, using 1753 cm^{-1} as the baseline. Area 2 was considered between 1660 and 1719 cm^{-1} and taking 1753 cm^{-1} as the baseline as well. Thus, Area 1 was

attributed to additive composition, and the effects of oxidation were measured by tracking the changes in Area 2, considering only positive areas relative to the baseline. The sulfoxide region remained unchanged in this second approach and was also considered for the evaluation of oxidation.

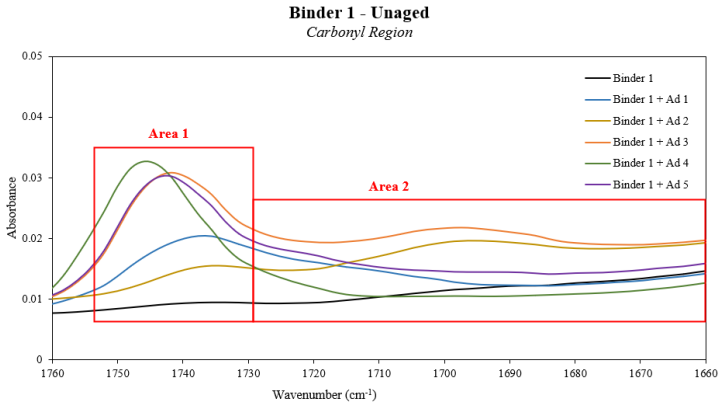

Figure 35. Example of Carbonyl Region divided into Area 1 and Area 2

For the second approach, aging indices were also calculated to track the effects of aging on modified binders relative to the base binders. In this case, it was hypothesized that the effects of aging would be more directly observed in the wavelengths between 1719 and 1660 cm^{-1}, designated as Area 2. The sulfoxide area calculation was unchanged. The aging index can be determined using Equation 11. Aging indices less than 1 would indicate slower formation of oxidation products, suggesting enhanced aging resistance of the modified binders. Both approaches were compared and correlated to rheological properties of binders to determine what region of the FTIR spectra was a more accurate predictor of oxidative aging when considering modified binders.

Equation 11. Carbonyl and Sulfoxide Aging Index for modified binders – Approach 2

$$(C=O_{Area\ 2}+S=O)Aging\ Index=\frac{(C=O_{Area\ 2}\ +S=O\ Area)_{RTFO+60hr\ PAV\ Modified}}{(C=O_{Area\ 2}+S=O\ Area)_{RTFO+60hr\ PAV\ Control\ binder}}$$

3.6.2. SARA fractions

As part of the chemical characterization plan, the binders were also separated into four chemical fractions based on their differences in solubility and polarity. These four fractions are designated as saturates (S), aromatics (A), resins (R), and asphaltenes (A), which are also known as SARA.

In the chemical separation procedure, the asphaltenes were first extracted per Institute of Petroleum (IP) standard 143 *Determination of Asphaltenes (Heptane Insoluble) in Crude Petroleum and Petroleum Products.* The remaining fractions, known as maltenes, which include saturates, aromatics and resins, were then separated per IP 469 standard *Determination of Saturated, Aromatic and Polar Compounds in Petroleum Products by Thin Layer Chromatography and Flame Ionization Detection* with dichloromethane:methanol (67:3 v/v) solution using Iatroscan.

For this study, SARA analysis was conducted to select the two base binders and to evaluate for the changes in chemical composition SARA fractions of the base and modified binders before and after extended aging. Therefore, testing was conducted on the unaged and RTFO + 60-hour PAV aged samples, and the changes

in each fraction were studied. SARA testing was conducted by industry partners participating in this study, and only base and modified binders without RAP were tested.

3.6.3. Differential Scanning Calorimetry

Modulated Differential Scanning Calorimetry (DSC) was selected to evaluate the glass transition behavior of the unmodified and modified binders after the RTFO + 60-hour PAV aging. Testing was conducted by WRI for this study.

The selected test method was Modulated DSC, which consisted of a series of linear heating and cooling rates with a periodic wave form of small amplitude being added within each cycle. The addition of a sinusoidal wave in Modulated DSC allows for each cycle to include both heating and cooling, though the overall trend is linear. The glass transition behavior is observed on the plot of reversed heat capacity with respect to temperature (Bricker & Hesp, 2013). Modulated DSC testing began by heating the samples up to 165℃, to fully anneal the binders and thus break any molecular association that may be present in binders at room temperatures prior to testing. The first cycle cools the sample at a rate of $5℃/min$, to -90℃, which is then kept for 5 minutes. The second cycle is a heating ramp at a $10℃/min$ rate up to 165℃. The sample is afterwards exposed to a modulated wave of $+/-0.5℃$ every 60 seconds. The next cycle cools down the sample once again at a $2℃/min$ to -90℃, and the last cycle heats the sample up to 165℃ at the same rate of $2℃/min$.

Test output includes the reversed heat capacity as a function of temperature, and four glass transition temperatures were identified: half-height ($T_g(H)$), inflection point ($T_g(I)$), onset ($T_g(O)$) , and end point ($T_g(E)$). Additionally, the width of the glass transition region was obtained as $T_g(W)$. These temperatures showed the effects of modification on the thermal properties of the binders. Additionally, $T_g(H)$ and $T_g(I)$ were compared, one of which was selected as the conditioning and testing temperature to study the hardening behavior of the binders using the extended BBR test.

3.6.4. Gel Permeation Chromatography

Binder molecular size distribution was evaluated using Gel Permeation Chromatography (GPC). Aging directly impacts the relative presence of SARA fractions in the neat and modified binders, changing their molecular size distribution, due to molecular agglomerations and formation of oxidation products. These changes in molecular size distribution (MSD) can have a significant impact on binder properties and stability.

GPC was conducted on the base and modified binders without RAP that were unaged and after 60 hours of PAV aging. Testing was conducted by an industry partner participating in this study. The test results were then analyzed and presented later in this thesis.

In this method, the asphalt binder was dissolved in a solvent (i.e., tetrahydrofuran) and was injected into the GPC system (Figure 36). The injected sample travels through a series of columns which separates the sample based on molecular size. The larger molecular size particles exit the columns first and are detected by the system's detectors. The smaller molecular size particles travel into the pores of the columns and, therefore, have longer retention times.

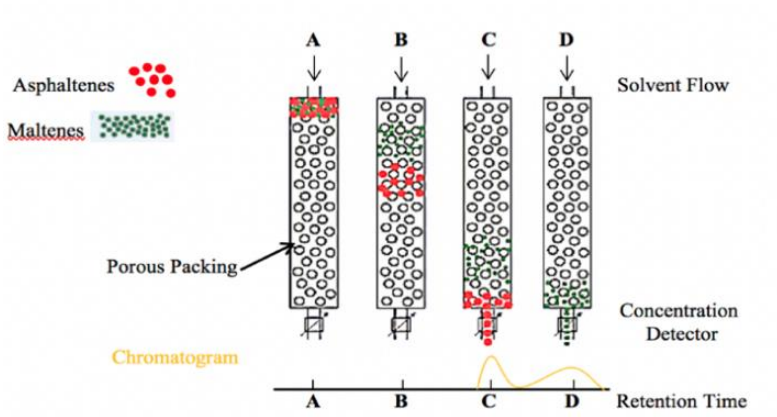

Figure 36. Schematic of Gel Permeation Chromatography (Moraes & Bahia, 2015)

The GPC output consists of a distinct and reproducible molecular-size distribution curve (chromatogram) (Figure 37). Several representative molecular weights can be determined, including Mw (weight average molecular weight), Mn (number average molecular weight), Mz (z-average molecular weight) and Mp (peak molecular weight). The presence of modifiers altered the shape of the distribution, leading to the appearance of multiple peaks. Therefore, these parameters are studied at the range where the asphalt peak is typically observed, which is between 500 and 1300 Daltons.

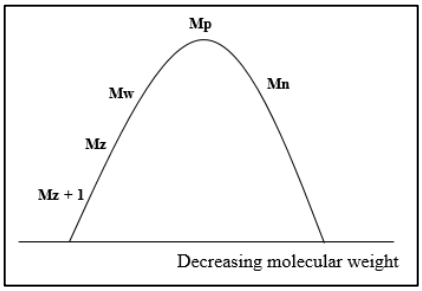

Figure 37. Typical GPC chromatogram curve with Mw (weight-average molecular weight), Mn (number-average molecular weight), Mz (z-average molecular weight), Mz+1 ((z+1)-average molecular weight), and Mp (peak molecular weight) (Moraes & Bahia, 2015)

CHAPTER 4 - RESULTS AND DISCUSSION

4.1. Base Binder Selection

Six asphalt binders from different sources were sampled as potential base binders for this study. Based on a rheological evaluation, two binders with distinctly opposite aging susceptibility were selected for modification with each aging resistant technology. The test results used for the selection process are discussed in this section.

Superpave PG was evaluated on unaged and aged (i.e., RTFO, 20-hour PAV and 60-hour PAV) samples to evaluate the aging susceptibility of the six binders. The PG test results, particularly low critical temperatures and ΔT_C parameter, having a good correlation to age-related cracking (R. M. Anderson et al., 2011; Elwardany, Planche, et al., 2020), were then used to evaluate the aging resistance of each binder.

TABLE 11 shows the performance grades and sources of the six binders. The high temperature true grade was determined for each binder, as shown in Figure 38. Binders 1, 5 and 6 had similar high temperature true grades that are higher than that of Binder 2 but lower than those of Binders 3 and 4.

TABLE 11. Base Binder Identification

Binder ID	PG Grade	Binder Source
Binder 1	64-16	West Texas
Binder 2	58-22	California Valley
Binder 3	67-22	Southeast US
Binder 4	64-22	California Coastal
Binder 5	64-22	West Canadian
Binder 6	64-22	Midwest US

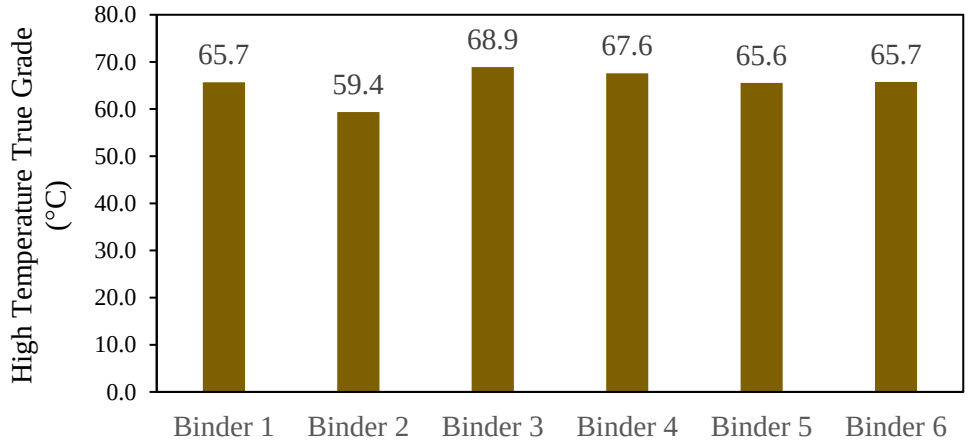

Figure 38. High Temperature True Grade for Base Binders

Figure 39 shows the intermediate temperature true grades after 20-hour PAV aging, as required in AASHTO M320. Despite having similar high temperature true grades as discussed earlier, Binder 1, 5 and 6 show different intermediate temperature fatigue parameters with Binder 5 having the highest fatigue cracking resistance, followed by Binder 6 and then Binder 1 with the lowest fatigue cracking performance.

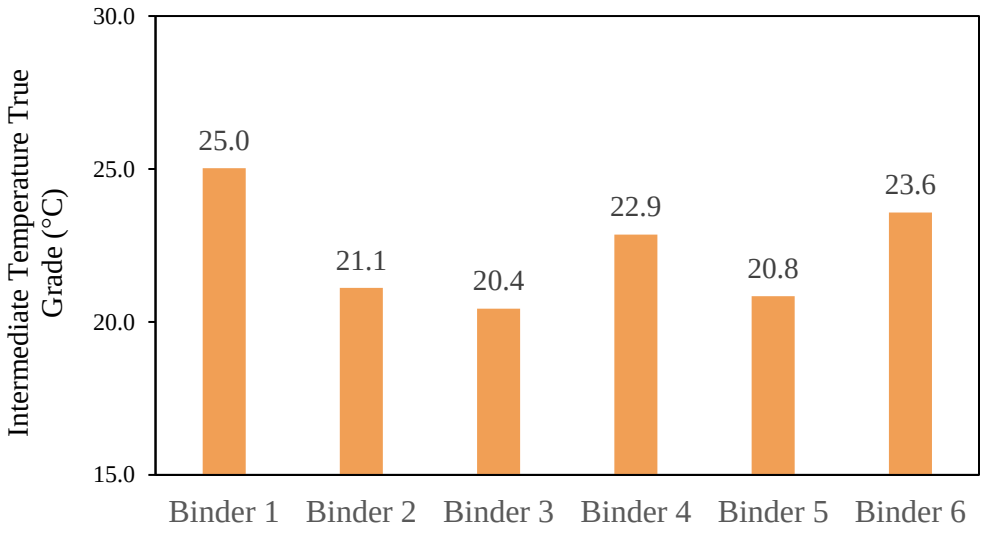

Figure 39. Intermediate Temperature True Grade for Base Binders

Furthermore, low critical temperatures based on Stiffness (S) and m-value were determined after 20-hour PAV aging, as shown in Figure 40. Binder 1 showed the warmest critical low temperature (-19.9°C), and it was m-controlled, meaning it failed at a warmer low temperature due to poor relaxation properties when subjected to thermal stresses. Binder 3 was also m-controlled but failed at a considerably lower temperature (-25.7°C).

In addition, these binders were also tested after RTFO followed by 60-hour PAV aging. Compared to the 20-hour PAV aged samples, the continuous low temperature grades of 60-hour PAV aged samples are expected to be higher as the binders become stiffer and lose relaxation properties, affecting their ability to withstand thermal stresses, which would reduce their cracking resistance. Therefore, binders with smaller increases in low critical temperatures from 20 hours to 60 hours of PAV aging would likely have higher cracking resistance. Additionally, due to the effect of aging, ΔT_C becomes more negative as the binder becomes more m-controlled.

Figure 41 compares the low temperature true grades for the six binders after 20 and 60 hours of PAV aging. The extended PAV aging changed Binder 5's low PG from a PG 64-28 to a PG 64-22, while Binder 6 retained its low PG at PG 64-22. Binder 1 showed a drop of two PG grades, going from a PG 64-16 to a PG 64-4, while Binder 3 went from a PG 64-22 to a PG 64-10. The differences in the low temperature true grades after 20 and 60 hours of PAV aging are presented in Figure 42. As previously noted, Binder 3 showed the largest increase in low temperature true grade while Binder 6 experienced the smallest increase, remaining a PG 64-22, even after extended PAV aging.

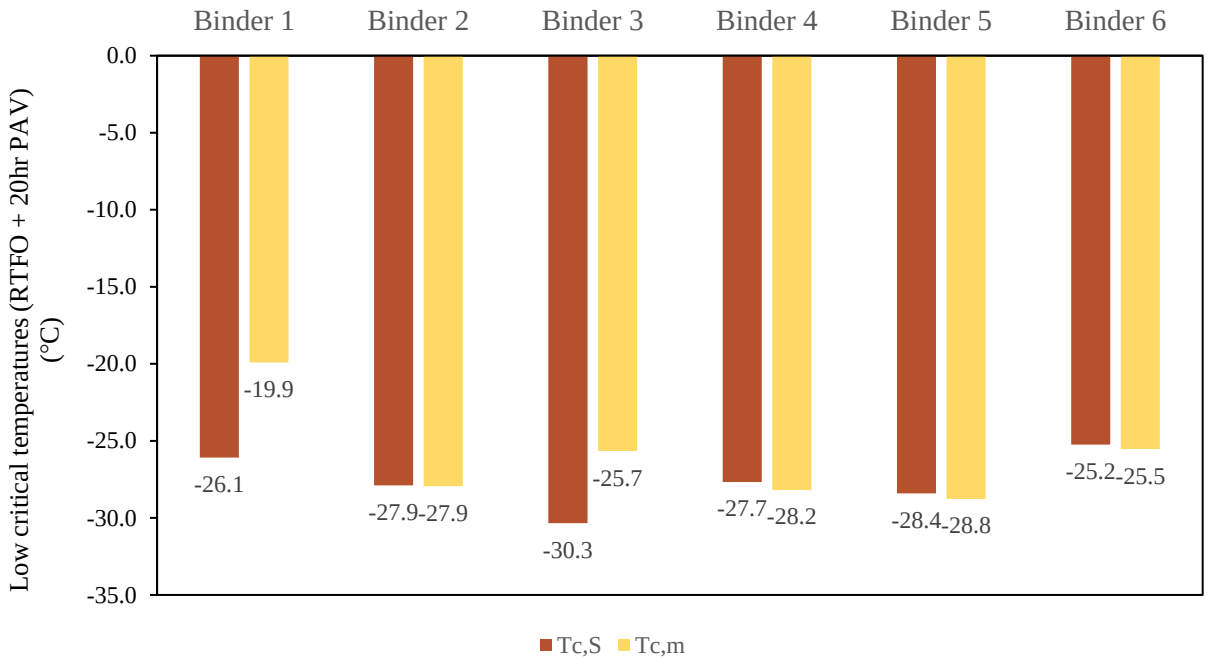

Figure 40. Low critical temperatures after RTFO + 20 hr PAV

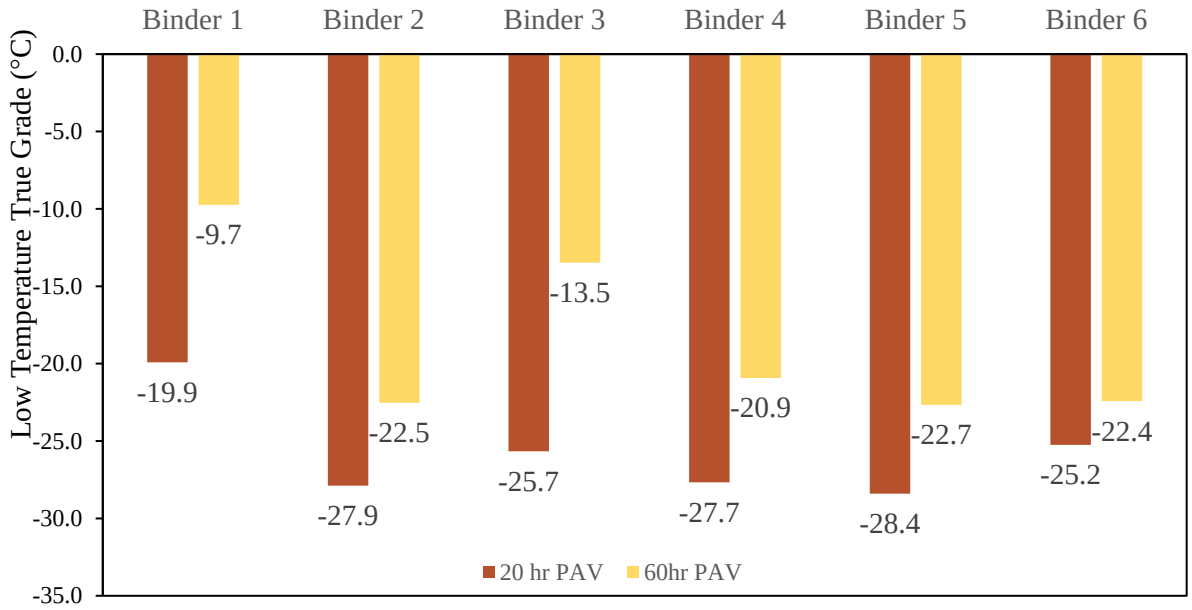

Figure 41. Low temperature true grade after RTFO + 20 and 60 hours of PAV aging

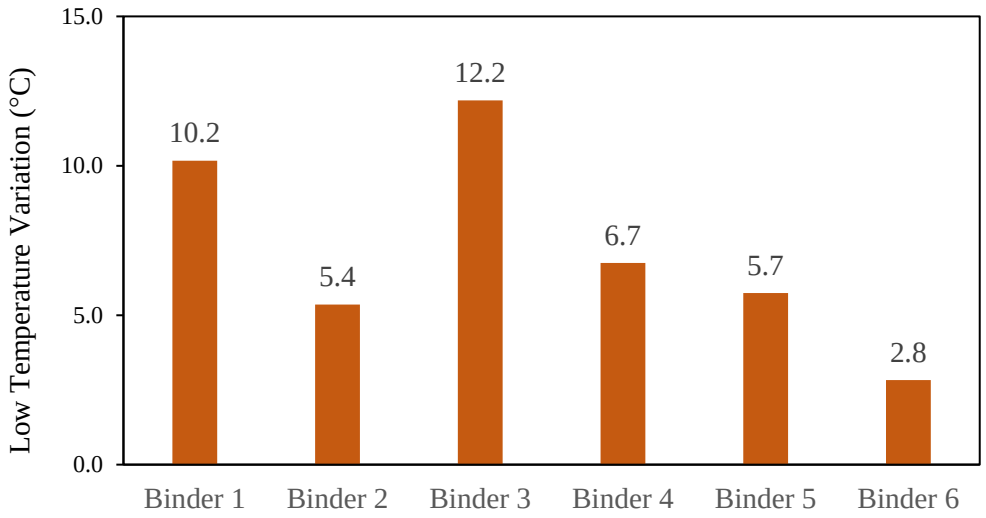

Figure 42. Difference in low temperature true grades after RTFO + 20- and 60-hour PAV aging

Figure 43 compares ΔT_C results after 20 and 60 hours of PAV aging. Lower (more negative) ΔT_C values would be indicative of binders with lower resistance to non-load associated cracking. After 20-hour PAV aging, Binders 3 and 1 had the lowest ΔT_C values while the other binders showed similar ΔT_C results. The ΔT_C values for all binders reduced after 60-hour PAV aging with Binders 3 and 1 showing the lowest ΔT_C and Binder 6 having the highest ΔT_C. The difference in ΔT_C after 20 hours and 60 hours of PAV aging were also determined and shown in Figure 44. Binders 3 and 1 showed the largest reductions, potentially indicating higher susceptibility to aging, while Binders 6 and 2 had the smallest changes, which would indicate lower aging susceptibility.

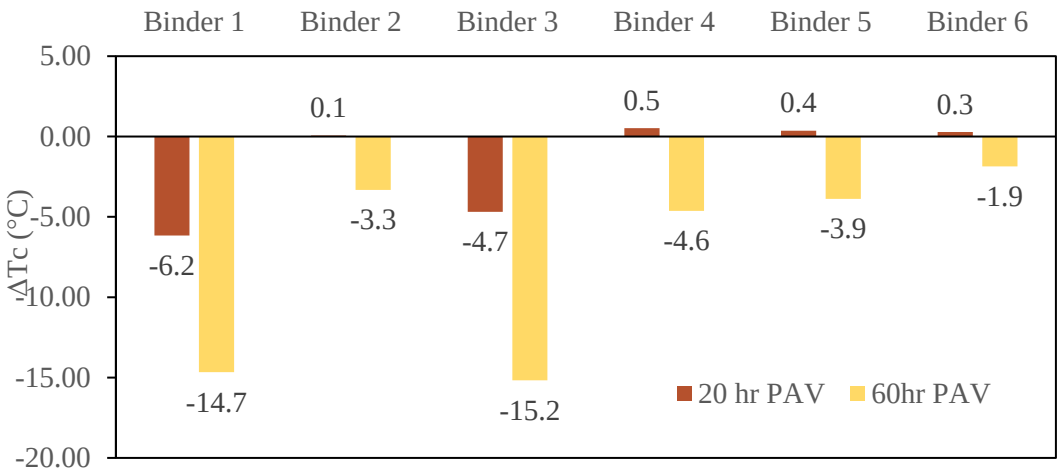

Figure 43. ΔTc after RTFO + 20 and 60 hours of PAV aging

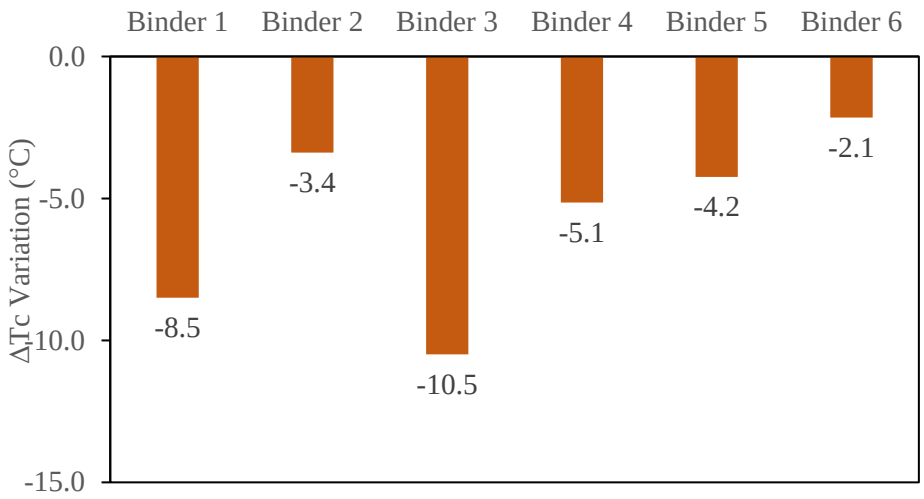

Figure 44. Difference in ΔTc after between RFTO + 20 and 60 hours of PAV aging

4.1.1 Summary of Results

Rheological properties determined on the unaged, RTFO aged, and 20- and 60-hour PAV aged samples of the six binders are summarized in TABLE 12.

TABLE 12. Summary of Results for Base Binders

	High Temperature True Grade (°C)	Intermediate Temperature (°C)	LT True Grade (°C) - 20hr PAV	ΔTc (°C) - 20hr PAV	LT True Grade (°C) - 60hr PAV	ΔTc (°C) - 60hr PAV
Binder 1	65.7	25.0	-19.9	-6.2	-9.7	-14.7
Binder 2	59.4	21.1	-27.9	0.1	-22.5	-3.3
Binder 3	68.9	20.4	-25.7	-4.7	-13.5	-15.2
Binder 4	67.6	22.9	-27.7	0.5	-20.9	-4.6
Binder 5	65.6	20.8	-28.4	0.4	-22.7	-3.9
Binder 6	65.7	23.6	-25.2	0.3	-22.4	-1.9

The candidate base binders had similar high temperature true grades, except for Binder 2. However, they had very different low temperature true grades and ΔT_C results after PAV aging, especially after the 60-hour cycle. For example, Binders 1, 5 and 6 had very similar high temperature true grades, but their low temperature true grades were distinctly different after 20- and 60-hour PAV aging. Changes in the low temperature true grade and ΔT_C of each base binder after 20- and 60-hour PAV aging are summarized in TABLE 13, including a relative ranking to illustrate their aging susceptibility. Binder 6 had the lowest aging susceptibility and was assigned a ranking of 1, while Binder 3 showed the highest aging susceptibility and was thus given a ranking of 6.

TABLE 13. Aged Properties of Base Binders and Relative Rankings

Binder ID	Low Temperature Increase (°C)	Relative Ranking	ΔTc after RTFO + 60-hour PAV(°C)	Relative Ranking	ΔTc Variation (°C)	Relative Ranking
Binder 1	10.2	5	-14.7	5	-8.5	5
Binder 2	5.4	2	-3.3	2	-3.4	2
Binder 3	12.2	6	-15.2	6	-10.5	6
Binder 4	6.7	4	-4.6	4	-5.1	4
Binder 5	5.7	3	-3.9	3	-4.2	3
Binder 6	2.8	1	-1.9	1	-2.1	1

In summary, the two binders selected for modification with the proposed aging resistant technologies were Binder 1 and Binder 5. These binders presented no compatibility issues with any technology, and had distinctly different aging behavior despite their comparable properties prior to aging.

4.1.2 RAP Binder and RAP Blend Characterization

In addition to Binder 1 and Binder 5, one RAP source from Alabama was selected as part of the control materials of the project. The RAP binder was extracted and recovered, and later blended at 20% by weight with each base binder. Superpave PG was followed for unaged and aged (RTFO followed by 20 and 60 hours of PAV aging) extracted RAP binder and RAP binder blends.

TABLE 14 details the results at the unaged condition. The addition of the RAP binder caused an increase on the high temperature PG of the base binders, going from a PG 64 to a PG 70. With regards to the low temperature PG, Binder 1 remained at PG -16, while Binder 5 went from a PG-28 to a PG-22.

TABLE 14. Unaged PG Grading of Base Binders and RAP Blends

Binder ID	HT Unaged (°C)	HT RTFO (°C)	IT RTFO + 20 hr PAV (°C)	Tc, S – RTF0 + 20hr PAV (°C)	Tc, m - RTF0 + 20hr PAV (°C)	ΔTc - RTF0 + 20hr PAV (°C)	PG Grade
RAP	107.4	107.7	40.0	-17.1	-8.5	-8.6	106 - 4
Binder 1	65.7	66.6	25.0	-26.1	-19.9	-6.2	64 - 16
Binder 1 + 20% RAP	73.4	73.2	27.1	-24.9	-18.7	-6.2	70 - 16
Binder 5	65.6	67.4	20.8	-28.4	-28.8	0.4	64 - 28
Binder 5 + 20% RAP	73.1	74.6	23.8	-26.2	-25.7	-0.5	70 - 22

TABLE 15 presents PG after RTFO plus 60 hours of PAV aging. The low temperature PG of base Binder 1 and the 20% RAP blend increased from -16 to -4 when going from 20 to 60 hours of PAV aging. On the other hand, Binder 5 experienced a reduction in low PG by only one grade, from -28 to -22, while the 20% RAP blend increased from -22 to -16.

TABLE 15. PG Grading of Virgin Binders and RAP Blends after RTFO + 60 Hours of PAV Aging

Binder ID	HT 60 hr PAV (°C)	IT RTF0 + 60 hr PAV (°C)	Tc, S - RTF0 + 60hr PAV (°C)	Tc, m - RTF0 + 60hr PAV (°C)	Delta Tc - RTF0 + 60hr PAV (°C)	PG
RAP		44.4	-16.9	-1.6	-15.3	XX – (+2)
Binder 1	100.7	30.2	-24.4	-9.7	-14.7	100 - 4
Binder 1 + 20% RAP	105.7	28.9	-23.4	-8.0	-15.4	100 - 4
Binder 5	103.4	25.2	-26.5	-22.7	-3.9	100 - 22
Binder 5 + 20% RAP	110.3	31.8	-24.7	-17.0	-7.7	106 - 16

4.2. Rheological Evaluation of Aging Resistant Technologies

4.2.1 Superpave Performance Grading

Every additive was blended with the selected base binders and with the RAP binder blends and evaluated per AASHTO M320. High temperature properties were evaluated at the unaged condition and after short-term RTFO aging, while intermediate and low temperature properties were evaluated after RTFO plus 20 hours of PAV aging. In addition, Superpave PG was evaluated for base binders and modified blends after RTFO plus 60 hours of PAV aging.

Statistical significance of the results with respect to the control binders and RAP blends was evaluated using ANOVA analysis followed by Tukey pairings at a 95% significance level, based on two replicate measurements per sample. Each base binder was designated with a letter to indicate a statistical group. When no statistical significance was found between results for a modified binder and the control, the same letter designation was assigned to the two binders.

a. High Temperature Evaluation

The different nature of the additives caused varying effects on the unaged properties of the virgin binders, as summarized in TABLE 16. At the unaged condition, Additives 1, 2 and 3 increase the high temperature PG of the control binders. On the other hand, additive 5 did not cause an increase on the high PG of the control binder, while Additive 4 had a softening effect on both binders 1 and 5, causing a loss of two PG grades from 64 to 58. The nature of each modifier can be interpreted based on their effects at high temperatures, as polymer modifiers increased the true grade of both base binders. Although Additive 1 would typically develop a polymeric network expected to improve high temperature properties it is hypothesized that the increase in high temperature true grade would be dependent on the degree of dilution, as has been found in the literature (Apostolidis et al., 2020).

TABLE 16. High Temperature True Grade for Binders Without RAP

	HT True Grade – Unaged (℃)	HT True Grade - RTFO (℃)	HT True Grade (℃)	High PG
Binder 1	65.7	66.6	65.7	64
Binder 1 + Additive 1 OD	70.5	68.5	68.5	64
Binder 1 + Additive 1 AD	70.6	68.7	68.7	64
Binder 1 + Additive 2	85.1	85.4	85.1	82
Binder 1 + Additive 3	102.2	93.6	93.6	88
Binder 1 + Additive 4	57.3	57.6	57.3	52
Binder 1 + Additive 5	65.4	65.1	65.1	64
Binder 5	65.6	67.4	65.6	64
Binder 5 + Additive 1 OD	78.6	76.8	76.8	76
Binder 5 + Additive 1 AD	79.0	77.4	77.4	76
Binder 5 + Additive 2	85.3	88.9	85.3	82
Binder 5 + Additive 3	97.2	95.8	95.8	94
Binder 5 + Additive 4	56.9	57.2	56.9	52
Binder 5 + Additive 5	64.9	65.7	64.9	64

High temperature performance is most strongly associated with permanent deformation, thus the increase on true grade caused by Additives 1 (for Binder 5 only), 2 and 3 would appear to improve rutting resistance with respect to control binders. Even though certain additives had a stiffening effect on the control binders, evaluating high temperature true grade before and after extended aging could indicate the extent of stiffening caused by aging. Among the additives, Additive 4 behaved as a softening agent on both binders, reducing the high PG of both base binders by two grades, from 64 to 52.

The continuous high temperature true grade of RAP binder blends is presented in TABLE 17, and the overall trends observed for neat binders were also found for RAP blends. Additive 4 decreased the high PG grade of the controls, while Additives 2 and 3 caused an increase of at least two grades for both recycled binder blends.

TABLE 17. High Temperature True Grade for Modified Binders With RAP

	HT True grade – Unaged (℃)	**HT True grade - RTFO** (℃)	**HT True grade** (℃)	**High PG**
Binder 1 + RAP	73.4	73.2	73.2	70
Binder 1 + RAP + Ad 2 OD	89.9	88.9	88.9	88
Binder 1 + RAP + Ad 2 AD	86.7	85.3	85.3	82
Binder 1 + RAP + Ad 3 OD	100.7	95.2	95.2	94
Binder 1 + RAP + Ad 3 AD	95.5	89.8	89.8	88
Binder 1 + RAP + Ad 4 OD	67.0	67.0	67.0	64
Binder 1 + RAP + Ad 4 AD	65.6	65.9	65.6	64
Binder 1 + RAP + Ad 5 OD	75.5	75.3	75.3	70
Binder 1 + RAP + Ad 5 AD	74.9	75.2	74.9	70
Binder 5 + RAP	73.1	74.6	73.1	70
Binder 5 + RAP + Ad 2 OD	89.4	90.3	89.4	88
Binder 5 + RAP + Ad 2 AD	91.2	90.4	90.4	88
Binder 5 + RAP + Ad 3 OD	98.4	95.4	95.4	94
Binder 5 + RAP + Ad 3 AD	102.8	97.4	97.4	94
Binder 5 + RAP + Ad 4 OD	66.6	66.3	66.3	64
Binder 5 + RAP + Ad 4 AD	67.7	67.5	67.5	64
Binder 5 + RAP + Ad 5 OD	75.3	75.4	75.3	70
Binder 5 + RAP + Ad 5 AD	76.8	76.4	76.4	76

b. Intermediate Temperature Evaluation

Intermediate temperature true grade was determined through DSR testing after 20 hours of PAV aging, to evaluate fatigue resistance of binders. A higher value of $G^* \sin \delta$ is indicative of the binder dissipating more energy per unit cycle, thus experiencing more damage, or fatigue cracking. Therefore, lower intermediate temperatures would indicate improved fatigue resistance. However, fatigue cracking characterization using the DSR parameter has presented some limitations (Hajj & Bhasin, 2018), particularly for the evaluation of polymer modified binders.

Continuous intermediate temperature true grade of modified binders without RAP are presented in TABLE 18. Binder 1 had a higher intermediate temperature than Binder 5, meaning lower fatigue resistance, which supports its selection as having higher aging susceptibility. Additive 1 (at the Alternative Dosage) and Additive 2 caused no significant changes with respect to the base binder. On the other hand, Additives 3, 4 and 5 reduced the intermediate temperature true grade with respect to the control and therefore appeared to improve fatigue resistance as given by the DSR parameter.

TABLE 18. Continuous Intermediate Temperature True Grade (RTFO + 20 Hr PAV) - Without RAP

	IT True grade - RTFO + 20hr PAV (℃)
Binder 1	25.0
Binder 1 + Additive 1 OD	22.8
Binder 1 + Additive 1 AD	24.8
Binder 1 + Additive 2	24.2
Binder 1 + Additive 3	20.7
Binder 1 + Additive 4	17.0
Binder 1 + Additive 5	18.9
Binder 5	20.8
Binder 5 + Additive 1 OD	22.7
Binder 5 + Additive 1 AD	23.2
Binder 5 + Additive 2	22.1
Binder 5 + Additive 3	12.3
Binder 5 + Additive 4	12.1
Binder 5 + Additive 5	15.1

Improvements in fatigue resistance showed some degree of base binder dependency, as shown in Figure 45 and Figure 46. Additives 3,4 and 5 showed consistent performance with both base binders, Additive 1 appeared more effective with Binder 1. Additive 2, on the other hand, provided no significant improvements.

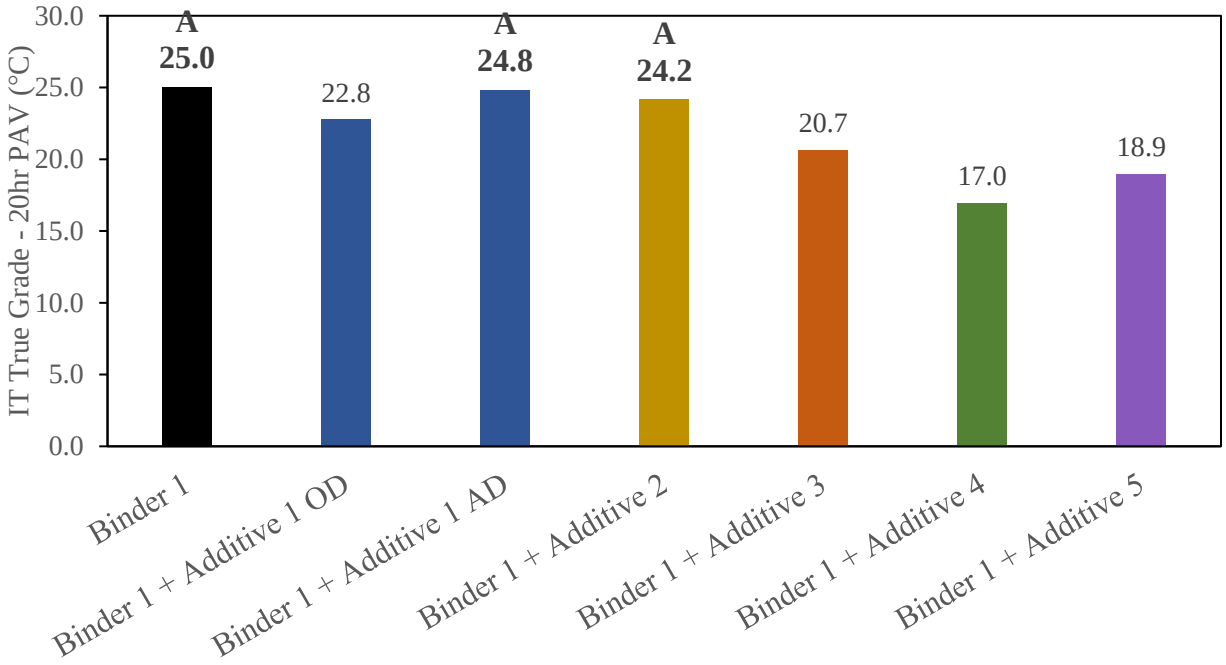

Figure 45. Intermediate temperature True Grade - RTFO + 20hr PAV - Binder 1

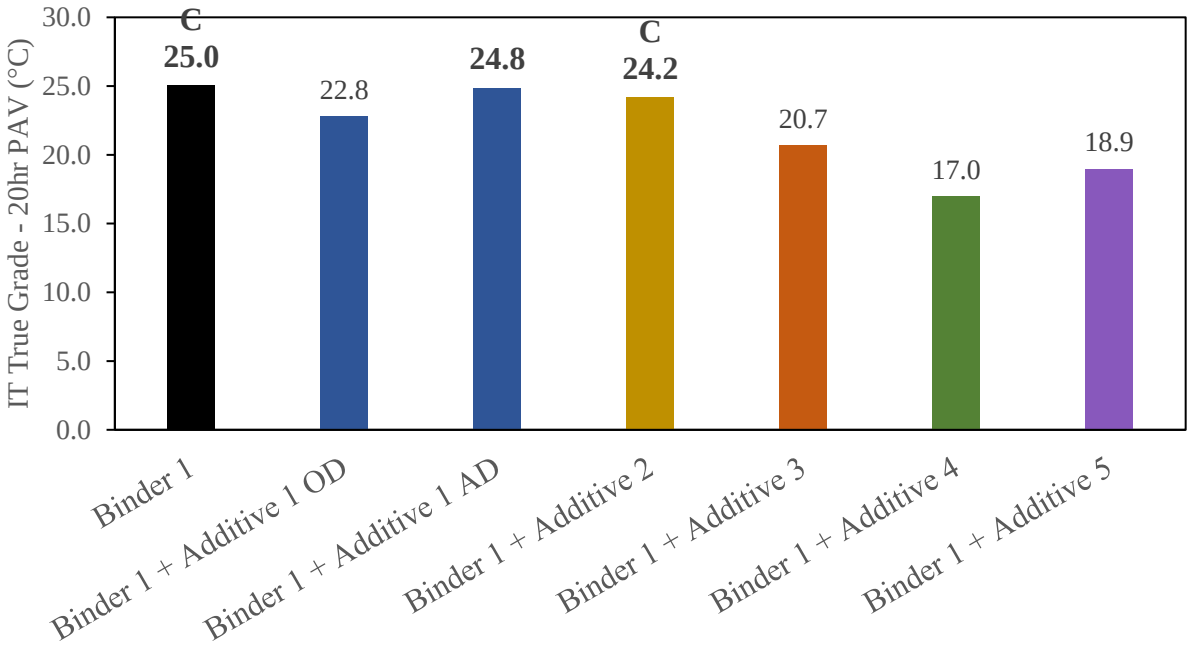

Figure 46. Intermediate temperature True Grade - RTFO + 20hr PAV - Binder 5

The intermediate temperature true grade of RAP blends shows all additives improved fatigue resistance, as indicated in TABLE 19. For both recycled binder blends, significant reductions in intermediate temperatures were found with the use of every additive, which might lead to improvements in fatigue cracking resistance with respect to the control.

TABLE 19. Continuous Intermediate Temperature True Grade (RTFO + 20 hr PAV) - with RAP

	IT True grade - RTFO + 20hr PAV (℃)
Binder 1 + RAP	27.1
Binder 1 + RAP + Ad 2 OD	21.6
Binder 1 + RAP + Ad 2 AD	22.9
Binder 1 + RAP + Ad 3 OD	21.5
Binder 1 + RAP + Ad 3 AD	18.1
Binder 1 + RAP + Ad 4 OD	18.1
Binder 1 + RAP + Ad 4 AD	20.2
Binder 1 + RAP + Ad 5 OD	23.4
Binder 1 + RAP + Ad 5 AD	25.0
Binder 5 + RAP	23.8
Binder 5 + RAP + Ad 2 OD	20.7
Binder 5 + RAP + Ad 2 AD	19.5
Binder 5 + RAP + Ad 3 OD	16.4
Binder 5 + RAP + Ad 3 AD	18.9
Binder 5 + RAP + Ad 4 OD	18.4
Binder 5 + RAP + Ad 4 AD	18.1
Binder 5 + RAP + Ad 5 OD	20.0
Binder 5 + RAP + Ad 5 AD	21.8

c. Low Temperature Evaluation

Low temperature properties of modified binders were evaluated through BBR testing after RTFO aging followed by 20 hours of PAV aging. ΔT_c was calculated, as it has been strongly correlated with binder ductility and resistance to age-related distresses (King et al., 2012; G. Rowe et al., 2014). TABLE 20 details critical temperatures, low temperature PG and ΔT_c for modified binders with no RAP.

TABLE 20. Low Critical Temperatures and ΔTc - RTFO + 20hr PAV – Without RAP

	Tc, S (℃)	**Tc, m** (℃)	**LT True grade**(℃)	ΔT_c (℃)	**PG LT**
Binder 1	-26.1	-19.9	-19.9	-6.2	-16
Binder 1 + Additive 1 OD	-25.9	-22.6	-22.6	-3.3	-22
Binder 1 + Additive 1 AD	-25.4	-23.8	-23.8	-1.6	-22
Binder 1 + Additive 2	-27.2	-18.7	-18.7	-8.5	-16
Binder 1 + Additive 3	-29.3	-25.3	-25.3	-4.0	-22
Binder 1 + Additive 4	-30.8	-28.7	-28.7	-2.1	-28
Binder 1 + Additive 5	-31.0	-27.3	-27.3	-3.7	-22
Binder 5	-28.4	-28.8	-28.4	0.4	-28
Binder 5 + Additive 1 OD	-26.1	-24.2	-24.2	-1.9	-22
Binder 5 + Additive 1 AD	-25.3	-23.4	-23.4	-1.9	-22
Binder 5 + Additive 2	-28	-23.4	-23.4	-4.6	-22
Binder 5 + Additive 3	-36.5	-38.1	-36.5	1.6	-34
Binder 5 + Additive 4	-34.2	-36	-34.2	1.8	-28
Binder 5 + Additive 5	-34.1	-33.8	-33.8	-0.3	-28

Improvements in low temperature properties are observed for Binder 1, as every additive caused a reduction in low critical temperatures. Overall, low temperature true grade was reduced indicating enhanced resistance to non-load related cracking and improved relaxation properties. Results for Binder 5, however, reiterate the base binder dependence previously noted, as improvements in low temperature properties were found for Additives 3, 4 and 5. Additives 1 and 2, however, resulted on higher critical temperatures which might compromise thermal cracking resistance.

ΔT_C results for base binders after 20 hours of PAV aging are presented in Figure 48 and Figure 47. The better aging properties of Binder 5 become evident from its positive value of ΔT_C at 0.4 ℃. Binder 1, on the other hand exhibited considerably lower cracking resistance, as a ΔT_C of -6.2 ℃ is below the -5 ℃ preliminary threshold determined for the presence of surface cracking (Technical Advisory Committee, 2019). ΔT_C of Binder 1 increased, (i.e., becomes more positive) after modification with Additives 4 and 5, showing improvements in binder relaxation properties. A higher ΔT_C would indicate these additives are potentially effective at improving binder relaxation properties, thus mitigating the embrittlement caused by aging. Binder 5, on the other hand, showed improvements in ΔT_C only after modification with Additive 4, while Additive 2 decreased the ΔT_C with respect to both neat binders.

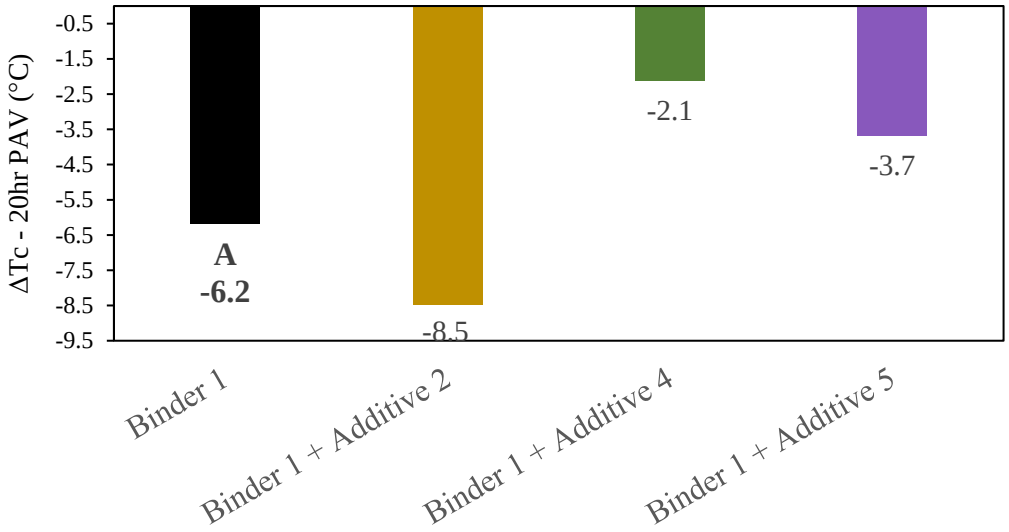

Figure 48. ΔTc for Binder 1 – RTFO + 20 hours PAV

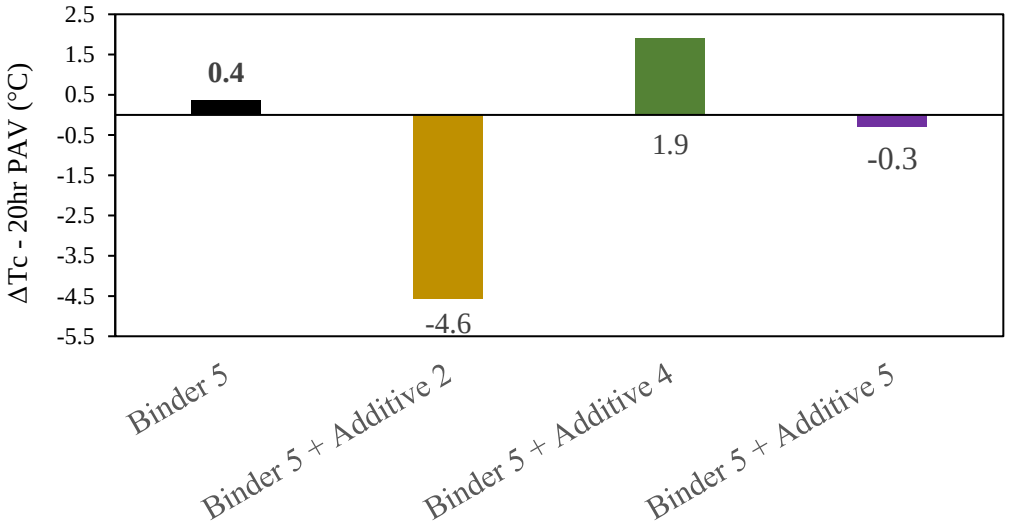

Figure 47. ΔTc for Binder 5 – RTFO +20 hours PAV

It is worth noting that the correlation of ΔT_C with cracking resistance and binder ductility has only been validated for unmodified binders (Christensen et al., 2019; Mensching et al., 2015). Limitations have been found with the use of this parameter as predictor of fatigue cracking resistance for polymer modified binders. Reductions in phase angle caused by the increased elastic response provided by these modifiers may result in more negative values of ΔT_C, which could be interpreted as a loss in relaxation properties (Aurilio et al., 2020). For this reason, the effects on ΔT_C of Additive 2 should be observed with caution since it contains polymer modifiers. A more negative value than the control may not necessarily indicate worse aging properties, so additional parameters to investigate durability of these materials are needed.

Low critical temperatures after 20 hours of PAV aging are presented in TABLE 21. All Additives reduced low critical temperatures of Binder 1 with RAP, in some cases by two grades, as observed for Additive 3. Improvements in thermal cracking resistance as well as relaxation properties after 20 hours of PAV aging indicate all additives mitigated the embrittlement of recycled blends with Binder 1. Varying effectiveness is observed for the different technologies and dosages, as Additive 2, for example, did not cause a reduction in low PG, while a reduction of two grades was observed for Additive 3.

Recycled binder blends with Binder 5 reflect improved low temperature performance for most additives. However, additive 2 presented reduced effectiveness with this base binder, as low critical temperatures increased for both dosages, indicating a loss in relaxation properties relative to the control. This Additive reduced the stiffness critical temperature, but the effect of polymer modification caused a reduction in m-value. Thus, the m-value critical temperature (and the low temperature true grade) increased relative to the control.

TABLE 21. Low Critical Temperatures and ΔTc - RTFO + 20hr PAV – With RAP

	Tc, S (℃)	**Tc, m** (℃)	**LT True grade**(℃)	ΔT_c (℃)	**PG LT**
Binder 1 + RAP	-24.9	-18.7	-18.7	-6.2	-16
Binder 1 + RAP + Ad 2 OD	-29.7	-20.1	-20.1	-9.6	-16
Binder 1 + RAP + Ad 2 AD	-27.8	-20.0	-20.0	-7.8	-16
Binder 1 + RAP + Ad 3 OD	-27.7	-19.6	-19.6	-8.1	-16
Binder 1 + RAP + Ad 3 AD	-30.6	-25.3	-25.3	-5.3	-22
Binder 1 + RAP + Ad 4 OD	-30.3	-30.5	-30.3	0.2	-28
Binder 1 + RAP + Ad 4 AD	-28.8	-24.8	-24.8	-4.0	-22
Binder 1 + RAP + Ad 5 OD	-27.7	-22.7	-22.7	-5.0	-22
Binder 1 + RAP + Ad 5 AD	-27.1	-21.4	-21.4	-5.7	-16
Binder 5 + RAP	-26.2	-25.7	-25.7	-0.5	-22
Binder 5 + RAP + Ad 2 OD	-30.0	-24.0	-24.0	-6.0	-22
Binder 5 + RAP + Ad 2 AD	-30.6	-24.7	-24.7	-5.9	-22
Binder 5 + RAP + Ad 3 OD	-34.2	-33.6	-33.6	-0.6	-28
Binder 5 + RAP + Ad 3 AD	-31.6	-31.1	-31.1	-0.5	-28
Binder 5 + RAP + Ad 4 OD	-31.1	-29.7	-29.7	-1.4	-28
Binder 5 + RAP + Ad 4 AD	-30.4	-30.8	-30.4	0.4	-28
Binder 5 + RAP + Ad 5 OD	-30.5	-30.2	-30.2	-0.3	-28
Binder 5 + RAP + Ad 5 AD	-29.4	-28.4	-28.4	-1.0	-28

The effect of modifiers on ΔT_C of Binder 1 with RAP is shown in Figure 49. Improvement in binder relaxation properties and durability given by more positive (or less negative) values of ΔT_C can be observed for Additives 3 (at the alternative dosage), 4 and 5. Additive 2 appears to reduce ductility with respect to the control, but additional analyses are required to overcome the limitations of ΔT_C when it comes to polymeric modifiers.

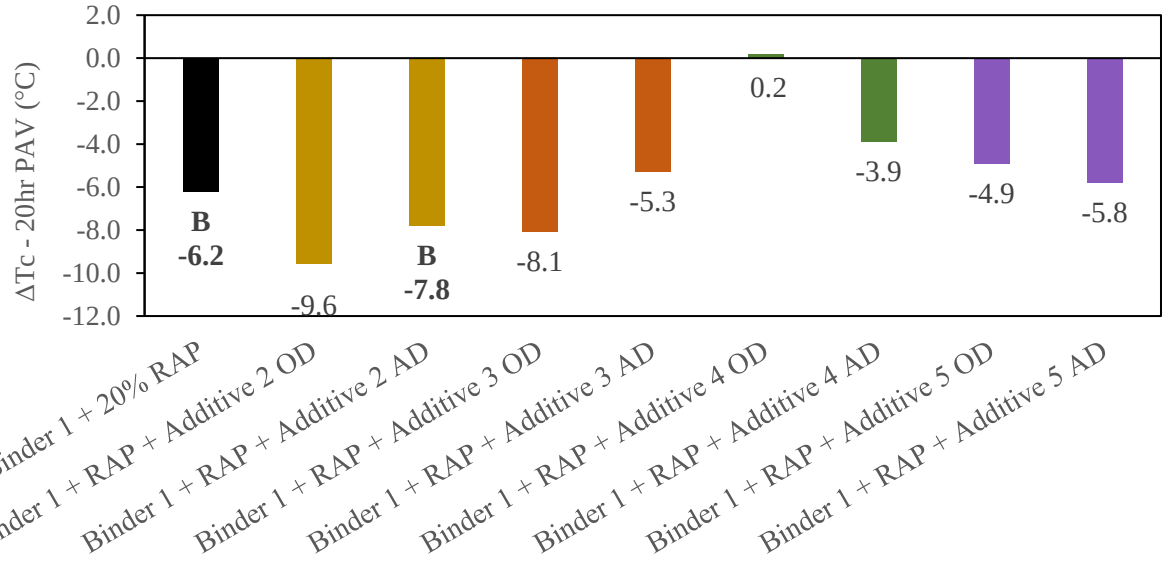

Figure 49. ΔTc for Binder 1 with RAP – RTFO + 20 hours PAV

No significant improvements were observed in ΔT_C of Binder 5 with RAP after 20 hours of PAV aging. Figure 50 shows Additive 2 reduced ΔT_C, and no significant differences were observed for the remaining materials. Thus, after 20 hours of PAV aging, durability of the control blend did not increase with these technologies. Testing ΔT_C after 60 hours of PAV will be useful to determine if modification has more significant effects after prolonged aging cycles which have not been captured at this stage.

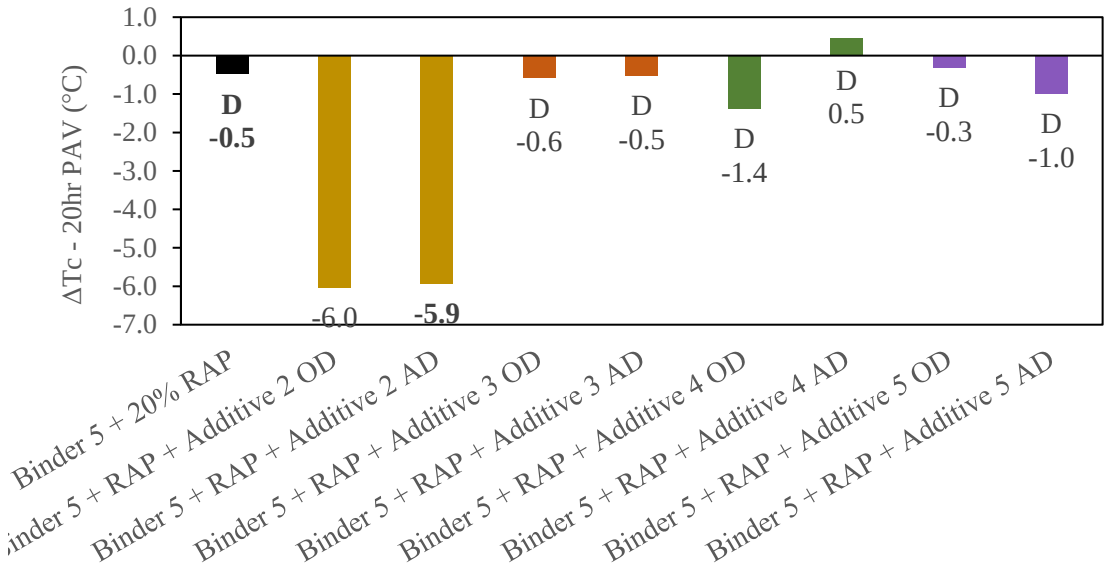

Figure 50. ΔTc for Binder 5 with RAP – RTFO + 20 hours PAV

d. Low Temperature Evaluation Using 4-mm DSR Approach

The considerably high stiffnesses of some modified binders after 60 hours of PAV aging caused difficulties when preparing beams for BBR testing. Therefore, as previously explained, the low temperature analysis for neat binders was divided between BBR and DSR evaluation. Additives 1 and 3, as well as the control binders were evaluated through DSR testing with 4 mm-diameter plates, following WRI recommendations (Sui et al., 2011) in terms of test procedure and conversions to BBR data. Low critical temperatures and ΔT_C after 20 hours of PAV aging are shown in TABLE 22.

TABLE 22. Critical Temperatures and ΔTc for RTFO + 20-Hour PAV Using DSR Testing

	Tc,S (°C)	Tc,m (°C)	True LT (°C)	ΔTc (°C)
Binder 1	-29.7	-26.6	-26.6	-3.1
Binder 1 + Additive 1 OD	-31.7	-29.9	-29.9	-1.8
Binder 1 + Additive 1 AD	-32.3	-31.2	-31.2	-1.1
Binder 1 + Additive 3	-32.2	-29.0	-29.0	-3.2
Binder 5	-32.3	-31.8	-31.8	-0.5
Binder 5 + Additive 1 OD	-32.2	-30.6	-30.6	-1.6
Binder 5 + Additive 1 AD	-33.1	-31.9	-31.9	-1.2
Binder 5 + Additive 3	-43.9	-40.4	-40.4	-3.6

It should first be noted that the correlation used for analysis yielded differences in low critical temperatures with respect to BBR measurements, resulting on colder temperatures when the DSR approach was used. For example, Binder 1 showed a Tc_S of -29.7 °C and Tc_m of -26.6 °C from DSR measurements, while BBR testing indicated -26.1 °C and -19.9 °C, respectively. Such a difference would cause Binder 1 to reduce its low PG from a -16 to a -22. Binder 5 showed a similar behavior, where DSR testing resulted in Tc_S of -32.3 °C and Tc_m of -31.8 °C, lower than low critical temperatures of -28.4 °C and -28.8 °C for stiffness and creep rate, respectively as determined through BBR testing. This finding supports the decision of testing not only the control but also the 20-hour PAV materials on the DSR, even though beam preparation was only unfeasible for the heavily aged materials. A more reliable comparison of additive performance would be obtained from the evaluation of every material under equal testing procedures.

Low temperature true grade after 20 hours of PAV aging is shown in Figure 51 for Binder 1 and Figure 52 for Binder 5. Improvements on low temperature properties were found for Binder 1, where both additives caused a reduction in true grade, therefore increasing binder resistance to thermal stresses. Reductions in low temperature true grade of Binder 5 were given by Additive 3, thus improving thermal cracking resistance. On the other hand, Additive 1 caused little to no improvement in low temperature performance, showing reduced effectiveness with his base binder.

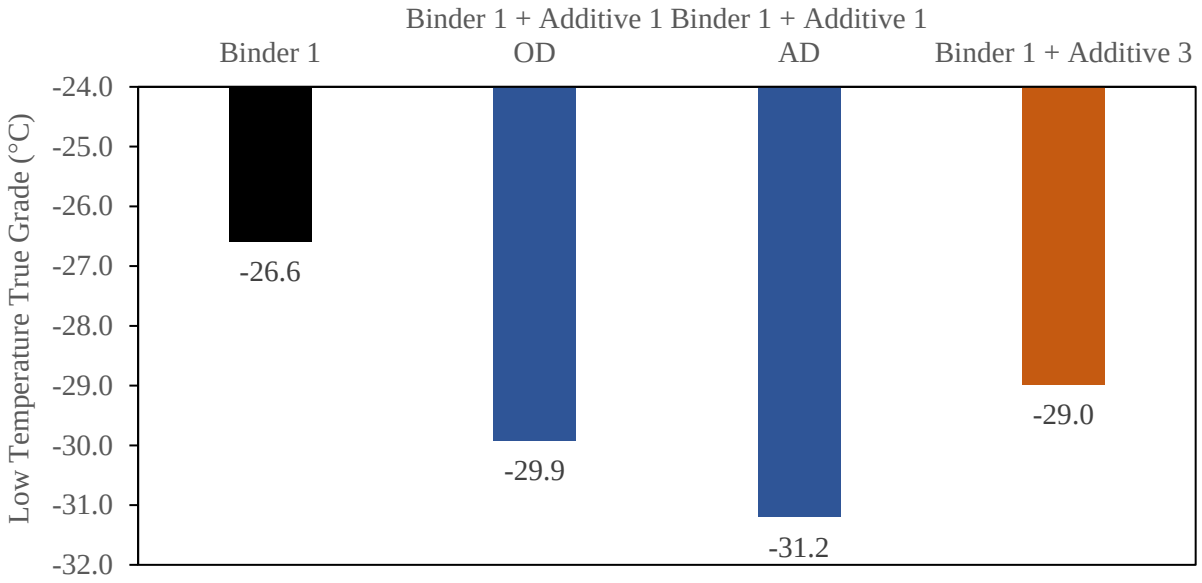

Figure 51. Low temperature true grade (RTFO+20hr PAV) for Binder 1 using DSR approach

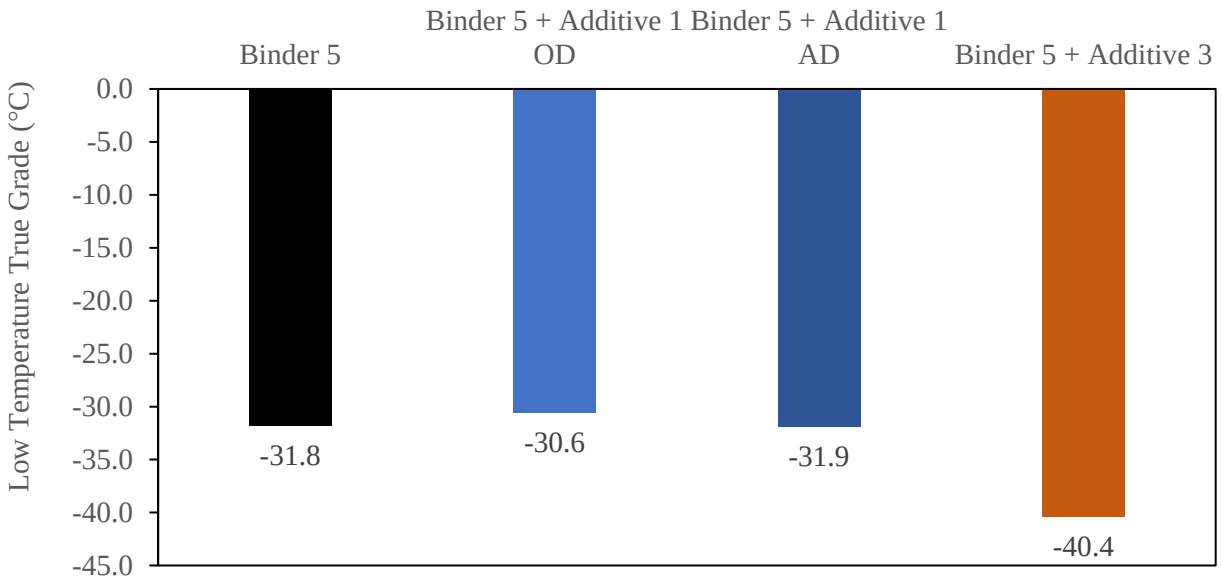

Figure 52. Low temperature true grade (RTFO+20hr PAV) for Binder 5 using DSR approach

Furthermore, ΔT_C was calculated at this aging condition, to assess any improvements in ductility of modified binders. Figure 53 and Figure 54 show results for Binder 1 and Binder 5, respectively.While Additive 1 resulted on more positive values for ΔT_C, therefore improving relaxation properties of Binder 1, Additive 3 showed a slighlty more negative value. Therefore, although modification shifted the critical temperatures to colder ranges, binder ductility did not see an equal improvement.

In terms of Binder 5, no improvements on ΔT_C were observed for any additive. Reduced effectiveness was observed for Additive 1, which shifted ΔT_C to more negative values. Additive 3 showed comparable effects on Binder 1 and 5. Although critical temperatures were shifted to more negative values, which is favorable, ΔT_C resulted on more negative values than both control binders, which would indicate a reduction in binder ductility.

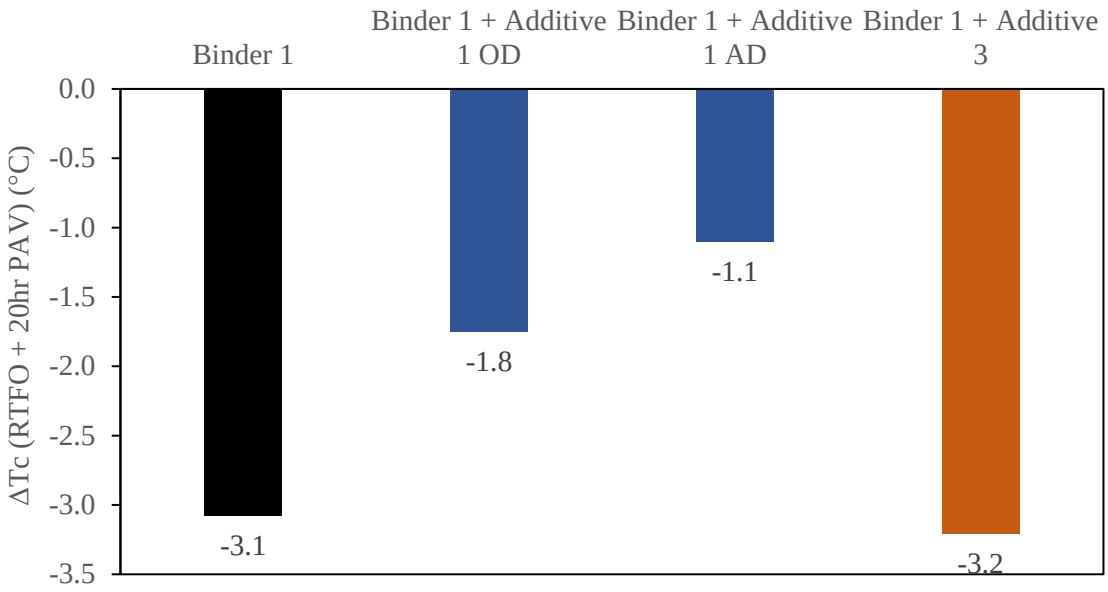

Figure 53. ΔTc after RTFO + 20-hour PAV for Binder 1 using DSR approach

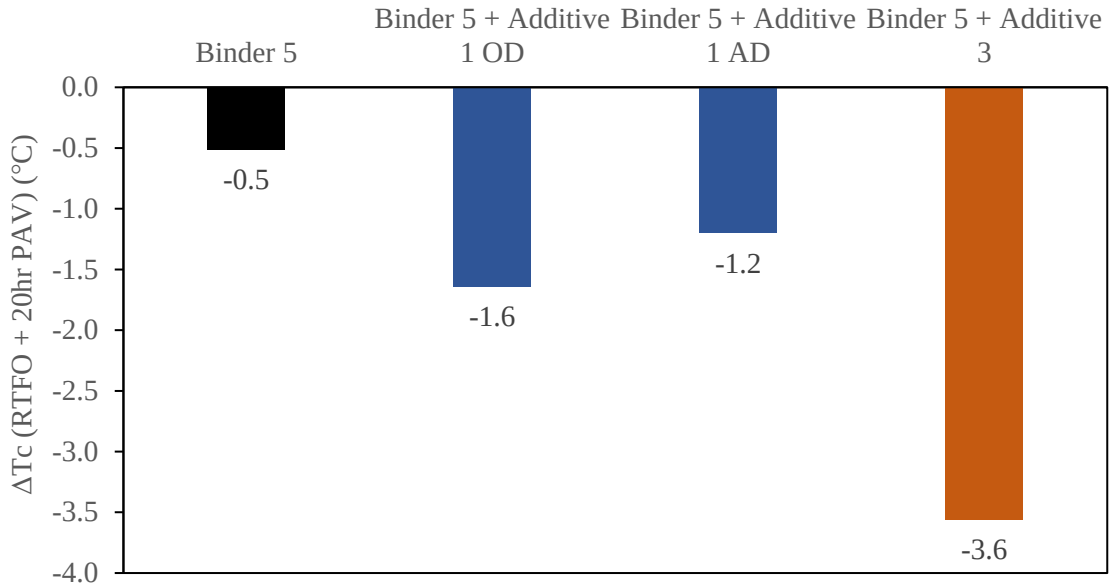

Figure 54. ΔTc after RTFO + 20-hour PAV for Binder 5 using DSR approach

4.2.2 Superpave Performance Grading after RTFO plus 60 hours PAV

PG grading was also performed on every material after the aging protocol of RTFO plus 60-hour PAV. In this case, all binders were treated "as is". In other words, high temperature DSR testing followed the unaged criterion of $G^*/\sin\delta \leq 1.00kPa$ at a 12% strain level and 10 rad/s, and no RTFO aging followed. PG testing at intermediate- and low-temperature was performed without additional PAV aging.

Superpave PG of base binders, recycled binder blends and modified binders at both aging conditions (i.e., after RTFO plus 20 and 60 hours of PAV aging) are presented in TABLE 23 through

TABLE 28. Binders characterized for low PG of binders through DSR testing are detailed separately for comparison. A detailed discussion on the changes in high-, intermediate- and low-temperature PG after extended aging will follow.

TABLE 23. PG of Base Binder 1 and Modified Blends – Unaged and RTFO + 20 and 60 Hours of PAV Aging (BBR Measurements)

		Superpave Continuous True Grades (°C)							
Asphalt Sample	**PAV Cycle**	T_{cont} High Original	T_{cont} High RTFO	T_{cont} Intermediate	T_{cont} Low S	T_{cont} Low m-value	$\triangle T_c$ (°C)	PG HT	PG LT
Binder 1	20-hour	65.7	66.6	25.0	-26.1	-19.9	-6.2	64	-16
	60-hour	100.7		30.2	-24.4	-9.7	-14.7		-4
Binder 1 + Additive 2 OD	20-hour	85.1	85.4	24.2	-27.2	-18.7	-8.5	82	-16
	60-hour	112.5		27.9	-26.7	-11.9	-14.8		-10
Binder 1 + Additive 4 OD	20-hour	57.3	57.6	17.0	-30.8	-28.7	-2.1	52	-28
	60-hour	89.5		23.0	-28.8	-22	-6.8		-22
Binder 1 + Additive 5 OD	20-hour	65.4	65.1	18.9	-31	-27.3	-3.7	64	-22
	60-hour	98.4		24.1	-28.9	-16.9	-12.1		-16

TABLE 24. PG of Base Binder 1 and Modified Blends - Unaged and RTFO + 20 and 60 Hours of PAV Aging (DSR measurements)

		Superpave Continuous True Grades (°C)							
Asphalt Sample	**PAV Cycle**	T_{cont} High Original	T_{cont} High RTFO	T_{cont} Intermediate	T_{cont} Low S	T_{cont} Low m-value	$\triangle T_c$ (°C)	PG HT	PG LT
Binder 1	20-hour	65.7	66.6	25.0	-29.7	-26.6	-3.1	64	-22
	60-hour	100.7		30.2	-29.6	-16.3	-13.3		-16
Binder 1 + Additive 1 OD	20-hour	70.5	68.5	22.8	-31.7	-29.9	-1.8	64	-28
	60-hour	95.6		26.1	-32	-27.1	-4.9		-22
Binder 1 + Additive 1 AD	20-hour	70.6	68.7	24.8	-32.3	-31.2	-1.1	64	-28
	60-hour	94.5		24.8	-31.2	-27.8	-3.4		-22
Binder 1 + Additive 3 OD	20-hour	102.2	93.6	20.7	-32.2	-29	-3.2	88	-28
	60-hour	126.0		24.7	-31.5	-23.2	-8.3		-22

TABLE 25. PG of Base Binder 5 and Modified Blends - Unaged, RTFO + 20 and 60 Hours of PAV Aging (BBR Measurements)

		Superpave Continuous True Grades (°C)							
Asphalt Sample	**PAV Cycle**	T_{cont} High Original	T_{cont} High RTFO	T_{cont} Intermediate	T_{cont} Low S	T_{cont} Low m-value	$\triangle T_c$ (°C)	PG HT	PG LT
Binder 5	20-hour	65.6	67.4	20.8	-28.4	-28.8	0.4	64	-28
	60-hour	103.4		25.2	-26.5	-22.7	-3.8		-22
Binder 5 + Additive 2 OD	20-hour	85.3	88.9	22.1	-28	-23.4	-4.6	82	-22
	60-hour	121.7		24.0	-27.7	-18.5	-9.2		-16
Binder 5 + Additive 4 OD	20-hour	56.9	57.2	12.1	-34.2	-36	1.9	52	-34
	60-hour	94.5		19.2	-31.6	-28.8	-2.9		-28
Binder 5 + Additive 5 OD	20-hour	64.9	65.7	15.1	-34.1	-33.8	-0.3	64	-28
	60-hour	103.2		20.1	-31.3	-28.6	-2.7		-28

TABLE 26. PG of Base Binder 5 and Modified Blends - Unaged, RTFO + 20 and 60 hours of PAV Aging (DSR measurements)

		Superpave Continuous True Grades (°C)							
Asphalt Sample	**PAV Cycle**	T_{cont} High Original	T_{cont} High RTFO	T_{cont} Intermediate	T_{cont} Low S	T_{cont} Low m-value	$\triangle T_c$ (°C)	PG HT	PG LT
Binder 5	20-hour	65.6	67.4	20.8	-32.3	-31.8	-0.5	64	-28
	60-hour	103.4		25.2	-32.9	-27.3	-5.6		-22
Binder 5 + Additive 1 OD	20-hour	78.6	76.8	22.7	-32.2	-30.6	-1.6	76	-28
	60-hour	122.4		27.6	-31	-25.6	-5.4		-22
Binder 5 + Additive 1 AD	20-hour	79	77.4	23.2	-33.1	-31.9	-1.2	76	-28
	60-hour	127.4		28.1	-31.9	-24.8	-7.1		-22
Binder 5 + Additive 3 OD	20-hour	97.2	95.8	12.3	-43.9	-40.4	-3.5	94	-40
	60-hour	136.3		17.8	-28.4	-24.1	-4.3		-22

TABLE 27. PG of Binder 1 Blends with 20% RAP and Modified Blends - Unaged, RTFO + 20 and 60 Hours of PAV Aging

		Superpave Continuous True Grades (°C)							
Asphalt Sample	**PAV Cycle**	T_{cont} High Original	T_{cont} High RTFO	T_{cont} Intermediate	T_{cont} Low S	T_{cont} Low m-value	$\triangle T_c$ (°C)	PG HT	PG LT
Binder 1 + RAP	20-hour	73.4	73.2	27.1	-24.9	-18.7	-6.2	70	-16
	60-hour	105.7		28.9	-23.4	-8	-15.4		-4
Binder 1 + RAP + Additive 2 OD	20-hour	89.9	88.9	21.6	-29.7	-20.1	-9.6	88	-16
	60-hour	114.3		27.9	-28.9	-12.8	-16.1		-10
Binder 1 + RAP + Additive 2 AD	20-hour	86.7	85.3	22.9	-27.8	-20	-7.8	82	-16
	60-hour	112.5		26.7	-27.6	-12.2	-15.4		-10
Binder 1 + RAP + Additive 3 OD	20-hour	100.7	95.2	21.5	-27.7	-19.6	-8.1	94	-16
	60-hour	126		29.4	-26.6	-11	-15.6		-10
Binder 1 + RAP + Additive 3 AD	20-hour	95.5	89.8	18.1	-30.6	-25.3	-5.3	88	-22
	60-hour	120.6		25.7	-29.3	-16.7	-12.6		-16
Binder 1 + RAP + Additive 4 OD	20-hour	67	67.0	18.1	-30.3	-30.5	0.2	64	-28
	60-hour	98.2		25.0	-28	-21.5	-6.5		-16
Binder 1 + RAP + Additive 4 AD	20-hour	65.6	65.9	20.2	-28.8	-24.8	-3.9	64	-22
	60-hour	95.8		26.6	-26.3	-16.2	-10		-16
Binder 1 + RAP + Additive 5 OD	20-hour	75.5	75.3	23.4	-27.7	-22.7	-4.9	70	-22
	60-hour	107.1		29.3	-25.3	-12.5	-12.8		-10
Binder 1 + RAP + Additive 5 AD	20-hour	74.9	75.2	25.0	-27.1	-21.4	-5.8	70	-16
	60-hour	105.1		29.7	-25	-12	-13		-10

TABLE 28. PG of Binder 5 Blends with 20% RAP and Modified Blends - Unaged, RTFO + 20 and 60 Hours of PAV Aging

		Superpave Continuous True Grades (°C)							
Asphalt Sample	**PAV Cycle**	T_{cont} High Original	T_{cont} High RTFO	T_{cont} Intermediate	T_{cont} Low S	T_{cont} Low m-value	$\triangle T_c$ (°C)	PG HT	PG LT
Binder 5 + RAP	20-hour	73.1	74.6	23.8	-26.2	-25.7	-0.5	70	-22
	60-hour	110.5		31.8	-24.7	-17	-7.7		-16
Binder 5 + RAP + Additive 2 OD	20-hour	89.4	90.3	20.7	-30	-24	-6	88	-22
	60-hour	122.4		24.2	-27.2	-18.2	-9		-16
Binder 5 + RAP + Additive 2 AD	20-hour	91.2	90.4	19.5	-30.6	-24.7	-5.9	88	-22
	60-hour	127.1		23.2	-29.8	-17.7	-12.1		-16
Binder 5 + RAP + Additive 3 OD	20-hour	98.4	95.4	16.4	-34.2	-33.6	-0.6	94	-28
	60-hour	161		20.9	-33	-26	-7		-22
Binder 5 + RAP + Additive 3 AD	20-hour	102.8	97.4	18.9	-31.6	-31.1	-0.5	94	-28
	60-hour	153.6		23.6	-30.6	-24.5	-6.1		-22
Binder 5 + RAP + Additive 4 OD	20-hour	66.6	66.3	18.4	-31.1	-29.7	-1.4	64	-28
	60-hour	101.4		23.6	-28.7	-23.3	-5.4		-22
Binder 5 + RAP + Additive 4 AD	20-hour	67.7	67.5	18.1	-30.4	-30.8	0.5	64	-28
	60-hour	101.5		24.7	-28.7	-24.8	-3.9		-22
Binder 5 + RAP + Additive 5 OD	20-hour	75.3	75.4	20.0	-30.5	-30.2	-0.3	70	-28
	60-hour	110.8		24.6	-27.9	-22.9	-5		-22
Binder 5 + RAP + Additive 5 AD	20-hour	76.8	76.4	21.8	-29.4	-28.4	-1	76	-28
	60-hour	110.1		26.9	-26.8	-20.4	-6.4		-16

a. High Temperature Evaluation

High temperature properties were also evaluated after RTFO followed by 60 hours of PAV aging, to determine additive performance after an extended aging cycle. The continuous high temperature true grades were obtained by DSR testing with every binder considered "as is" and are presented in TABLE 29 for neat binders.

TABLE 29. High Temperature True Grade (RTFO + 60 Hr PAV) - Without RAP

	HT True grade (RTFO + 60 hr PAV) (℃)
Binder 1	100.7
Binder 1 + Additive 1 OD	95.6
Binder 1 + Additive 1 AD	94.5
Binder 1 + Additive 2	112.5
Binder 1 + Additive 3	126.0
Binder 1 + Additive 4	89.5
Binder 1 + Additive 5	98.4
Binder 5	103.4
Binder 5 + Additive 1 OD	122.4
Binder 5 + Additive 1 AD	127.4
Binder 5 + Additive 2	121.7
Binder 5 + Additive 3	136.3
Binder 5 + Additive 4	94.5
Binder 5 + Additive 5	103.2

The increase in high temperature true grade was studied to evaluate the stiffening effects of aging on all binders. Smaller increases in high temperature true grade could indicate that additives decreased the stiffening rate of control binders, therefore reducing their aging susceptibility. Figure 55 for Binder 1 shows lower stiffening rates for most additives, therefore the effects of aging on binder stiffness were successfully mitigated. An ANOVA analysis followed by Tukey pairings was conducted on the difference in high temperature true grade of each replicate measurement, at a significance level of 95%. Each control binder was assigned a letter to indicate a statistical group, and Figure 55 indicates Additive 5 belonged to the same statistical group and therefore caused no significant difference relative to the control.

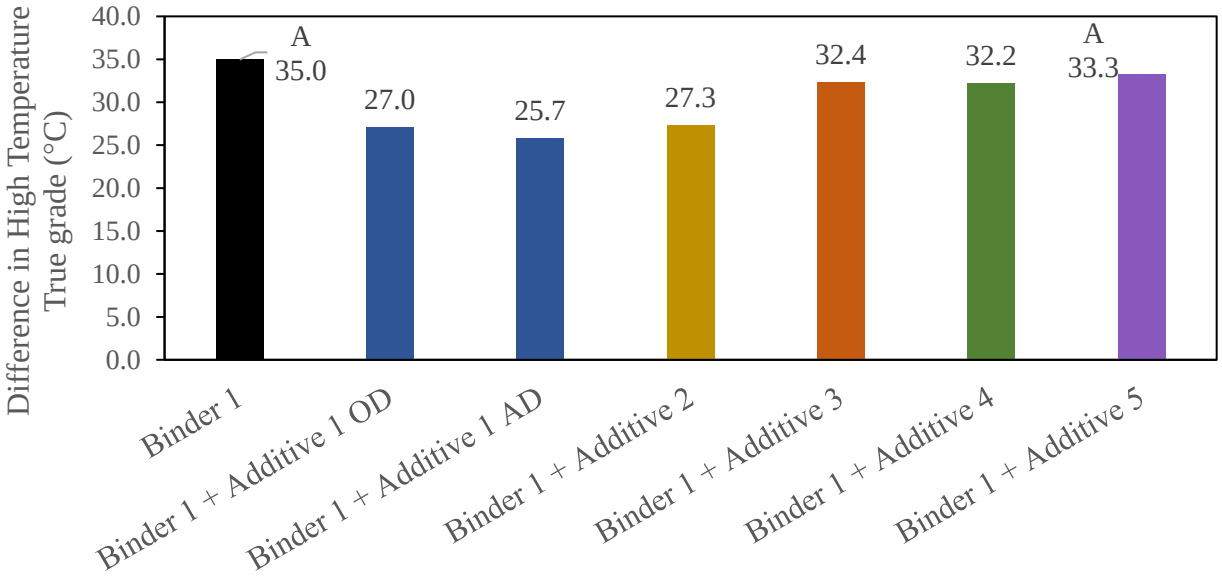

Figure 55. Difference In High Temperature True Grade (RTFO+60hr PAV – Unaged) - Binder 1

Binder 5, on the other hand, saw no reduction on the stiffening effects of aging from the evaluated additives. While no significant differences were observed for Additives 2, 4 and 5, Additives 1 and 3 resulted on greater increases in high temperature true grade, as shown in Figure 56.

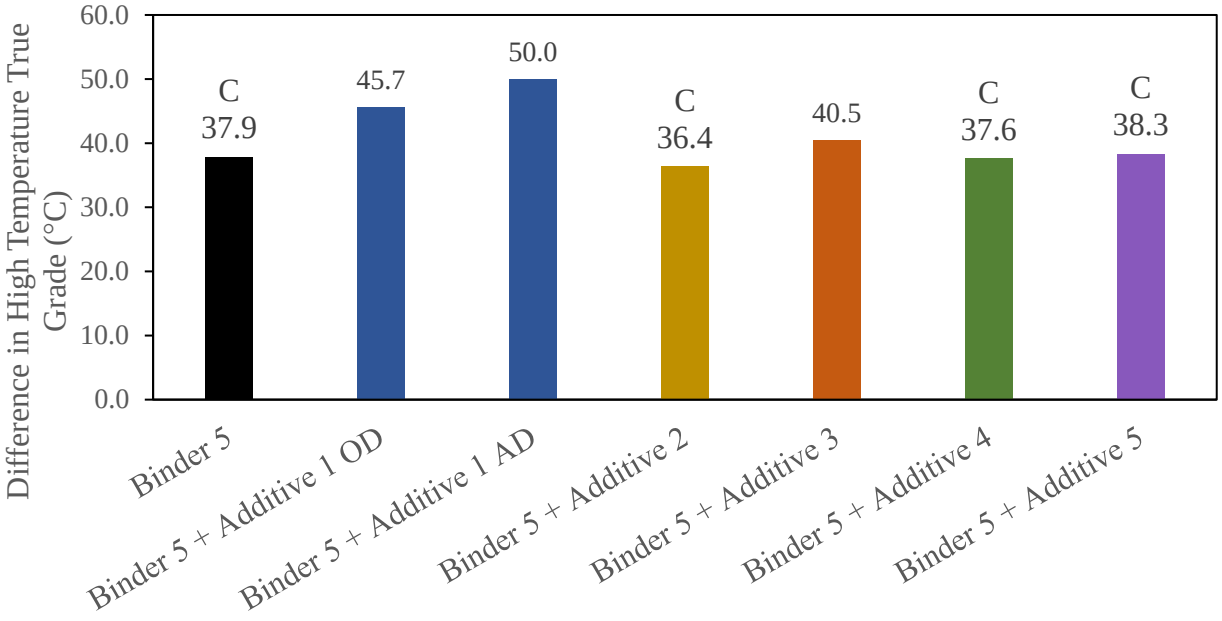

Figure 56. Difference In High Temperature True Grade (RTFO+60hr PAV – Unaged) - Binder 5

Therefore, the stiffening effect of aging was more effectively mitigated for Binder 1. Additives have shown varying effectiveness when interacting with different base binders, which has previously been reported in the literature (Apostolidis et al., 2020; Elkashef & Williams, 2017).

The high temperature true grade of recycled binder blends is detailed in TABLE 30. The changes between the unaged condition and 60 hours of PAV aging were also evaluated to determine the stiffening rates of modified binders and are shown in Figure 57 and Figure 58.

TABLE 30. Continuous High Temperature True Grade (RTFO + 60 Hr PAV) - With RAP

	HT True grade (RTFO + 60 hr PAV) (℃)
Binder 1 + RAP	105.7
Binder 1 + RAP + Ad 2 OD	114.3
Binder 1 + RAP + Ad 2 AD	112.5
Binder 1 + RAP + Ad 3 OD	161.0
Binder 1 + RAP + Ad 3 AD	153.6
Binder 1 + RAP + Ad 4 OD	98.2
Binder 1 + RAP + Ad 4 AD	95.8
Binder 1 + RAP + Ad 5 OD	107.1
Binder 1 + RAP + Ad 5 AD	105.1
Binder 5 + RAP	110.5
Binder 5 + RAP + Ad 2 OD	122.4
Binder 5 + RAP + Ad 2 AD	127.1
Binder 5 + RAP + Ad 3 OD	126
Binder 5 + RAP + Ad 3 AD	120.6
Binder 5 + RAP + Ad 4 OD	101.4
Binder 5 + RAP + Ad 4 AD	101.5
Binder 5 + RAP + Ad 5 OD	110.8
Binder 5 + RAP + Ad 5 AD	110.1

A reduction of the stiffening rate of Binder 1 RAP blends was achieved by Additive 2, and Additives 4 and 5 at their alternative dosages. Overall, no statistically significant results were observed fo Additive 3. The changes in continuous high temperature true grade have shown that, regardless of the effects on the unaged properties, additives reduced the stiffening effects of aging on RAP blends with Binder 1. The stiffening rate of Binder 5 with RAP was reduced by Additive 2 at the optimum dosage, and Additive 4 and 5 at the alternative dosage, as shown by Figure 58. Additive 3, however, presented higher stiffening rates than the control.

Overall, aging susceptibility at high temperatures was decreased by Additive 2 at both dosages for Binder 1 and the optimum dosage for Binder 5, and the alternative dosage of Additive 4 and 5 (with respect to both RAP blends). Additive 3 showed no statistical difference with Binder 1 and presented higher rates for Binder 5. It is worth noting that each additive caused different effects at the unaged condition: Additive 2 increased the high temperature PG, while Additive 4 acted as a softener, and Additive 5 did not change the high temperature PG. Despite of their varying effects at the unaged condition, given by their diverse nature, these additives reduced the high temperature aging susceptibility of the control RAP blends with varying effectiveness for Binder 1 and Binder 5.

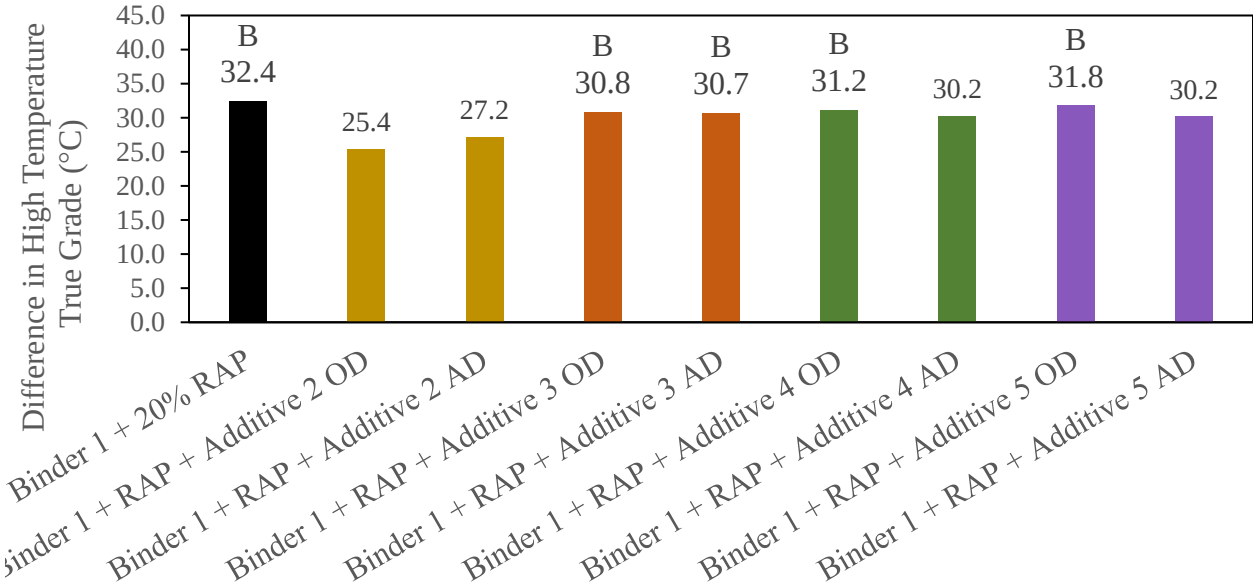

Figure 57. Difference In High Temperature True Grade (RTFO+60hr PAV – Unaged) - Binder 1+RAP

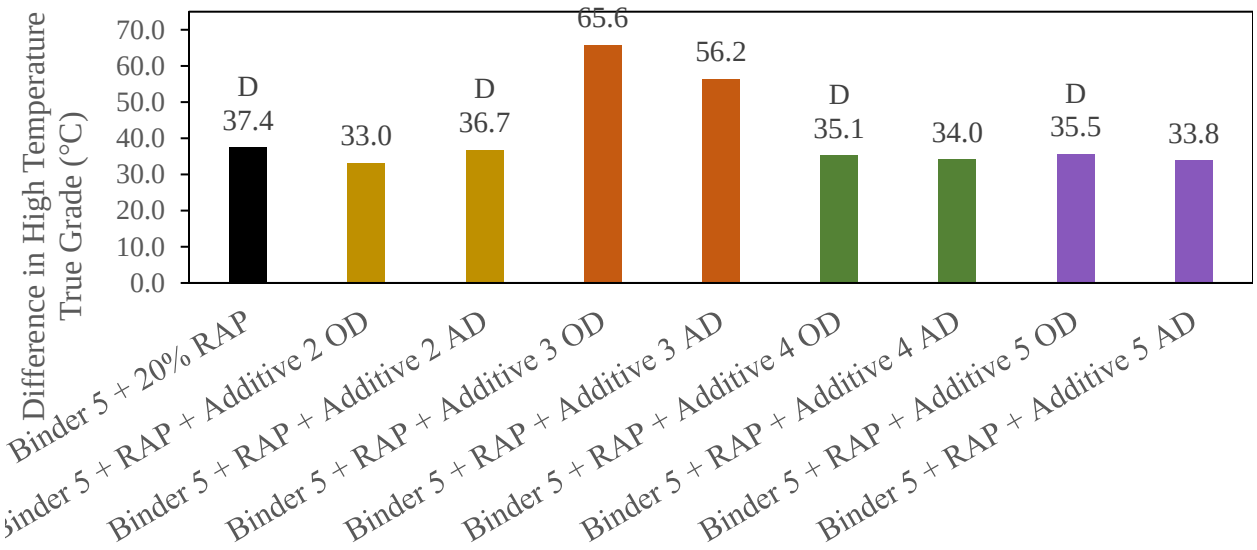

Figure 58. Difference In High Temperature True Grade (RTFO+60hr PAV – Unaged) - Binder 5+RAP

b. Intermediate Temperature Evaluation

All binders were tested for fatigue performance after RTFO plus 60 hours of PAV aging, considering the material "as is". Thus, the fatigue criterion of $G^* \sin\delta \leq 5{,}000\, kPa$ was followed to determine true intermediate temperatures after extended aging cycles.

A significant reduction in intermediate temperature for every additive was found with respect to the Binder 1, as shown in Figure 59. Therefore, modification appears to improve fatigue resistance after RTFO plus 60 hours of PAV aging. As noted in Section 4.2.1, fatigue characterization following AASHTO M320 has presented limitations, so fatigue resistance was further evaluated using LAS after 60 hours of PAV aging.

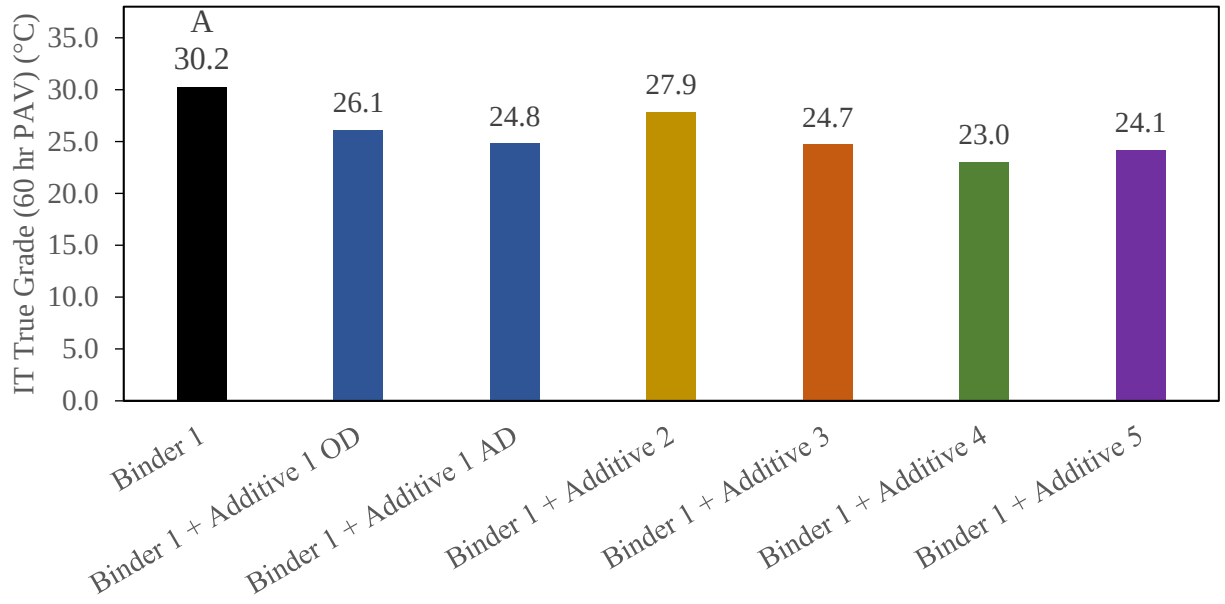

Figure 59. Intermediate Temperature True Grade (RTFO + 60hr PAV) - Binder 1

Modification of Binder 5 shows improved fatigue performance for Additives 2, 3, 4 and 5, as indicated by Figure 60. On the other hand, higher intermediate temperatures were found for Additive 1, which may suggest poorer fatigue resistance relative to the control. As with previous results, additives display varying effectiveness with each base binder.

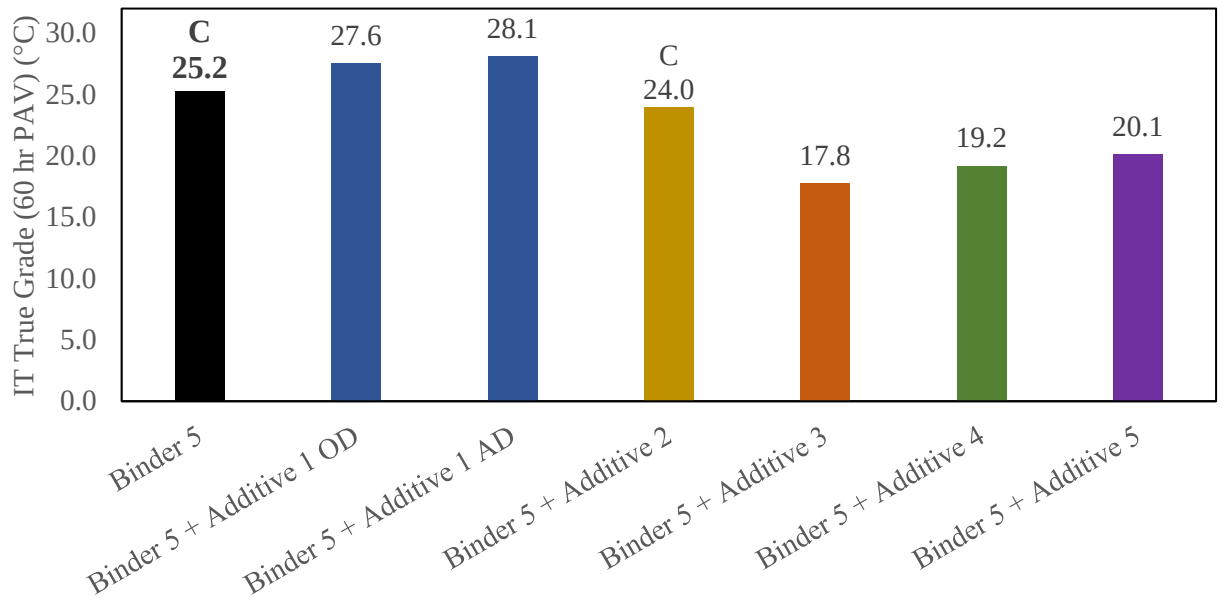

Figure 60. Intermediate Temperature True Grade (RTFO + 60hr PAV) - Binder 5

Fatigue evaluation of Binder 1 with RAP was performed after 60 hours of PAV aging, and improvements were observed for Additive 4 and the alternative dosage of Additives 2 and 3, shown by the reduction in intermediate temperatures. Additive 5, on the other hand, caused no significant differences relative to the control. On the other hand, every additive reduced the intermediate temperature true grade of Binder 5 with RAP, as shown by Figure 62. Therefore, modifiers showed improved effectiveness on RAP blends containing RAP, and improved fatigue cracking resistance relative to the control after extended aging.

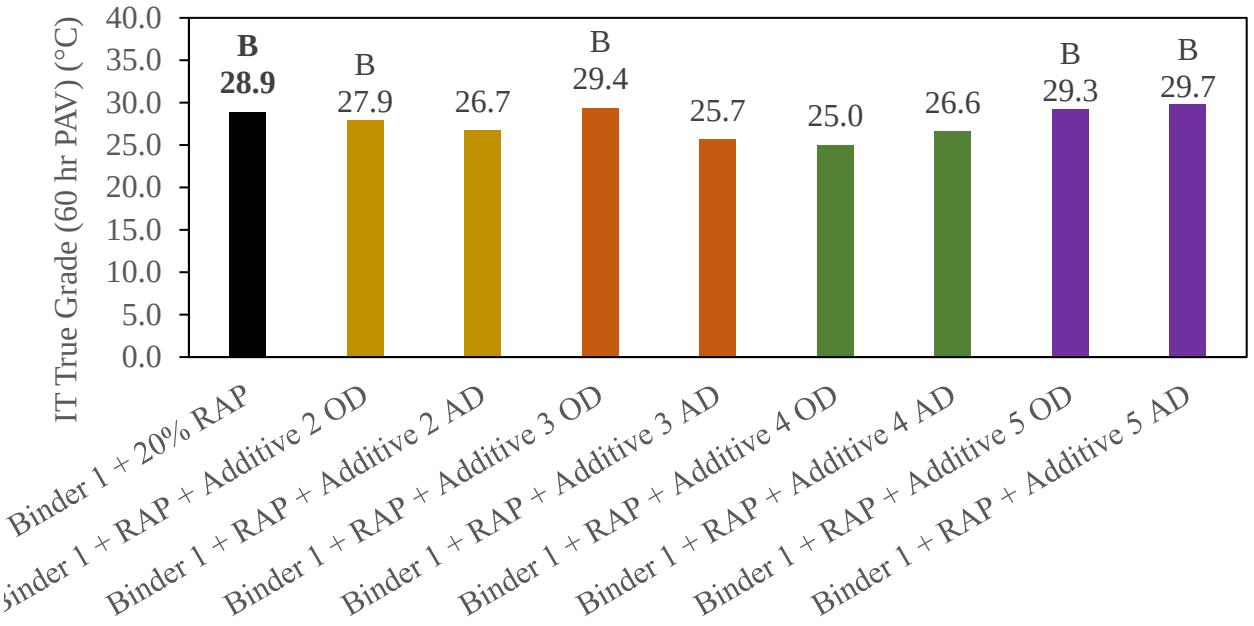

Figure 61. Intermediate Temperature True Grade (RTFO + 60hr PAV) - Binder 1 with RAP

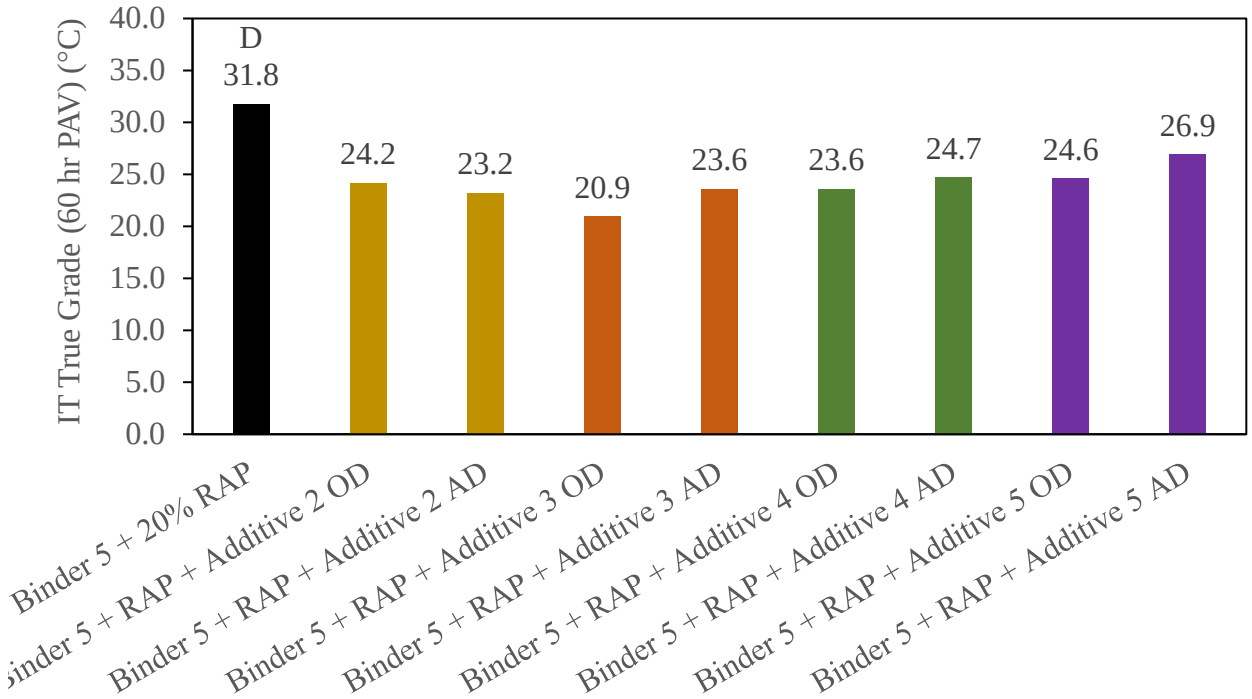

Figure 62. Intermediate Temperature True Grade (RTFO + 60hr PAV) - Binder 5 with RAP

c. Low Temperature Evaluation

As previously explained, low temperature analysis for 60 hours of PAV aging was performed separately using BBR and DSR testing, for binders without RAP. Thus, the present section will cover results for Additive 2, 4 and 5 whose properties were determined using BBR testing. Low critical temperatures and ΔT_C of neat and modified binders are presented in TABLE 31.

TABLE 31. Low Critical Temperatures and ΔTc - RTFO + 60hr PAV – Without RAP

	Tc, S (℃)	**Tc, m** (℃)	**LT True grade**(℃)	ΔT_c (℃)	**PG LT**
Binder 1	-24.4	-9.7	-9.7	-14.7	-4
Binder 1 + Additive 1 OD					
Binder 1 + Additive 1 AD					
Binder 1 + Additive 2	-26.7	-11.9	-11.9	-14.8	-10
Binder 1 + Additive 3					
Binder 1 + Additive 4	-28.8	-22.0	-22.0	-6.8	-22
Binder 1 + Additive 5	-28.9	-16.9	-16.9	-12.0	-16
Binder 5	-26.5	-22.7	-22.7	-3.8	-22
Binder 5 + Additive 1 OD					
Binder 5 + Additive 1 AD					
Binder 5 + Additive 2	-27.7	-18.5	-18.5	-9.2	-16
Binder 5 + Additive 3					
Binder 5 + Additive 4	-31.6	-28.8	-28.8	-2.8	-28
Binder 5 + Additive 5	-31.3	-28.6	-28.6	-2.7	-28

Every additive improved the low temperature properties of Binder 1, given by the reduction in low critical temperatures. Results showed that the low temperature PG of the control was shifted, by one, two and three grades by Additives 2, 5 and 4, respectively. Stiffness as well as m-value- based critical temperatures were reduced, thus enhancing binder thermal cracking resistance and relaxation properties.

Low temperature properties of Binder 5 were improved after modification with Additives 4 and 5, which shifted by one the low temperature PG of the control. Additive 2, despite improving binder stiffness at low temperatures, increased the m-value, which may be attributable to the nature of this modifier.

Furthermore, ΔT_C of Binder 1 improved (i.e., became more positive) with Additive 4 and 5, while Additive 2 showed no significant change, as shown in Figure 63. Therefore, Additives 4 and 5 increased ductility relative to the control, which favors resistance to age-related surface distresses. Binder 5, on the other hand, saw no significant improvements in ΔT_C, as indicated in Figure 64, despite improvements in low critical temperatures.

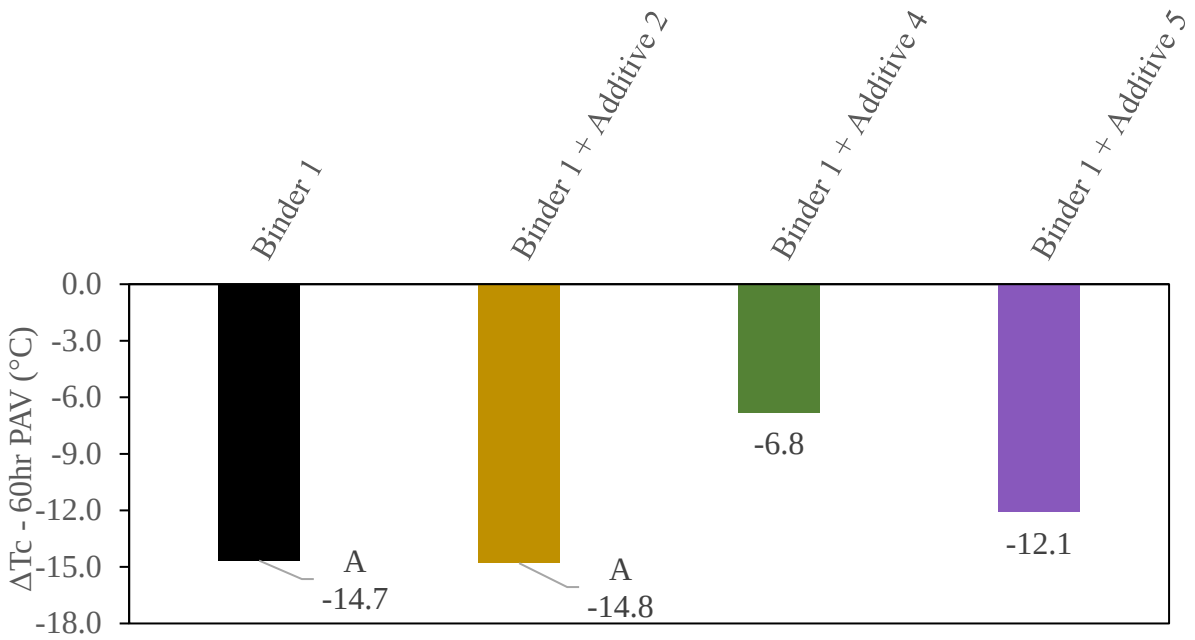

Figure 63. ΔTc - RTFO + 60hr PAV – Binder 1

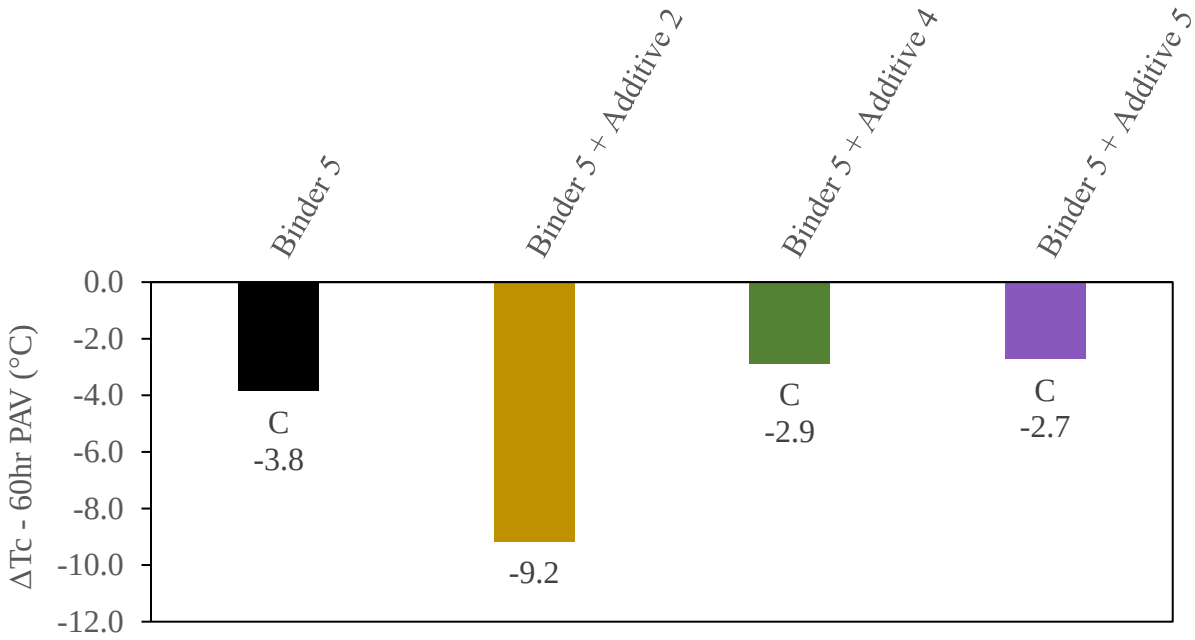

Figure 64. ΔTc - RTFO + 60hr PAV – Binder 5

Changes in low temperature properties between 20 and 60 hours of PAV aging were studied to investigate the loss in relaxation properties caused by aging. As aging durations increase low critical temperatures increase (i.e, become more positive) as binders become stiffer and more brittle. Thus, smaller increases in low temperature true grade with respect to the control would be indicative of lower aging susceptibility. The increase in low temperature true grade of Binder 1 was significantly reduced by Additives 2 and 4 as shown in Figure 65. It is worth noting how Additive 2 did not cause a significant reduction in low temperature true grade after 20 hours of PAV aging, but still caused a smaller increase than the control after extended aging. Therefore, Additive 2 resulted on a lower susceptibility to aging on the low temperature end. Conversely, Additive 5 improved low temperature properties at 20 hours of PAV aging, but experienced changes comparable to the control after extended aging. Therefore, Additive 5 did not improve the aging susceptibility at low temperatures.

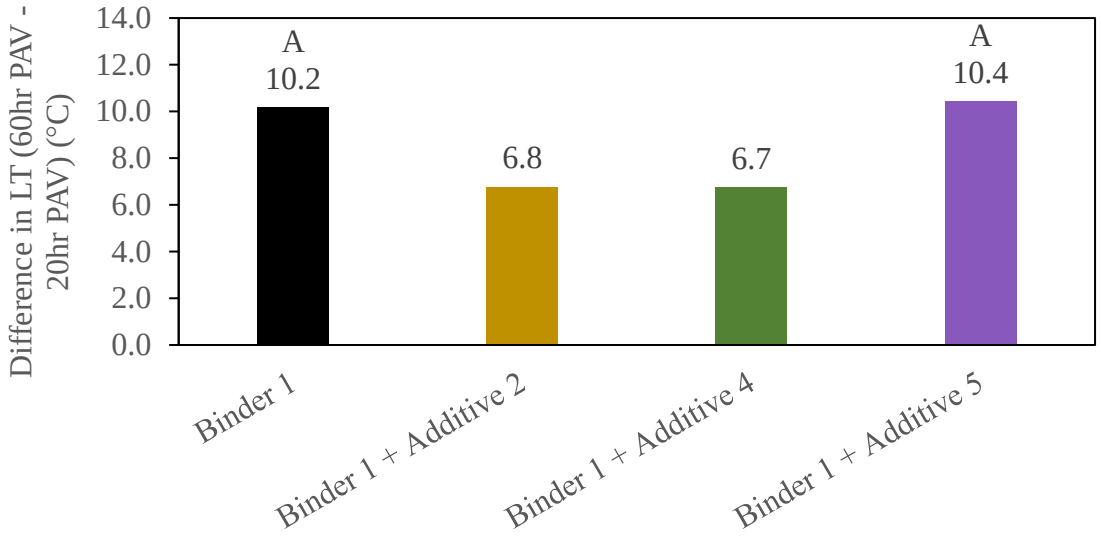

Figure 65. Difference in Low Temperature true Grade (60hr PAV - 20hr PAV) – Binder 1

The increase in low temperature true grade of Binder 5 shown in Figure 66, and no significant differences were observed between the control and modified binders. Therefore, the changes in low temperature properties occur at a comparable rate to the control, indicating no improvements in aging susceptibility relative to the base binder. However, Additives 4 and 5 resulted on lower critical temperatures than the control after aging, which would still indicate enhanced resistance to thermal stresses after extended aging.

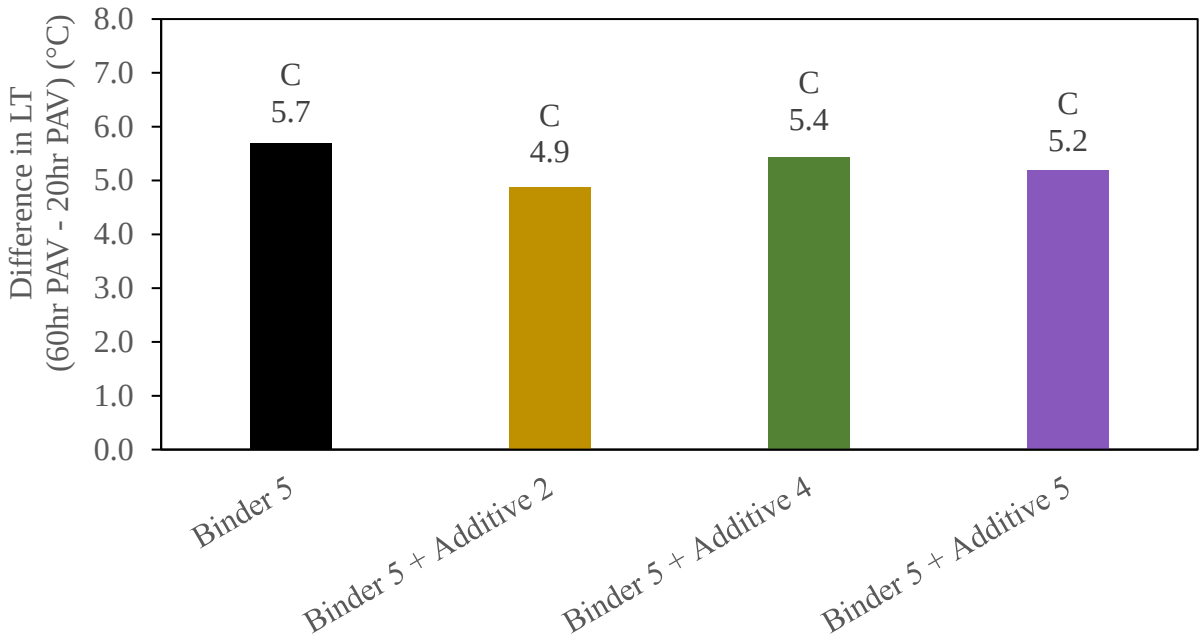

Figure 66. Difference in Low Temperature true Grade (60hr PAV - 20hr PAV) – Binder 5

The changes on ΔT_C were studied after 60 hours of PAV aging. As aging progresses ΔT_C would become more negative due to the loss in binder relaxation properties. Therefore, a smaller reduction in comparison to the control would indicate enhanced aging susceptibility. Additive 4 caused smaller increases in ΔT_C of Binder 1, while 2 and 5 did not provide significant improvements, as shown in Figure 67. Figure 68 shows the loss in ductility of Binder 5, as evaluated by the reduction in ΔT_C, was not mitigated by any of the additives.

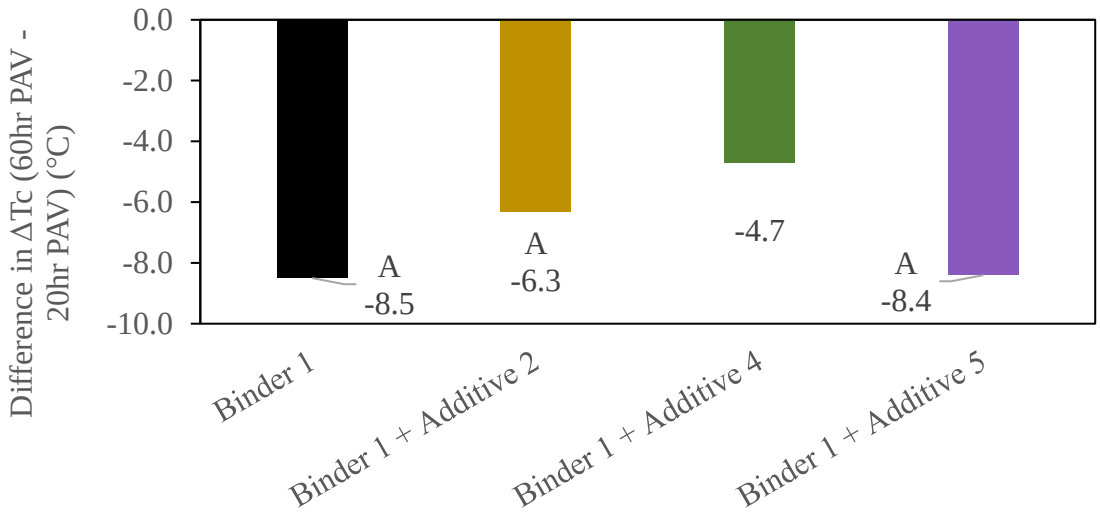

Figure 67. Difference in ΔTc for Binder 1 - (60hr PAV - 20 hr PAV)

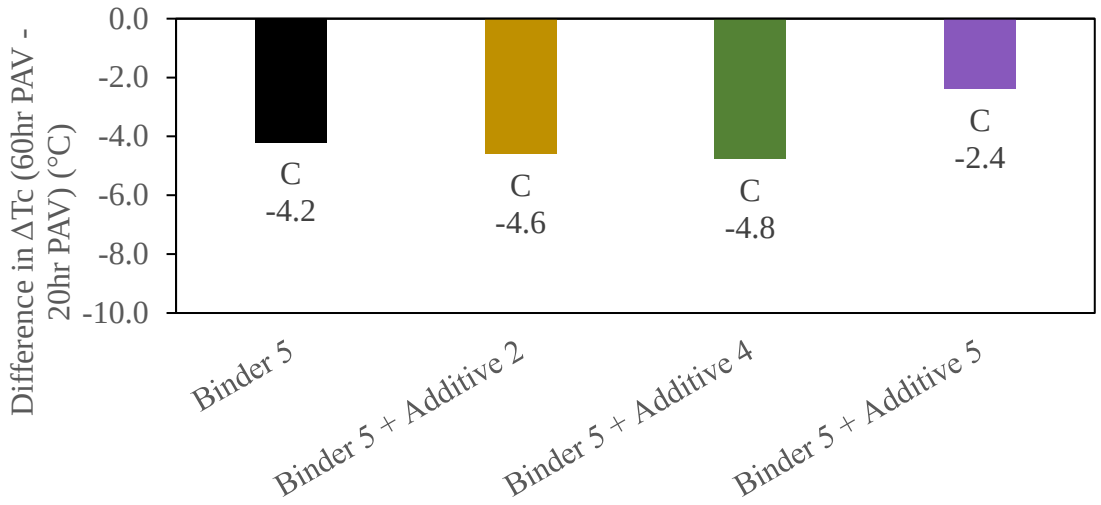

Figure 68. Difference in ΔTc for Binder 5 (60hr PAV - 20hr PAV)

Low critical temperatures and ΔT_c of recycled binder blends after RTFO plus 60 hours of PAV aging are presented in TABLE 32. Lower stiffness-based critical temperatures were observed for all additives (and dosages), which would indicate all additives reduced the embrittlement of binders at low temperatures. In addition, the m-value critical temperature of Binder 1 with RAP was reduced by all additives, indicating better relaxation properties after extended aging cycles. Overall, RAP blends with binder 1 showed a reduction of at least one grade on the low temperature end. On the other hand, additive effectiveness was reduced on Binder 5 with RAP: m-value critical temperature was increased by Additive 3, and Additive 2 reduced low temperature true grade, but not enough to reduce the low PG.

TABLE 32. Low Critical Temperatures and ΔTc - RTFO + 60hr PAV – with RAP

	Tc, S (℃)	**Tc, m** (℃)	**LT True grade**(℃)	ΔT_c (℃)	**PG LT**
Binder 1 + RAP	-23.4	-8.0	-8.0	-15.4	-4
Binder 1 + RAP + Ad 2 OD	-28.9	-12.8	-12.8	-16.1	-10
Binder 1 + RAP + Ad 2 AD	-27.6	-12.2	-12.2	-15.4	-10
Binder 1 + RAP + Ad 3 OD	-33.0	-26.0	-26.0	-7.0	-22
Binder 1 + RAP + Ad 3 AD	-30.6	-24.5	-24.5	-6.1	-22
Binder 1 + RAP + Ad 4 OD	-28.0	-21.5	-21.5	-6.5	-16
Binder 1 + RAP + Ad 4 AD	-26.3	-16.2	-16.2	-10.1	-16
Binder 1 + RAP + Ad 5 OD	-25.3	-12.5	-12.5	-12.8	-10
Binder 1 + RAP + Ad 5 AD	-25.0	-12.0	-12.0	-13.0	-10
Binder 5 + RAP	-24.7	-17	-17.0	-7.7	-16
Binder 5 + RAP + Ad 2 OD	-27.2	-18.2	-18.2	-9	-16
Binder 5 + RAP + Ad 2 AD	-29.8	-17.7	-17.7	-12.1	-16
Binder 5 + RAP + Ad 3 OD	-26.6	-11	-11	-15.6	-10
Binder 5 + RAP + Ad 3 AD	-29.3	-16.7	-16.7	-12.6	-16
Binder 5 + RAP + Ad 4 OD	-28.7	-23.3	-23.3	-5.4	-22
Binder 5 + RAP + Ad 4 AD	-28.7	-24.8	-24.8	-3.9	-22
Binder 5 + RAP + Ad 5 OD	-27.9	-22.9	-22.9	-5	-22
Binder 5 + RAP + Ad 5 AD	-26.8	-20.4	-20.4	-6.4	-16

RAP blends with Binder 1 showed more positive values of ΔT_C with Additives 3, 4 and 5, as shown in Figure 69. Thus, these additives effectively mitigated the loss in binder ductility due to aging. Additionally, TABLE 30 showed these additives reduced the low PG of recycled binder blends by as much as two grades, while simultaneously increasing ΔT_C. Therefore, they improved thermal cracking resistance and increased the ability of recycled binder blends to withstand age-related surface distresses. Additive 2, despite reducing continuous low temperature true grade did not cause a significant increase in ΔT_C.

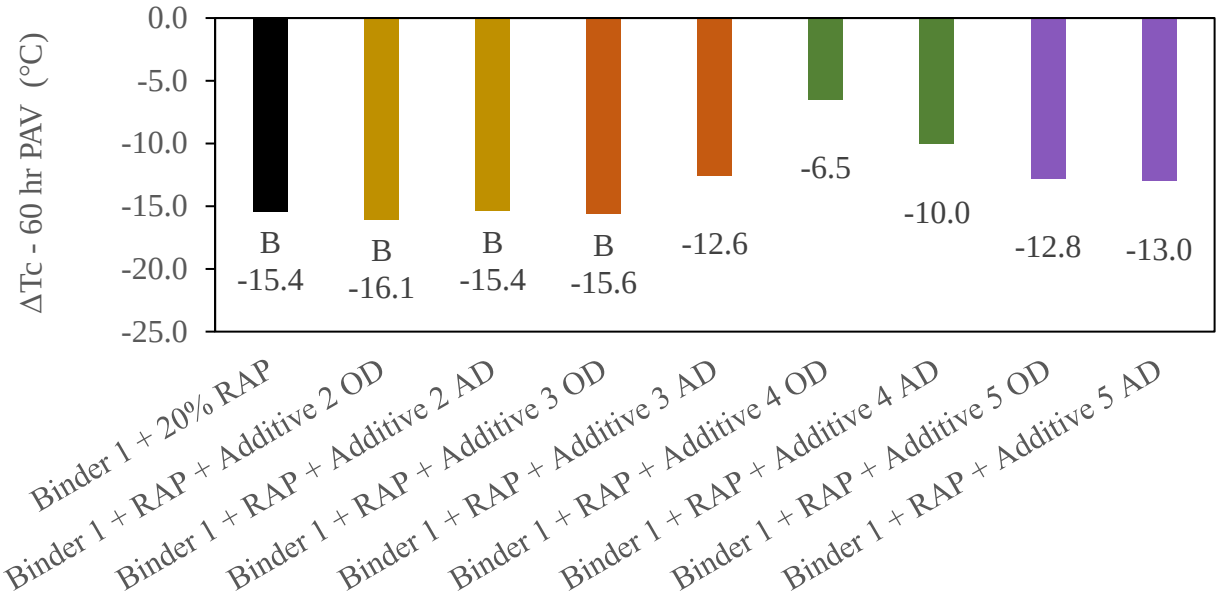

Figure 69. ΔTc (60hr PAV) - Binder 1 with RAP

Improvements in ΔT_C of recycled binder blends with binder 5 were also found for Additives 4 and 5 (at the optimum dosage), as shown by the more positive values of ΔT_C in Figure 70. Therefore, these modifiers enhanced durability of the control through a reduction in critical low temperatures but also from more positive values of ΔT_C, similarly to their effects on Binder 1 with RAP. On the other hand, only the alternative dosage of Additive 3 improved ΔT_C of recycled binder blends with Binder 5, thus showing less effectiveness than for recycled binder blends with Binder 1.

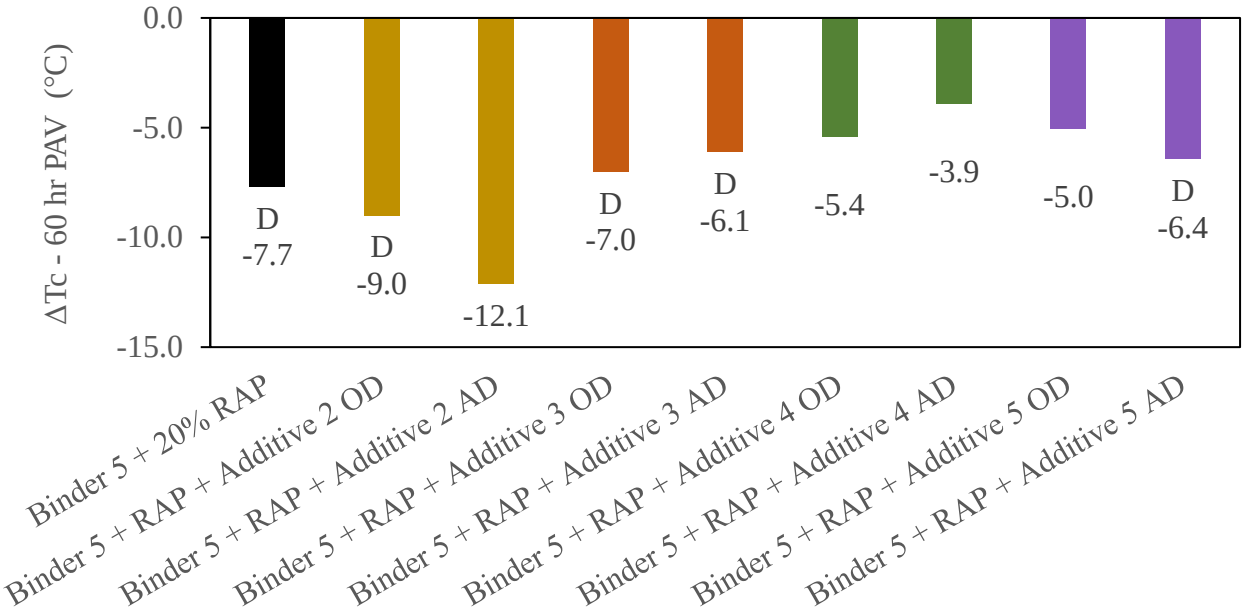

Figure 70. ΔTc (60hr PAV) - Binder 5 with RAP

In addition, aging susceptibility at low temperatures was evaluated through the increase in continuous low temperature true grade between RTFO plus 20 and RTFO plus 60 hours of PAV aging. Every additive but number 5 mitigated the increase in low temperature true grade of Binder 1 with RAP, as shown in Figure 71 . Therefore, the aging susceptibility of Binder 1 with RAP was improved after modification. Even though the grade loss is comparable to the control, Additive 5 resulted on lower critical temperatures after 60 hours of aging, thus the aged properties of Additive 5 still indicated improved performance properties than the control.

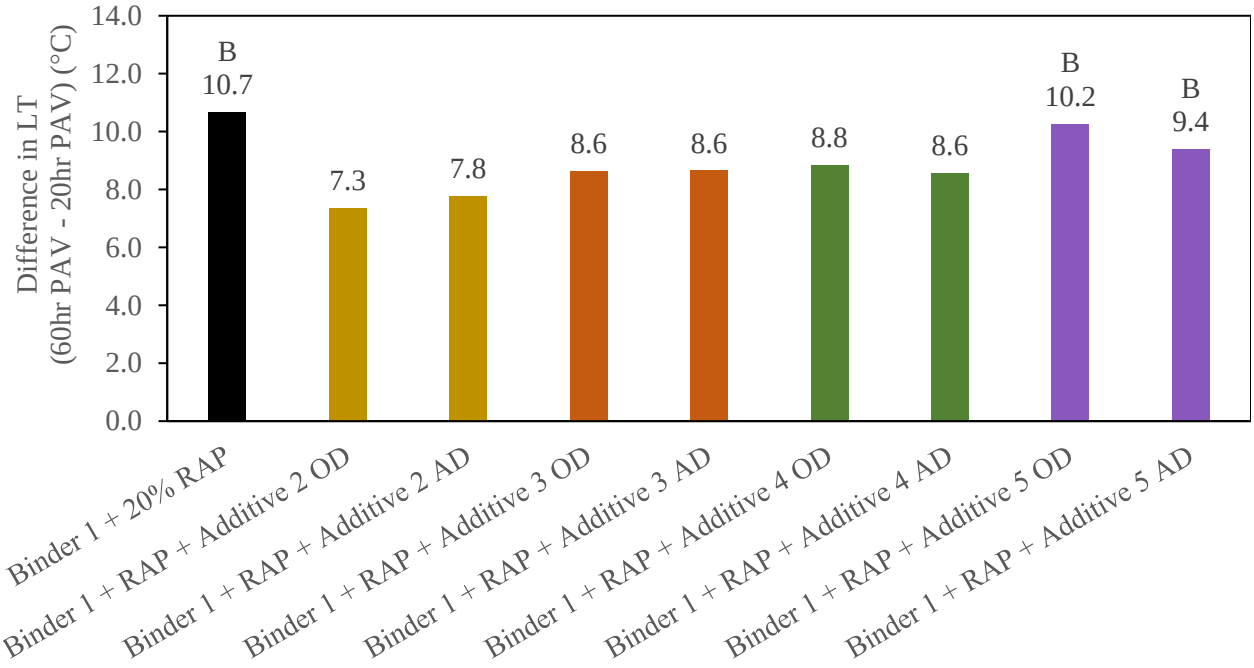

Figure 71. Difference in Low temperature true grade (60hr PAV - 20hr PAV) - Binder 1 with RAP

Recycled binder blends with base Binder 5 in Figure 72 showed smaller grade losses for Additive 4, Additive 2 at the optimum dosage and Additive 3 at the alternative dosage, meaning improved aging susceptibility. Additive 5, the alternative dosage of Additive 2 and the optimum dosage of Additive 3 caused no statistical differences. Thus, effectiveness of Additives 2 and 3 was conditioned by dosage. Although the aging susceptibility of the recycled binder blend was not improved with Additive 5, TABLE 32 shows it reduced low critical temperatures after aging, thus improving both stiffness and relaxation properties. This result matches findings obtained for recycled binder blends with base Binder 1. On the other hand, Additive 3 provided a less susceptible binder to the effect of aging, but stiffness and creep rate were not improved, as critical temperatures in TABLE 32 were warmer than the control.

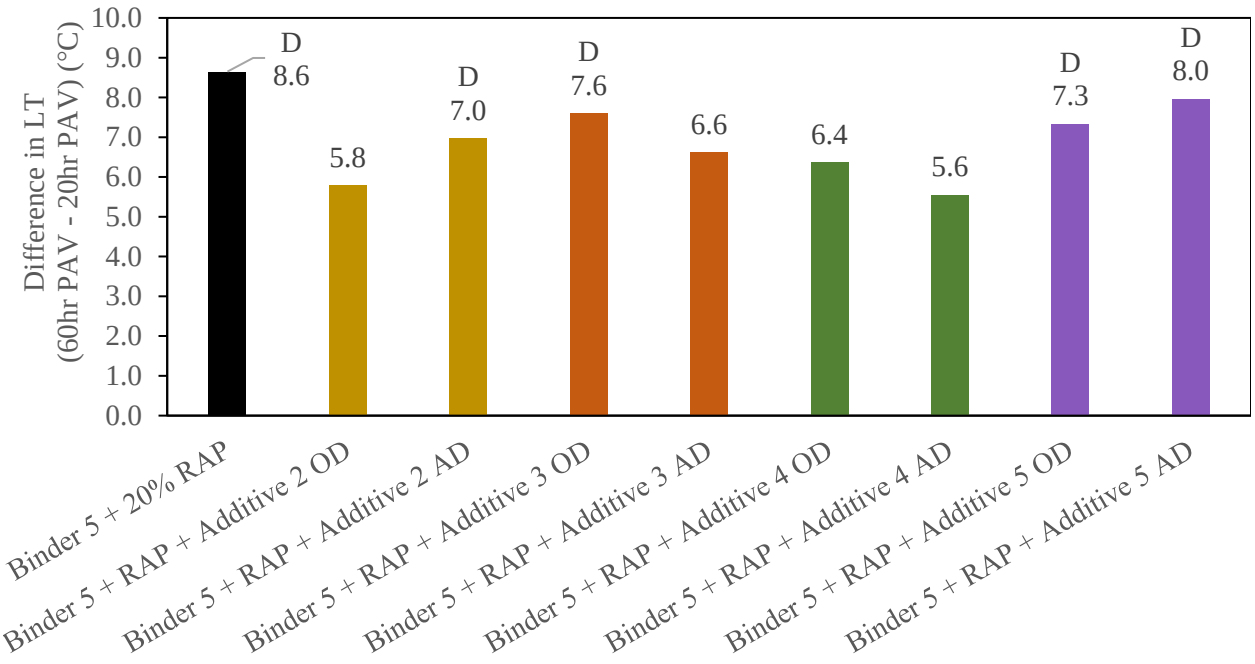

Figure 72. Difference in Low temperature true grade (60hr PAV - 20hr PAV) - Binder 5 with RAP

Changes in ΔT_C of Binder 1 RAP blends show Additive 4 was the only modifier that significantly improved the loss in ductility with extended aging cycles, as indicated in Figure 73. The remaining additives showed comparable reductions in ΔT_C, thus the susceptibility of ΔT_C to extended aging remained unchanged. Nevertheless, Additives 3 and 5 did provide more positive values of ΔT_C after aging, which favored the aged properties of recycled binder blends.

Figure 74 shows Additive 2 (at the optimum dosage) and Additives 4 and 5 caused smaller reductions in ΔT_C of recycled binder blends with base Binder 5. Thus, these modifiers mitigated the loss in ductility experienced by the base binder, which would indicate enhanced aging susceptibility. In addition to providing smaller reductions in ΔT_C, Additives 4 and 5 shifted ΔT_C to more positive values. Therefore, these additives improved the aging susceptibility with respect to the control while providing more positive values of ΔT_C after aging, which would indicate improvements in ductility and relaxation properties.

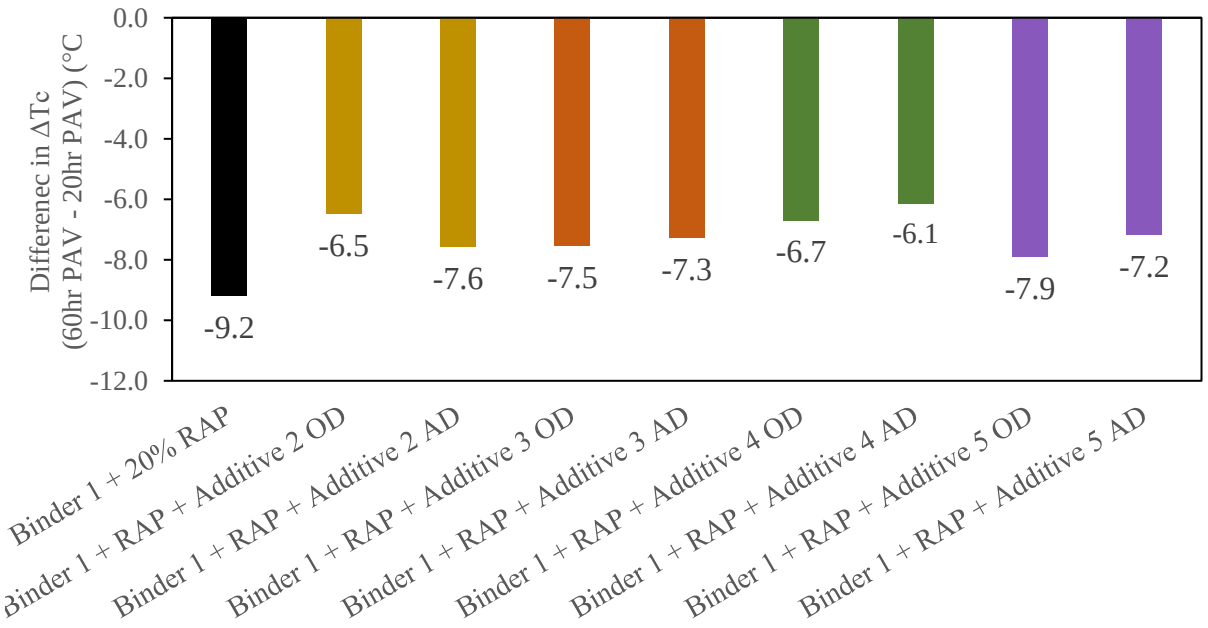

Figure 73. Differences in ΔTc for Binder 1 with RAP (60hr PAV - 20hr PAV)

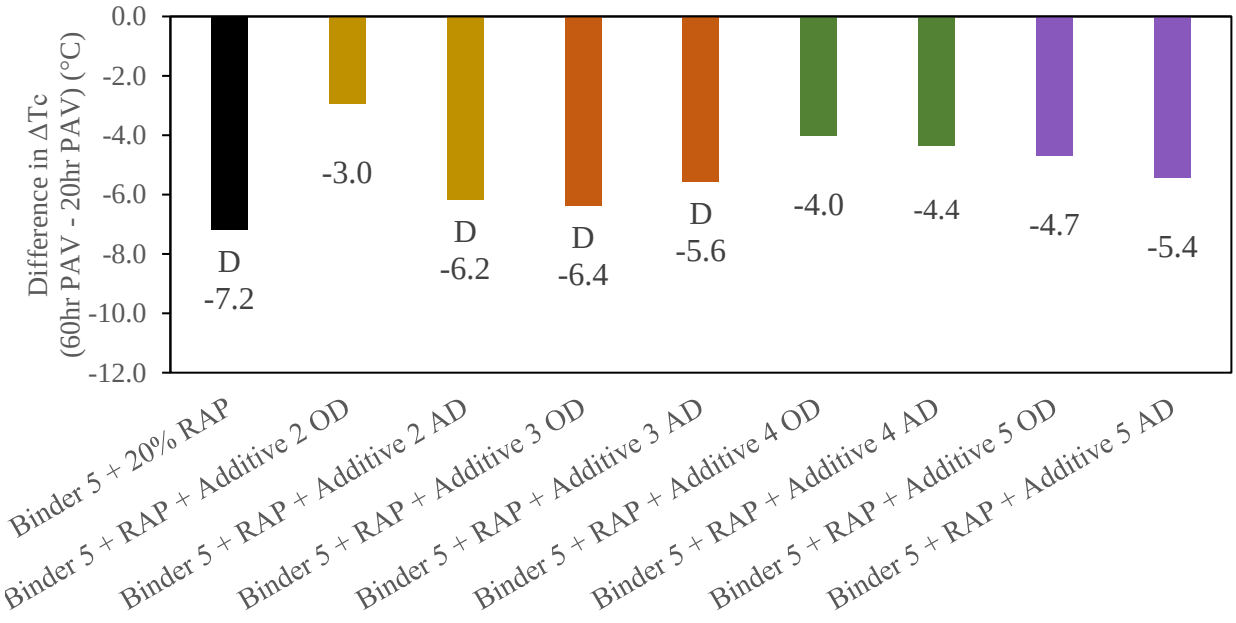

Figure 74. Difference in ΔTc for Binder 5 with RAP (60hr PAV - 20hr PAV)

d. Low Temperature Evaluation Using 4-mm DSR Approach

Base and modified binders were tested after RTFO plus 60 hours of PAV aging to determine critical low temperatures as well as ΔT_C, as shown in TABLE 33. Base binders were tested using BBR (TABLE 31) and DSR; and the comparison between both results showed considerably lower critical temperatures from DSR measurements. Binder 1 critical temperatures were -24.4 °C for Tc_s and -9.7 °C for Tc_m using BBR testing, while DSR measurements indicated -29.6 °C for Tc_s and -16.3 °C for Tc_m. Similarly, Binder 5 showed critical BBR temperatures of -26.5 °C for Tc_s and -22.7 °C for Tc_m, while DSR correlations resulted on -32.9 °C for Tc_s and -27.3 °C for Tc_m.

TABLE 33. Critical Temperatures and ΔTc for RTFO + 60-Hour PAV Using DSR Testing

	Tc,S (°C)	Tc,m (°C)	True LT (°C)	ΔTc (°C)
Binder 1	-29.6	-16.3	-16.3	-13.3
Binder 1 + Additive 1 OD	-32.0	-27.1	-27.1	-4.8
Binder 1 + Additive 1 AD	-31.2	-27.8	-27.8	-3.4
Binder 1 + Additive 3	-31.5	-23.2	-23.2	-8.4
Binder 5	-32.9	-27.3	-27.3	-5.6
Binder 5 + Additive 1 OD	-31.0	-25.6	-25.6	-5.4
Binder 5 + Additive 1 AD	-31.9	-24.8	-24.8	-7.1
Binder 5 + Additive 3	-28.4	-24.1	-24.1	-4.3

The changes in low temperature true grade as well as ΔT_C between 20 and 60 hours of PAV aging were also evaluated. Results for Binder 1 are presented in **Error! Reference source not found.** and Figure 76.

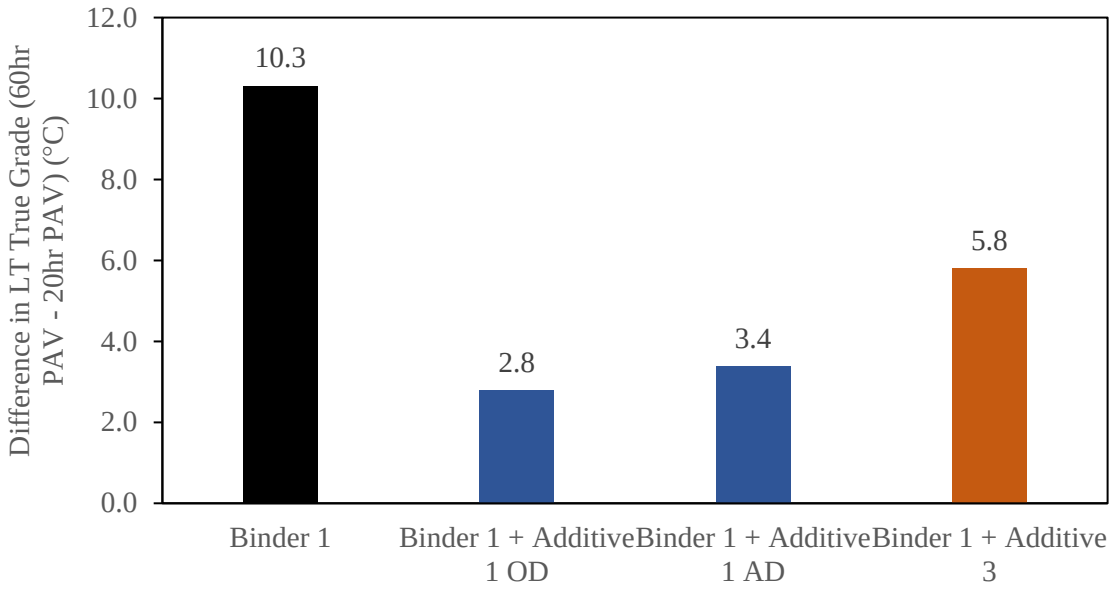

Figure 75. Difference in low temperature true grade (60hr PAV – 20hr PAV) for Binder 1 using DSR testing

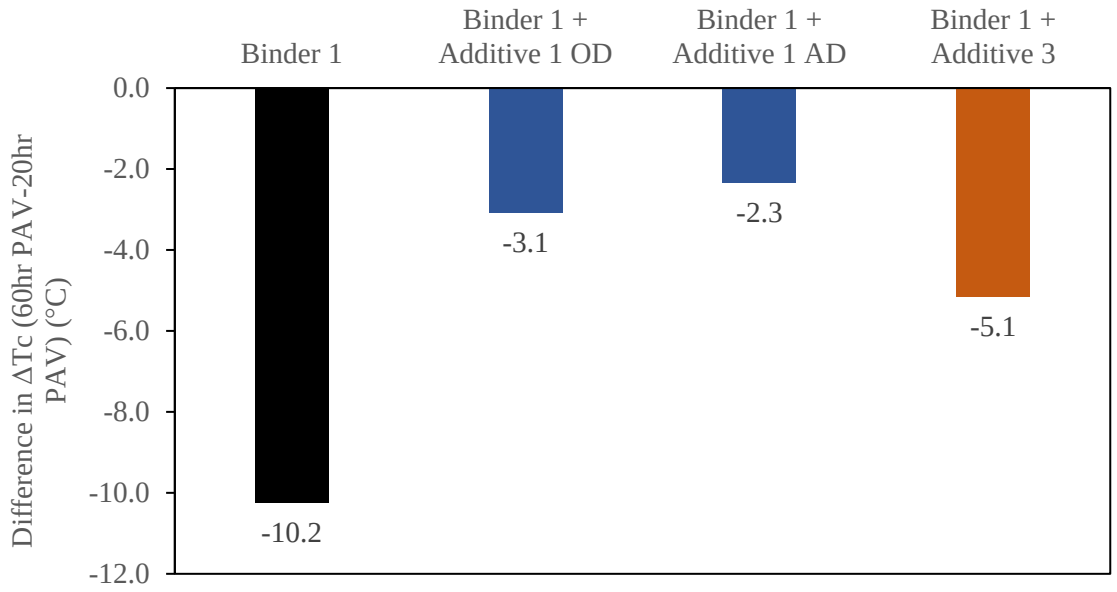

Figure 76. Difference in ΔTc (60hr PAV – 20hr PAV) for Binder 1 using DSR testing

When compared against the control, both additives caused a smaller loss in continuous low temperature true grade, meaning that modified binders presented enhanced resistance to thermal stresses after extended aging cycles. Not only was the low temperature true grade reduced, but when exposed to extended aging between 20- and 60-hours PAV, the increase in low temperature true grade was lower for modified binders, indicating improved aging susceptibility.

Additionally, the changes in ΔT_C showed that modified binders with Additives 1 and 3 lost relaxation properties at a slower rate than the control. The reduction in ΔT_C shown by Binder 1 was greater than that of modified binders, indicating greater susceptibility to the effects of aging. Overall, Additive 1 improved ΔT_C at the 20-hour PAV condition and then experienced a smaller reduction after extended aging. Additive 3, however, did not provide improvements after a 20-hour cycle, but showed a smaller reduction than the control after an extended aging cycle.

Changes in continuous low temperature true grade and ΔT_C for Binder 5 are shown in Figure 77 and Figure 78, respectively. In this case, additive effectiveness was greater on Binder 1 than on Binder 5. Additives 1 and 3 caused higher increase in low temperature true grade than the control, meaning these additives were not as effective at reducing aging susceptibility of Binder 5.

Figure 78 shows smaller reductions in ΔT_C relative to the control were observed for Additive 3 and the optimum dosage of Additive 1. This could indicate that ductility of modified binders was less susceptible to the effects of aging. It should also be observed that although Additive 3 resulted on more negative values of ΔT_C after RTFO plus 20 hours of PAV aging, an improvement in aging susceptibility could still be observed as it provided more positive ΔT_C after the extended aging cycle of RTFO plus 60 hours of PAV aging.

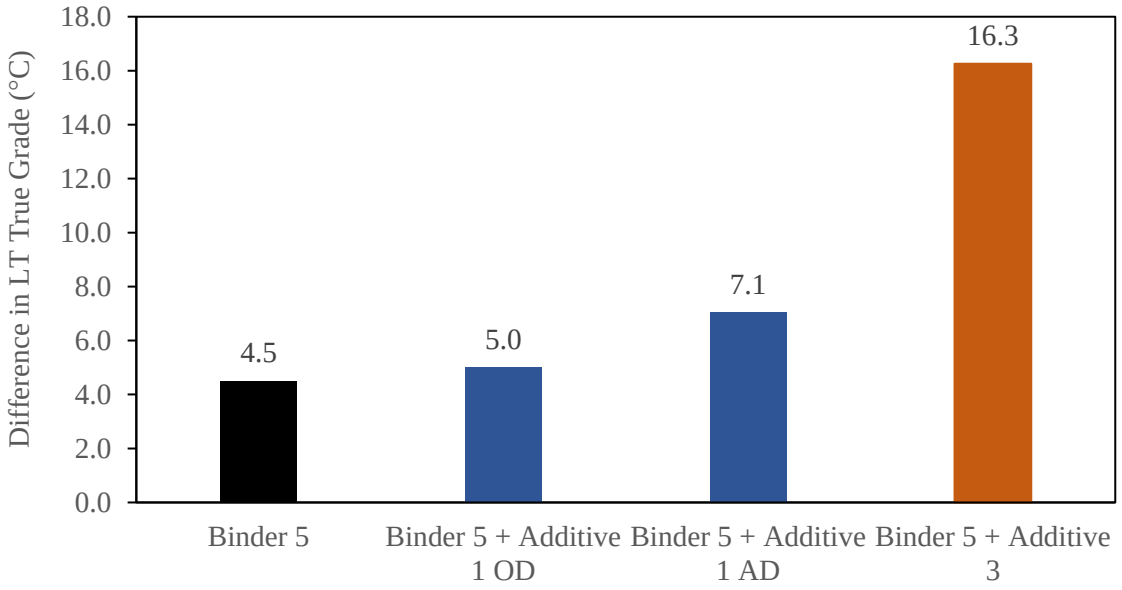

Figure 77. Difference in low temperature true grade (60hr PAV – 20hr PAV) for Binder 5 using DSR testing

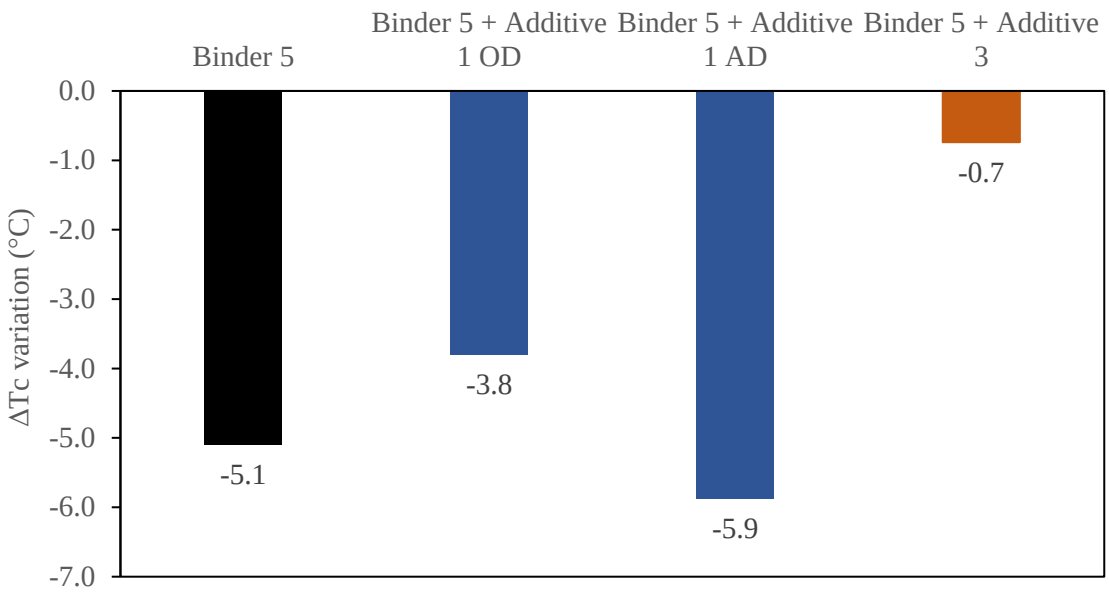

Figure 78. Difference in ΔTc (60hr PAV – 20hr PAV) for Binder 5 using DSR testing

Overall, Additives 1 and 3 showed varying effectiveness on the low temperature properties of the control binders. Both Additives reduced the continuous low temperature true grade of Binder 1 and shifted ΔT_C to more positive values. In addition, smaller reductions in ΔT_C after 60 hours PAV indicated better resistance to the effects of extended aging. Therefore, Additives 1 and 3 showed better resistance to thermal stresses as well as increased ductility and relaxation capability with respect to Binder 1. Binder 5 showed improvements after modification with Additive 3, which caused a reduction in low temperature true grade and improved ΔT_C after extended aging cycles. Additive 1 at the optimum dosage led to more positive values of ΔT_C, but overall showed better effectiveness with Binder 1.

4.2.3 Multiple Stress Creep and Recovery

Multiple Stress Creep and Recovery (MSCR) tests were performed on every binder, at the RTFO aged condition following AASHTO T350 standard. Elastic recovery and non-recoverable creep compliance (J_{nr}) were determined at a stress level of 3.2 kPa and binders were subsequently graded according to AASHTO M332, at a test temperature of 64℃, to match the state of Alabama climatic PG requirements.

Elastic recovery and J_{nr} provide insight into binder's high temperature properties, particularly rutting resistance. By applying higher strain levels that those applied during DSR testing for compliance with AASHTHO M320 (i.e., through $|G^*|/\sin\delta$) polymeric networks many become engaged and differences in rutting performance of modified binders would be observed. Therefore, MSCR results were helpful on the characterization of modified binders with polymer modifiers such as additives 2 and 3.

Elastic recovery and J_{nr} results for neat binders are presented in Figure 80 through Figure 82. Consistent trends are observed on both binders, where Additives 2 and 3 caused an improvement in elastic recovery accompanied by a reduction in J_{nr}. Such improvements in high temperature performance caused Binder 1 to go from an "S" or Standard Designation, suitable for less than 10 million ESALs and traffic speeds greater than 70 km/h to an "E" or Extremely High designation, capable of withstanding more than 30 million ESALs and standing traffic speeds (of less than 20 km/h). Binder 5 experienced an equal upgrade on its designation after the use of both additives.

The softening nature of Additive 4 was clearly captured by the increase in J_{nr}, which fell outside the 4.5 kPa^{-1} limit established in AASHTO M332. Such an effect may compromise rutting resistance, which has been previously found in the literature for some rejuvenators of similar nature (Yin et al., 2017). As 64℃ was the selected test temperature for climatic requirements but Additive 4 fell outside the M332 specification limits, it was retested at 52 ℃ for an accurate J_{nr} result, which determined an "H" designation.

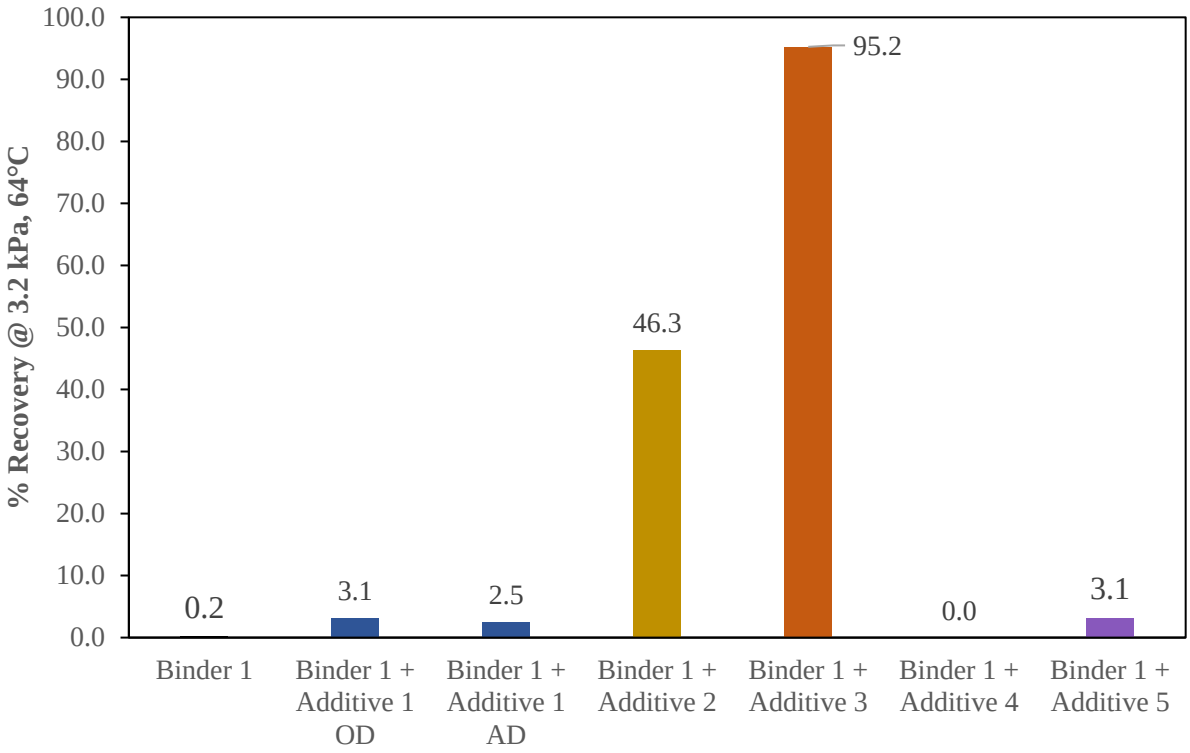

Figure 80. % Recovery at 3.2 kPa - Binder 1

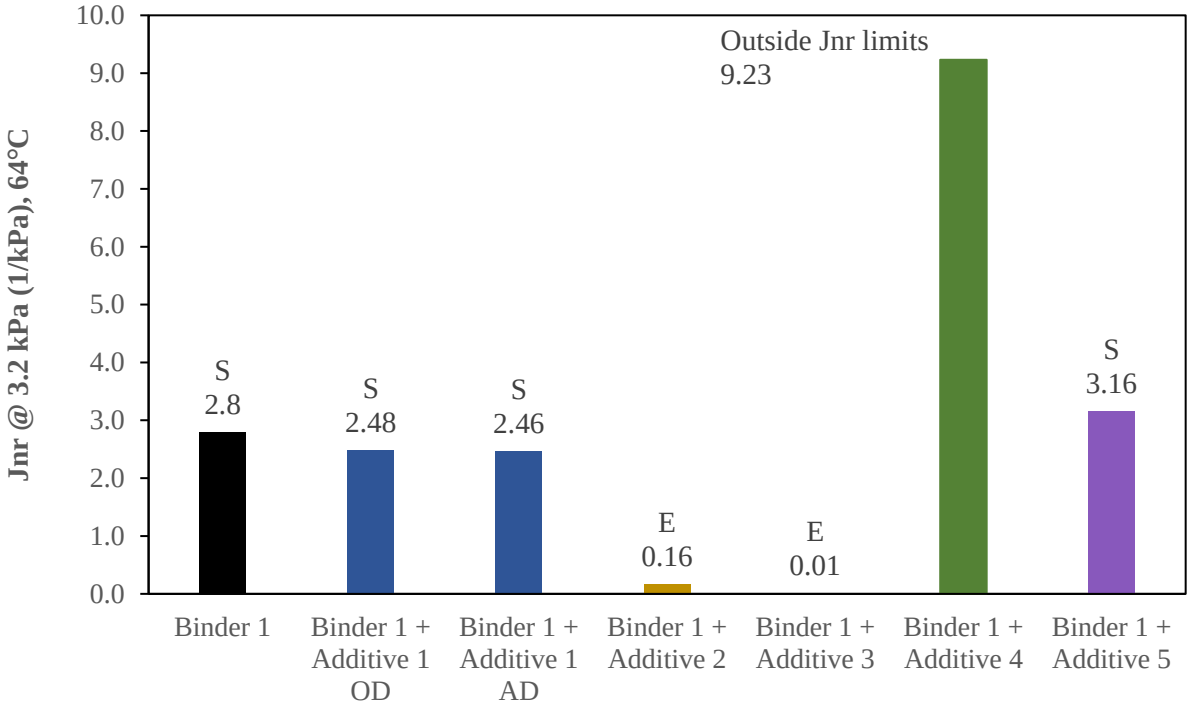

Figure 79. Jnr at 3.2 kPa - Binder 1

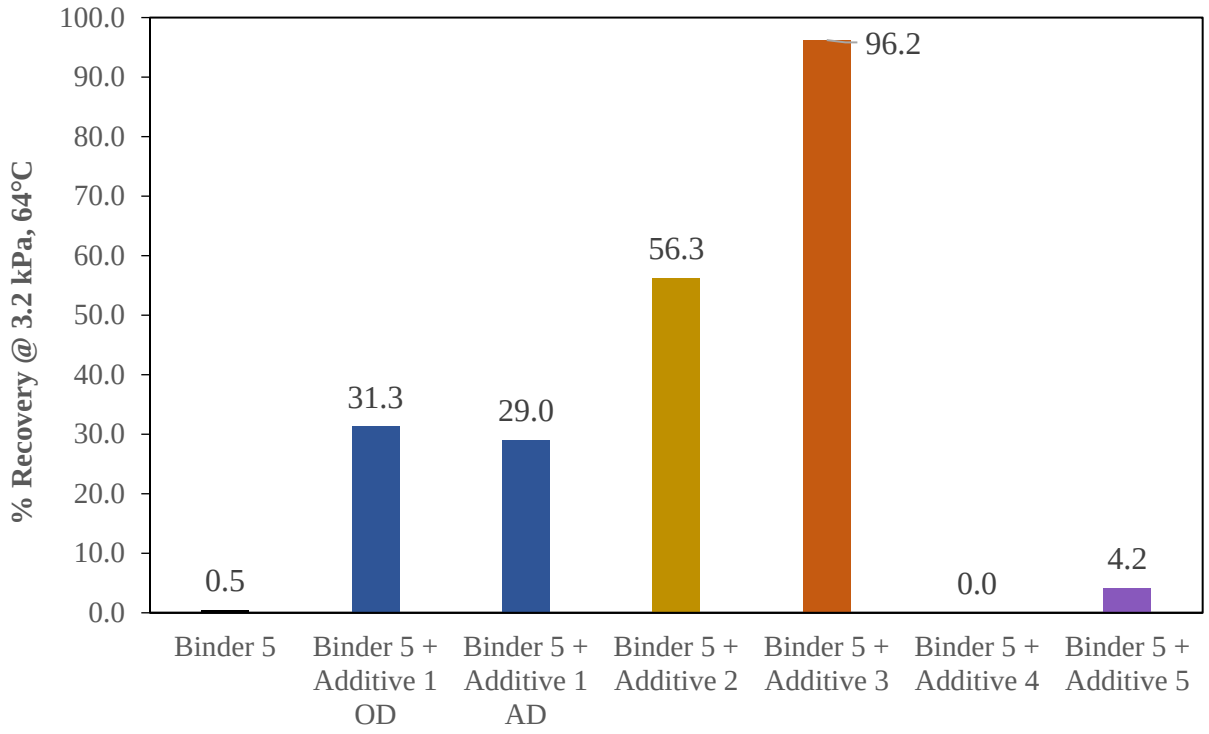

Figure 81. Elastic Recovery at 3.2 kPa - Binder 5

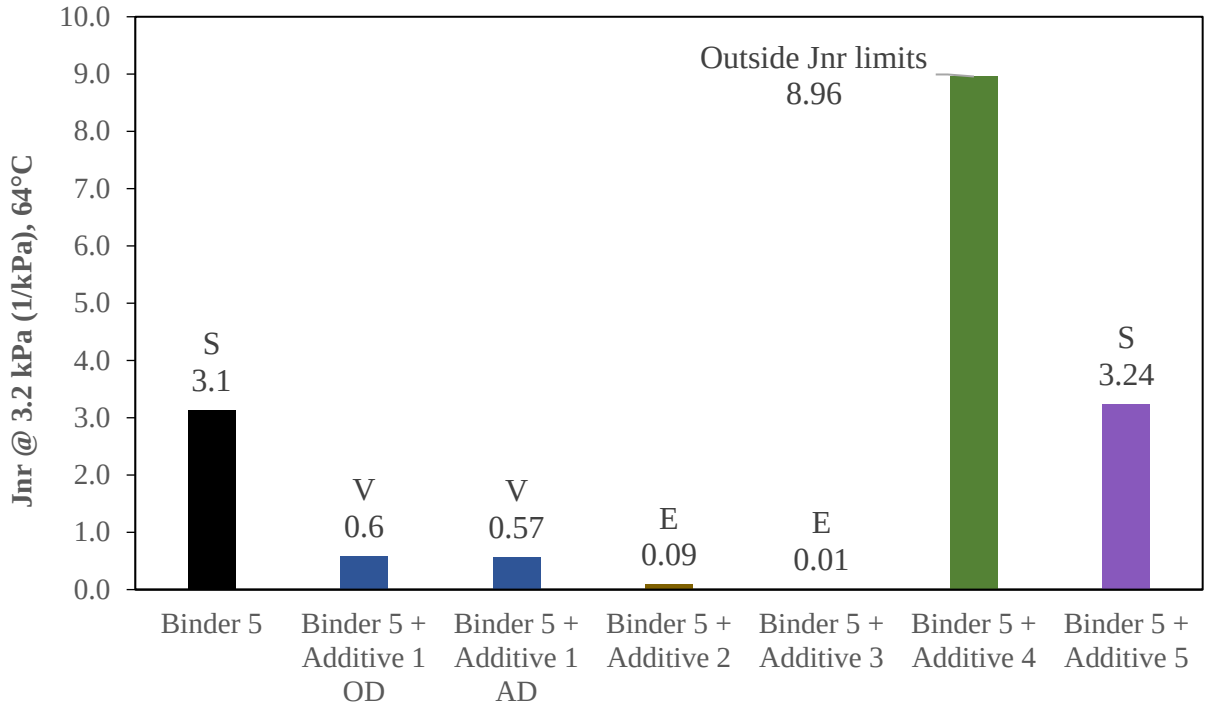

Figure 82. Jnr at 3.2 kPa - Binder 5

MSCR results for Binder 1 with RAP are presented in Figure 83 and
Figure 84. Improvements in rutting resistance were evident for Additives 2 and 3, particularly the latter as it can be characterized as a highly polymer-modified technology. Additive 4 shifted Binder 1 + RAP from a “V” to an “S” designation, showing a softening effect on the control. Additive 5 did not change the “V” traffic level of the control binder.

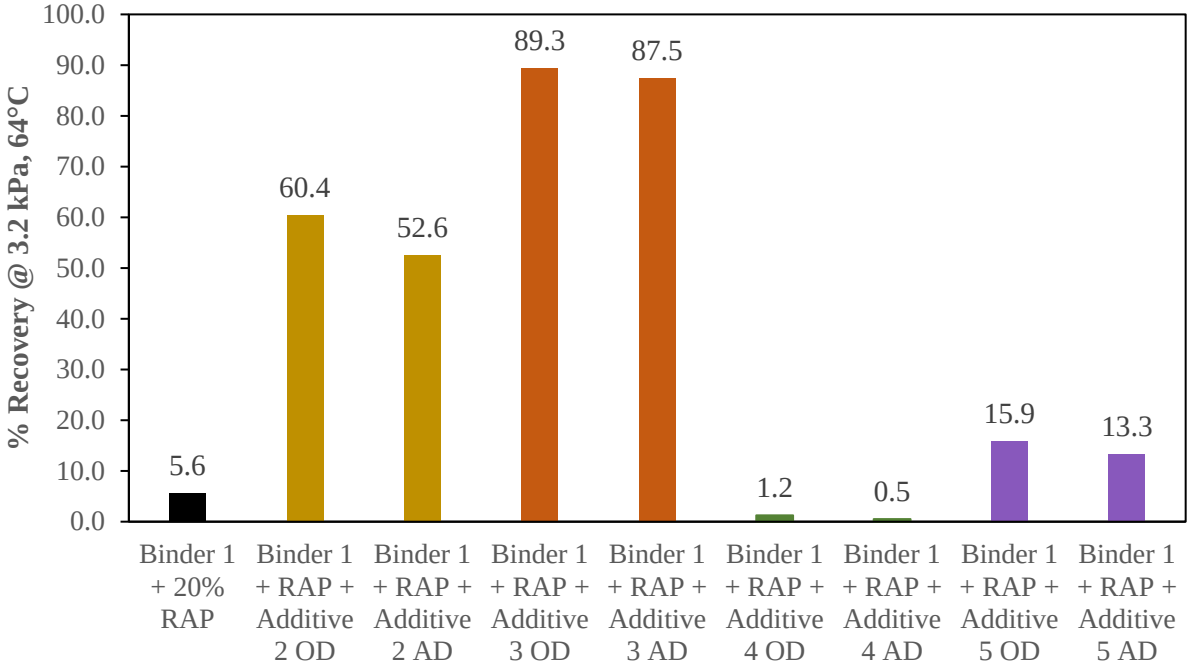

Figure 83. Elastic Recovery at 3.2 kPa - Binder 1 with RAP

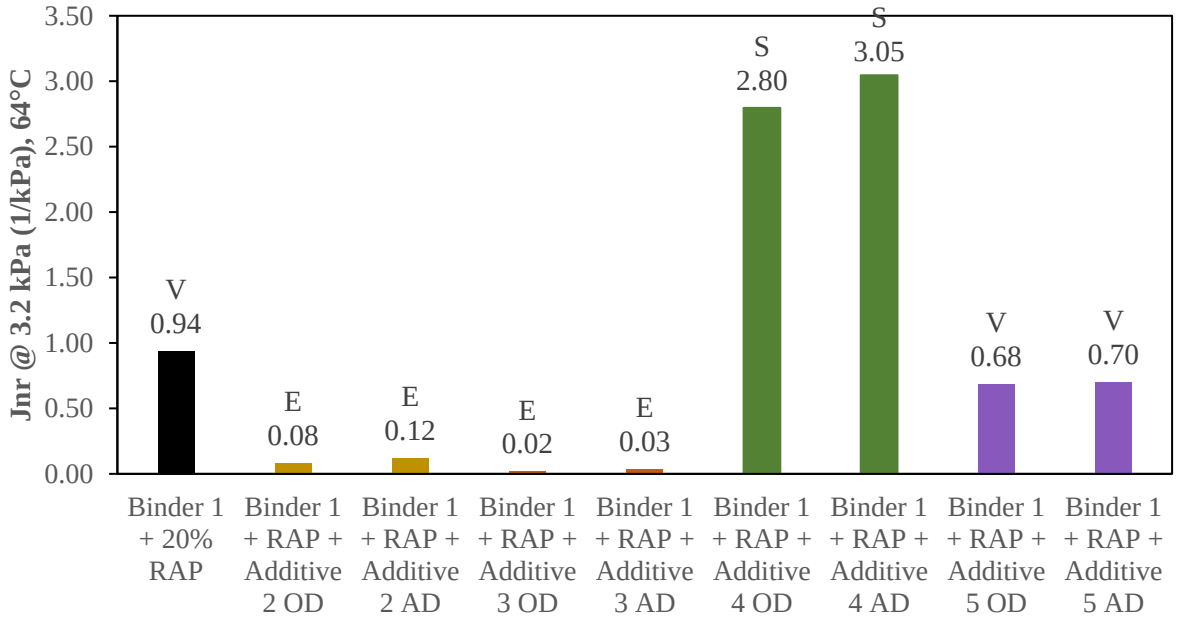

Figure 84. Jnr at 3.2 kPa - Binder 1 with RAP

Figure 85 and Figure 86 present MSCR results for binder 5 RAP blends, and similar trends were found: enhanced rutting performance for Additives 2 and 3, softening of the base binder for Additive 4 and no change for Additive 5.

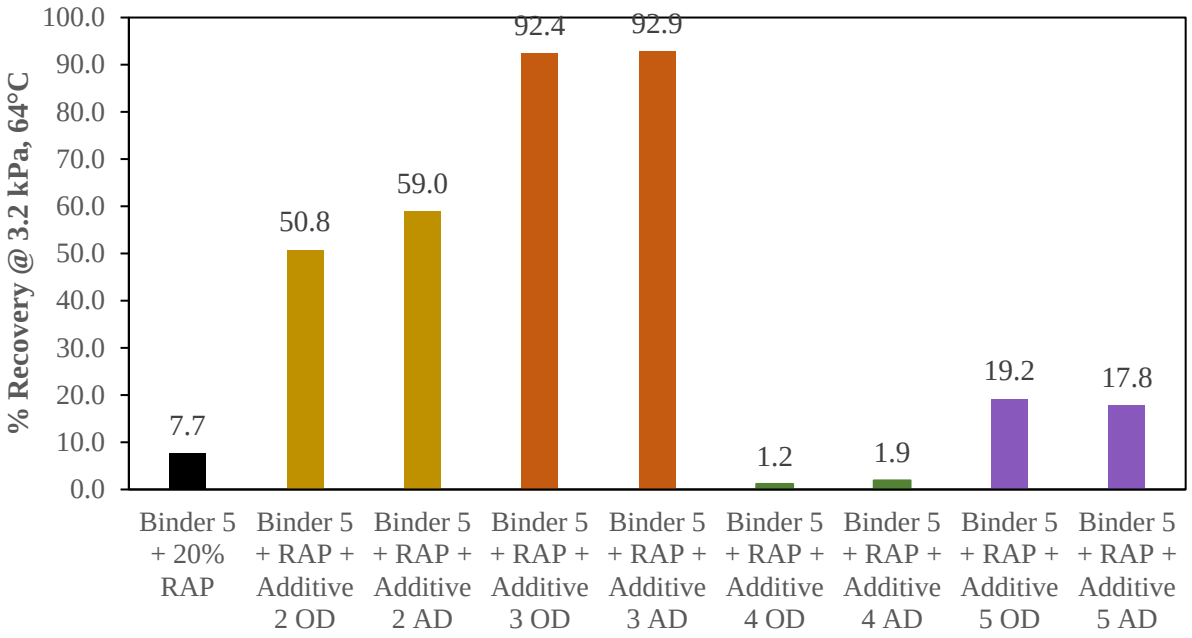

Figure 85. Elastic Recovery at 3.2 kPa - Binder 5 with RAP

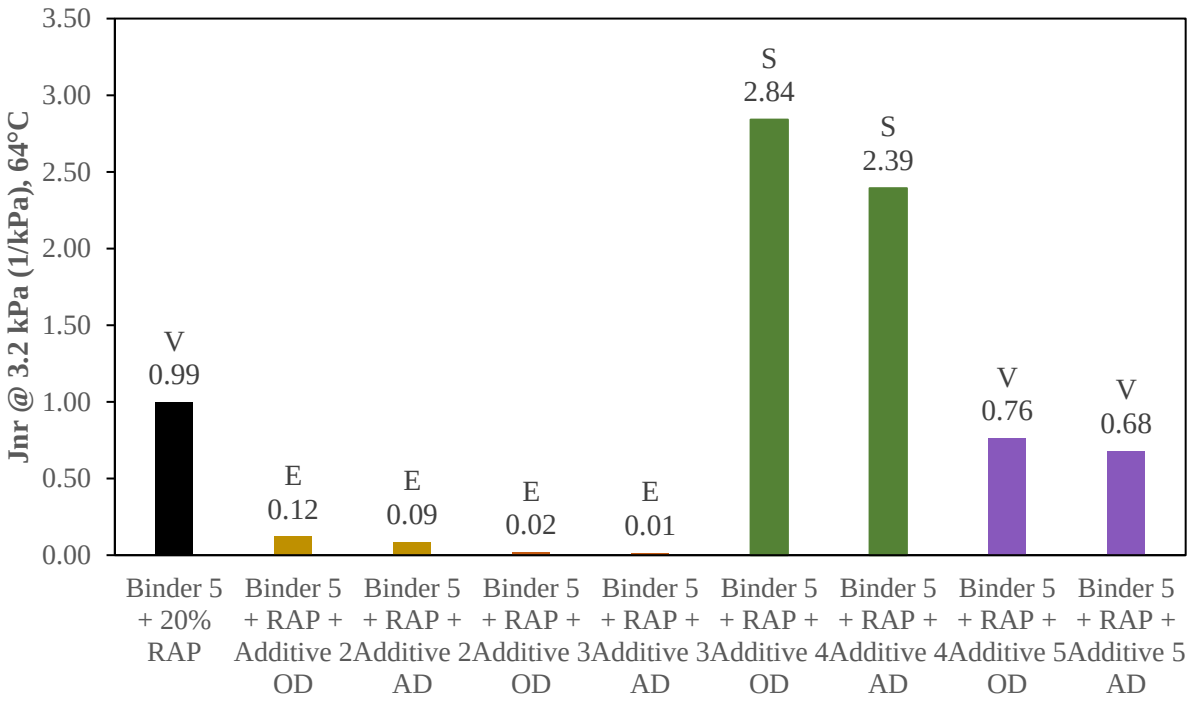

Figure 86. Jnr at 3.2 kPa - Binder 5 with RAP

4.2.4 Linear Amplitude Sweep

LAS tests were conducted on every sample after 60 hours of PAV aging, following AASHTO T391 at a temperature of 20℃, as previously described. Fatigue life of modified and unmodified binders was evaluated through N_f and $|B| - parameter$.

Binder 1 showed improvements in fatigue life after modification with every additive. Figure 87 shows additives increased N_f at 5% strain, although Additive 1 OD showed no significant difference based on Tukey pairings. Additionally, Figure 88 shows damage accumulation rate was improved with every modifier, as the fatigue parameter B was reduced with respect to the control. Therefore, fatigue life of Binder 1 after aging was enhanced after modification.

These findings appear in agreement with improvements in intermediate temperatures after 60 hours of PAV aging, as shown in Section 4.2.2.b. where all additives caused a reduction in intermediate temperature true grade with respect to the control.

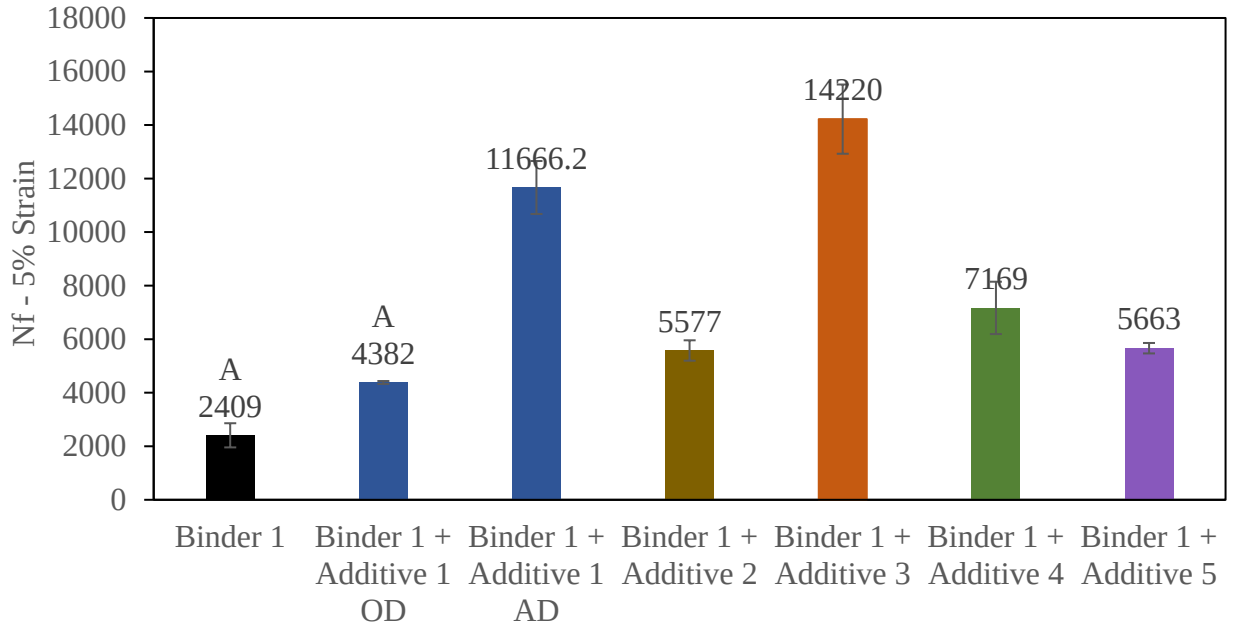

Figure 87. Nf at 5% strain - Binder 1

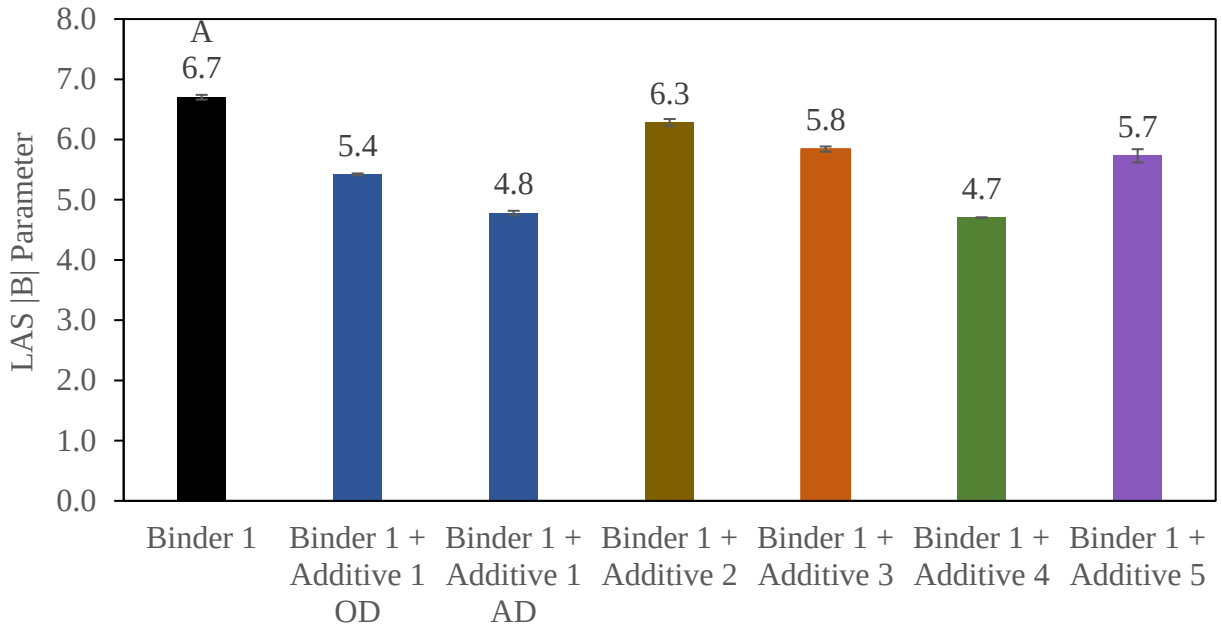

Figure 88. |B| Parameter from LAS - Binder 1

N_f for Binder 5 are shown in Figure 89, where Additives 3, 4 and 5 showed higher values of N_f, indicating imrpovement in fatigue cracking resistance. Additives 1 and 2, on the other hand, caused no significant difference with respect to the control. Of particular interest may be the number of cycles to failure of Additive 3, as it is considerably higher than any other material. The nature of the modifier may be generating this confounding result, which may question the definition of the failure definition, which has been reported by other researchers (R. Zhang et al., 2020). For this reason, and to provide a more robust ranking tool across technologies, strain tolerance will also be discussed below. In this case, the ranking obtained from LAS appears in agreement with intermediate temperatures from DSR measurements after 60 hours of PAV aging (Section 4.2.2).

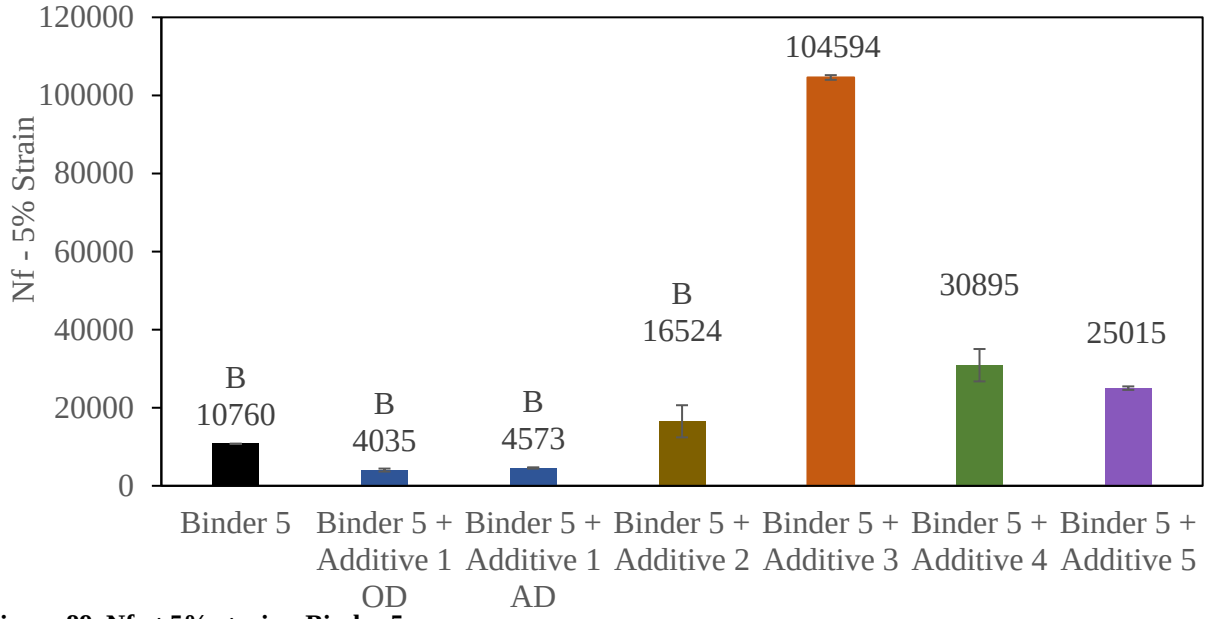

Figure 89. Nf at 5% strain - Binder 5

The $|B|$ parameter for base Binder 5 and modified blends shown in Figure 90 indicated Additive 4 significantly improved damage accumulation rate of Binder 5. No significant differences were found for Additives 1, 3 and 5. Therefore, reduced effectiveness of some additives was found upon interactions with Binder 5.

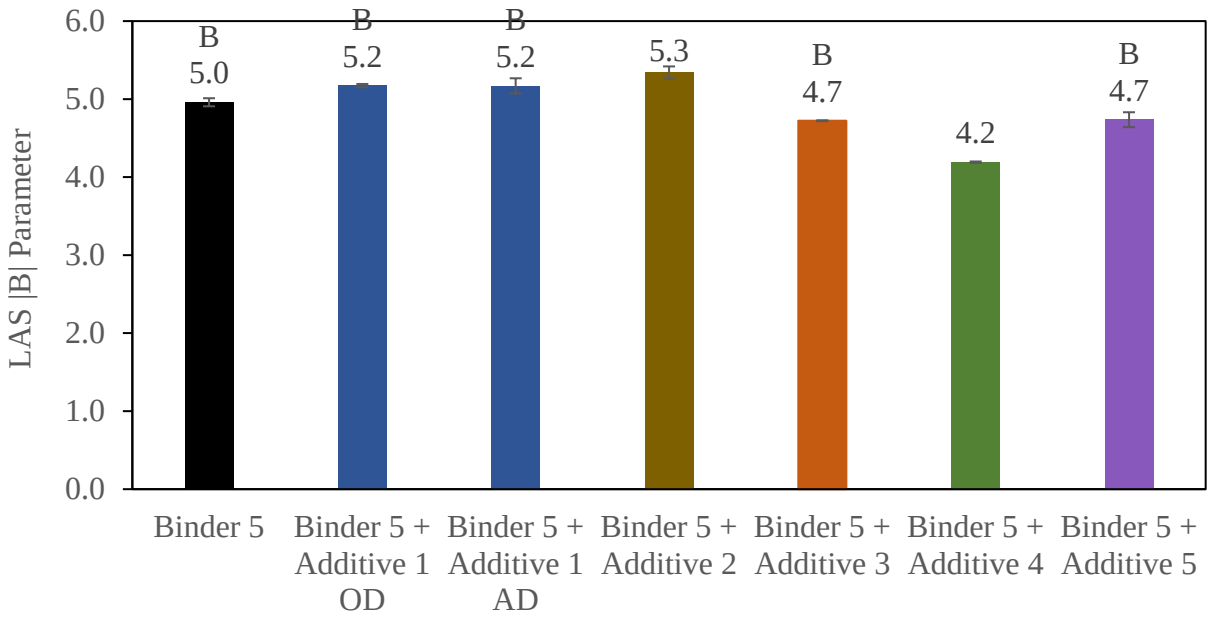

Figure 90. |B| Parameter for Binder 5

N_f results for Binder 1 with RAP are shown in Figure 91, where improved fatigue life was observed for Additives 2, 3 and 4 at the optimum dosage. N_f appeared to increase for every additive, but statistical groupings indicated that Additive 5 and the alternative dosage od Additive 4 were not statistically significant.

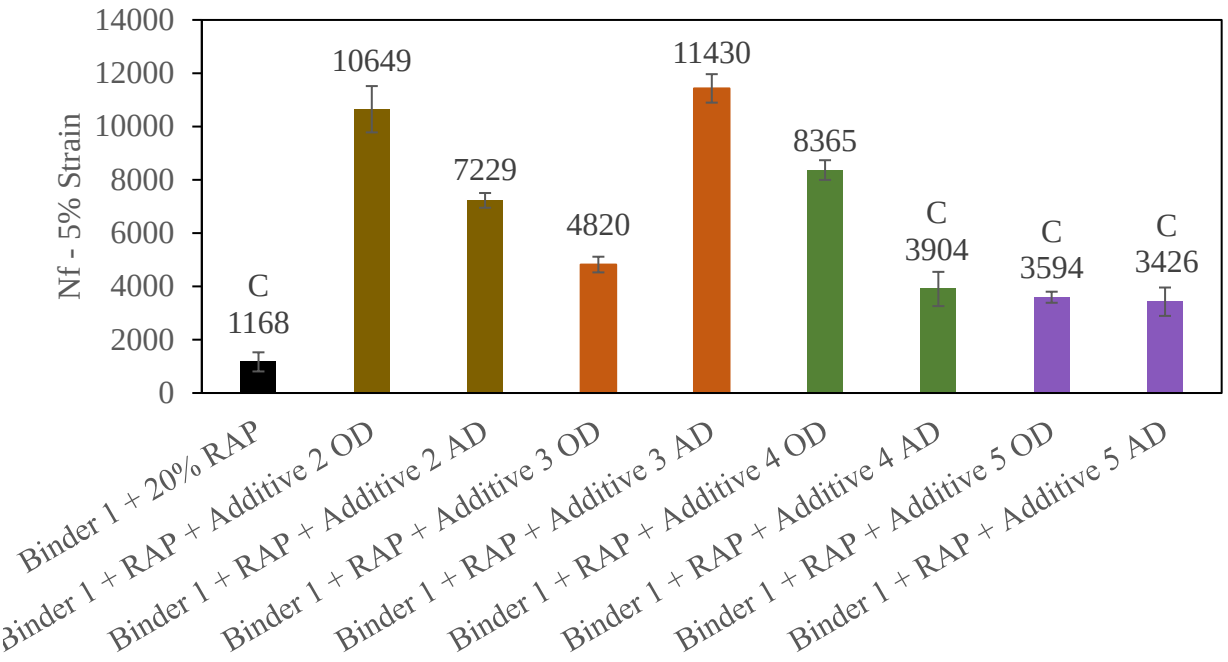

Figure 91. Nf at 5% strain - Binder 1 + RAP

Nevertheless, every additive reduced the $|B| - parameter$ with respect to the control, as indicated in Figure 92. Statistically significant reductions in $|B| - parameter$ were found for all additives at both dosages, indicating improvements in the damage accumulation rate of the base binders.

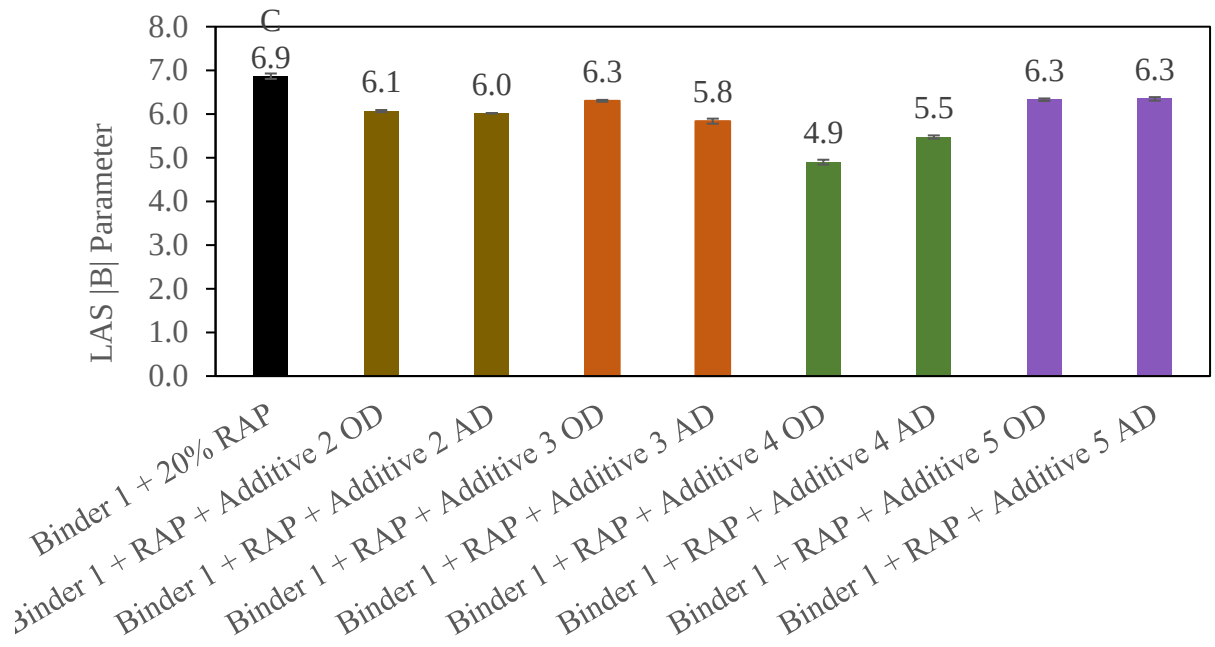

Figure 92. $|B| - parameter$ - Binder 1 + RAP

Figure 93 shows cycles to failure for Binder 5 with RAP, where Additives 2 and 3, as well as the alternative dosage of Additive 4 and the Optimum dosage of Additive 5 caused statistically significant increases. Therefore, these additives showed enhanced fatigue life with respect to the control. On the other hand, Additive 4 at the optimum dosage and Additive 5 at the alternative dosage did not cause statistically significant results, and therefore presented lower effectiveness at improving fatigue life of the control RAP blend. In addition, Figure 94 shows significant reductions in $|B| - parameter$ for Additive 4 and the optimum dosage of Additive 3 and 5, indicating these Additives reduced the damage accumulation rate with respect to the control RAP blend.

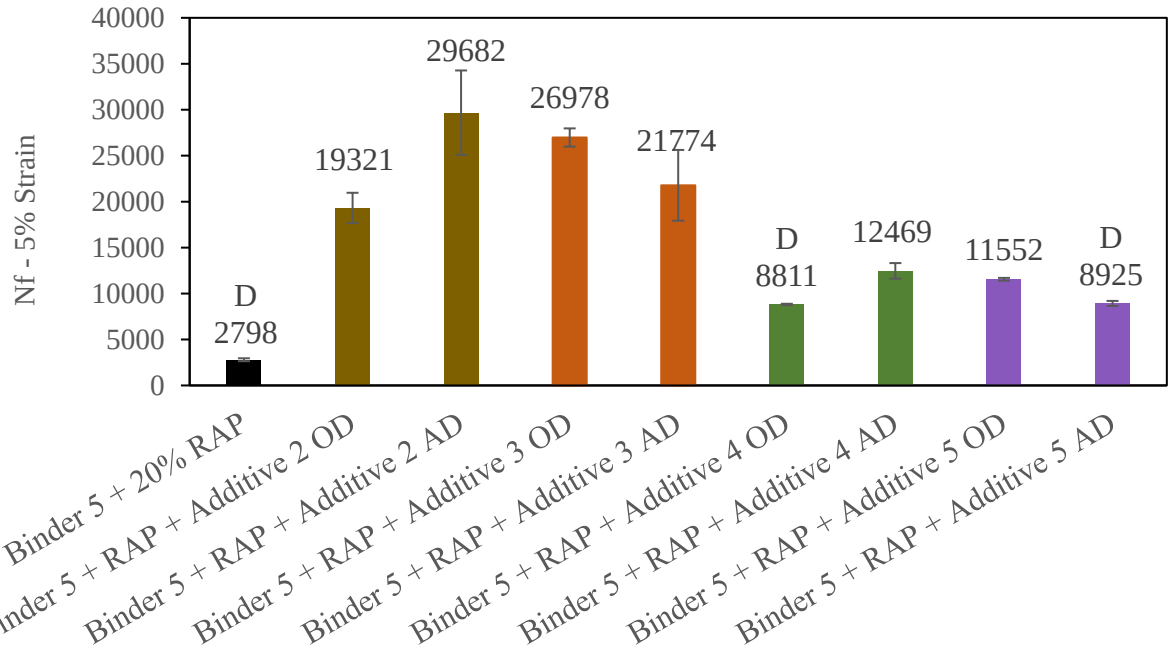

Figure 93. Nf at 5% strain - Binder 5 + RAP

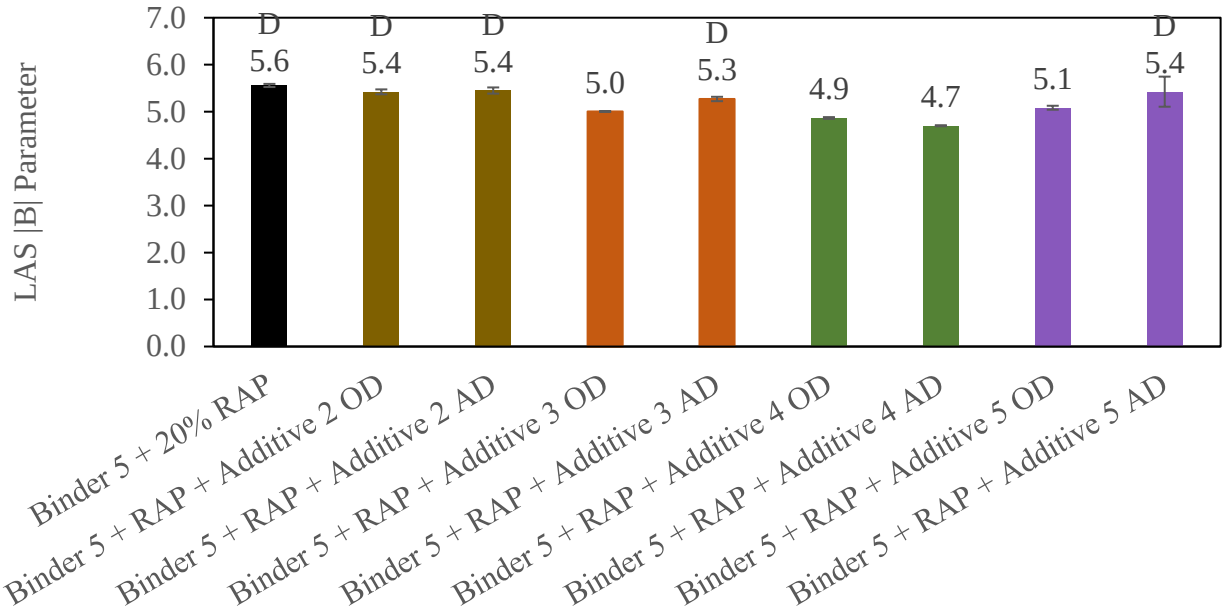

Figure 94. $|B| - parameter$ for Binder 5 with RAP

Overall, LAS test results showed improvement in fatigue cracking resistance with respect to the control binders for most additives. However, effectiveness was dependent on the base binder, presence of RAP and dosage: Additives 1 and 2 showed lower effectiveness with Binder 5 than Binder 1, as they caused no significant improvements in cycles to failure of the former. In addition, Additive 5 and the alternative dosage of Additive 4 did not improve cycles to failure of recycled binder blends with Binder 1, while recycled blends with binder 5 did not show improvements in N_f with the optimum dosage of Additive 4 or the alternative dosage of Additive 5.

Increases in cycles to failure showed enhanced fatigue cracking resistance of modified binders, but some additives (e.g., Additive 3) led to magnitudes of N_f that compromised the statistical results and thus lead to misleading comparisons across technologies. The $|B| - parameter$, which is obtained is obtained from the frequency sweep step of the LAS test, captured improvements in fatigue cracking resistance and statistical differences across technologies. However, researchers have also found limitations with $|B| - parameter$ when capturing the effects of aging (R. Zhang et al., 2020). Thus, the strain at peak stress was determined for each material. Evaluation of strain at peak stress indicates the strain tolerance of the binder prior to cracking. Aging causes an embritllement of the binder which would cause it to crack at lower strains, thus reducing fatigue resistance (Miró et al., 2015).

a. Analysis of Strain at Peak Stress

Stress versus strain curves of Binder 1 and modified blends is presented in Figure 95, to illustrate the strain at peak stress evaluated for strain tolerance (indicated as the dashed red line for Binder 1). In addition to illustrating the peaks, curves are helpful to further understand the effects of modification on the base binder. After peak stress Binder shows a fast drop for higher strain levels, while modified binders present a longer and flatter post-peak behavior, which would be indicative of enhanced resistance to loss in material integrity. Better responses at high strain levels are observed for Additives 2, 3, and 5, which would be consistent with polymeric modifiers, particularly in the formulations of Additives 2 and 3.

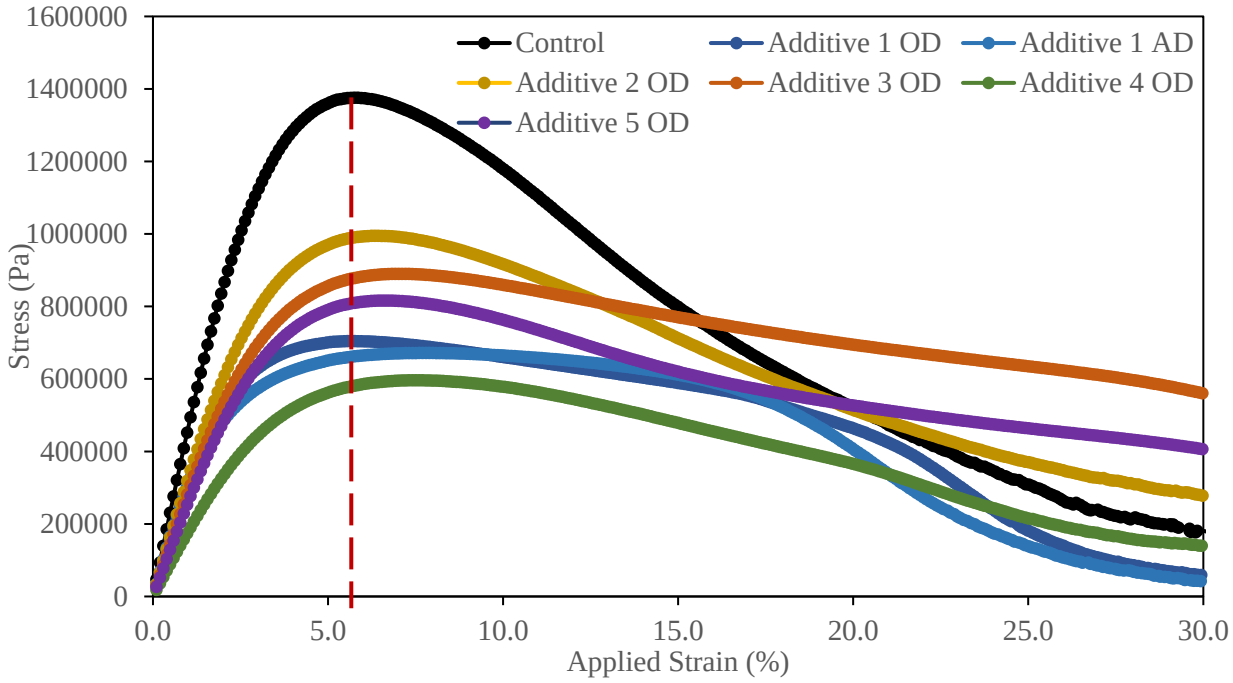

Figure 95. Stress versus strain for Binder 1

Strain at peak stress, determined as illustrated above, is shown in Figure 96 for Binder 1. Additives 2 through 5 showed increased strain tolerance relative to the control, except for Additive 1 at the optimum dosage, which caused no significant difference. Results were consistent with the number of cycles to failure, which means a comparable ranking was obtained across additives.

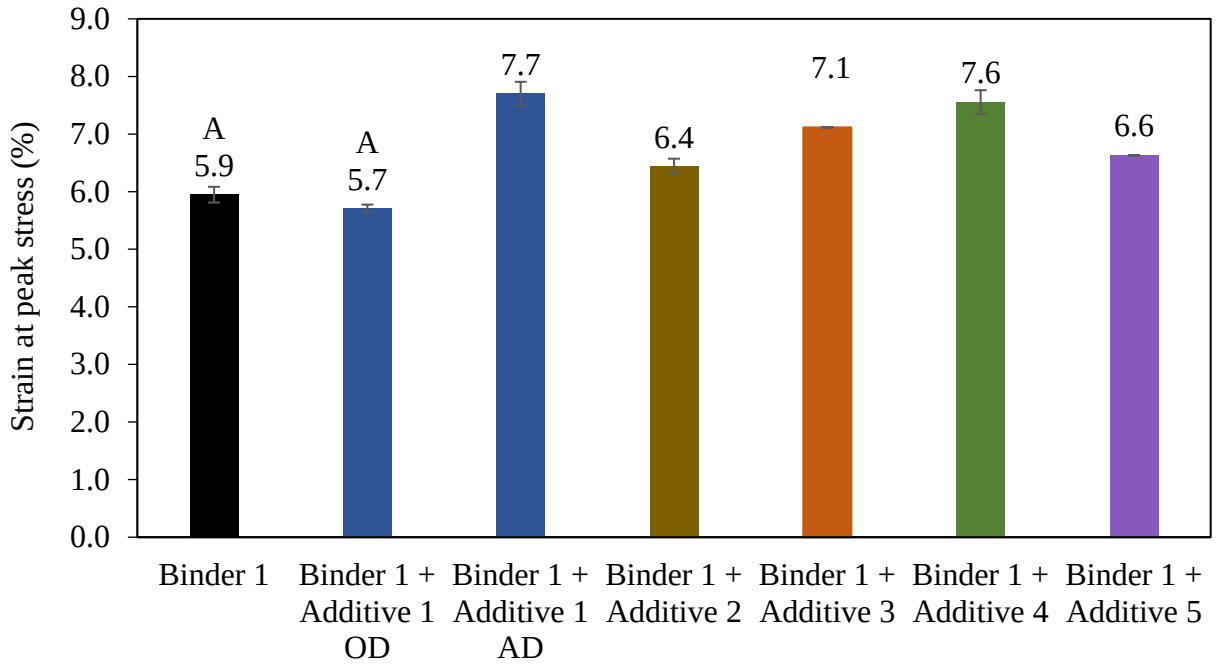

Figure 96. Strain at Peak Stress for Binder 1

Stress-strain curves of Binder 5 and modified binders are presented in Figure 97. The difference among the base binders (which prompted base binder selection) can be observed through differences in the post-peak behavior of Binder 5, which shows better tolerance to damage accumulation than Binder 1, as the drop in stress is not as pronounced for higher strain levels. In addition, the stress-strain curve of Additive 3 is helpful to illustrate the N_f previously discussed. The flat and long curve after peak stress may suggest the material did not experience true failure and thus the cycles to failure showed considerably high values.

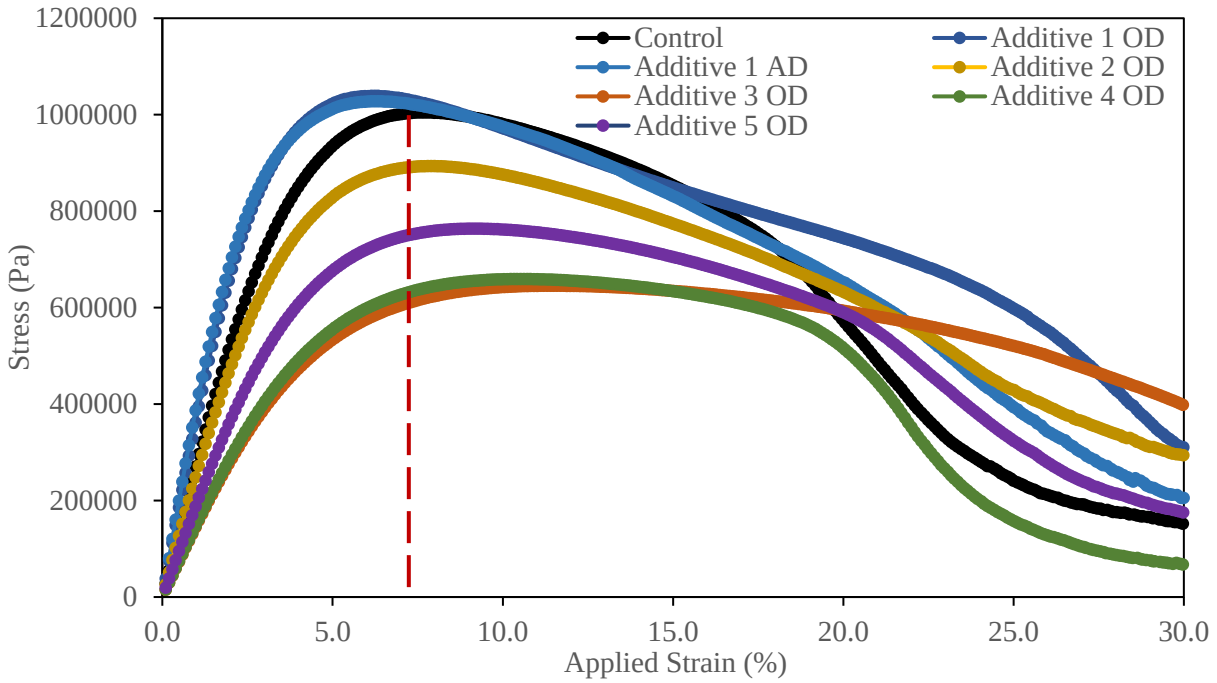

Figure 97. Stress-strain curves for Binder 5

Strain tolerance of Binder 5 improved with Additives 3, 4 and 5, while Additive 2 showed no significant improvement as indicated in Figure 98. Reduced effectiveness was found for Additive 1 with Binder 5, as strain tolerance was reduced with respect to the control. Thus, improvements in fatigue life of the base binders were given by Additives 3, 4 and 5, while greater base binder dependency was observed for Additives 1 and 2, which only caused improvements on Binder 1.

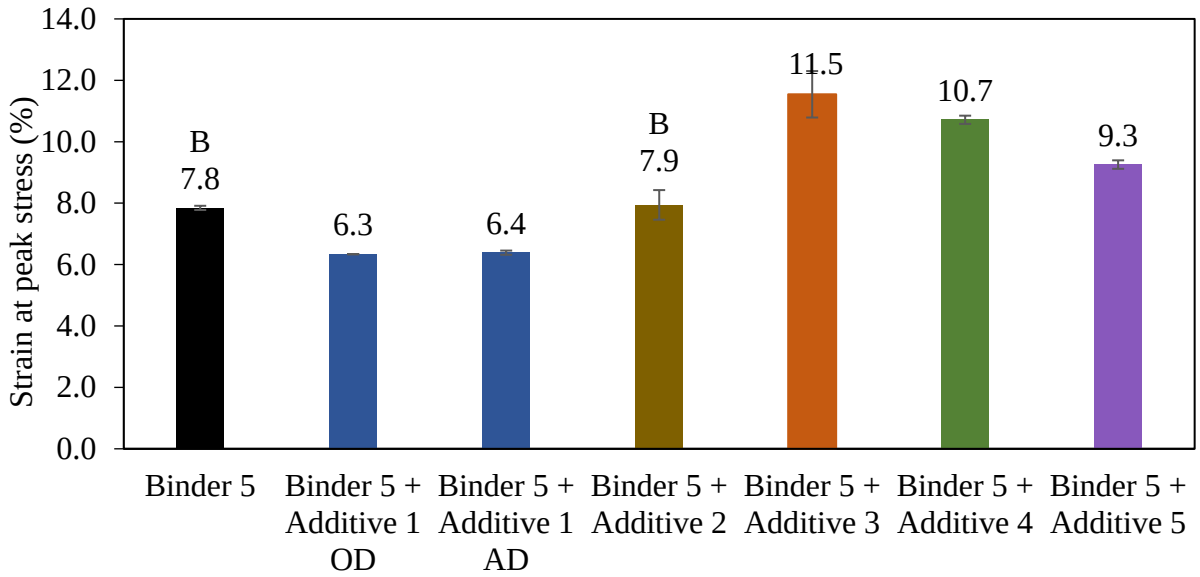

Figure 98. Strain at peak stress for Binder 5

Stress versus strain curves for RAP blends with Binder 1 are presented in Figure 99, where only optimum dosages are included for clarity. Once again, modifiers result on a flatter and longer post-peak behavior, indicative of better ability to withstand stresses at higher strain levels. These findings highlight the usefulness of the LAS test to illustrate enhanced performance of modified binders.

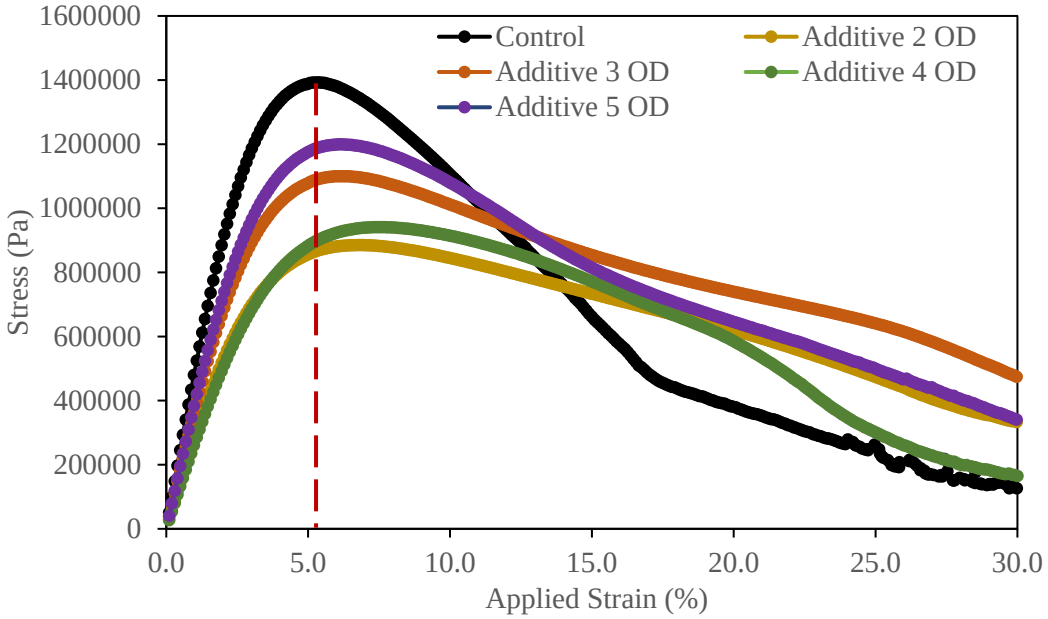

Figure 99. Stress-strain curves for Binder 1 with RAP

Results for strain at peak stress for Binder 1 with RAP are presented in Figure 100. Every modified binder showed higher strain tolerance than the control, potentially indicating enhanced fatigue cracking resistance. Figure 91 showed an increase in number of cycles to failure for every additive relative to the control, but statistical analyses only showed significant improvements for Additives 2, 3 and 4 at the optimum dosage. Therefore, a more accurate comparison across additives was achieved by evaluating strain levels at failure.

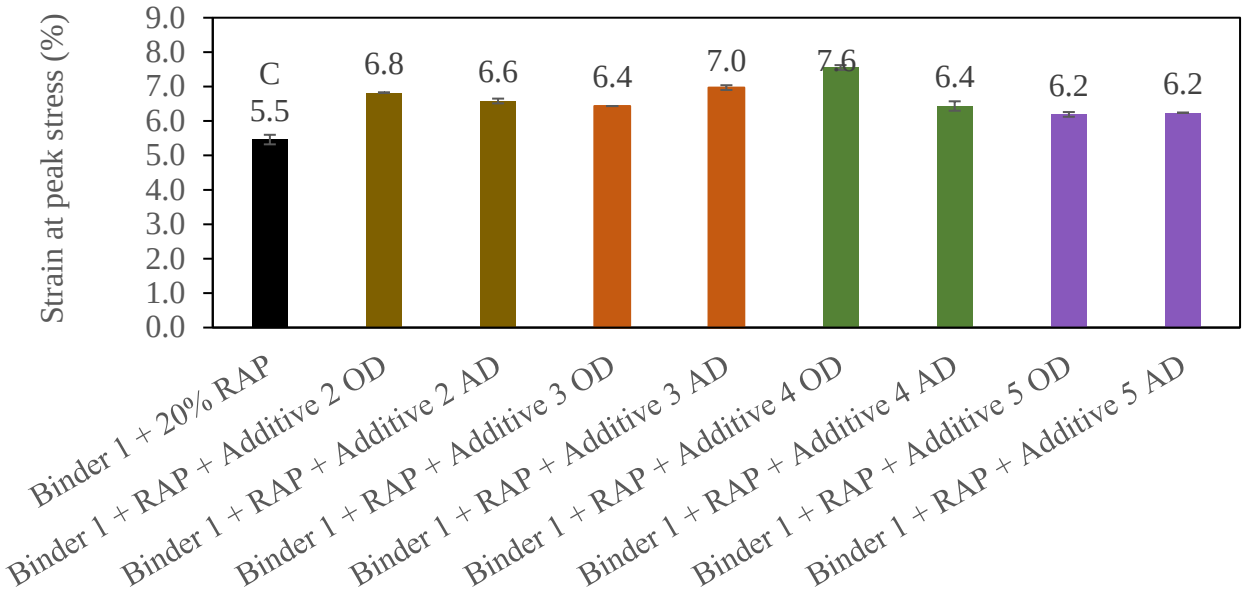

Figure 100. Strain at peak stress for Binder 1 with RAP

Stress-strain curves of Binder 5 with RAP and modified binders (at the optimum dosage) are shown in Figure 101. Improvements in material integrity at high strain levels can be observed as a result of modification, which would lead to improvement in fatigue life of base binders.

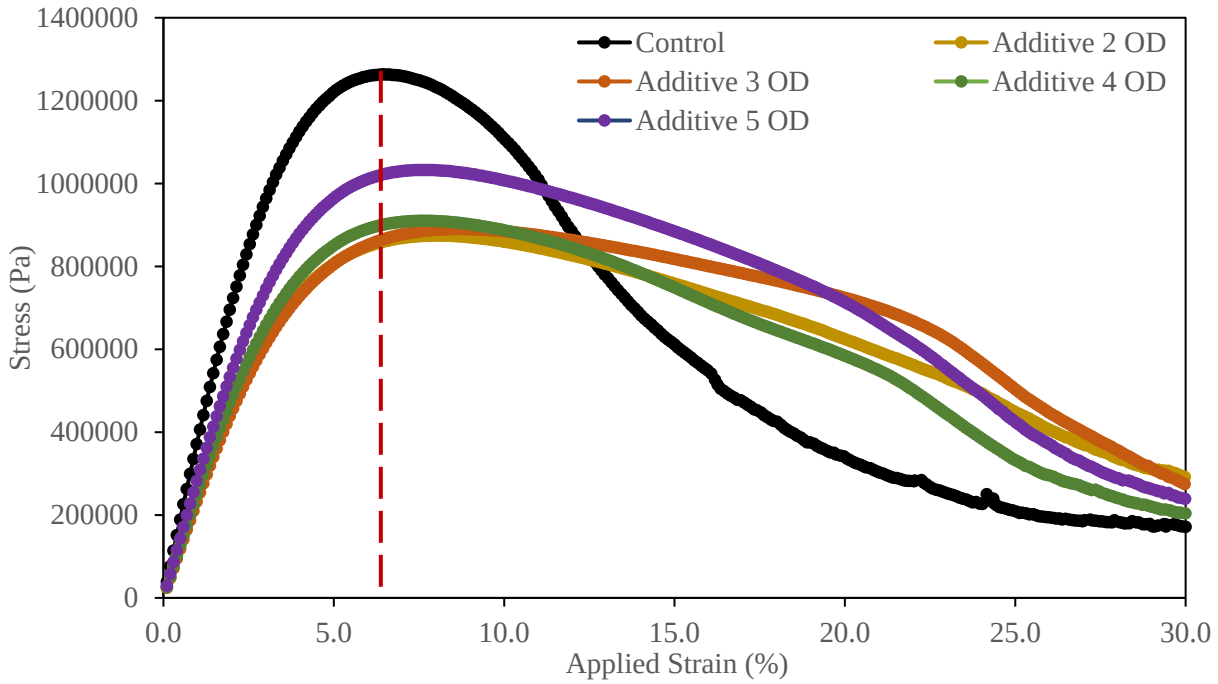

Figure 101. Stress-strain curves for Binder 5 with RAP

Strain tolerance of Binder 5 + RAP improved after the addition of every technology, as shown in Figure 102. Additive 5, however, was only effective at the optimum dosage, as the alternative dosage did not show statistical difference.

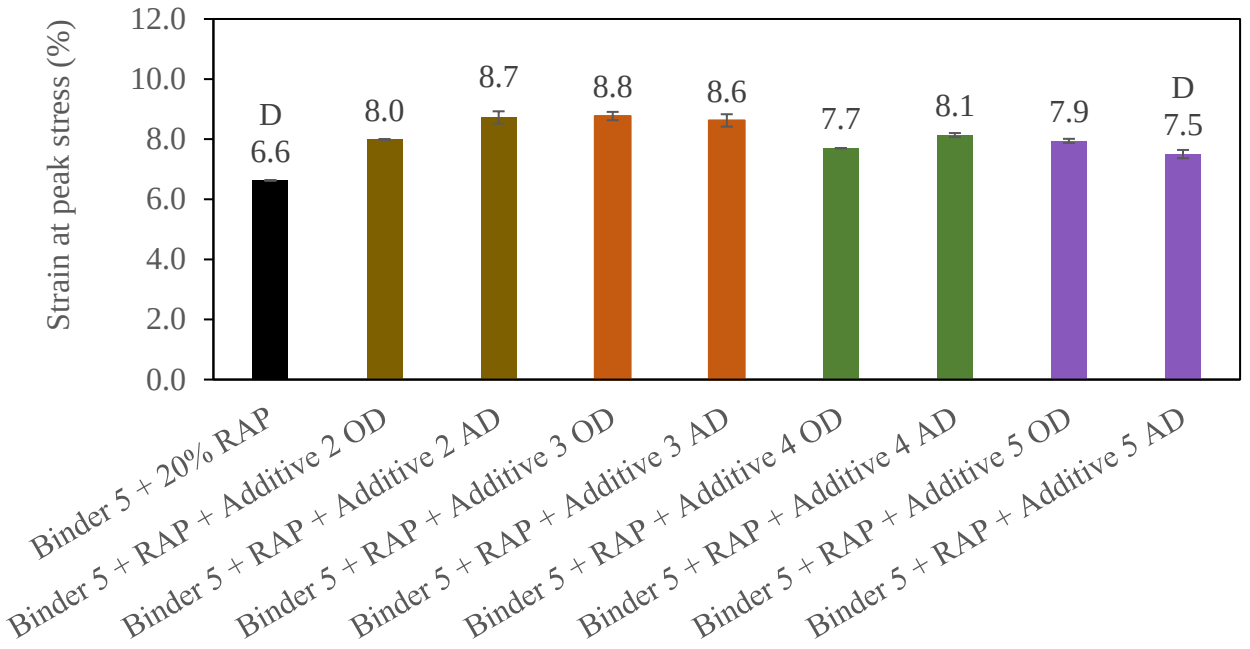

Figure 102. Strain at peak stress for Binder 5 with RAP

Overall, fatigue life of RAP blends was improved by every technology after extended aging cycles. Additive 5 showed a slightly reduced effectiveness on Binder 5 with RAP, as improvements were only given by its optimum dosage.

LAS results showed modifiers were successful at increasing binder durability. Furthermore, the relationship between strain at peak stress and ΔT_C was explored, as it has been related to ductility and resistance to age-related distresses (R. M. Anderson et al., 2011; Elwardany, Planche, et al., 2020). A good level of agreement was found for base binders, as shown in Figure 103 by the R^2 value of 0.93. Higher strain levels are accompanied by more positive values of ΔT_C, therefore higher ductility would also be indicative of improved fatigue resistance. However, evaluation of modified binders led to more scattered relationships (R^2 = 0.57), as shown in Figure 104 possibly caused by the varying nature of these materials. It should be noted that this analysis only included ΔT_C obtained from BBR testing. Figure 104 shows that Additives 2 and 3, in yellow and orange, appear to follow a common trend, while Additives 4 and 5 in green and purple appear to share a trend as well. This is consistent with additive composition, as the former contain polymer modifiers. Figure 105 shows a similar approach where additives have been grouped. The improvements in strain tolerance and ΔT_C are in better agreement for Additives 4 and 5. Although the overall trend is followed by the polymeric additives, correlation is limited by the ability of ΔT_C to characetrize these materials. Therefore, both parameters (ΔT_C and strain at peak stress) captured improvements in aging resistance of modified binders.

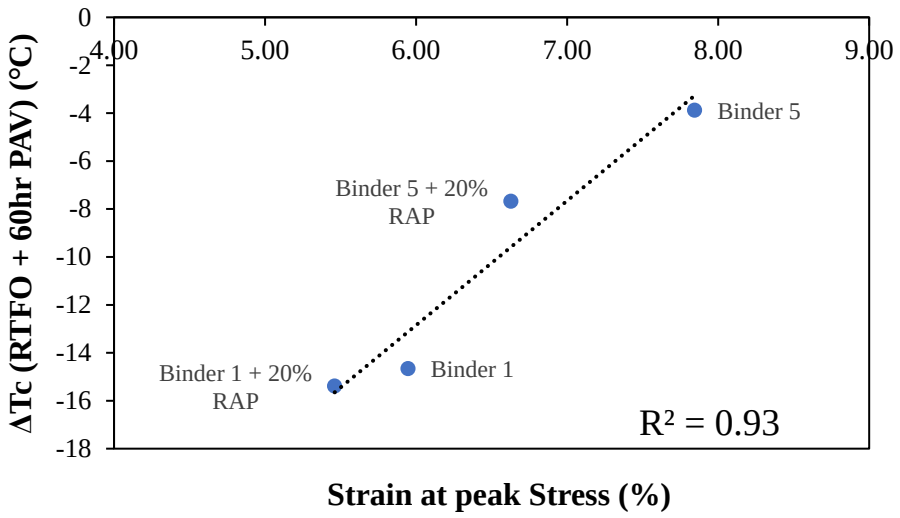

Figure 103. Strain tolerance and ΔTc for base binders

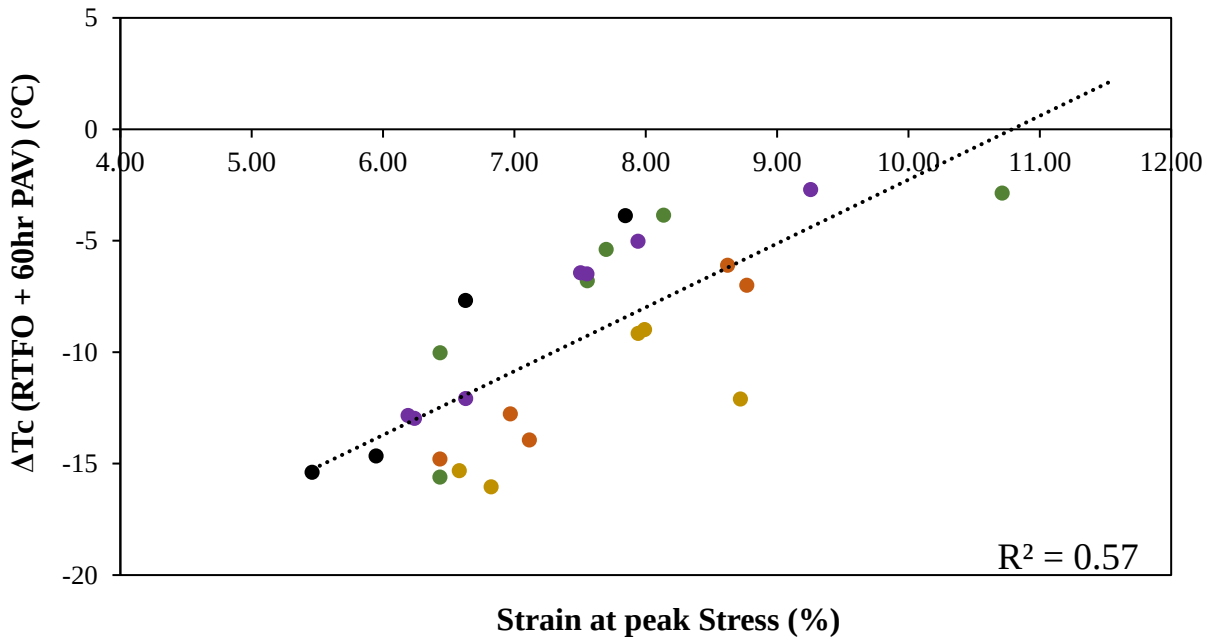

Figure 104. Strain tolerance and ΔTc for base binders and modified blends

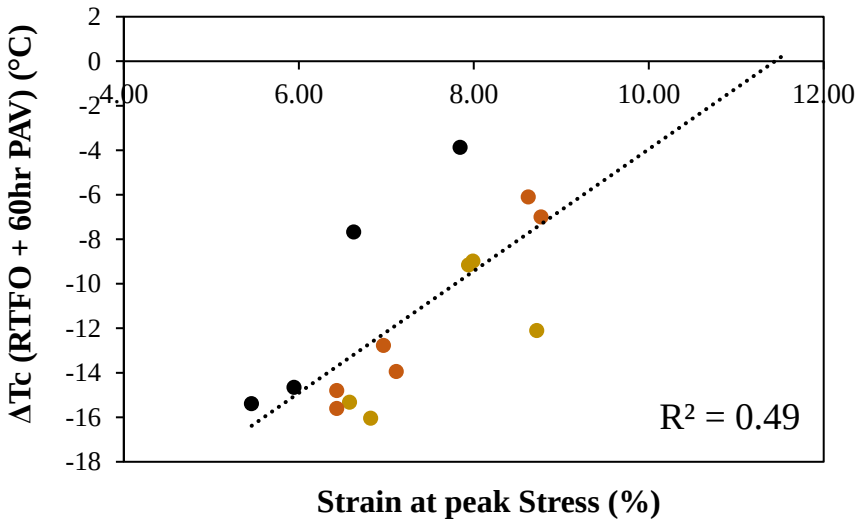

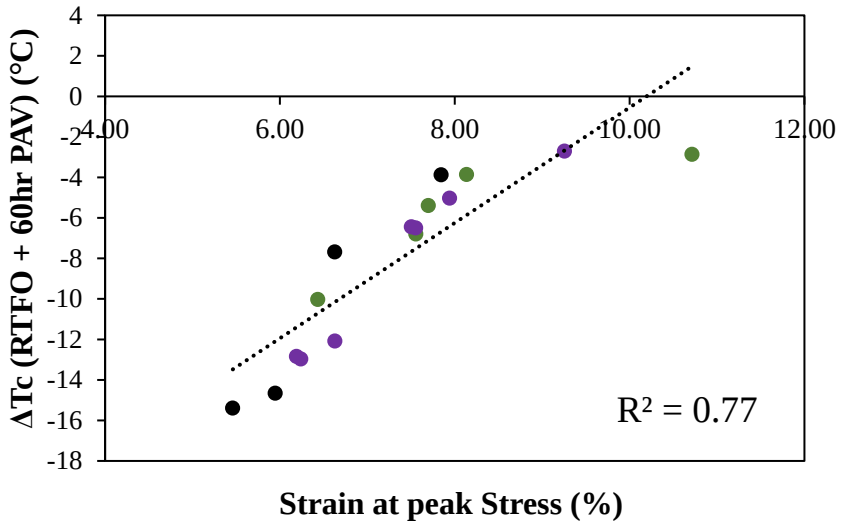

Figure 105. Strain tolerance and ΔTc for base binders and modified blends per Additive type

4.2.5 Temperature – frequency sweeps and master curve creation

Temperature frequency sweeps were conducted on the DSR for unaged samples as well as after RTFO plus 60 hours of PAV aging. RHEA software was used to build master curves of complex modulus G^* and phase angle δ. The curve fitting model followed a "free fitting" approach, as the traditional Christensen Anderson model was not applicable for those technologies containing higher dosage of SBS. A reference temperature of 15 ℃ was selected for the subsequent analysis of the Glover-Rowe parameter.

Master curves for every evaluated technology will be presented in Appendix 1. Each additive will be shown relative to the control binder to identify specific changes on rheology caused by each of the technologies. The following sections will focus on the Glover-Rowe analysis that resulted from master curves, as it is more closely related to the effects of aging and durability of binders.

a. Glover-Rowe Parameter and Black Space Diagrams

The Glover-Rowe parameter for every material was calculated from master curve data at a frequency of $0.005\ rad/s$ and the reference temperature of 15℃, as given by Equation 12. This parameter has been closely correlated with ductility, and has therefore been used as a predictor of fatigue and thermal cracking resistance. Complex modulus $|G^*|$, phase angle (δ) and resulting Glover-Rowe (G-R) parameter values for base binders and modified blends are presented in TABLE 34, for the unaged condition and after RTFO plus 60 hours of PAV aging.

Equation 12. Glover-Rowe parameter

$$G - R\ parameter = G^* \frac{(\cos \delta)^2}{\sin \delta}$$

Black Space diagrams have been used to track the impacts of aging on binder ductility (Habbouche et al., 2020; King et al., 2012; G. Rowe et al., 2014; G. M. Rowe & Sharrock, 2016). After aging, the increase in G^* and reduction in phase angle can be observed as movements along Black Space from bottom right locations towards the top left quadrant. Final locations in Black Space as well as the movements along Black Space following oxidative aging have been linked to the progression of cracking distresses observed in the field (Mensching et al., 2015). The damage zone defined by Rowe was developed for the evaluation of cracking resistance of unmodified binders, so the the nature of some additives in this study may limit its applicability (G. Rowe et al., 2014). Nevertheless, the changes in rheology as observed in Black Space were still useful to determine improvements in aging susceptibility with respect to the control binders.

TABLE 34. $|G^*|$, δ and Glover-Rowe Parameter for Base and Modified Binders

	Unaged			RTFO + 60hr PAV		
	$\|G^*\|(kPa)$	$\delta(°)$	G-R (kPa)	$\|G^*\|(kPa)$	$\delta(°)$	G-R (kPa)
Binder 1	49	77.8	2.3	4746	36.0	5274.9
Binder 1 + Additive 1 OD	40	76.1	2.4	1695	46.0	1136.0
Binder 1 + Additive 1 AD	31	75.9	1.9	1371	51.1	693.1
Binder 1 + Additive 2	233	59.5	69.7	2052	39.4	1930.5
Binder 1 + Additive 3	94	60.2	26.7	1822	38.6	1780.0
Binder 1 + Additive 4	3	84.9	0.03	718	50.1	386.1
Binder 1 + Additive 5	13	76.6	0.70	1022	45.1	719.3
Binder 5	12	79.9	0.4	1056	45.4	731.2
Binder 5 + Additive 1 OD	42	66.3	7.4	1641	47.2	1034.2
Binder 5 + Additive 1 AD	48	65.2	8.2	1900	48.0	1235.5
Binder 5 + Additive 2	111	59.1	127.8	1266	42.1	1222.2
Binder 5 + Additive 3	18	47.9	10.8	525	42.8	416.5
Binder 5 + Additive 4	1	85.2	0.01	263	52.3	124.2
Binder 5 + Additive 5	5	75.2	0.32	464	47.4	289.0
Binder 1 + RAP	304	64.7	61.4	3964	37.3	4145.9
Binder 1 + RAP + Additive 2 OD	256	56.3	95.1	1459	40.8	1278.0
Binder 1 + RAP + Additive 2 AD	229	57.9	76.2	1465	41.1	1263.5
Binder 1 + RAP + Additive 3 OD	183	51.1	92.6	2682	37.9	2713.8
Binder 1 + RAP + Additive 3 AD	118	57.5	40.5	1830	39.8	1683.2
Binder 1 + RAP + Additive 4 OD	11	76.8	0.60	783	49.8	428.0
Binder 1 + RAP + Additive 4 AD	16	78.2	0.70	1491	46.2	991.6
Binder 1 + RAP + Additive 5 OD	68	69.3	9.1	2719	39.9	2492.7
Binder 1 + RAP + Additive 5 AD	83	69.3	11.1	2886	40.3	2593.3
Binder 5 + RAP	235	63.3	53.3	2027	41.4	1724.9
Binder 5 + RAP + Additive 2 OD	146	56.2	54.2	1386	42.3	1125.0
Binder 5 + RAP + Additive 2 AD	151	54.7	188.7	1229	41.3	1052.5
Binder 5 + RAP + Additive 3 OD	50	50.0	92.6	655	44.8	468.9
Binder 5 + RAP + Additive 3 AD	74	52.9	33.8	974	41.6	819.9
Binder 5 + RAP + Additive 4 OD	13	77.1	0.67	723	49.0	412.1
Binder 5 + RAP + Additive 4 AD	11	76.4	0.61	732	48.0	440.7
Binder 5 + RAP + Additive 5 OD	28	68.0	4.2	1068	45.5	734.5
Binder 5 + RAP + Additive 5 AD	42	67.2	6.9	1296	45.4	899.9

Figure 106 and Figure 107 show the Black Space diagrams for neat binders 1 and 5, respectively. Round, filled markers indicate the location of the RTFO plus 60 hr PAV aged materials and triangular, blank markers correspond to the unaged condition. The progression of aging can be seen on movements from the bottom right corner, at lower stiffnesses and greater phase angles, towards the top left corner, given by the greater stiffnesses and more elastic responses observed after aging

.

Figure 106 shows Binder 1 at the top left location, falling within the region of visible surface damage, given by a 600 kPa threshold on the Glover-Rowe parameter. All of the modified binders result on improved locations relative to Binder 1, indicating improvements in cracking performance and durability after 60

hours of PAV aging. More specifically, Additive 4 remained below the visible surface cracking threshold. Superpave PG evaluation showed that Additives 2 and 3 increased the high PG of binders, which can be observed on Black Space as driven mostly by an increase in elastic response (i.e., reduction in phase angle) and to a lesser extent an increase in complex modulus. On the other hand, the softening effect of Additive 4 can also be observed on Black Space, as the unaged condition of the base binder was shifted to a lower stiffness and higher phase angle.. This was also observed for Additive 1, whose unaged properties located in proximity of binder 1. Overall, Black Space illustrated how each technology, despite causing varying effects at the unaged condition, could potentially provide improvements in cracking resistance relative to the base binder after an extended PAV aging cycle.

In addition to final locations in Black Space, the path followed with progressive aging was of interest. The length of the path followed by each binder could potentially indicate their susceptibility to aging. The higher aging susceptibility of Binder 1 was confirmed, as it presented a long displacement on Black Space supporting previous findings that motivated binder selection. Shorter paths were observed for Additives 2 and 3, showing that not only they improved the cracking resistance of the base binder 1, but also reduced its aging susceptibility, which is consistent with other findings for similar modifiers (Habbouche et al., 2021; Heitzman, 1992). On the other hand, Additives 4 and 5 presented longer paths along Black Space, indicating higher aging susceptibility. Thus, it can be argued that the improved final location in Black Space was obtained as a result of a more favourable starting condition.

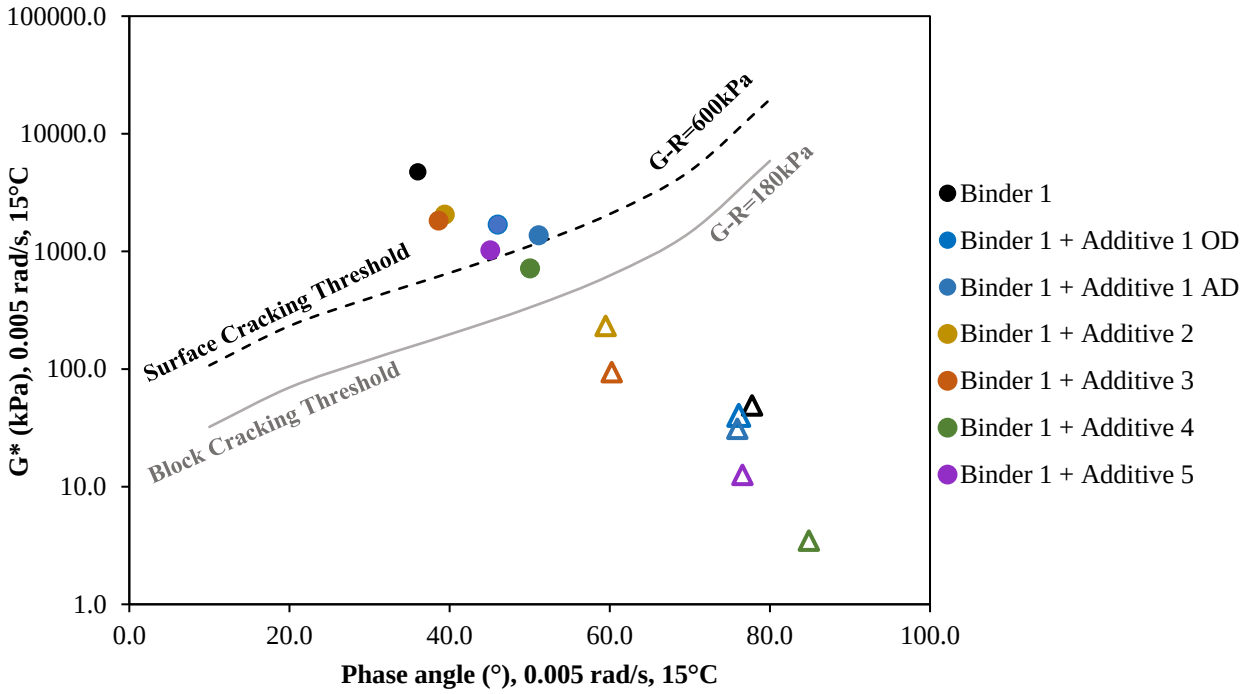

Figure 106. Black Space diagram for Binder 1

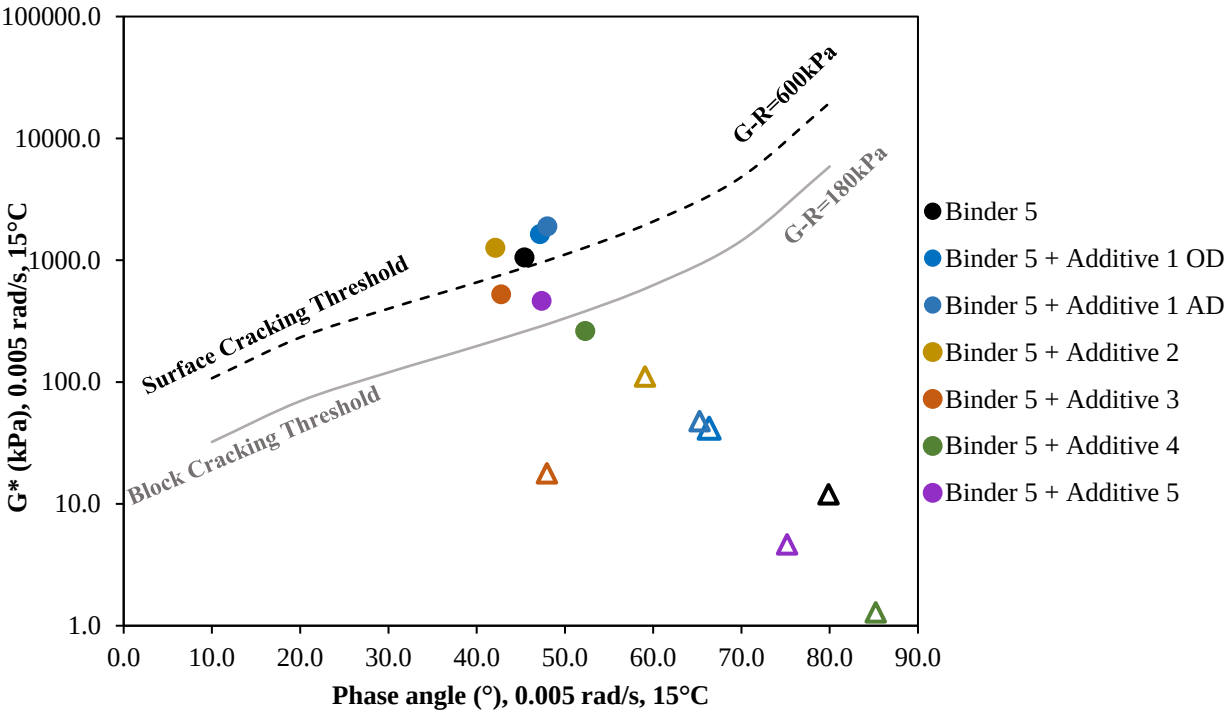

Figure 107. Black Space diagram for Binder 5

Figure 107 presents the effects of modification on Binder 5 on Black Space. Rounded markers showing locations after RTFO plus 60 hours of PAV aging indicated that Additives 1 and 2 resulted on poorer performance than the control binder. After 60 hours of PAV aging these additives showed higher stiffness and lower phase angle relative to the control, suggesting lower ductility and fatigue resistance. Therefore, additive effectiveness at enhancing long-term cracking resistance was found as base binder dependent, which is consistent with other findings for similar additives (Heitzman, 1992).

The overall trends for modified binders match those encountered for Binder 1. Greater susceptibility to oxidation was encountered after modification with Additive 4 and 5, but improvements in cracking resistance were still obtained due to the better starting location of the binder to withstand stiffening due to aging. Additive 4 fell below the threshold for block cracking (180 kPa) while Additive 5 remained below 600 kPa. Additive 3 also fell below this threshold, showing improved cracking resistance which was accompanied by improved aging susceptibility, as given by the shorter path along Black Space.

Overall, most of the technologies under consideration improved the cracking resistance of base binders after extended cycles of PAV aging, shown by the final location of modified binders on Black Space. It was found, however, that modifier effectiveness depended on interactions with the base binders: while Additives 3, 4 and 5 enhanced cracking resistance of both binders, Additives 1 and 2 presented greater effectiveness with Binder 1.

Figure 108 and Figure 109 present the Black Space diagrams for RAP blends. Round markers show the location of binders after RTFO plus 60 hours of PAV aging, while the triangular markers indicate the unaged condition. Final locations in Black Space indicate improvements in cracking resistance and durability of both base binders. Findings for Binder 1 + RAP in Figure 108 show optimum dosage of Additive 4 fell below the 600 kPa threshold of significant surface cracking. Similar trends were observed with the presence of RAP: shorter paths along Black Space were found for Additives 2 and 3. Thus, improved cracking resistance was achieved as well as enhanced aging susceptibility. Lower Glover-Rowe parameters after aging and improved locations in Black Space are in agreement with LAS findings of higher strain tolerance after modification, as presented in Section 4.2.4. Therefore, every technology provided enhanced fatigue resistance and thus greater durability of recycled binder blends with base Binder 1.

Figure 109 shows all additives improved cracking resistance of recycled binder blends with Binder 5. Particularly, Additive 3 and 4 fell below the visible surface cracking threshold after RTFO plus 60 hours of PAV aging. Improved aging susceptibililty was also observed for Additives 2 and 3. As noted for recycled binder blends with Binder 1, Glover-Rowe parameters are in agreement with LAS results.

Overall, RAP blends showed improvements in resistance to fatigue cracking after aging, as given by the location of modified binders in Black Space. Additive effectiveness was consistent across both RAP blends, as opposed to neat binders where poorer performance was observed for Binder 5. Additives 2 and 3, both polymeric modifiers in nature, presented lower susceptibility oxidation, shown by their shorter displacements along Black Space diagrams. Additives 4 and 5, which share an oil-based nature, improve the unaged properties of th ebase bidners (i.e., better starting location on Black Space diagram) and enhanced cracking resistance at the expense of higher aging susceptibility.

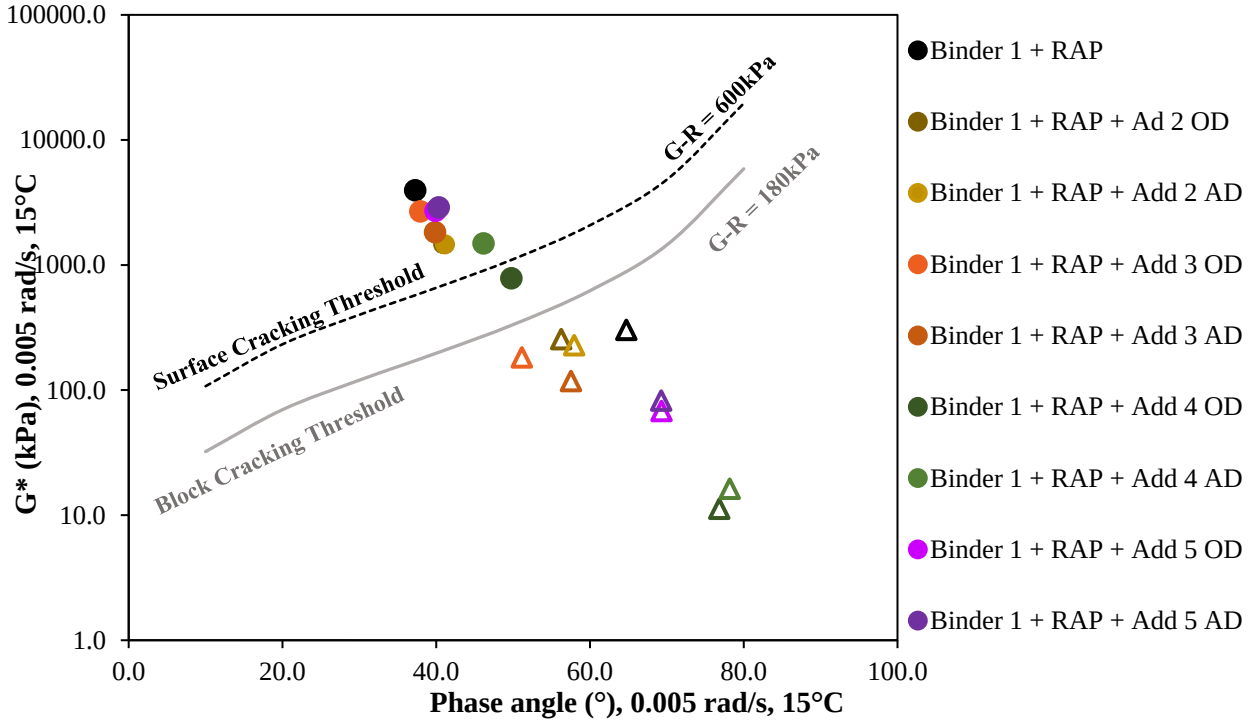

Figure 108. Black Space diagram for Binder 1 with RAP

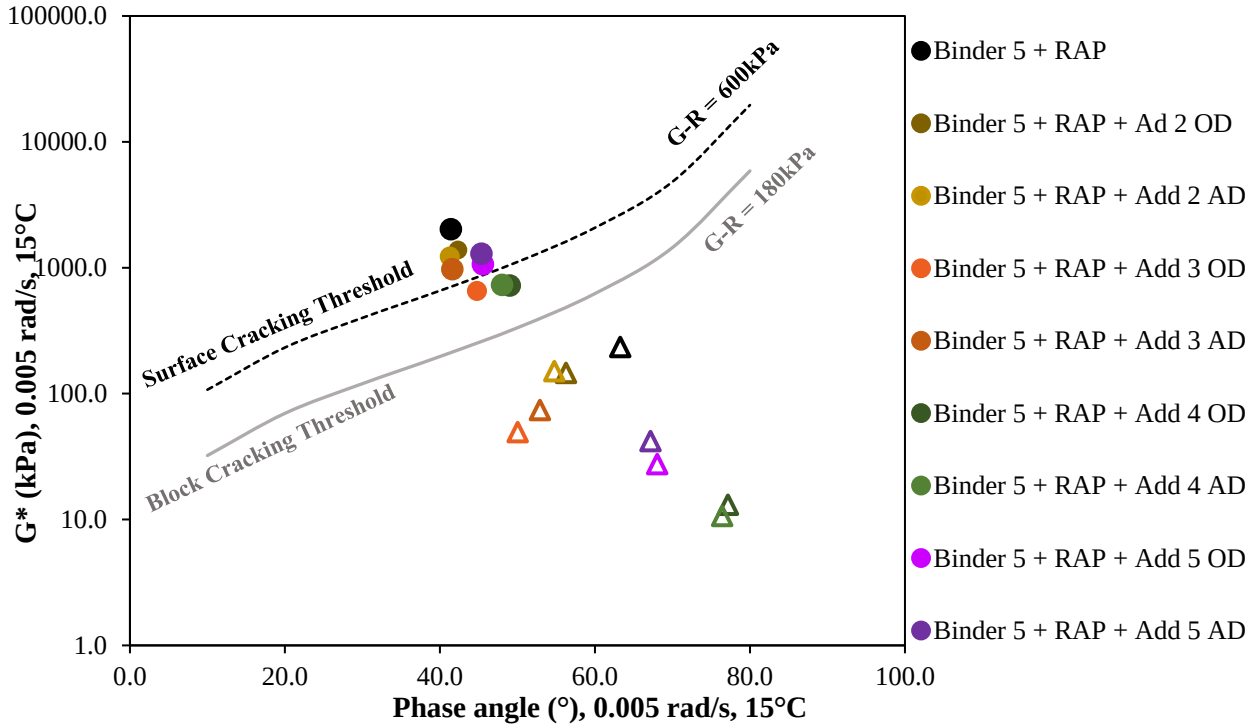

Figure 109. Black Space diagram for Binder 5 with RAP

b. Rheological Aging Indices

Results observed on Black Space diagrams were illustrated through aging indices using the Glover Rowe parameter. Two ratios were evaluated, as shown by Equations (13) and (14). First, aged properties were evaluated with respect to the control binders, to determine the improvement on cracking resistance after the use of each technology. This parameter was defined as Glover-Rowe Effectiveness Index.

Additionally, the Glover-Rowe Aging Index as indicated in Equation (3) was also studied. This parameter has been used by researchers to determine the aging susceptibility of binders (Apeagyei, 2011; J.C. Petersen, 2009; Xiao et al., 2009).

Equation 13. Glover-Rowe Effectiveness Index

$$Glover - Rowe\ Effectiveness\ Index = \frac{(G - R_{RTFO+60\ hr\ PAV})_{Binder\ with\ Additive}}{(G - R_{RTFO+60\ hr\ PAV})_{Control\ Binder}}$$

Equation 14. Glover-Rowe Aging Index

$$Glover - Rowe\ Aging\ Index = \frac{(G - R_{RTFO+60\ hr\ PAV})_{Binder\ with\ Additive}}{(G - R_{Unaged})_{Binder\ with\ Additive}}$$

The Glover-Rowe Effectiveness illustrates the final locations of modified binders on Black Space diagrams relative to the control. Locations to the bottom right of the control after RTFO plus 60 hours of PAV aging are indicative of better Glover-Rowe values and improved fatigue cracking resistance. This will be reflected by a Glover-Rowe Aging Effectiveness smaller than 1. Even smaller values will be indicative of greater additive effectiveness. The Glover-Rowe Aging Index represents the path and distance travelled by modified binders along Black Space and shows additive aging susceptibility. Higher values indicate the modified binder experienced greater changes for equal aging durations.

Glover-Rowe Effectiveness Indices for base binder 1 and 5 are presented in Figure 110 and Figure 111, respectively. Additives 3, 4 and 5 showed values smaller than 1 for both base binders, thus reducing the stiffening and embrittlement effects of aging. However, Additives 1 and 2 showed improvements on Binder 1, but were less effective on Binder 5. In this case, indices greater than 1 for modified binders indicate fatigue cracking resistance and durability was not improved after modification. In addition, LAS results (Section 4.2.4) showed lower or no significant increase in strain tolerance, which agrees with the above findings.

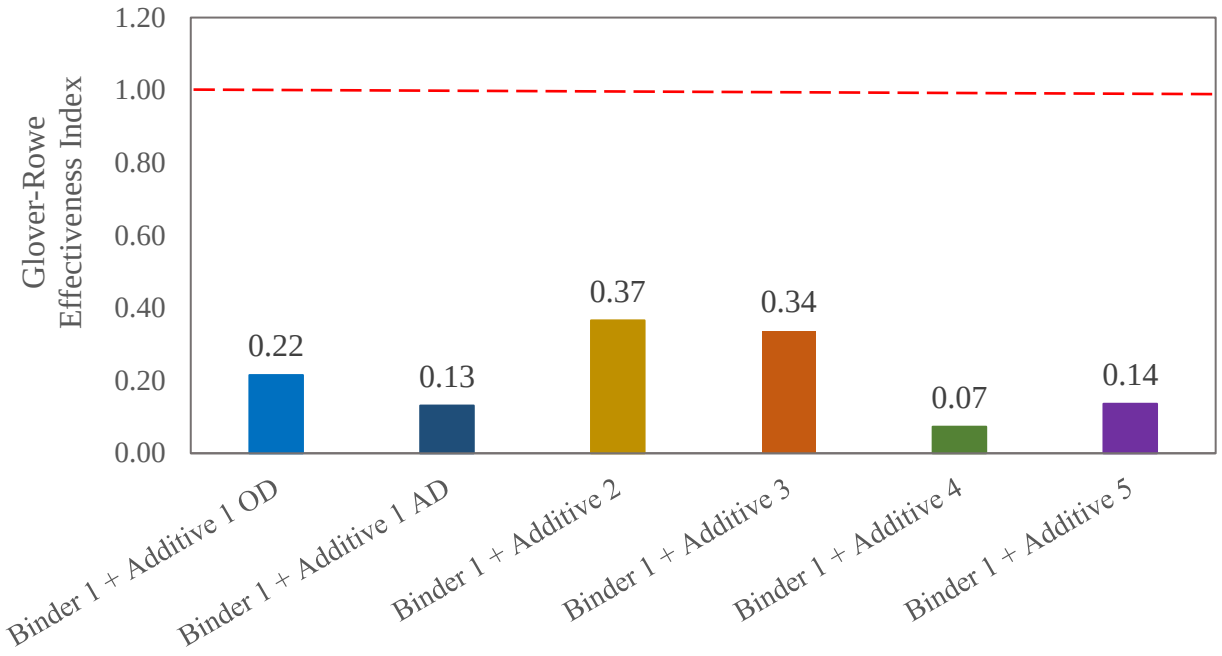

Figure 110. Glover-Rowe Effectiveness Index for Binder 1

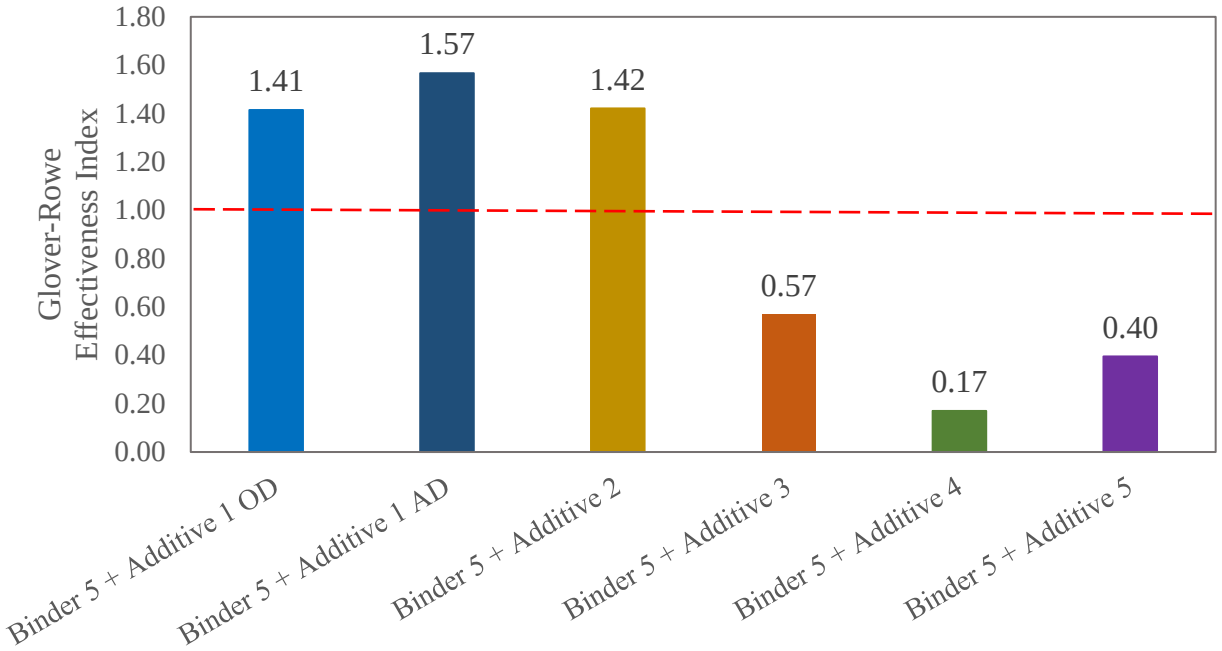

Figure 111. Glover-Rowe Effectiveness Index For Binder 5

Glover-Rowe Effectiveness Indices for recycled binder blends with Binder 1 and Binder 5 are shown in Figure 112 and Figure 113, respectively. Results showed every additive improved fatigue cracking resistance with respect to the control blends, , as indices fell consistently below 1.

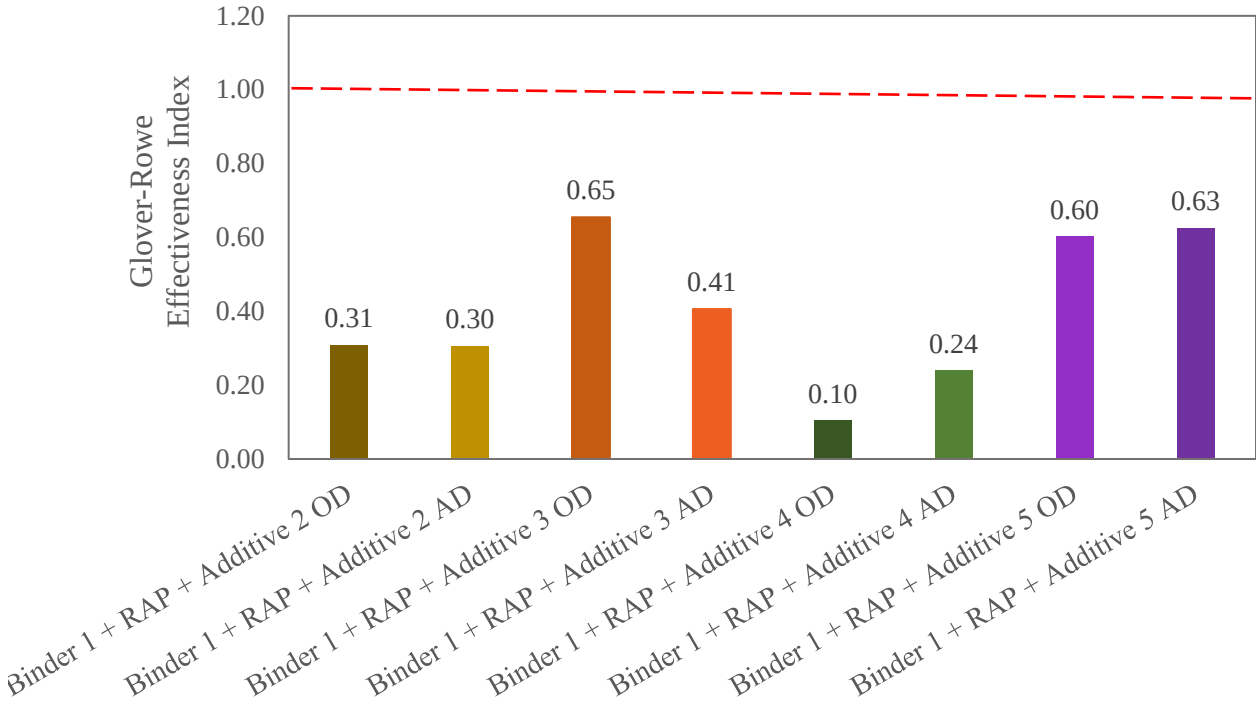

Figure 112. Glover-Rowe Aging Effectiveness Index For Binder 1 + RAP

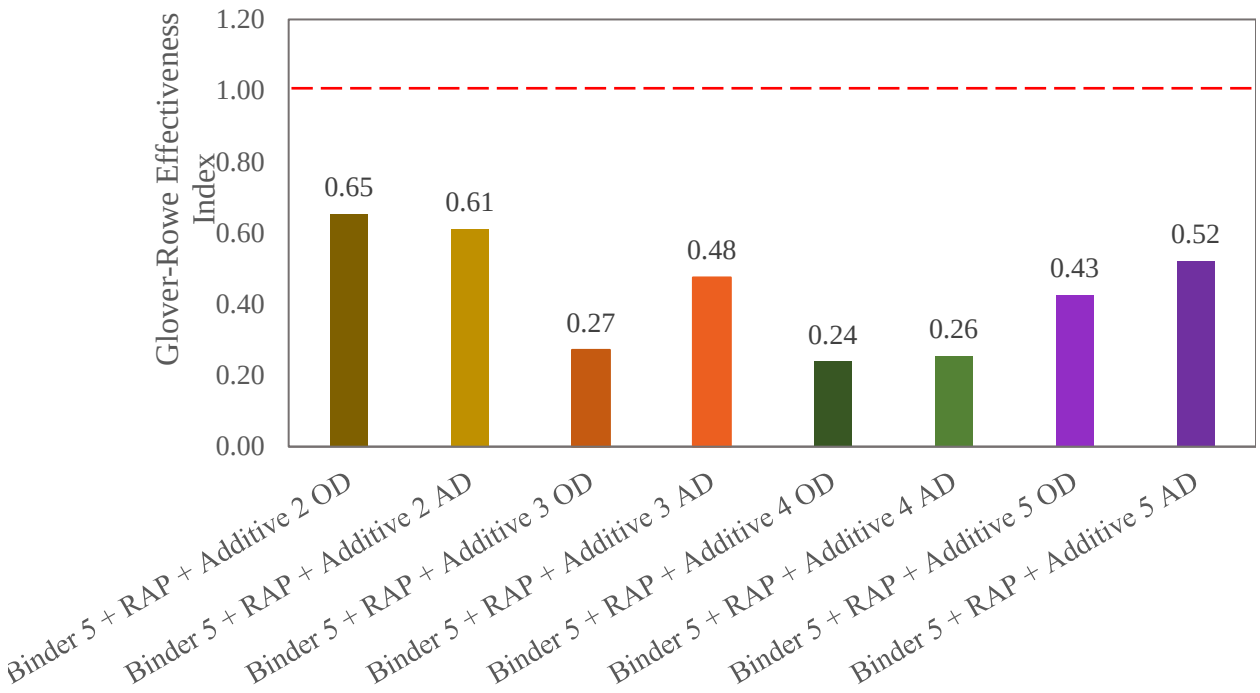

Figure 113. Glover-Rowe Effectiveness Index for Binder 5 + RAP

Glover-Rowe Aging Indices for base binders 1 and 5 are shown in Figure 114 and Figure 115, respectively. Binder 1 showed a higher Aging Index than Binder 5, indicating higher aging susceptibility, and supports the results discussed in Section 4.1 for base binder selection. Additionally, improved aging susceptibility was found after modification with every additive except for number 4. The greater increase in Glover-Rowe relative to the control indicated that this additive, by itself, experienced greater changes due to aging. However, given the softening effect shown by its starting location on Black Space, the final position of the modified binder relative to the control was still indicative of improved rheological properties.

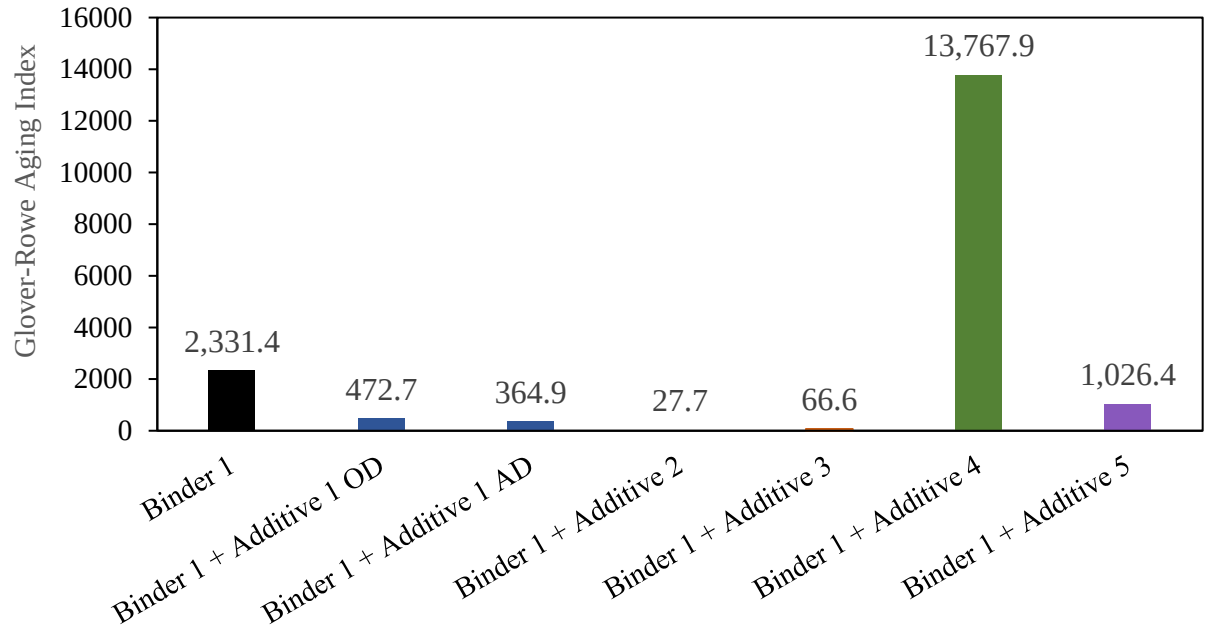

Figure 114. Glover-Rowe Aging Index of Binder 1 and modified binders

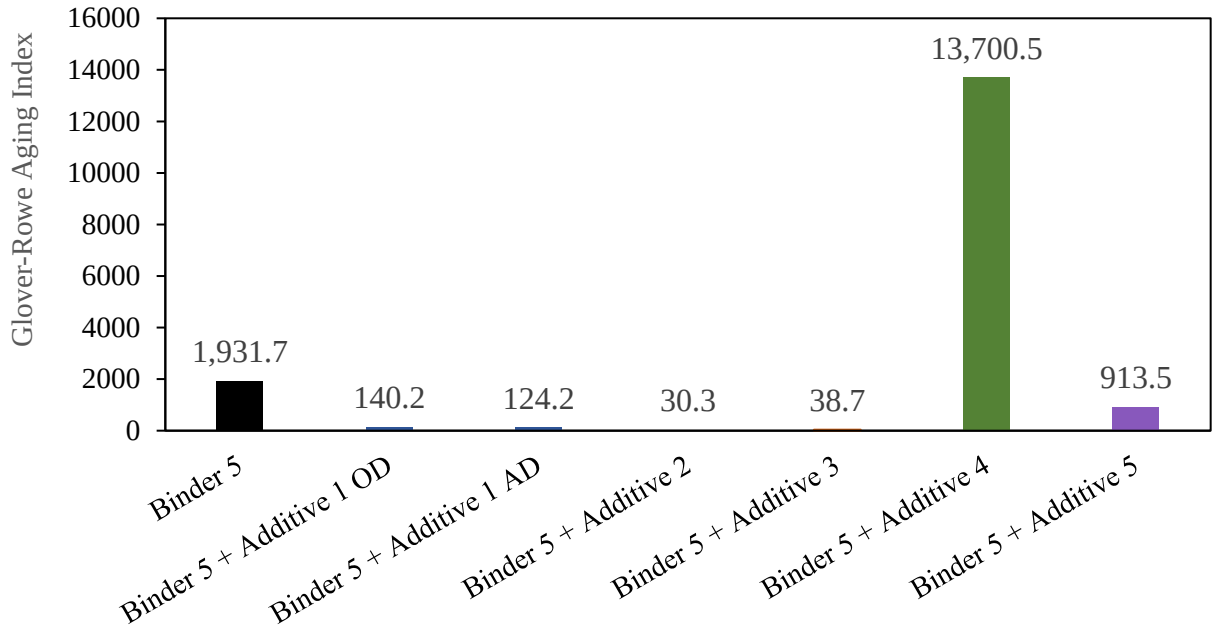

Figure 115. Glover-Rowe Aging Index of Binder 5 and modified binders

Glover Rowe Aging Indices for RAP blends with base binders 1 and 5 are shown in Figure 116 and Figure 117, respectively. Additive 4 showed a similar behavior when interacting with RAP blends as with base binders, with a greater aging susceptibility. In this case, Additive 5 also experienced more aging than the control blend while providing improvements on Glover-Rowe after aging. Thus, this finding further supports how starting locations on Black Space are equally important to final properties to track the effect of oxidative aging on cracking resistance (Elwardany, King, et al., 2020; King et al., 2012).

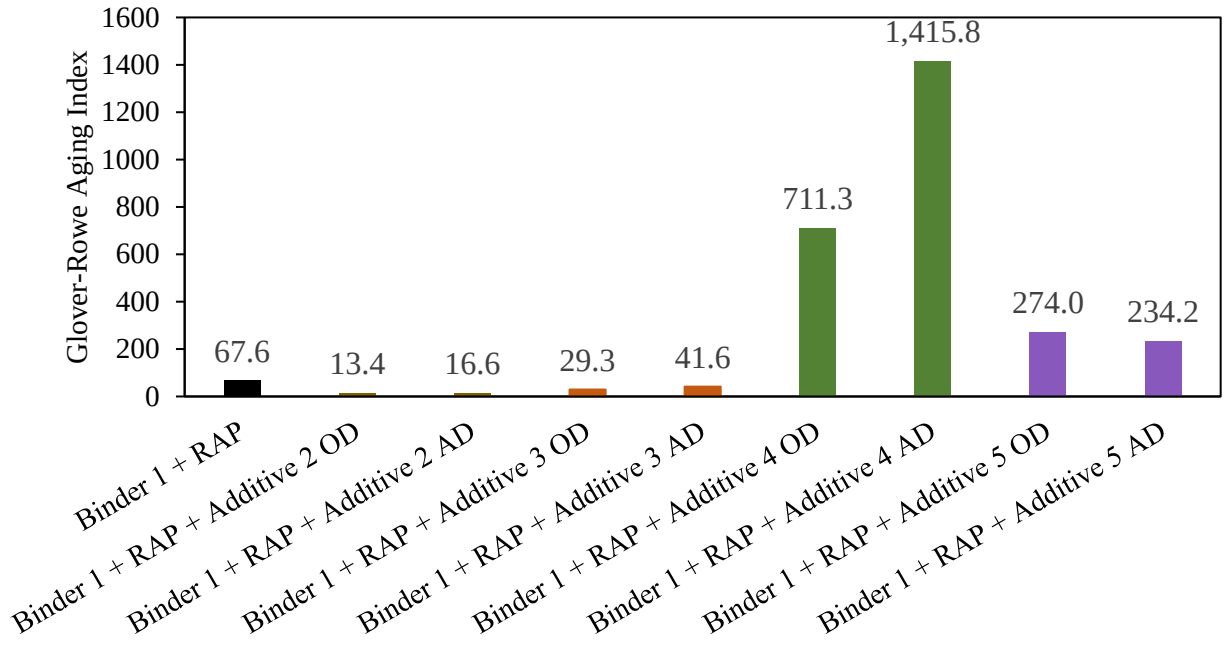

Figure 116. Glover-Rowe Aging Index of Binder 1 with RAP and modified binders

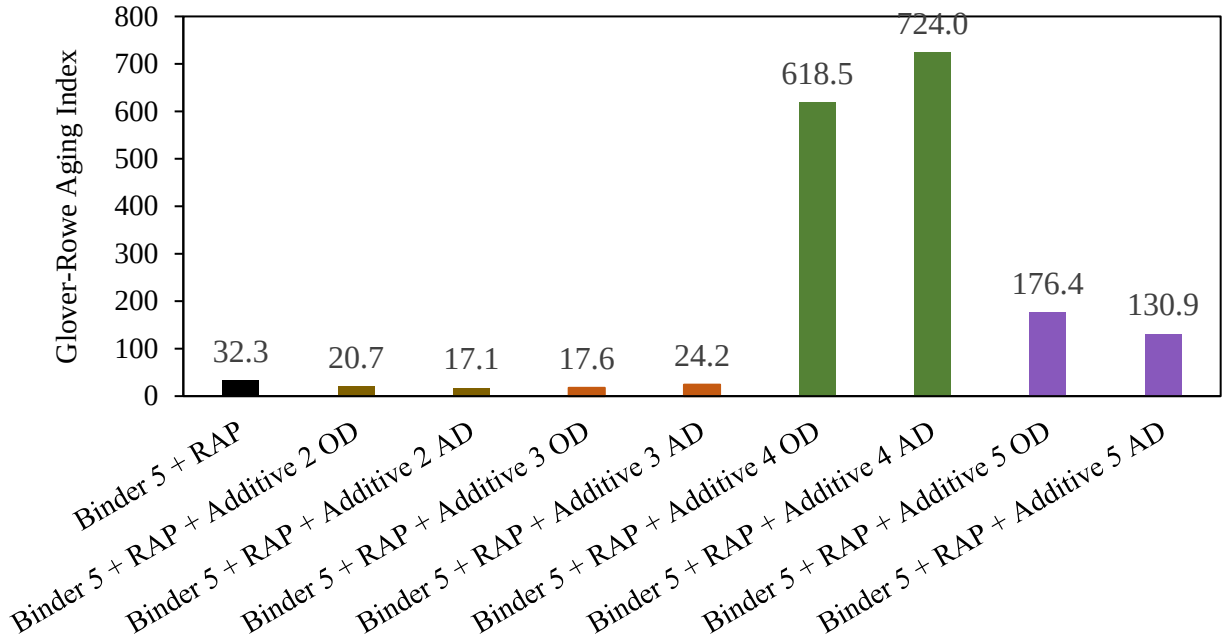

Figure 117. Glover-Rowe Aging Index of Binder 5 with RAP and modified binders

4.2.6 Extended BBR Test

The physical hardening behavior (i.e., the thermo-reversible relaxation process taking place in the glass transition region) of the base and modified binders was evaluated through extended BBR testing following an adapted version of AASHTO TP 122. In this study, the conditioning and testing temperature was the Glass Transition (T_g) of each base and modified binder, as research has shown that the maximum rate of physical hardening occurs at the T_g temperature (Hassan A Tabatabaee, Velasquez, & Bahia, 2012).

Differential Scanning Calorimetry (DSC) was used to measure the T_g temperature of the base binders and modified blends at selected dosages after RTFO plus 60 hours of PAV aging. The T_g at half-height was selected for extended BBR testing, as will be discussed detail in Section 4.3.3. The physical hardening rate of binders depends on chemical composition and therefore interactions with each Additive might cause changes in this behavior. A hardening index (S/S_0) was calculated as the ratio of the creep stiffness after 24 hours of isothermal conditioning at the T_g temperature of each modified blend to that of the base binder. Therefore, improvements in physical hardening behavior of the base binders would be given by indices lower than 1.

The T_g, extended BBR test results, and hardening indices are presented in TABLE 35 for base binder 1 and modified blends and TABLE 36 for Base binder 5 and modified blends.

TABLE 35. Tg(H) and Extended BBR Results for Binder 1 and Modified Blends

	Tg (H) (°C)	**Stiffness after 24-h conditioning at Tg (Mpa)**	**m-value after 24-h conditioning at Tg (Mpa)**	S/S_0
Binder 1	-17.2	485	0.190	
Binder 1 + Additive 1 OD	-13.9	363	0.209	0.75
Binder 1 + Additive 2 OD	-18.9	340	0.214	0.70
Binder 1 + Additive 3 AD	-15.6	345	0.220	0.71
Binder 1 + Additive 4 OD	-20.1	277	0.235	0.57
Binder 1 + Additive 5 OD	-18.1	279	0.233	0.57

TABLE 36. Tg(H) and Extended BBR Results for Binder 5 and Modified Blends

	Tg (°C)	**Stiffness after 24-h conditioning at Tg (Mpa)**	**m-value after 24-h conditioning at Tg (Mpa)**	S/S_0
Binder 5	-8.1	154	0.281	
Binder 5 + Additive 1 OD	-5.5	142	0.265	0.92
Binder 5 + Additive 2 AD	-19.6	343	0.225	2.22
Binder 5 + Additive 3 OD	-17.2	136	0.293	0.88
Binder 5 + Additive 4 OD	-17.2	217	0.285	1.41
Binder 5 + Additive 5 OD	-17.0	195	0.278	1.26

Hardening indices of modified blends with Binder 1 were smaller than 1 for every Additive, as shown in Figure 118. Thus, results showed that every additive improved the physical hardening behavior with respect to base Binder 1.

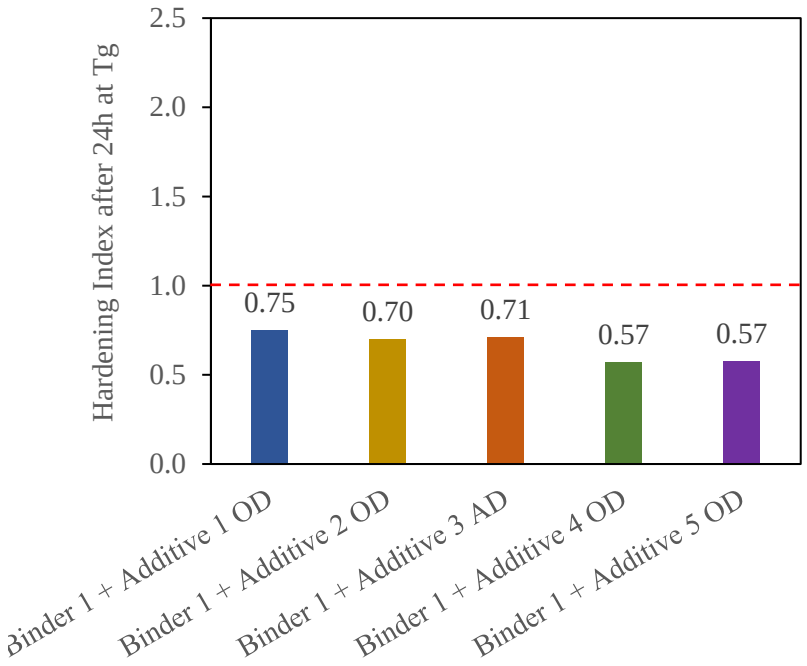

Figure 118. Hardening Indices for modified blends with base Binder 1

However, Figure 119 shows that only Additives 1 and 3 resulted in hardening indices smaller than 1 when blended with base Binder 5. Therefore, Additives 2, 4 and 5 showed lower effectiveness at improving the physical hardening behavior of base binder 5, as indicated by hardening indices greater than 1.

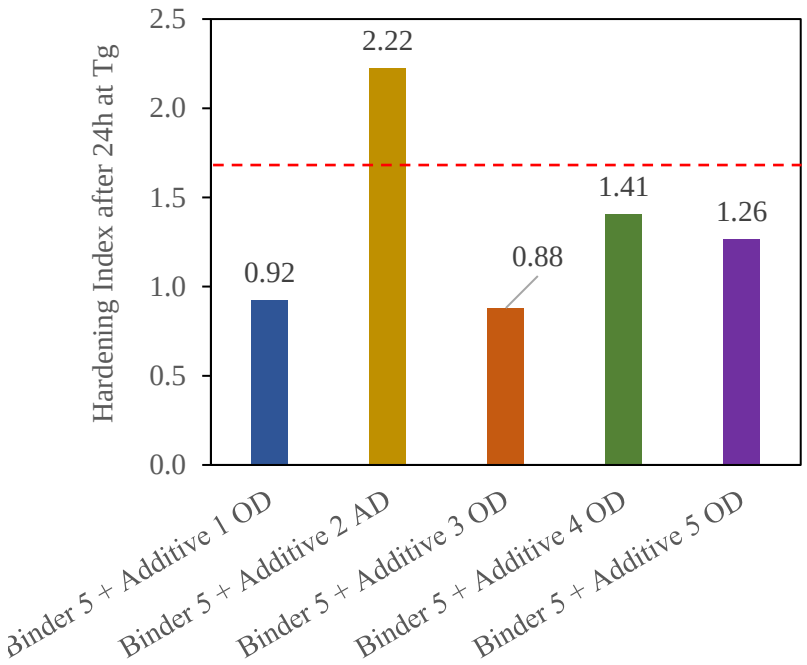

Figure 119. Hardening Indices for modified blends with base Binder 5

Overall, extended BBR testing evaluated the physical hardening behavior of base and modified binders following an adaptation of AASHTO TP 122. Every material was subjected to the highest physical hardening rate by testing and conditioning samples at the glass transition temperature (from DSC measurements). Results showed that Additives 1 and 3 improved the physical hardening behavior of both base binders, as shown by hardening indices smaller than 1. Additives 2, 4 and 5 improved the physical hardening behavior of Binder 1, but not for Binder 5, as their hardening indices were greater than 1. Thus, additives may improve the physical hardening behavior of the base binders, which would lead to improvements in thermal cracking resistance (Bricker & Hesp, 2013; Hesp et al., 2009).

4.2.7 Summary of Rheological findings and dosage selection

a. Superpave Performance Grading

Superpave PG showed that the proposed aging resistant technologies improved the high, intermediate, and low temperature properties of the control binders after laboratory aging. Performance grading of unmodified and modified binders was conducted at the unaged condition and after 20 and 60 hours of PAV aging and statistical analyses were performed to determine significant changes relative to the control binders. TABLE 37 summarizes how each rheological parameter was studied to determine improvements in durability of binders. TABLE 38 details the Additive and dosage that were statistically different relative to each of the control binders. It should be noted that statistical analyses were performed on BBR measurements. Since DSR testing was performed on single replicates, no statistical significance could be performed.

TABLE 37. Rheological Parameters and Effects on Aging Resistance of Binders

Superpave parameter	Evaluation	Effect on durability
High temperature True Grade	$HT_{(RTFO + 60hr\ PAV)} - HT_{(Unaged)}$	Smaller variation indicates lower stiffening rate
Intermediate temperature True Grade	$IT_{(RTFO + 60hr\ PAV)}$	Lower intermediate temperature after extended aging indicate improvement in fatigue resistance
Low critical temperatures	$LT_{(RTFO + 60hr\ PAV)}$	Lower critical temperature indicates better resistance to thermal stresses and better relaxation properties
	$LT_{(RTFO + 60hr\ PAV)} - LT_{(RTFO + 20hr\ PAV)}$	Smaller variation in critical low temperatures indicate smaller loss in relaxation properties
ΔT_C	$\Delta T_C(RTFO + 60hr\ PAV)$	Higher (more positive) values of ΔTc indicate improved resistance to non-load related distresses
	$\Delta T_C(RTFO + 60hr\ PAV) - \Delta T_C(RTFO + 20hr\ PAV)$	A smaller increase in ΔTc indicates a smaller loss in relaxation properties and thus, enhanced aging resistance

TABLE 38. Additive Improvements on Superpave Rheological Parameters

	Lower HT Variation	Lower IT After RTFO + 60 Hours Pav	Lower LT (RTFO + 60hr Pav)	Lower LT True Grade Variation	Higher (More Positive) ΔTc	Smaller Reduction In ΔTc
Binder 1	Additive 1 OD, AD Additive 2 OD Additive 4 OD	Additive 1 OD, AD Additive 2 OD Additive 3 OD Additive 4 OD Additive 5 OD	Additive 2 OD Additive 4 OD Additive 5 OD	Additive 2 OD Additive 4 OD	Additive 4 OD Additive 5 OD	Additive 3 OD Additive 4 OD
Binder 5	Additive 3 OD	Additive 3 OD Additive 4 OD Additive 5 OD	Additive 4 OD Additive 5 OD			
Binder 1 + RAP	Additive 2 OD, AD Additive 4 AD Additive 5 AD	Additive 2 AD Additive 3 OD, AD Additive 4 OD, AD	Additive 2 OD, AD Additive 3 OD, AD Additive 4 OD, AD Additive 5 OD, AD	Additive 2 OD, AD Additive 3 OD, AD Additive 4 OD, AD	Additive 3 OD, AD Additive 4 OD, AD Additive 5 OD, AD	Additive 3 OD, AD Additive 4 AD
Binder 5 + RAP	Additive 2 OD Additive 3 OD, AD Additive 4 OD, AD Additive 5 OD, AD	Additive 2 OD, AD Additive 3 OD, AD Additive 4 OD, AD Additive 5 OD, AD	Additive 4 OD, AD Additive 5 OD, AD	Additive 2 OD Additive 4 OD, AD	Additive 4 OD, AD Additive 5 OD	Additive 2 OD Additive 4 OD, AD Additive 5 OD

b. Linear Amplitude Sweep Test

Linear Amplitude Sweep tests were conducted after RTFO followed by 60 hours of PAV aging to determine improvement in fatigue life. TABLE 39 summarizes statistically significant results for each additive and control binder considering number of cycles to failure, |B|-parameter and strain at peak stress (i.e., strain tolerance).

TABLE 39. Additive Improvements on Fatigue Life from LAS Test

	Increase In Cycles to Failure (at 5% strain)	Reduction In |B| - Parameter	Increase In Strain Tolerance
Binder 1	Additive 1 AD Additive 2 OD Additive 3 OD Additive 4 OD Additive 5 OD	Additive 1 OD, AD Additive 2 OD Additive 3 OD Additive 4 OD Additive 5 OD	Additive 1 AD Additive 3 OD Additive 4 OD Additive 5 OD
Binder 5	Additive 3 OD Additive 4 OD Additive 5 OD	Additive 4 OD	Additive 3 OD Additive 4 OD Additive 5 OD
Binder 1 + RAP	Additive 2 OD, AD Additive 3 OD, AD Additive 4 OD	Additive 2 OD, AD Additive 3 OD, AD Additive 4 OD, AD Additive 5 OD, AD	Additive 2 OD, AD Additive 3 OD, AD Additive 4 OD, AD Additive 5 OD, AD
Binder 5 + RAP	Additive 2 OD, AD Additive 3 OD, AD Additive 4 AD Additive 5 OD	Additive 3 OD Additive 4 OD, AD Additive 5 OD	Additive 2 OD, AD Additive 3 OD, AD Additive 4 OD, AD Additive 5 OD

c. Glover-Rowe Parameter and Black Space Diagram

Improvement on binder cracking resistance after aging were evaluated by the Glover-Rowe parameter. The ratio of the $G - R$ between modified binders and the control (i.e., Glover-Rowe Aging Effectiveness) was calculated to determine the effectiveness of the additives in decreasing the stiffness and embrittlement of the control binders after aging. Improvement in fatigue cracking resistance was caused by the Additives in TABLE 40, which provided indices lower than 1.

TABLE 40. Additive Improvements on Fatigue Life from Glover-Rowe Parameter

	Glover-Rowe Aging Effectiveness Lower Than 1
Binder 1	Additive 1 OD, AD Additive 2 OD Additive 3 OD Additive 4 OD Additive 5 OD
Binder 5	Additive 3 OD Additive 4 OD Additive 5 OD
Binder 1 + RAP	Additive 2 OD, AD Additive 3 OD, AD Additive 4 OD, AD Additive 5 OD, AD
Binder 5 + RAP	Additive 2 OD, AD Additive 3 OD, AD Additive 4 OD, AD Additive 5 OD, AD

d. Relative Ranking of Cracking-Related Parameters

Improvements in aging resistance of binders have been observed through improvements in fatigue cracking resistance. Rheological findings have shown Additives mitigated the stiffening and embrittlement caused by aging, which would therefore enhance cracking resistance, providing longer fatigue lives. To illustrate additive effectiveness, a relative ranking for each Additive and dosage was studied in terms of three fatigue cracking parameters previously discussed: Glover-Rowe parameter, reduction in ΔT_C between 20 and 60 hours of PAV aging, and strain at peak stress.

Additive rankings for each base binder and RAP blend are presented in TABLE 41 through TABLE 44. The most effective additives are placed at the top of the table and were determined from the lowest G-R Effectiveness Index, the smallest reduction in ΔTc and the largest strain at peak stress. Differences in rankings resulted from the parameter under consideration, base binder type and the presence of RAP. Only two Additives showed consistent ranking across the three parameters: Additive 1 with Binder 5 and Additive 4 (at the OD) with Binder 1 with RAP. This highlights the need for a comprehensive evaluation of rheological properties and multiple parameters to determine improvements in cracking resistance given by such diverse array of modifiers.

In addition, base binder dependency as well as the influence of RAP can be captured through these rankings. For example, Additive 1 resulted on high ranking upon interactions with Binder 1, while leading to the least improvements in aging resistance of Binder 5, which supports the rationale behind binder selection.

TABLE 41. Additive Ranking for Cracking-Related Parameters Relative to Binder 1

Glover-Rowe Effectiveness Index	ΔTc Reduction (60hr PAV-20hr PAV)	Strain at Peak Stress
Additive 4 OD	Additive 1 AD	Additive 1 AD
Additive 1 AD	Additive 1 OD	Additive 4 OD
Additive 5 OD	Additive 3 OD	Additive 3 OD
Additive 1 OD	Additive 4 OD	Additive 5 OD
Additive 3 OD	Additive 2 OD	Additive 2 OD
Additive 2 OD	Additive 5 OD	Additive 1 OD

TABLE 42. Additive Ranking for Cracking-Related Parameters Relative to Binder 5

Glover-Rowe Effectiveness Index	ΔTc Reduction (60hr PAV-20hr PAV)	Strain at Peak Stress
Additive 4 OD	Additive 3 OD	Additive 3 OD
Additive 5 OD	Additive 5 OD	Additive 4 OD
Additive 3 OD	Additive 1 OD	Additive 5 OD
Additive 1 OD	Additive 2 OD	Additive 2 OD
Additive 2 OD	Additive 4 OD	Additive 1 AD
Additive 1 AD	Additive 1 AD	Additive 1 OD

TABLE 43. Additive Ranking for Cracking-Related Parameters Relative to Binder 1 RAP Blends

Glover-Rowe Effectiveness Index	ΔTc Reduction (60hr PAV-20hr PAV)	Strain at Peak Stress
Additive 4 OD	Additive 4 AD	Additive 4 OD
Additive 4 AD	Additive 2 OD	Additive 3 AD
Additive 2 AD	Additive 4 OD	Additive 2 OD
Additive 2 OD	Additive 5 AD	Additive 2 AD
Additive 3 AD	Additive 3 AD	Additive 4 AD
Additive 5 OD	Additive 3 OD	Additive 3 OD
Additive 5 AD	Additive 2 AD	Additive 5 AD
Additive 3 OD	Additive 5 OD	Additive 5 OD

TABLE 44. Additive Ranking for Cracking-Related Parameters Relative to Binder 5 RAP Blends

Glover-Rowe Effectiveness Index	ΔTc Reduction (60hr PAV-20hr PAV)	Strain at Peak Stress
Additive 4 OD	Additive 2 OD	Additive 3 OD
Additive 4 AD	Additive 4 OD	Additive 2 AD
Additive 3 OD	Additive 4 AD	Additive 3 AD
Additive 5 OD	Additive 5 OD	Additive 4 AD
Additive 3 AD	Additive 5 AD	Additive 2 OD
Additive 5 AD	Additive 3 AD	Additive 5 OD
Additive 2 AD	Additive 2 AD	Additive 4 OD
Additive 2 OD	Additive 3 OD	Additive 5 AD

e. Dosage selection from Rheological Evaluation

For each additive, the dosage [i.e., either Optimum (OD) or Alternative (AD)] that resulted in higher performance as determined by Superpave PG, MSCR, LAS and Glover-Rowe parameter was selected. TABLE 45 shows the dosage selection for Additive 1. Shaded values indicate the better performing dosage in comparison to the control binders. Better rheological properties were consistently observed for Binder 5 with the OD. For Binder 1, it appears AD resulted on better performance across more parameters. Due to the previously discussed limitations with BBR testing, and the curing challenges on the material, the OD was selected for the next testing step.

TABLE 45. Comparison Between Optimum and Alternative Dosages - Additive 1

	Additive 1					
Rheological parameter	**Binder 1**	**OD**	**AD**	**Binder 5**	**OD**	**AD**
HT Variation (°C)	35.0	27.0	25.7	37.9	45.7	50.0
IT after 60h PAV (°C)	30.2	26.1	24.8	25.2	27.6	28.1
LT Variation (°C)	10.3	2.8	3.4	4.5	5.0	7.1
ΔTc after aging (°C)	-13.3	-4.8	-3.4	-5.6	-5.4	-7.1
Reduction in ΔTc (°C)	-10.2	-3.1	-2.3	-5.1	-3.8	-5.9
MSCR Jnr (kPa $^{-1}$)	2.8	2.5	2.5	3.1	0.6	0.6
MSCR Jnr Grade	S	S	S	S	V	V
MSCR % Recovery	0.19	3.08	2.47	0.47	31.32	29.01
Strain tolerance (%)	5.948	5.707	7.701	7.846	6.337	6.388
B parameter	6.70	5.42	4.78	4.96	5.17	5.17
G-R after aging (kPa)	5274.9	1136.0	693.1	731.2	1034.2	1145.5
G-R effectiveness index		0.22	0.13		1.41	1.57

TABLE 46 compares the results for each dosage of Additive 2. Binder 1 with RAP showed greater improvements when modified at the optimum dosage. Conversely, Binder 5 with RAP did not show such a consistent trend. As the alternative dosage showed improved fatigue life given by a greater strain tolerance from LAS and better fatigue resistance due to a lower Glover-Rowe value, it was thus selected.

TABLE 46. Comparison Between Optimum and Alternative Dosages - Additive 2

	Additive 2					
Rheological parameter	**Binder 1 + RAP**	**OD**	**AD**	**Binder 5 + RAP**	**OD**	**AD**
HT Variation (°C)	32.4	25.4	27.2	37.4	33.0	36.7
IT after 60h PAV (°C)	28.9	27.9	26.7	31.8	24.2	23.2
LT Variation (°C)	10.7	7.3	7.8	8.6	5.8	7.0
ΔTc after aging (°C)	-15.4	-16.1	-15.4	-7.7	-9.0	-12.1
Reduction in ΔTc (°C)	-9.2	-6.5	-7.6	-7.2	-3.0	-6.2
MSCR Jnr (kPa -1)	0.9	0.1	0.1	1.0	0.1	0.1
MSCR Jnr Grade	V	E	E	V	E	E
MSCR % Recovery	5.64	60.37	52.57	7.74	50.81	58.97
Strain tolerance (%)	5.461	6.824	6.582	6.629	7.992	8.722
B parameter	6.87	6.07	6.02	5.56	5.42	5.45
G-R after aging (kPa)	4145.9	1278.0	1263.5	1724.9	1125.0	1052.5
G-R effectiveness index		0.31	0.30		0.65	0.61

Dosage comparison for Additive 3 is presented in TABLE 47. The alternative dosage showed consistently better performance than the optimum for RAP blends with Binder 1. Binder 5 RAP blends showed greater improvements in Superpave parameters with the alternative dosage. However, the parameters related to cracking resistance and durability (i.e., strain tolerance, |B| parameter and Glover-Rowe) showed greater improvement with the optimum dosage and was therefore preferred.

TABLE 47. Comparison Between Optimum and Alternative Dosages - Additive 3

	Additive 3					
Rheological parameter	**Binder 1 + RAP**	**OD**	**AD**	**Binder 5 + RAP**	**OD**	**AD**
HT Variation (°C)	32.4	30.8	30.7	37.4	65.6	56.2
IT after 60h PAV (°C)	28.9	29.4	25.7	31.8	20.9	23.6
LT Variation (°C)	10.7	8.6	8.6	8.6	7.6	6.6
ΔTc after aging (°C)	-15.4	-15.6	-12.6	-7.7	-7.0	-6.1
Reduction in ΔTc (°C)	-9.2	-7.5	-7.3	-7.2	-6.4	-5.6
MSCR Jnr (kPa^{-1})	0.9	0.0	0.0	1.0	0.0	0.0
MSCR Jnr Grade	V	E	E	V	E	E
MSCR % Recovery	5.64	89.34	87.49	7.74	92.39	92.90
Strain tolerance (%)	5.461	6.435	6.970	6.629	8.770	8.624
B parameter	6.87	6.30	5.84	5.56	5.00	5.27
G-R after aging (kPa)	4145.9	2713.8	1683.2	1724.9	468.9	819.9
G-R effectiveness index		0.65	0.41		0.27	0.48

The comparison between dosages of Additive 4 is presented in TABLE 48. Consistently better performance was observed with the optimum dosage for Binder 1 with RAP and was therefore selected. Results for Binder 5 with RAP showed that the alternative dosage showed higher strain tolerance, while the optimum dosage caused the greatest reduction in Glover-Rowe parameter. In this case, the Glover-Rowe parameter guided the selection of the optimum dosage.

TABLE 48. Comparison Between Optimum and Alternative Dosages - Additive 4

	Additive 4					
Rheological parameter	Binder 1 + RAP	OD	AD	Binder 5 + RAP	OD	AD
HT Variation (°C)	32.4	31.2	30.2	37.4	35.1	34.0
IT after 60h PAV (°C)	28.9	25.0	26.6	31.8	23.6	24.7
LT Variation (°C)	10.7	8.8	8.6	8.6	6.4	5.6
ΔTc after aging (°C)	-15.4	-6.5	-10.0	-7.7	-5.4	-3.9
Reduction in ΔTc (°C)	-9.2	-6.7	-6.1	-7.2	-4.0	-4.4
MSCR Jnr (kPa $^{-1}$)	0.9	2.8	3.0	1.0	2.8	2.4
MSCR Jnr Grade	V	S	S	V	S	S
MSCR % Recovery	5.64	1.25	0.51	7.74	1.17	1.92
Strain tolerance (%)	5.461	7.554	6.435	6.629	7.700	8.137
B parameter	6.87	4.90	5.47	5.56	4.87	4.70
G-R after aging (kPa)	4145.9	428.0	991.6	1724.9	412.1	440.7
G-R effectiveness index		0.10	0.24		0.24	0.26

Results for the optimum and alternative dosages of Additive 5 is detailed in TABLE 49. The optimum dosage was selected for recycled binder blends with base binders 1 and 5, as it caused more positive values of ΔT_c, lower |B| parameter from LAS (with lower strain tolerance for Binder 5), and lower Glover-Rowe parameter, all indicative of enhanced fatigue cracking resistance.

TABLE 49. Comparison Between Optimum and Alternative Dosages - Additive 5

	Additive 5					
Rheological parameter	Binder 1 + RAP	OD	AD	Binder 5 + RAP	OD	AD
HT Variation (°C)	32.4	31.8	30.2	37.4	35.5	33.8
IT after 60h PAV (°C)	28.9	29.3	29.7	31.8	24.6	26.9
LT Variation (°C)	10.7	10.2	9.4	8.6	7.3	8.0
ΔTc after aging (°C)	-15.4	-12.8	-13.0	-7.7	-5.0	-6.4
Reduction in ΔTc (°C)	-9.2	-7.9	-7.2	-7.2	-4.7	-5.4
MSCR Jnr (kPa $^{-1}$)	0.9	0.7	0.7	1.0	0.8	0.7
MSCR Jnr Grade	V	V	V	V	V	V
MSCR % Recovery	5.64	15.90	13.34	7.74	19.25	17.83
Strain tolerance (%)	5.461	6.192	6.240	6.629	7.943	7.505
B parameter	6.87	6.33	6.35	5.56	5.08	5.43
G-R after aging (kPa)	4145.9	2492.7	2593.3	1724.9	734.5	899.9
G-R effectiveness index		0.60	0.63		0.43	0.52

A final summary of the selected dosages, PG and resulting Useful temperature Interval (UTI) of the base and modified binders is presented in TABLE 50. The UTI of binders was calculated as the difference between the high and low PG (considering the negative sign on the low PG). It can be observed that Additives 1, 4 and 5 widen the UTI with respect to the control, the achieve that by lowering the low PG of the base binder. In addition, the softening effects of Additive 4 are also observed, as the wider UTI is obtained at the expense of two drops on the low PG, as the high PG was also reduced. Additives 2 and 3, on the other hand, widen the UTI to a greater extent through lower PG on the low temperature end and a higher PG on the high temperature end. Thus, these additives provided improvements in aging resistance while also enhancing the temperature interval where the binder would present satisfactory performance.

TABLE 50. Base Binders and Selected Dosage for Modified Blends

Binder ID	PG	UTI (°C)
Binder 1	**64 - 16**	**80**
Additive 1 + OD	64 - 28	92
Binder 1 + RAP	**70 - 16**	**86**
Binder 1 + RAP + Additive 2 OD	82 - 16	98
Binder 1 + RAP + Additive 3 AD	94 - 28	122
Binder 1 + RAP + Additive 4 OD	64 - 28	92
Binder 1 + RAP + Additive 5 OD	70 - 22	92
Binder 5	**64 - 28**	**92**
Additive 1 + OD	64 - 28	92
Binder 5 + RAP	**70 - 22**	**92**
Binder 5 + RAP + Additive 2 AD	88 - 22	110
Binder 5 + RAP + Additive 3 OD	94 - 16	110
Binder 5 + RAP + Additive 4 OD	64 - 28	92
Binder 5 + RAP + Additive 5 OD	70 - 28	98

4.3. Chemical Evaluation of Aging Resistant Technologies

4.3.1 Fourier Transformed Infrared Spectroscopy

Infrared spectra of modified and unmodified binders were analyzed before and after aging to study the effects of each technology on the rate of formation of oxidation products, i.e carbonyl (C=O) and sulfoxide (S=O) functional groups.

The carbonyl group is typically observed at wavelengths around 1741 cm^{-1}, corresponding to the stretch of the C=O bond, typically occurring in the asphaltenes (Elkashef et al., 2018; Habbouche et al., 2021). Additionally, the sulfoxide group manifests at wavelengths of 1030 cm^{-1}(Apostolidis et al., 2020; Lu & Isacsson, 2002; Qin et al., 2014). Carbonyl and sulfoxide regions of the FTIR spectra for each base binder and its blends are shown in Figure 120 through Figure 134 below. TABLE 51 shows the wavenumbers for the carbonyl and sulfoxide groups as well as other functional groups typically present in asphalt binders.

TABLE 51. Typical Functional Groups Observed in Binder FTIR Spectra

Wavenumber (cm^{-1})	Description
1030	Stretching vibration of S=O (Lu & Isacsson, 2002; Qin et al., 2014)
1600	C=C stretch from aromatic ring (Elkashef & Williams, 2017; Rios Carreno, 2021)
1741	Carbonyl stretch (Elkashef & Williams, 2017; Habbouche et al., 2021; Qin et al., 2014)
2955 - 2871, 1456 - 1377	Asymmetric deformation in CH_2 and CH_3 (Elkashef et al., 2018; Elkashef & Williams, 2017; Habbouche et al., 2021; Santos et al., 2021)
1375	Symmetrical and Asymmetrical angular vibrations of CH_3 (Rios Carreno, 2021)
2924 - 2853, 1496	Ethyl (aliphatic) (Elkashef & Williams, 2017)

Additionally, due to its formulation, each additive each additive also has distinct peaks in FTIR spectra. The available information on each product (Product 1-5 defined in Chapter 3) led to the identification of certain peaks, as indicated in TABLE 52. Although additional peaks were observed, an in-depth chemical characterization of each technology fell outside the scope of this work.

TABLE 52. FTIR Peaks Observed for Products 1- 5

	Wavenumber (cm^{-1})	Description
Product 1	700	Polystyrene
	965	Polybutadiene trans double bond
Product 2	828	p-phenylene groups (J. Yu, Cong, & Wu, 2009)
	1040	Ether (Apostolidis et al., 2020)
	1510	p-phenylene groups (J. Yu et al., 2009)
	1740	Ester carbonyl (J. Yu et al., 2009)
Product 3	1155	Ester moiety (Elkashef & Williams, 2017)
	1740	Ester (Santos et al., 2021)
Product 4	700	Styrene (Habbouche et al., 2021; Zhao et al., 2010)
	910	Polybutadiene vinyl double bond (Habbouche et al., 2021)
	965	Polybutadiene trans double bond (Habbouche et al., 2021; Zhao et al., 2010)
	1740	Ester (J. Yu et al., 2009)
Product 5	1600	Ester resulting from terpolymer reaction with binder (Keyf, 2015)
	1735	Ester resulting from terpolymer reaction with binder (Keyf, Ismail, Corbacıoglu, & Ozen, 2007)

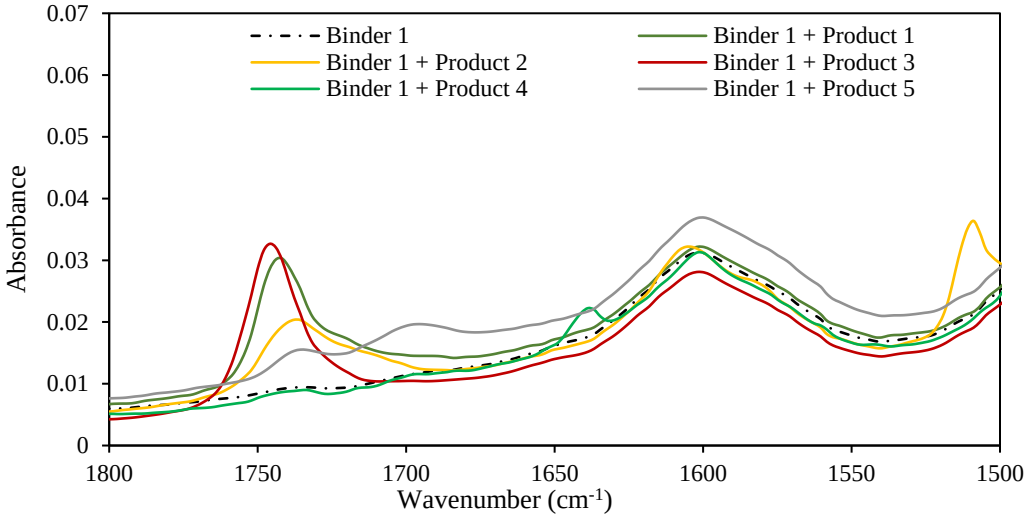

Figure 120. Carbonyl Region for Binder 1 - Unaged

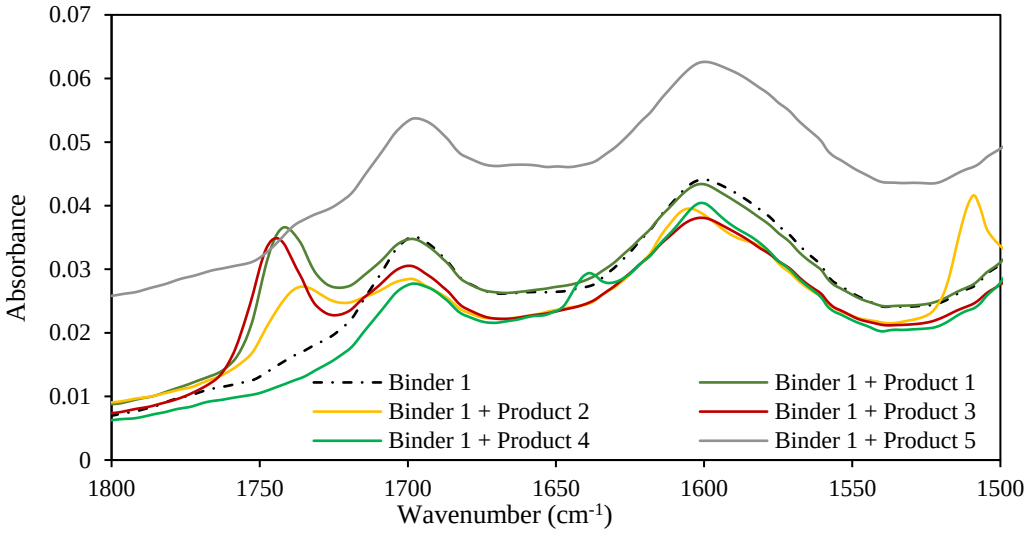

Figure 121. Carbonyl Region for Binder 1 - RTFO + 60h PAV

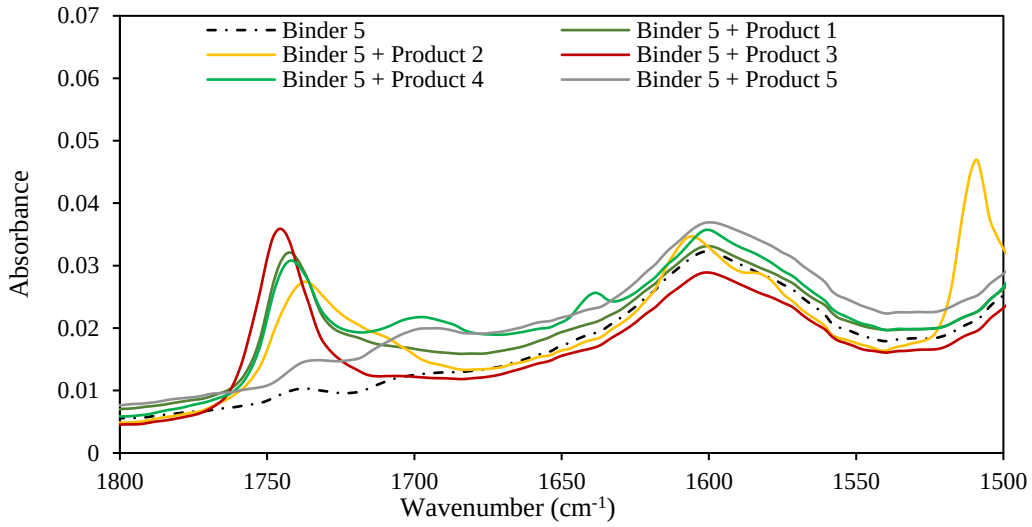

Figure 122. Carbonyl Region for Binder 5 - Unaged

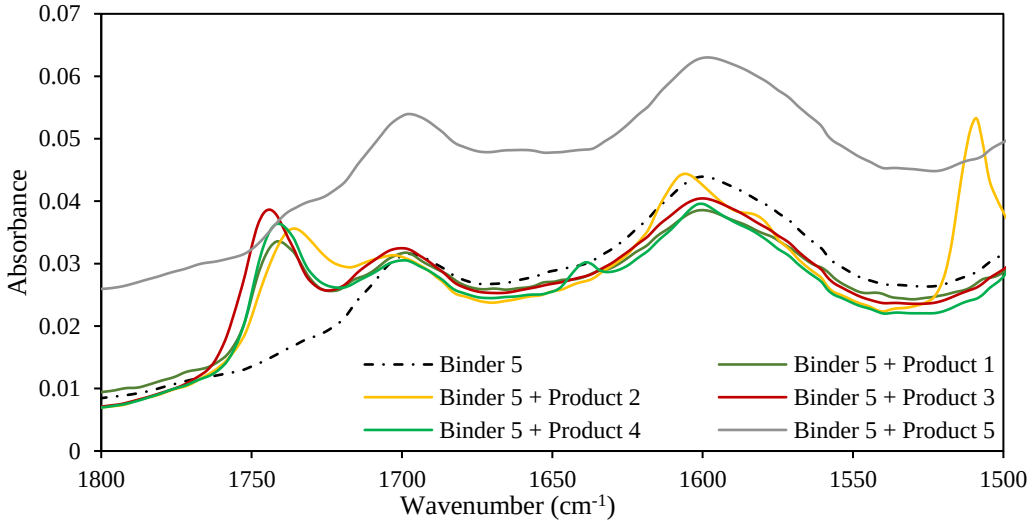

Figure 123. Carbonyl Region for Binder 5 - RTFO + 60hr PAV

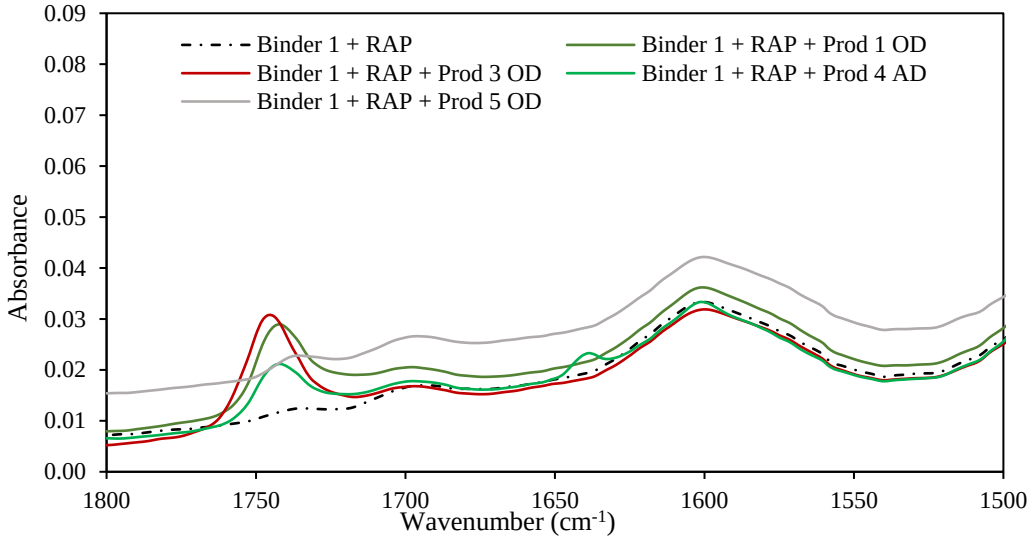

Figure 124. Carbonyl Region - Binder 1 with RAP Unaged

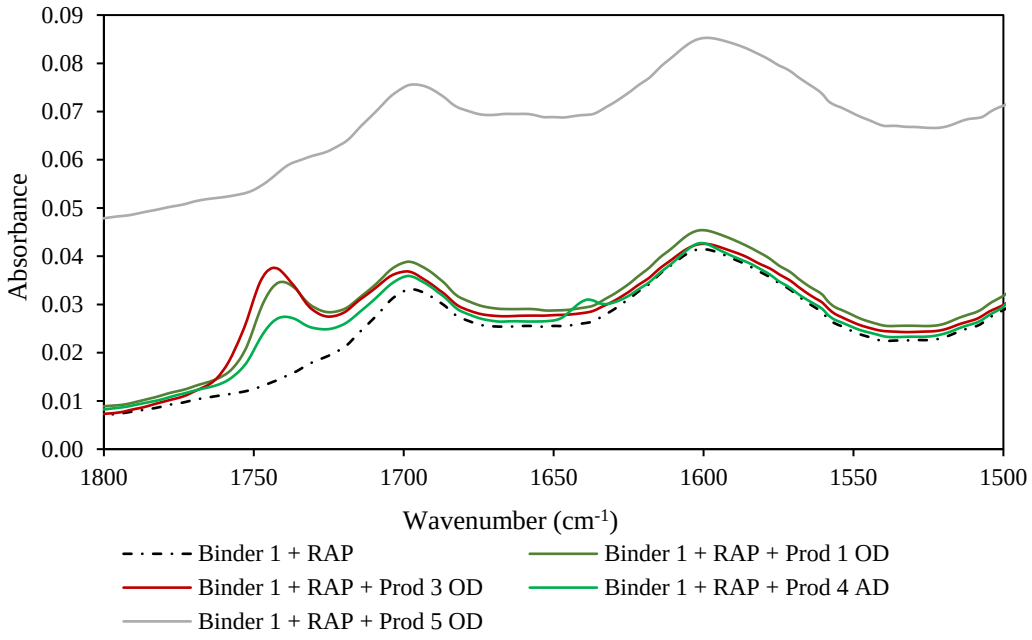

Figure 125. Carbonyl Region - Binder 1 with RAP RTFO + 60hr PAV

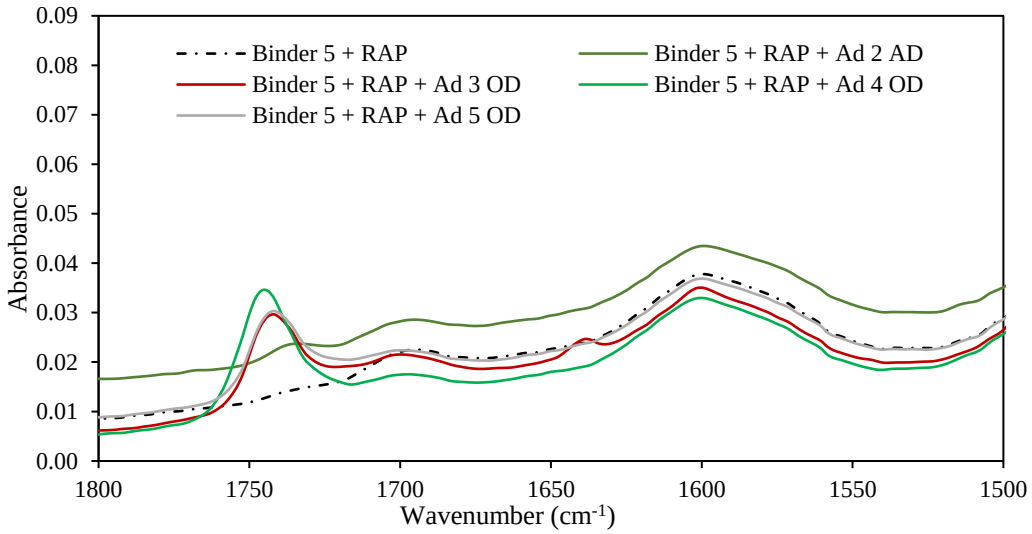

Figure 126. Carbonyl Region - Binder 5 with RAP Unaged

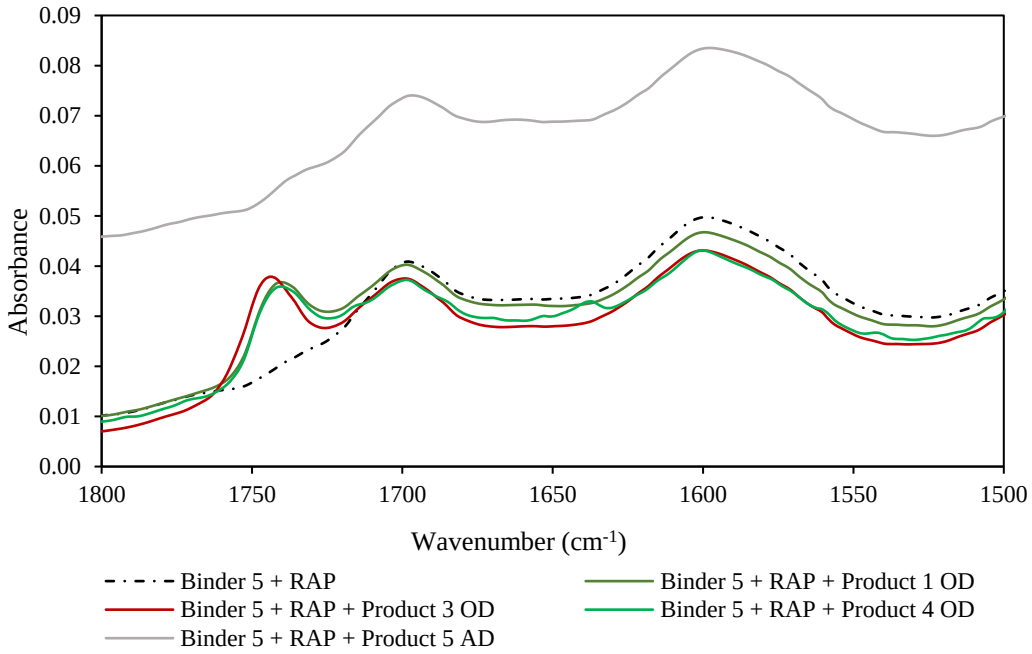

Figure 127. Carbonyl Region - Binder 5 with RAP RTFO+60hr PAV

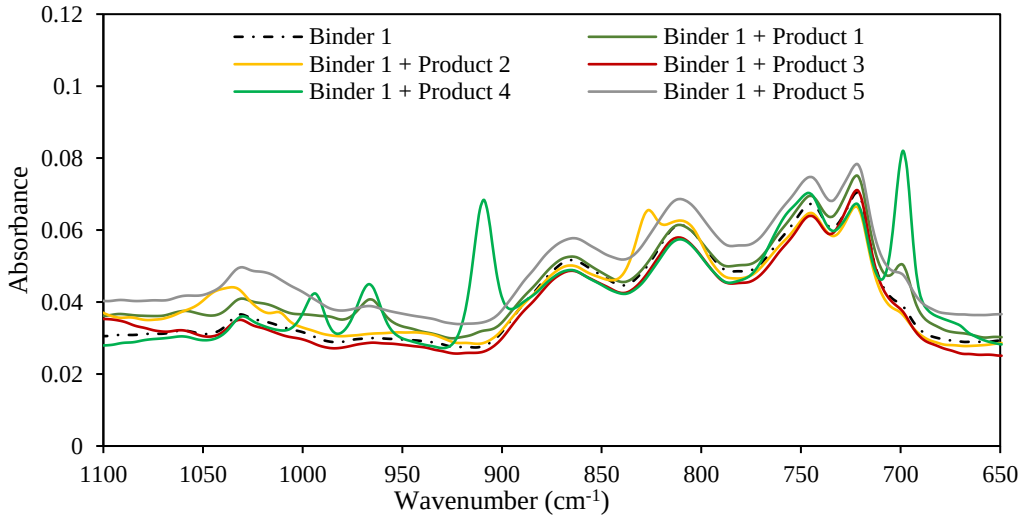

Figure 128. Sulfoxide region - Binder 1 Unaged

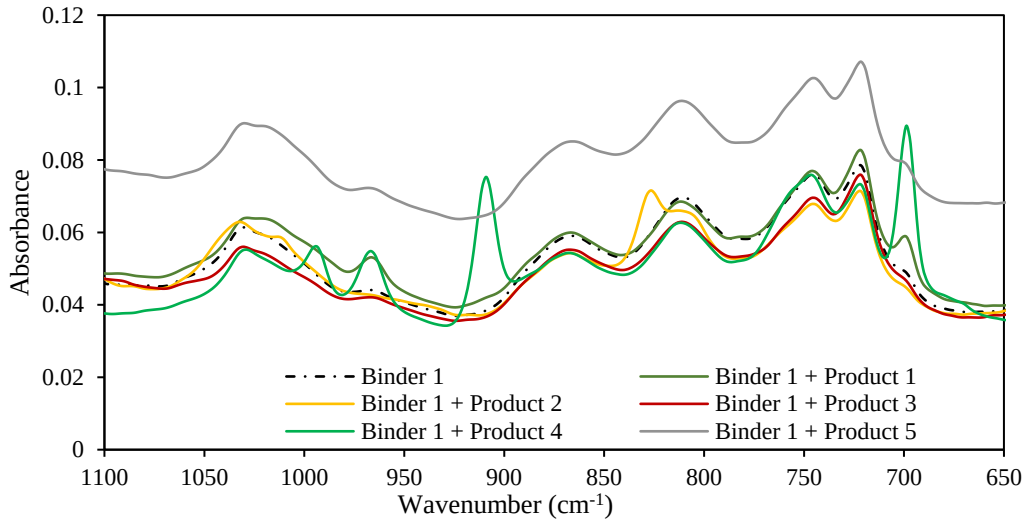

Figure 129. Sulfoxide region - Binder 1 RTFO + 60hr PAV

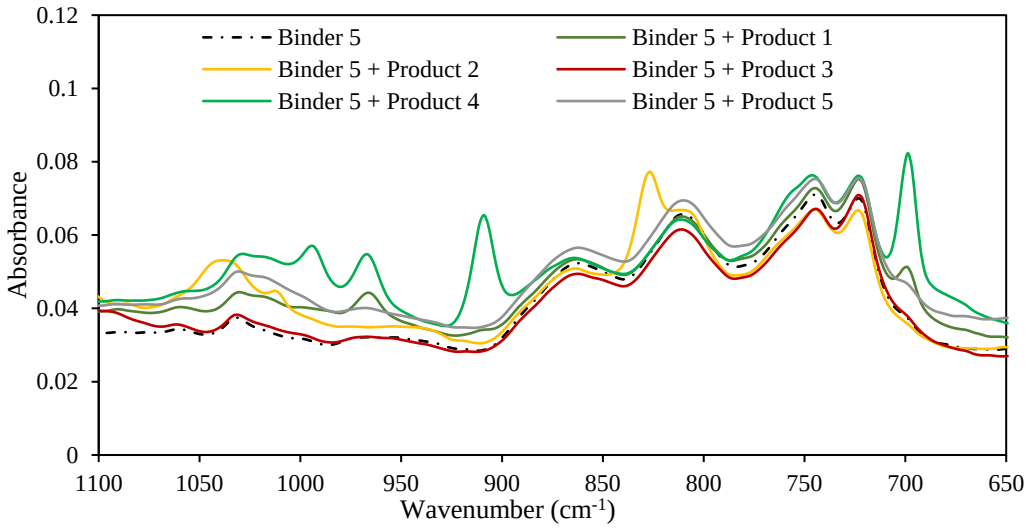

Figure 130. Sulfoxide region - Binder 5 Unaged

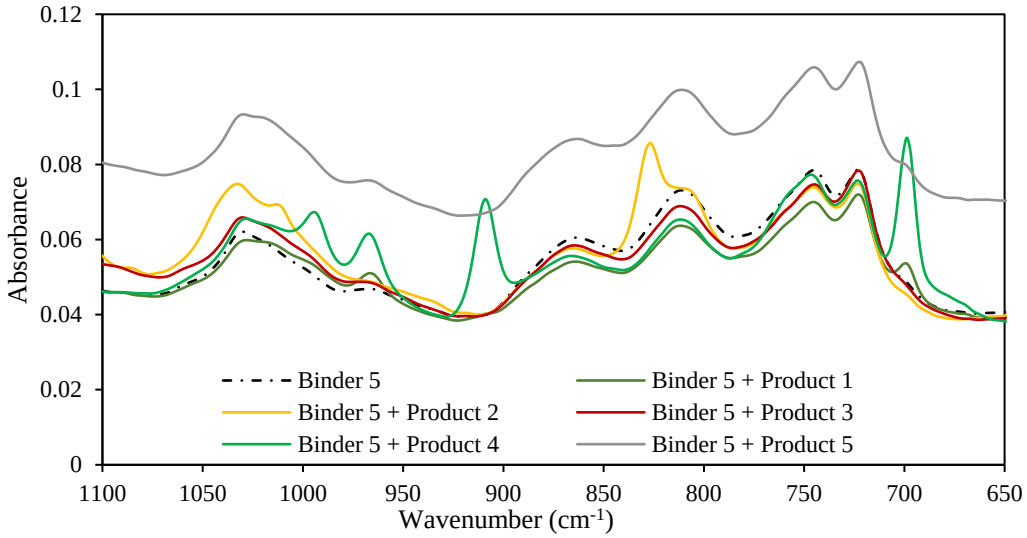

Figure 131. Sulfoxide region - Binder 5 RTFO + 60hr PAV

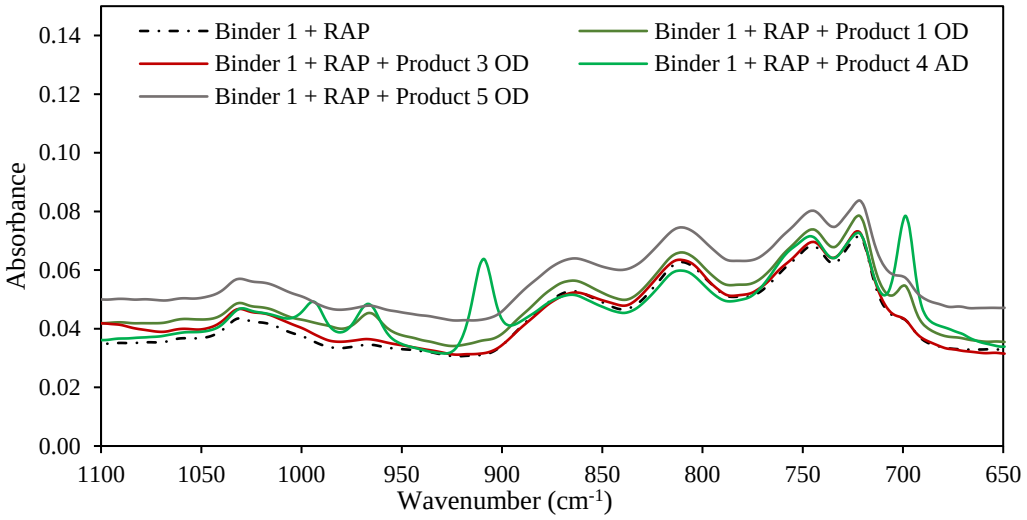

Figure 132. Sulfoxide region - Binder 1 with RAP Unaged

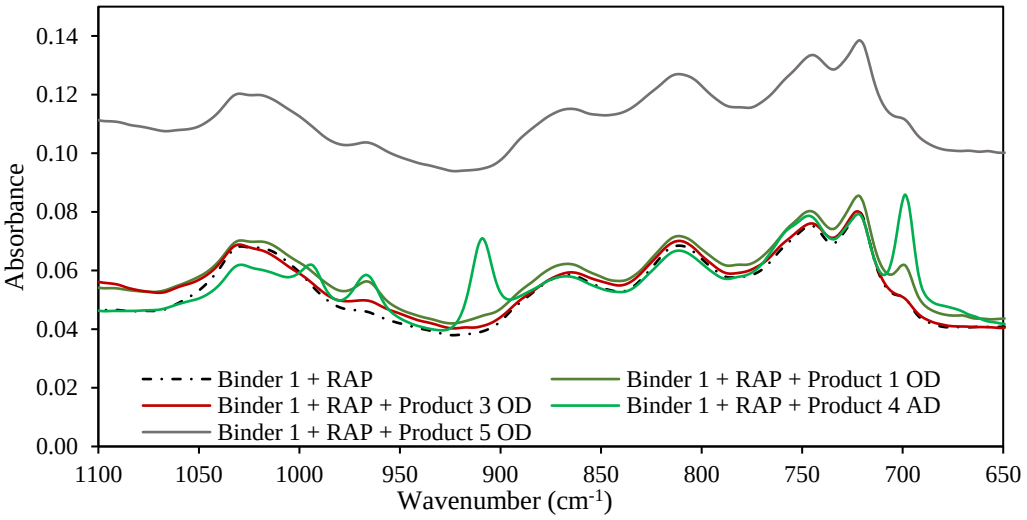

Figure 133. Sulfoxide region - Binder 1 with RAP RTFO + 60hr PAV

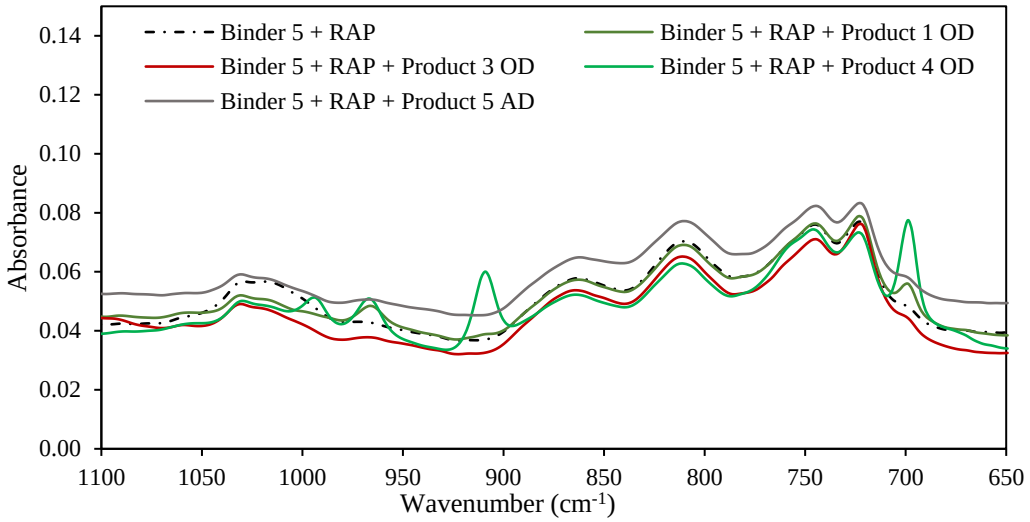

Figure 135. Sulfoxide region - Binder 5 with RAP Unaged

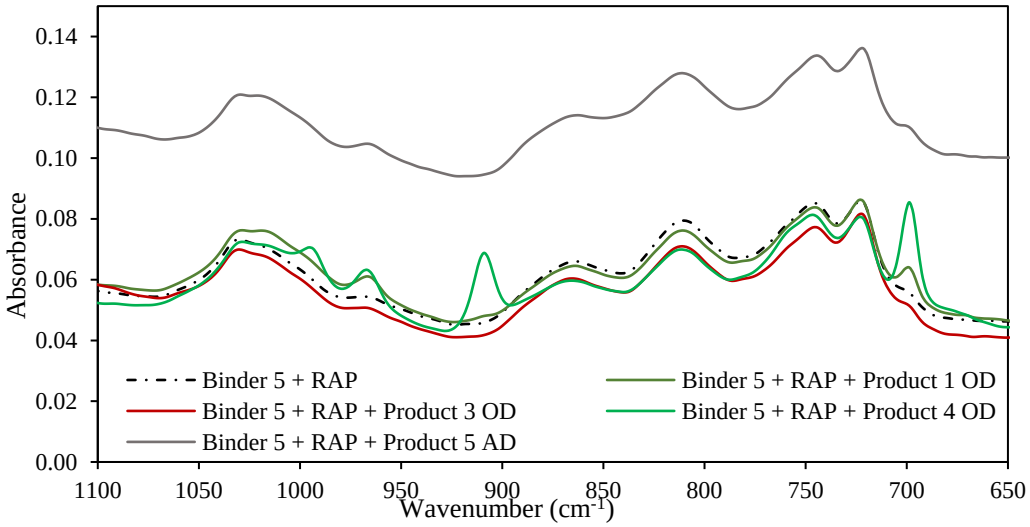

Figure 134. Sulfoxide region - Binder 5 with RAP RTFO + 60hr PAV

FTIR spectra and TABLE 52 showed how certain technologies present peaks at wavelengths that overlap with the carbonyl region typically evaluated after aging. Thus, two approaches were followed to determine the changes in carbonyl region between the unaged condition and after 60 hour of PAV aging.

a. Approach 1

The first approach considered the area of carbonyl functions (such as ketones, dicarboxylic anhydrides and carboxylic acids) between the wavelengths of 1660 and 1753 cm^{-1} and attributed the changes in the entire region to the effect of aging. The sulfoxide area was calculated between 1047 and 995 cm^{-1} and, as no interference was observed with additive peaks, remained unchanged for both approaches. Aging indices comparing the carbonyl and sulfoxide areas of modified binders with respect to the control were calculated as indicated by Equation 10 (Explained in Section 3.6.1 and reiterated below). Therefore, improvements in aging resistance would result from indices smaller than 1.

Equation 10. Carbonyl and Sulfoxide Aging Index for modified binders – Approach 1

$$(C=O+S=O)Aging\ Index = \frac{(C=O+S=O\ Area)_{RTFO+60hr\ PAV\ Modified}}{(C=O+S=O\ Area)_{RTFO+60hr\ PAV\ Control\ binder}}$$

Figure 136 and Figure 137 show the aging indices for the modified binders that were formulated with Binder 1 and Binder 5, respectively. Additives 1, 3 4 and 5 would improve the aging resistance of the two base binders when blended at the selected dosages, as their aging indices were less than 1 in both cases. Additive 2 showed aging indices greater than 1 for both base binders, suggesting this additive led to higher rate of formation of oxidation products, thus showing greater aging susceptibility than the control binders.

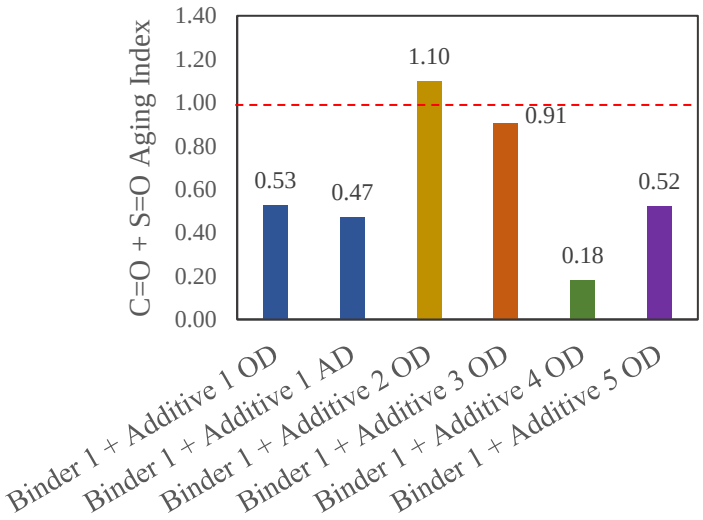

Figure 136. C=O + S=O Aging Indices for Binder 1 – Approach 1

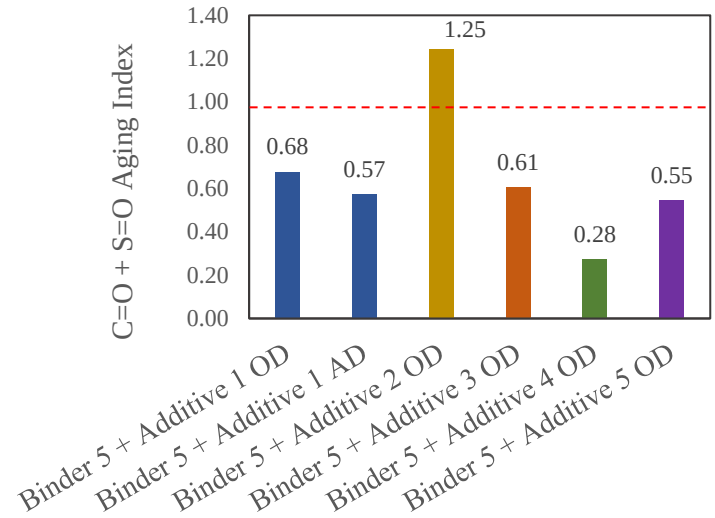

Figure 137. C=O + S=O Aging indices for Binder 5 – Approach 1

Figure 138 shows RAP blends with Binder 1 presented aging indices smaller than 1 after modification with every additive except for the optimum dosage of Additive 2. Therefore, all additives when blended at an appropriate dosage can improve the aging resistance of Binder 1 with 20% RAP binder.

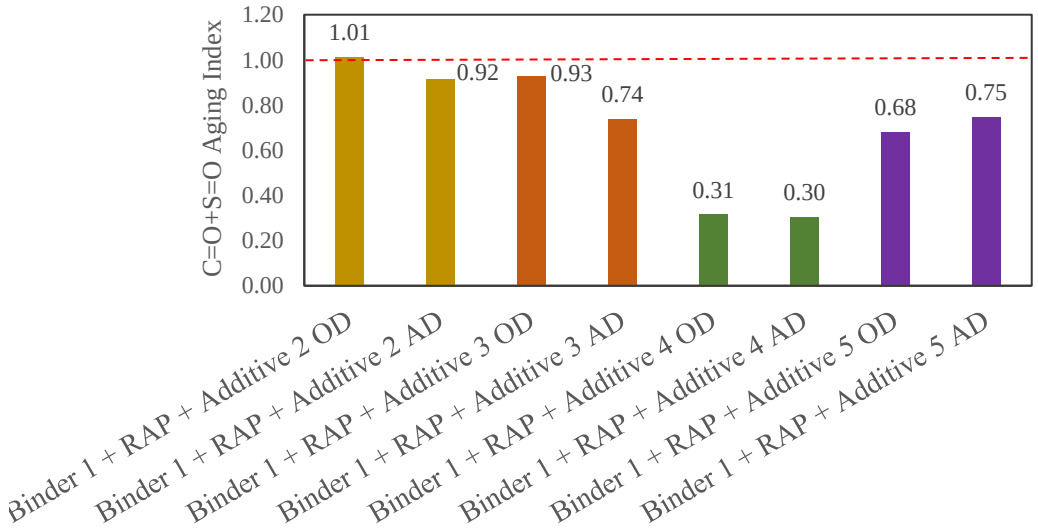

Figure 138. C=O + S=O Aging indices for Binder 1 with RAP – Approach 1

As shown in Figure 139, Binder 5 RAP blends with Additives 3, 4 and 5 had aging indices less than 1, suggesting these additives would mitigate the formation of oxidation products. Binder 5 RAP blends with Additive 2, on the other hand, had aging indices greater larger than 1 for both dosages, suggesting it was not effective in reducing aging susceptibility of Binder 5 with 20% RAP binder at the two selected dosages.

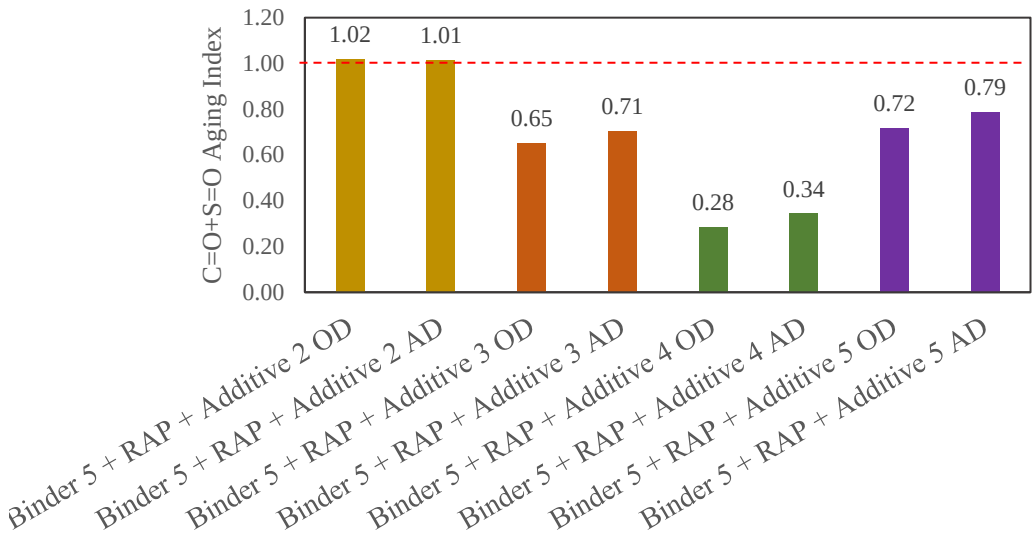

Figure 139. C=O + S=O Aging indices for Binder 5 with RAP – Approach 1

b. Approach 2

The carbonyl areas were also determined based on an alternative approach to separate the effect of C=O bonds present in some additives, which may lead to higher carbonyl area values but are not attributable to oxidation. Therefore, aging indices were calculated for wavenumbers between 1660 and 1719 cm^{-1} to account for C=O formation during aging (designated as Area 2), and the sulfoxide region remained at wavelengths between 995 and 1047 cm^{-1}, as indicated in Equation 11 (as explained in Section 3.6.1 and reiterated below)

Equation 11. Carbonyl and Sulfoxide Aging Index for modified binders – Approach 2

$$(C=O_{Area\ 2}+S=O)Aging\ Index=\frac{(C=O_{Area\ 2}\ +S=O\ Area)_{RTFO+60hr\ PAV\ Modified}}{(C=O_{Area\ 2}+S=O\ Area)_{RTFO+60hr\ PAV\ Control\ binder}}$$

Results for Binder 1 and Binder 5 are presented in Figure 141 and Figure 140, which are similar to Figure 136 and Figure 137 obtained per Approach 1. Additives 1, 3, 4 and 5 resulted on indices lower than 1 and therefore would improve the aging resistance of both base binders, while Additive 2 would not as its aging indices were greater than 1.

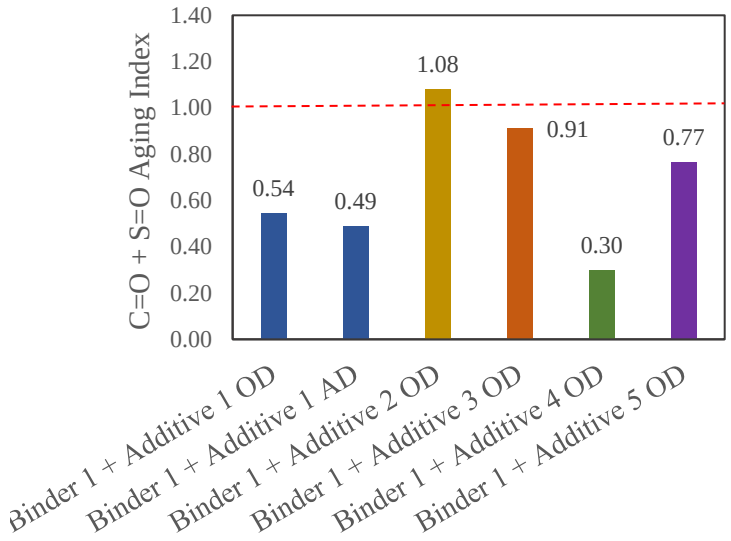

Figure 141. C=O + S=O Aging indices for Binder 1 – Approach 2

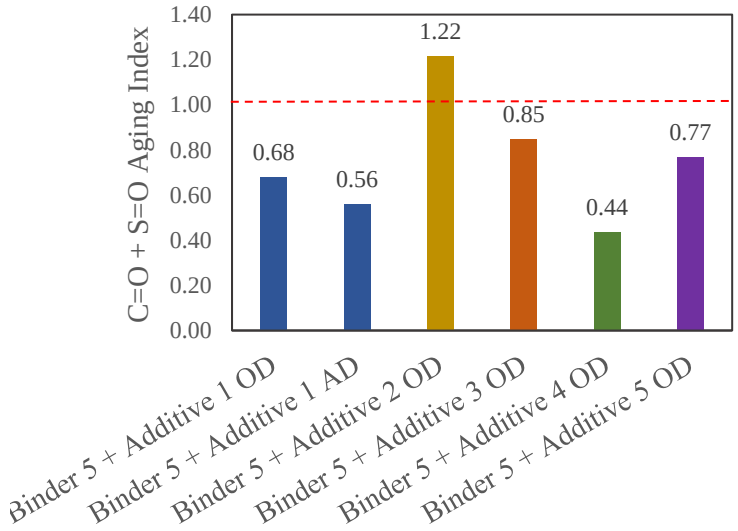

Figure 140. C=O + S=O Aging indices for Binder 5 – Approach 2

Based on the alternative analysis approach, all modified RAP blends with Binder 1 had aging indices less than 1, as shown in Figure 142. Aging indices smaller than 1 suggested modified binders were less sensitive to the effect of aging, due to a slower formation of carbonyl and sulfoxide oxidation products.

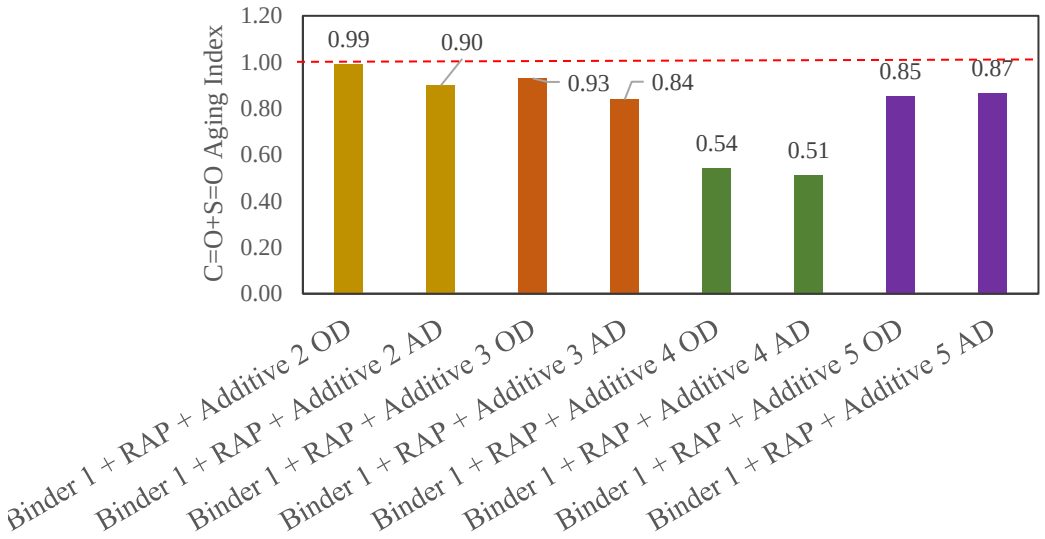

Figure 142. C=O + S=O Aging indices for Binder 1 with RAP – Approach 2

Finally, as shown in Figure 143, Additives 3, 4 and 5 would effectively improve the aging resistance of the Binder 5 RAP blends. Additive 2, on the other hand, showed little to no effect on carbonyl and sulfoxide areas as given by the aging indices of 1.00 and 0.99 for the selected dosages.

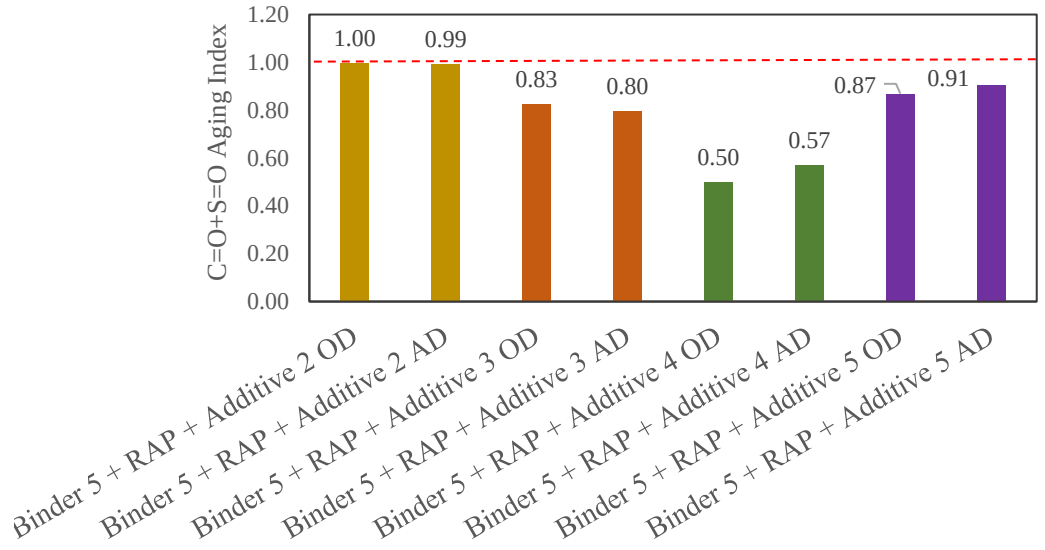

Figure 143. C=O + S=O Aging indices for Binder 5 with RAP – Approach 2

Overall, FTIR aging indices suggested that Additives 1, 3, 4 and 5 could reduce the formation of oxygen-containing functional groups observed due to oxidative aging. Thus, these additives can improve the aging resistance of Binders 1 and 5 as well as their blends with 20% RAP binders. Although improvements with respect to the control were observed through both approaches, the relative rankings provided by each aging index were compared, to understand whether peak interference caused misleading results in terms of aging resistance.

c. Relative Rankings based on Aging Indices

Relative rankings for Binder 1 are presented in TABLE 53, where Additives are ranked from most to less effective in decreasing the aging susceptibility of the control binder in accordance to approaches 1 and 2. Although both indices ranked the least and most effective additives equally, differences were observed for Additive 5 and the optimum dosage of number 1.

TABLE 53. Relative Rankings for C=O+S=O Aging Indices - Binder 1

Binder 1	
Approach 1	**Approach 2**
Additive 4	Additive 4
Additive 1 AD	Additive 1 AD
Additive 5	Additive 1 OD
Additive 1 OD	Additive 5
Additive 3	Additive 3
Additive 2	Additive 2

Both approaches led to equal top and bottom rankings for modifiers with Binder 5, but more pronounced differences were observed. TABLE 54 indicates, for example, that while Additive 5 was among the best ranked with Approach 1, the same was not observed when following approach 2. Therefore, potential overestimations in carbonyl area due to additive interference when following approach 1, in this case, did not negatively affect the aging index, as initially hypothesized.

TABLE 54. Relative Rankings for C=O+S=O Aging Indices - Binder 5

Binder 5	
Approach 1	**Approach 2**
Additive 4	Additive 4
Additive 5	Additive 1 AD
Additive 1 AD	Additive 1 OD
Additive 3	Additive 5
Additive 1 OD	Additive 3
Additive 2	Additive 2

When ranking the additives based on the aging indices determined with respect to Binder 1 and 20% RAP, their rankings are similar based on the two analysis approaches, except for Additive 5 at the optimum dosage and Additive 3 at the alternative dosage, as shown in TABLE 55. When looking at its effectiveness relative to the control, Additive 2 at the optimum dosage had an aging index greater than 1 in analysis approach 1, but it was less than 1 in analysis approach 2.

TABLE 55. Relative Rankings for C=O+S=O Aging Indices - Binder 1 with RAP

Binder 1 + RAP	
Approach 1	**Approach 2**
Additive 4 AD	Additive 4 AD
Additive 4 OD	Additive 4 OD
Additive 5 OD	Additive 3 AD
Additive 3 AD	Additive 5 OD
Additive 5 AD	Additive 5 AD
Additive 2 AD	Additive 2 AD
Additive 3 OD	Additive 3 OD
Additive 2 OD	Additive 2 OD

The rankings of the additives based on the aging indices of blends with Binder 5 and 20% RAP were the same based on the two analysis approaches, except for the two dosages of Additive 3, as shown in TABLE 56.

TABLE 56. Relative Rankings for C=O+S=O Aging Indices - Binder 5 with RAP

Binder 5 + RAP	
Approach 1	**Approach 2**
Additive 4 OD	Additive 4 OD
Additive 4 AD	Additive 4 AD
Additive 3 OD	Additive 3 AD
Additive 3 AD	Additive 3 OD
Additive 5 OD	Additive 5 OD
Additive 5 AD	Additive 5 AD
Additive 2 AD	Additive 2 AD
Additive 2 OD	Additive 2 OD

d. Correlations between Carbonyl Areas and Glover Rowe Parameters

The aging process can change both chemical and rheological properties of asphalt binders. The chemical changes include the formation of oxidation products, resulting in an increase in the carbonyl area, while the rheological change may affect both stiffness and relaxation, which can be captured in the Glover-Rowe parameter. Thus, the correlations between the carbonyl areas determined by both analysis approaches and the Glover-Rowe parameters were evaluated in this study. Specifically, the carbonyl areas were correlated with the Glover-Rowe parameters for unaged binders, while the change in carbonyl areas (difference between RTFO + 60-hour PAV aged and unaged areas) were correlated with the Glover-Rowe parameter for RTFO + 60-hour PAV aged samples.

The correlations comparing both analysis approaches are presented for both base binders and recycled binder blends in Figure 144 through Figure 159. It was initially hypothesized that Approach 2 would eliminate peak interference, however, it was found that carbonyl areas determined through Approach 2 showed poorer correlations with the Glover-Rowe parameter, before and after aging. In addition, such behavior was consistent across both base binders and was also observed for recycled binder blends. Although an increasing trend was observed, where higher C=O area correlated to higher Glover-Rowe values and thus higher binder stiffness, considering narrower regions did not improve the accuracy of the prediction. Therefore, peak interference did not mislead the aging susceptibility evaluation of binders.

Approach 1

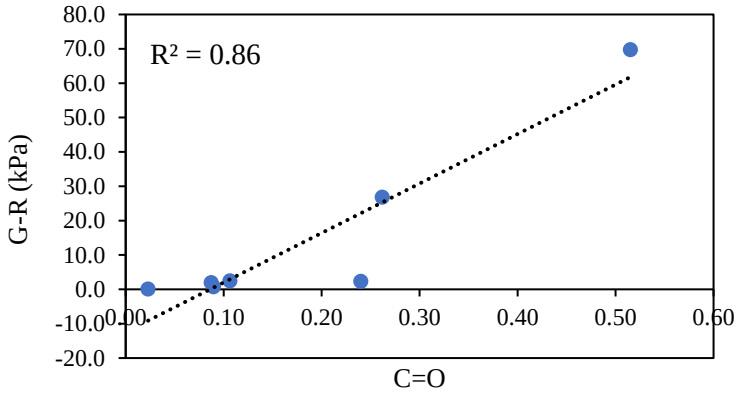

Figure 144. Carbonyl Area from Approach 1 and Glover-Rowe parameter for neat and modified blends with Binder 1 - Unaged

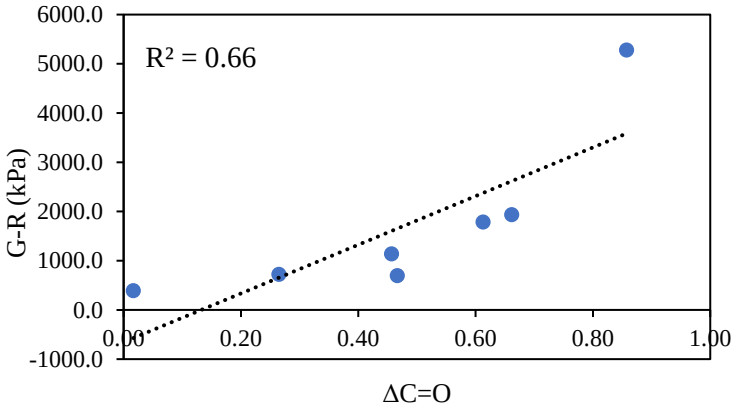

Figure 145. Carbonyl Area variation from Approach 1 and Glover-Rowe parameter for neat and modified blends with Binder 1 - RTFO + 60hr PAV

Approach 2

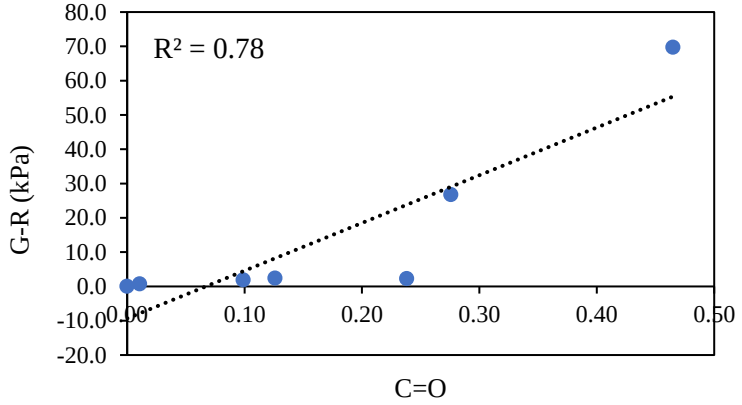

Figure 146. Carbonyl Area from Approach 2 and Glover-Rowe parameter for neat and modified blends with Binder 1 - Unaged

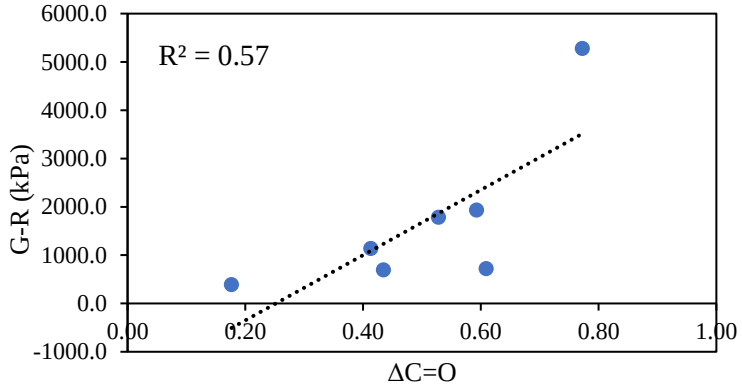

Figure 147. Carbonyl Area variation from Approach 2 and Glover-Rowe parameter for neat and modified blends with Binder 1 - RTFO + 60hr PAV

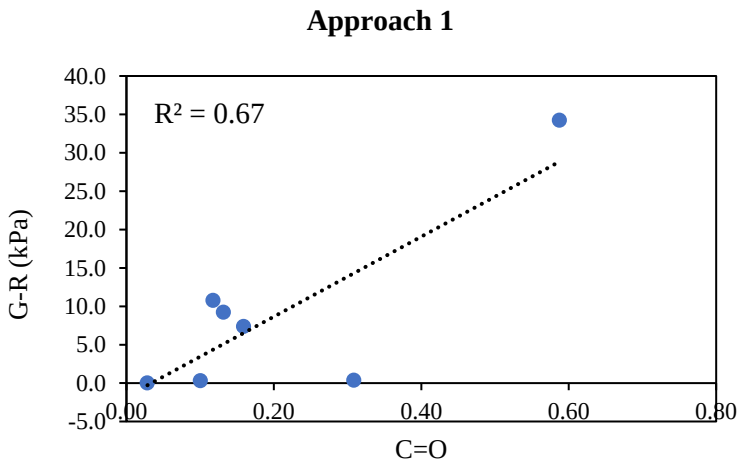

Figure 148. Carbonyl Area from Approach 1 and Glover-Rowe parameter for neat and modified blends with Binder 5 - Unaged

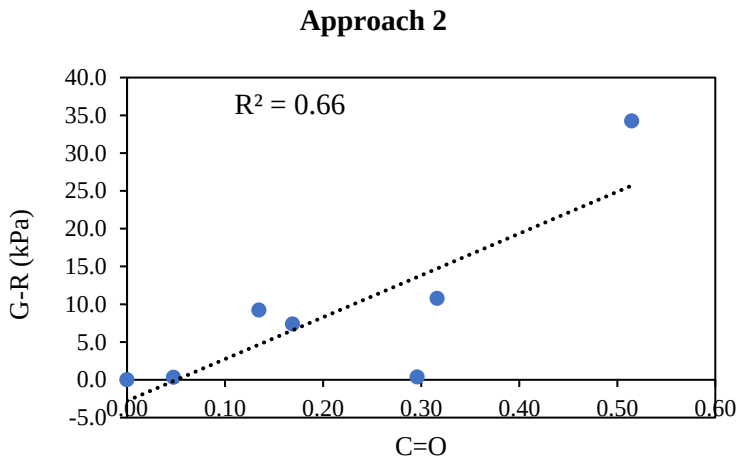

Figure 149. Carbonyl Area from Approach 2 and Glover-Rowe parameter for neat and modified blends with Binder 5 - Unaged

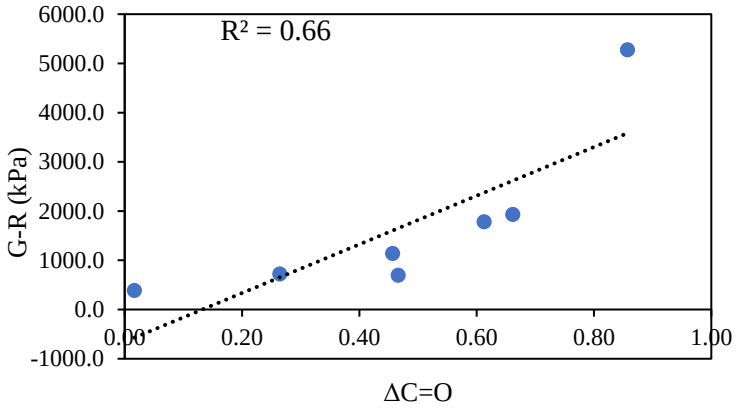

Figure 150. Carbonyl Area variation from Approach 1 and Glover-Rowe parameter for neat and modified blends with Binder 5 - RTFO + 60hr PAV

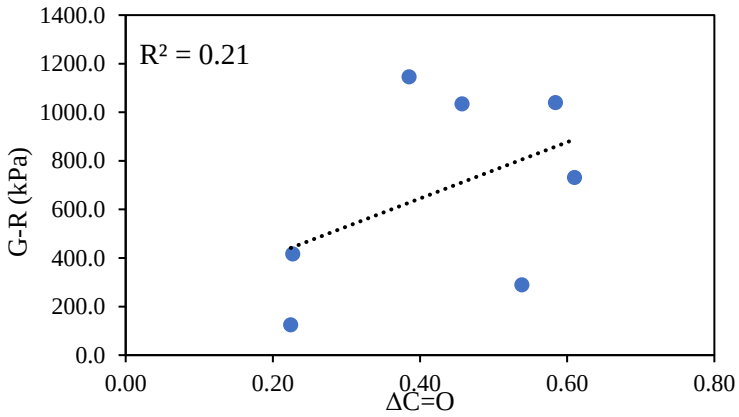

Figure 151. Carbonyl Area variation from Approach 2 and Glover-Rowe parameter for neat and modified blends with Binder 5 - RTFO + 60hr PAV

Approach 1

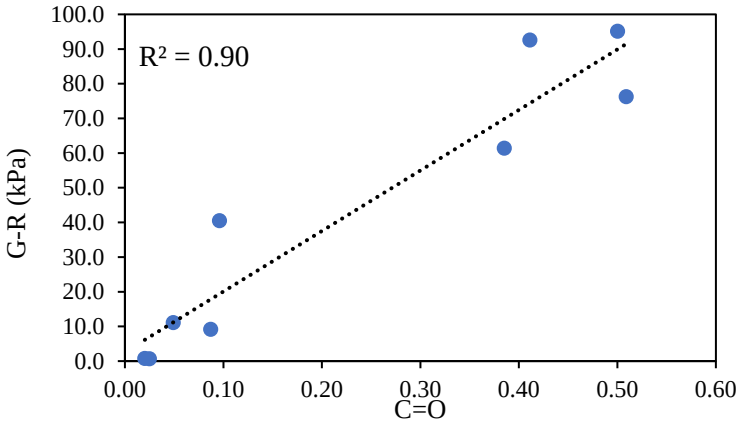

Figure 152. Carbonyl Area from Approach 1 and Glover-Rowe parameter for neat and modified blends with Binder 1 with RAP - Unaged

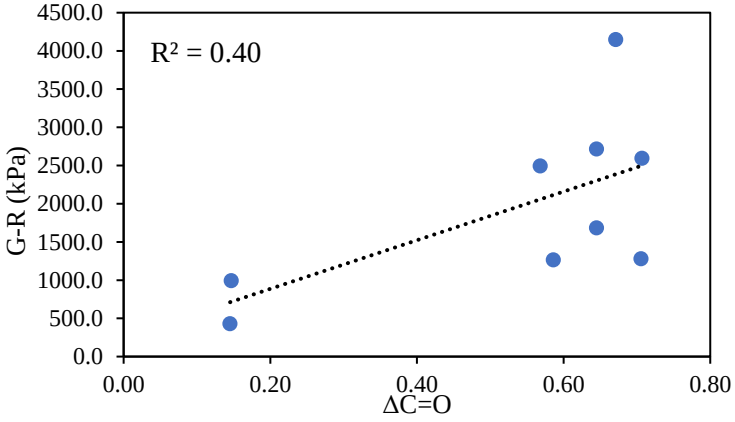

Figure 153. Carbonyl Area variation from Approach 1 and Glover-Rowe parameter for neat and modified blends with Binder 1 with RAP - RTFO + 60hr PAV

Approach 2

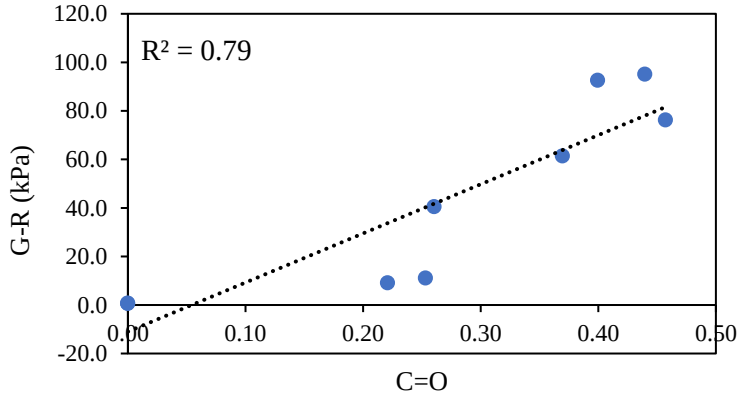

Figure 154. Carbonyl Area from Approach 2 and Glover-Rowe parameter for neat and modified blends with Binder 1 with RAP - Unaged

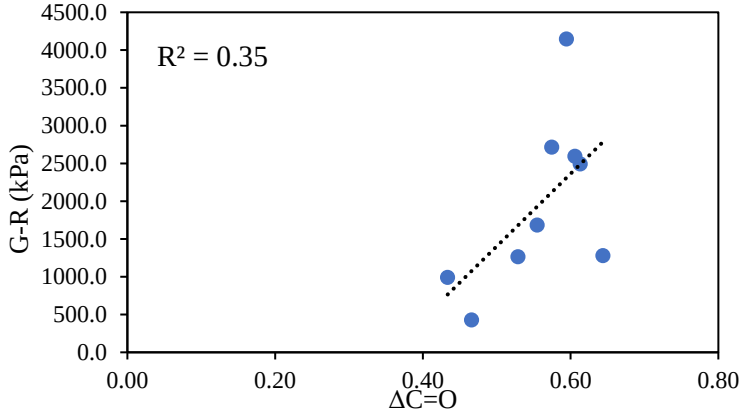

Figure 155. Carbonyl Area variation from Approach 2 and Glover-Rowe parameter for neat and modified blends with Binder 1 with RAP - RTFO + 60hr PAV

Approach 1

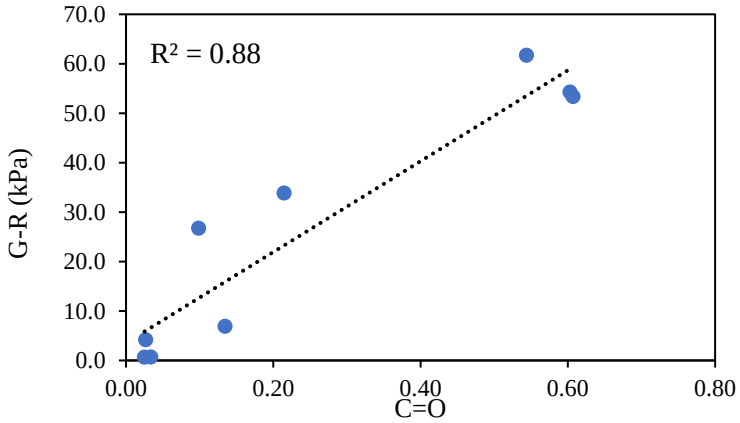

Figure 156. Carbonyl Area from Approach 1 and Glover-Rowe parameter for neat and modified blends with Binder 5 with RAP - Unaged

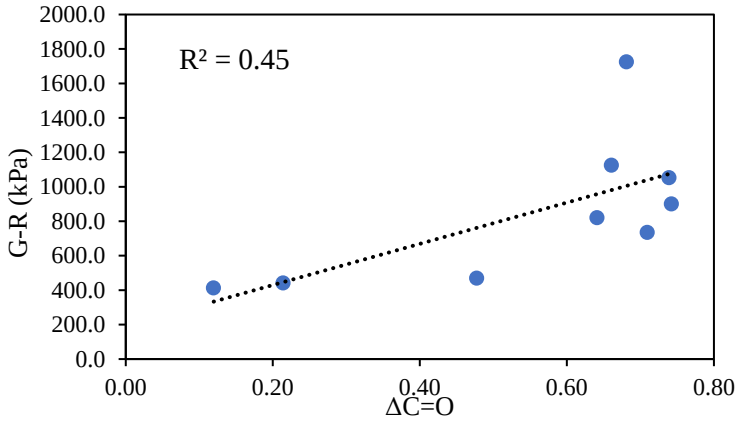

Figure 157. Carbonyl Area variation from Approach 1 and Glover-Rowe parameter for neat and modified blends with Binder 5 with RAP - RTFO + 60hr PAV

Approach 2

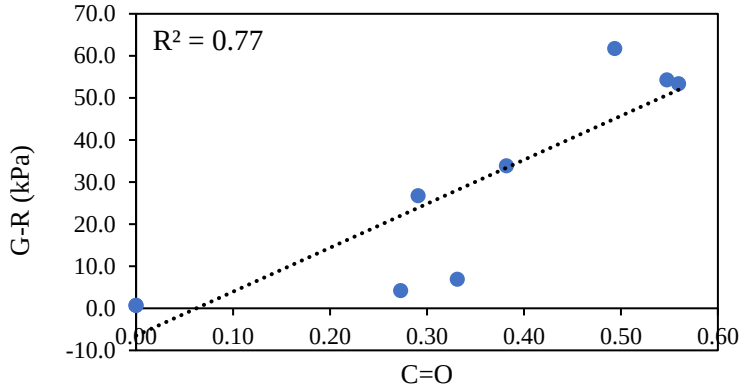

Figure 158. Carbonyl Area from Approach 2 and Glover-Rowe parameter for neat and modified blends with Binder 5 with RAP - Unaged

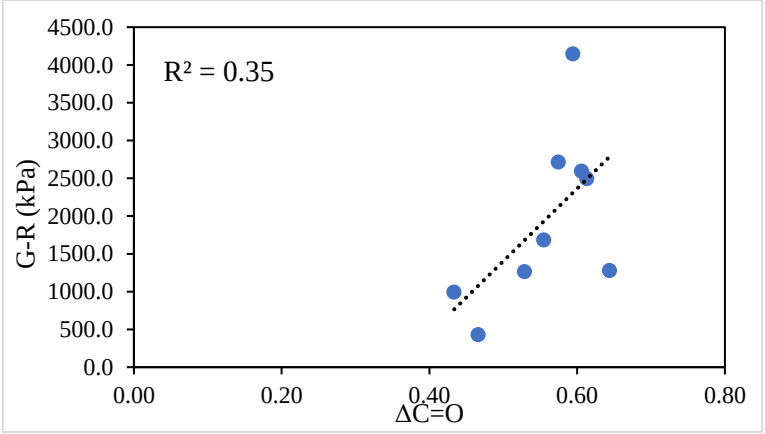

Figure 159. Carbonyl Area variation from Approach 2 and Glover-Rowe parameter for neat and modified blends with Binder 5 with RAP - RTFO + 60hr PAV

To summarize, two approaches were followed for the study of binder aging susceptibility in terms of carbonyl functions (such as ketones, dicarboxylic anhydrides, and carboxylic acids) as well as sulfoxides area through FTIR. First, the carbonyl area was calculated between wavenumbers of 1660 and 1753 cm^{-1}, and the growth observed in the entire region was attributed to the effects of aging. The second analysis approach accounted for the presence of C=O bonds inherent to additive composition, leading to potential overestimations of the carbonyl area and therefore worse aging susceptibility. Thus, the effect of aging on carbonyl functions was considered between 1660 and 1719 cm^{-1}, removing potential interferences with additive-specific peaks (found between 1719 and 1753 cm-1).

Results from both approaches showed additives 1, 3, 4 and 5 consistently inhibited the formation of oxidation products with respect to both base binders and recycled binder blends, thus potentially reducing their aging susceptibility. Additive 2 showed varying effectiveness; no improvements were observed for either base binder, recycled binder blends with Binder 1 were improved after modification with both dosages, but only the alternative dosage improved the aging susceptibility of the recycled blend with Binder 5.

Both approaches successfully identified improvements with respect to the control binders, and therefore captured additive effectiveness. Additionally, they ranked the better and worst additives equally, showing differences in intermediate rankings. The relation between C=O area and Glover-Rowe parameter was evaluated for each approach to determine their accuracy at predicting binder stiffening as a result of aging. Overall, better correlations were found for all base binders using Approach 1. Additionally, it was found that the presence of C=O peaks in modifiers did not influence the calculated aging indices and, therefore, did not compromise the understanding of additive effect.

4.3.2 SARA Fractions

SARA fractions were determined for modified and unmodified neat binders, at the unaged condition and after 60 hours of PAV aging. The effect of each modifier on the four fractions of both base binders was evaluated, as well as the stability of each material as given by the Colloidal Instability Index in Equation 15.

Equation 15. Colloidal Instability Index

$$Colloidal\ Instability\ Index\ (CII) = \frac{Asphaltenes + Saturates}{Resins + Aromatics}$$

Research has shown that binder dispersion is very closely related with aging susceptibility (J.C. Petersen, 2009; Hassan A. Tabatabaee & Kurth, 2017). Higher values of CII indicate binders that are poorly dispersed and therefore more susceptible to aging. CII of base binders before and after aging in Figure 160 confirm the worse aging properties of Binder 1 relative to Binder 5, supporting the base binder selection of this study. Binder 1 showed a greater increase on CII, while Binder 5 experienced a smaller increase in CII.

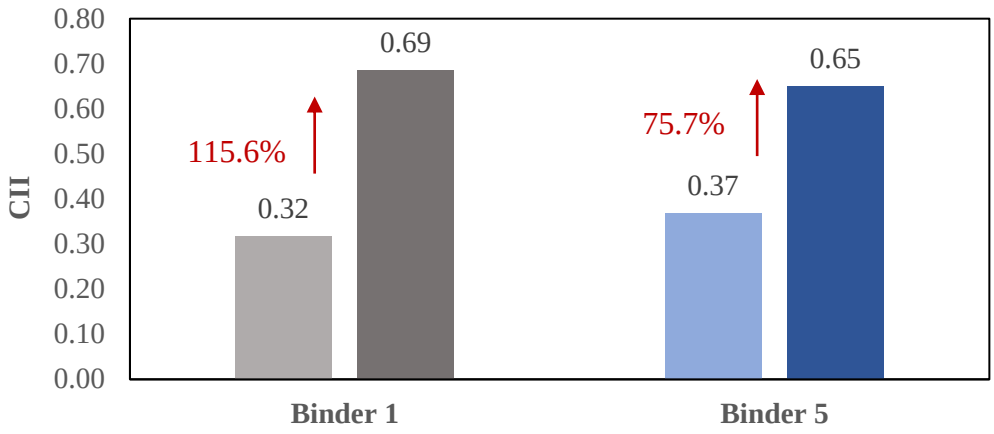

Figure 160. CII of base binders before and after aging.

The changes in SARA fractions of binders 1 and 5, before and after aging, are shown in Figure 161 through Figure 165. The observed trends for both base binders match the findings encountered in the literature. Overall, aging caused a reduction in aromatics and an increase in asphaltenes, while saturates remained mostly unchanged, given their inert nature (Lesueur, 2009; J.C. Petersen, 2009; Weigel & Stephan, 2017). Resins, however, can potentially increase or decrease after aging, as they increase due to the decay of aromatics but progressively oxidize and produce asphaltenes. Although more typically they increase, this might depend on the base binder (Mirwald et al., 2020). In this case, resins decreased for Binder 5 and mostly increased for Binder 1. An increase in resins would indicate an increase in the polar components of binders (Isacsson & Zeng, 1997; Lu & Isacsson, 2002), which, in addition to the loss in aromatics, could relate to the overall higher stiffness found for Binder 1 and its modified blends.

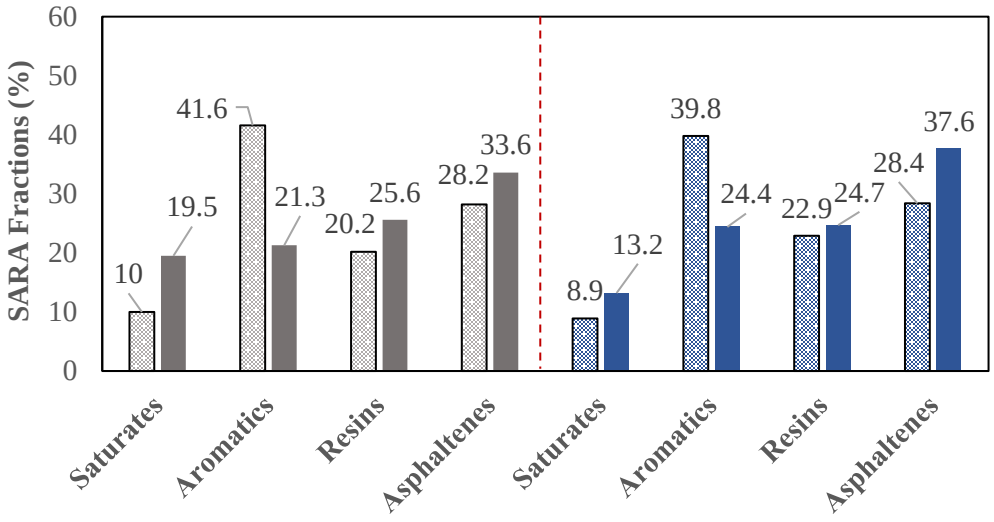

Figure 161. SARA fractions for Additive 1 with Binder 1 (grey) and Binder 5 (blue) before and after aging

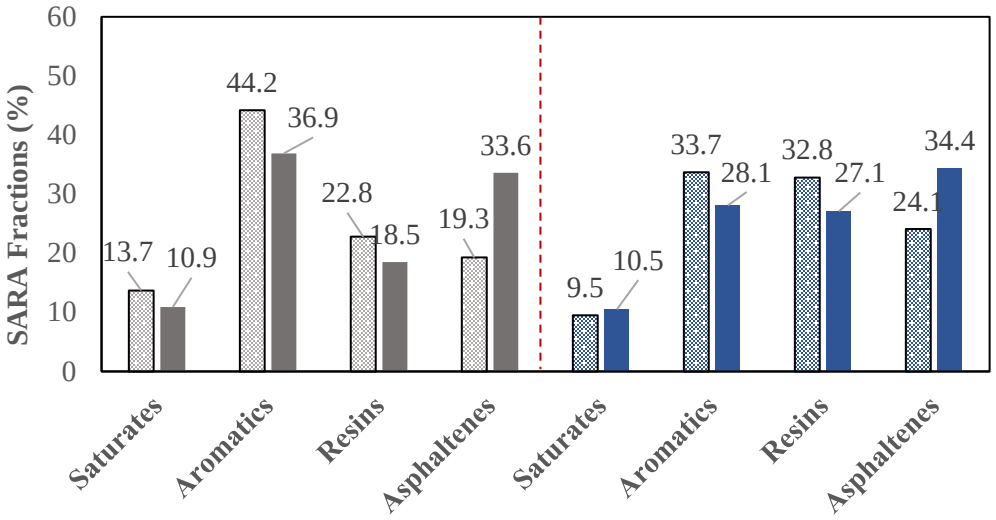

Figure 162. SARA fractions for Additive 2 with Binder 1 (grey) and Binder 5 (blue) before and after aging

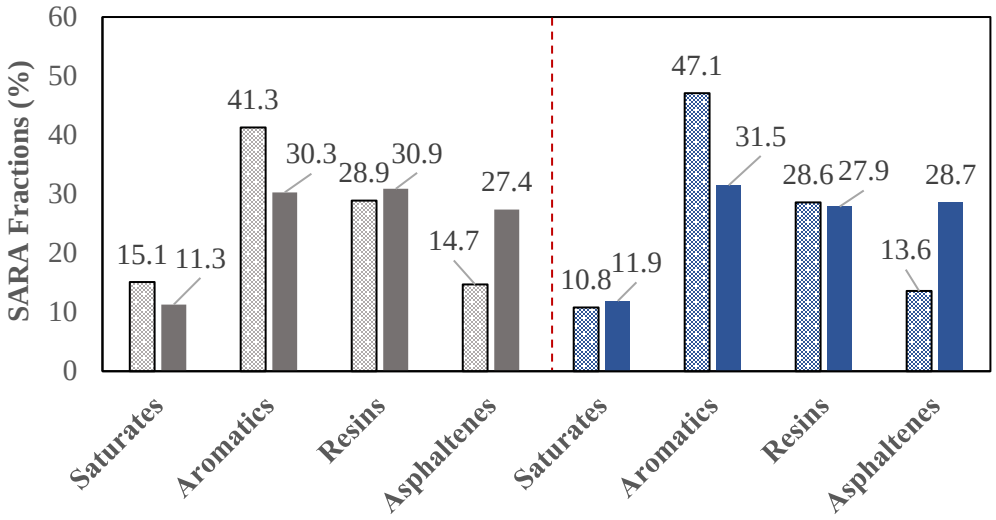

Figure 163. SARA fractions for Additive 3 with Binder 1 (grey) and Binder 5 (blue) before and after aging

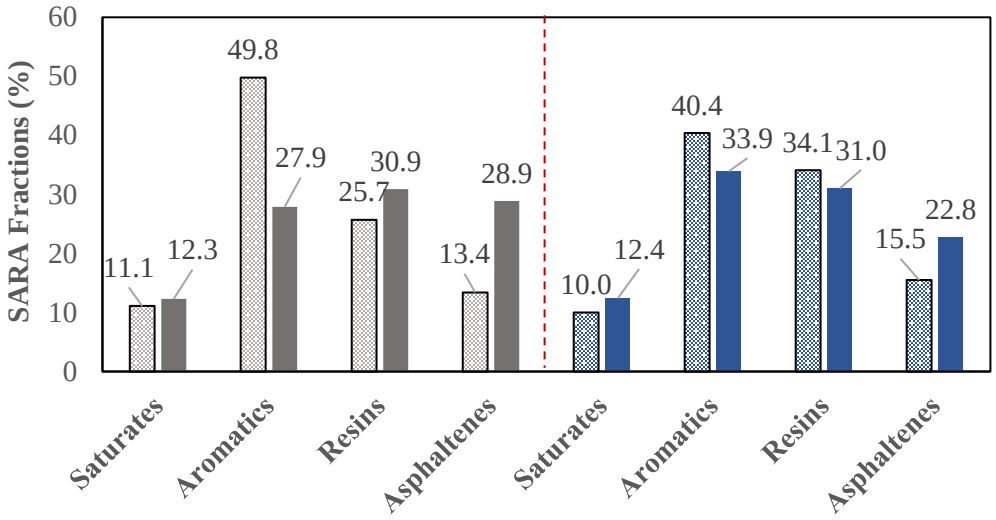

Figure 164. SARA fractions for Additive 4 with Binder 1 (grey) and Binder 5 (blue) before and after aging

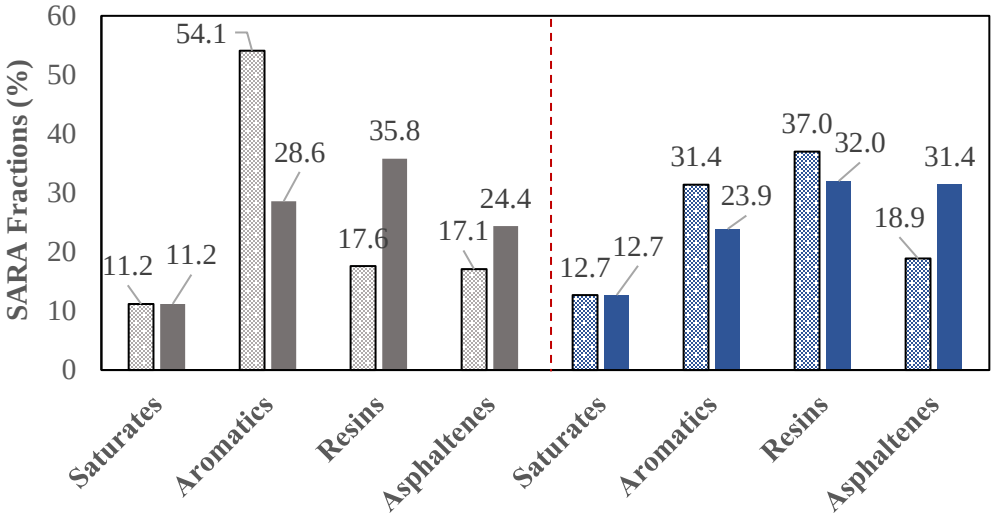

Figure 165. SARA fractions for Additive 5 with Binder 1 (grey) and Binder 5 (blue) before and after aging

The effect of each additive on the SARA fractions of base binders was studied by calculating the percent change of each fraction after RTFO plus 60 hours of aging, as indicated in Equation 16. Percent change in SARA fractions of modified blends with respect to base binders

Equation 16. Percent change in SARA fractions of modified blends with respect to base binders

$$\%\ Change\ in\ Fraction\ i = \frac{(Fraction\ i)_{Modified\ blend} - (Fraction\ i)_{Base\ binder}}{(Fraction\ i)_{Base\ binder}} \times 100$$

where:

$$Fraction\ i = Saturates, Aromatics, Resins, Asphaltenes\ content\ at\ RTFO\ plus\ 60\ hours\ of\ PAV\ aging$$

The effects of modification on the SARA fractions of Binder 1 are presented in Figure 166. Additive 1 showed greater saturates and asphaltenes contents than the control, in addition to lower aromatics and resins. Saturates content after PAV aging is roughly 60% higher than the control, which may appear unusual as this fraction is mostly inert, meaning it would not be significantly affected by aging. Such an increase in saturates reflects an increase in the less polar fraction of the binder, which could imply weaker molecular interactions in the modified binder after aging (Lesueur, 2009; J.C. Petersen, 2009). Therefore, this would contribute to better flow properties, which may be observed from the greater phase angles and lower stiffnesses reported in Section 4.2.5. It should be noted, however, that such an increase in saturates may also be resulting from potential interactions between the solvents used for SARA extraction and the nature of this modifier.

Additives 2,3 and 5 increased the aromatics content with respect to the control, which favors binder dispersion after aging and thus may result on less brittle binders (Hassan A. Tabatabaee & Kurth, 2017). Resins, on the other hand, were reduced by additives 2 and 3, which would compromise binder dispersion.

Overall, modification with Additive 4 caused the least changes in SARA fractions of the control binder. Therefore, it may be argued that the softening effects resulting from this additive come from a decrease in asphaltenes agglomerations more than a re-balancing of the four SARA fractions.

Asphaltenes content was reduced by Additives 3 and 5, indicating that these additives could potentially mitigate asphaltenes formation after aging (J Claine Petersen & Glaser, 2011). Additionally, both resulted on fewer saturates than the control, which also favors binder stability (J.C. Petersen, 2009). Additives 2 and 4 showed higher asphaltenes content than the control. Although asphaltenes are mostly associated with binder stiffness, every modified blend presented lower complex modulus than the control after aging (see section 4.2.4). This supports literature findings indicating that stiffness may also depend on binder dispersion (J.C. Petersen, 2009; J. C. Petersen, Robertson, R.E, Branthaver, J.F., Harnsberger, P.M, Duvall, J.J., Kim, S.S., Anderson, D.A, Christiansen, D.W., Bahia, U.H. , 1994), which was explored using CII.

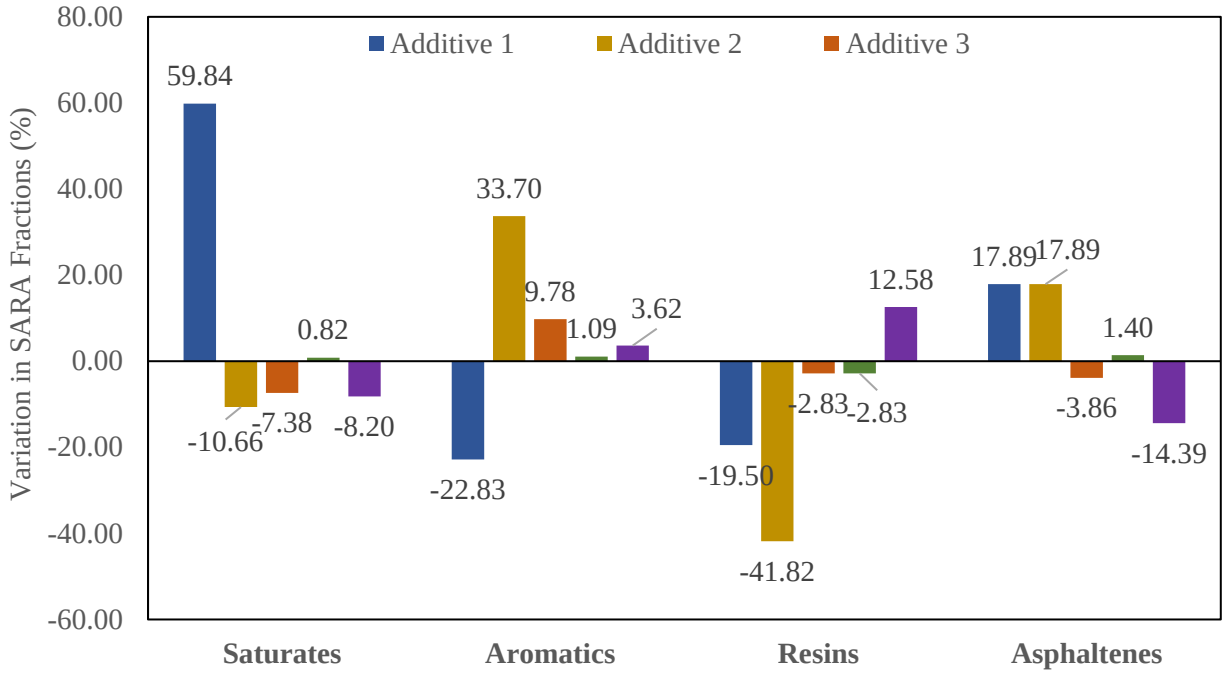

Figure 166. Effects of modification on SARA fractions of Binder 1 after aging

In comparison to Binder 1 (Figure 166), all additives showed greater interactions with Binder 5 (Figure 167). Every modified binder showed greater aromatics content and lower resins than the control after aging. This may indicate that additives prevented the oxidation of aromatics and the subsequent formation of resins, one of the typical effects of aging on SARA fractions. Therefore, all additives could have potentially reduced the formation of oxidation products, which may favor the aging resistance of Binder 5 (Mirwald et al., 2020; J Claine Petersen & Glaser, 2011).

Despite reducing the oxidation of the aromatics, Additives 1 and 2 increased asphaltenes content, which was accompanied by greater stiffnesses after aging (see section 4.2.4). On the other hand, Additive 3 caused a marginal increase (i.e., less than 1%), while Additive 4 caused a reduction in asphaltenes content. Therefore, these additives could have potentially prevented the oxidation of aromatics and mitigate the asphaltenes formation, resulting on improved aging resistance. Although Additive 5 resulted on greater asphaltenes content, rheological findings indicate improvements in brittleness after aging, which supports the analysis of aging stability in terms of CII.

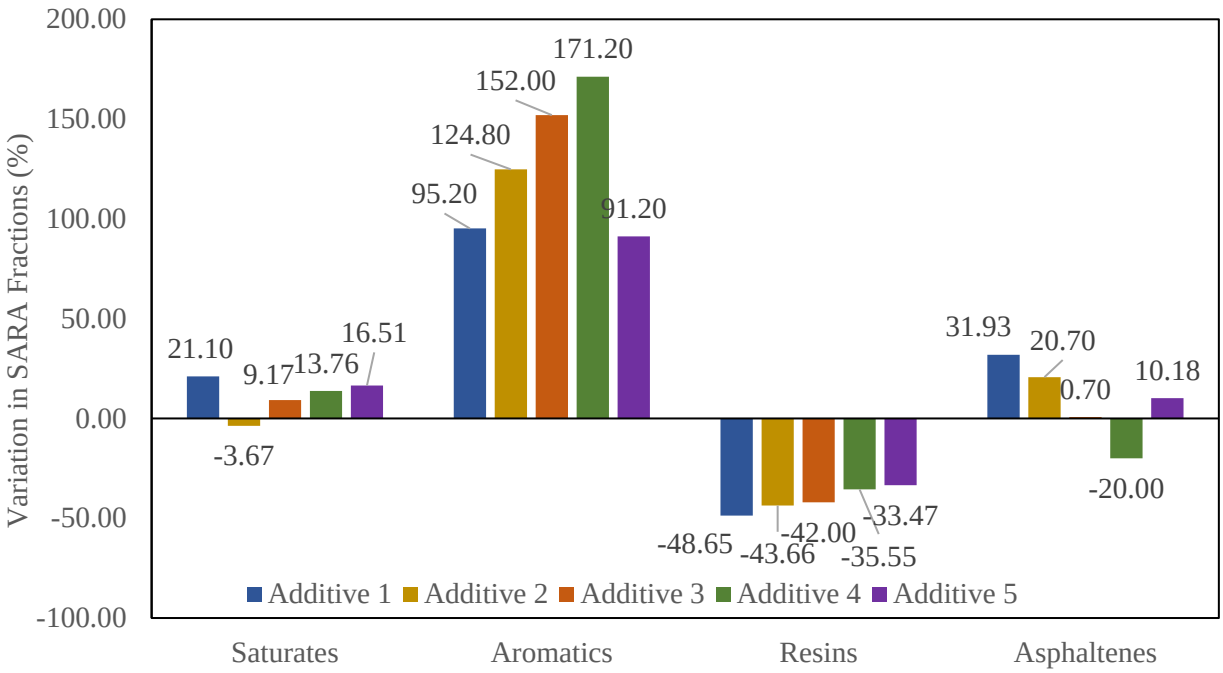

Figure 167. Effect of modification on SARA fractions of Binder 5

CII indices after aging for base Binder 1 and modified blends are presented in Figure 168. Additive 4 showed a comparable CII to the control, which agrees with the above findings of little interactions with its SARA fractions. Additives 1 and 2 showed higher CII than the control after aging, which may be indicative of a higher aging susceptibility. On the other hand, Additive 3 and Additive 5 cause a reduction in CII relative to Binder 1. These results may suggest a greater degree of dispersion of the asphaltenes and thus, decreased susceptibility to aging (J.C. Petersen, 2009). Aging indices calculated with the Glover-Rowe parameter support these findings.

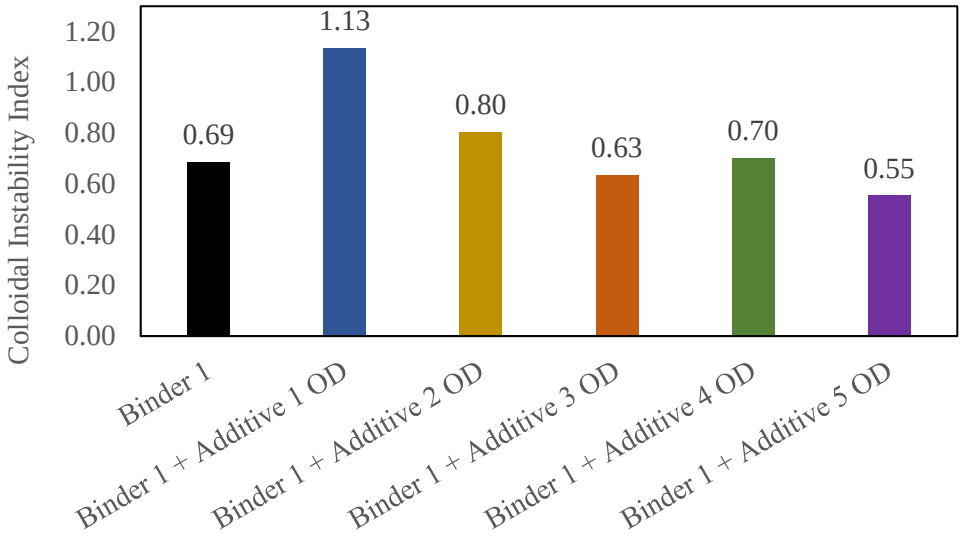

Figure 168. CII after 60 hours PAV aging for Binder 1

CII values after aging for Binder 5 are presented in Figure 169. CII of modified binders with Additives 1, 2, 3 and 5 were higher than the control, indicating poorer dispersion and therefore higher susceptibility to aging (J.C. Petersen, 2009; Hassan A. Tabatabaee & Kurth, 2017). Additive 4 improved the aging properties of Binder 5 in terms of CII. The Glover-Rowe Aging Index indicated otherwise.

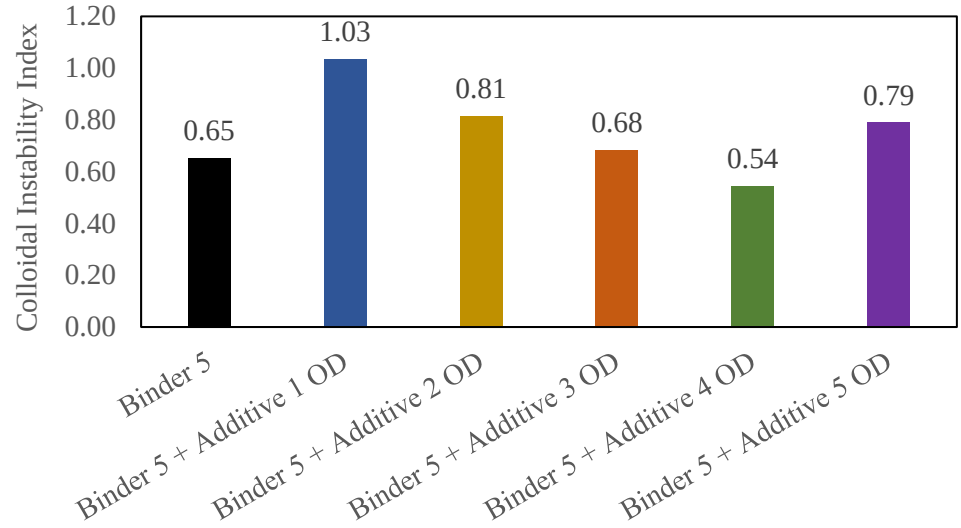

Figure 169. CII after 60 hours PAV aging for Binder 5

The CII ratio between the PAV aged materials and the unaged condition was calculated using Equation 17.
CII Ratio for base and modified binders

Equation 17. CII Ratio for base and modified binders

$$CII\ Ratio = \frac{(CII)_{RTFO+60hr\ PAV}}{(CII)_{Unaged}}$$

Binder 1 results are shown in Figure 170. Additive 4 caused a comparable increase in CII to the control. Additives 1, 2, 3 and 5 decreased CII ratio relative to the control, which is in agreement with the improved rheological properties after aging. The changes in SARA fractions relative to the control (Figure 166) show that this improved stability was achieved by different mechanisms; while Additive 2 reduced resins and increased asphaltenes, Additive 5 showed opposite effects. This result highlights the importance of the characterization of the four fractions to explain binder properties. Dispersion may play an equal role on binder aging behavior as the overall asphaltenes content, although this is the fraction most typically associated with the detrimental effects of aging.

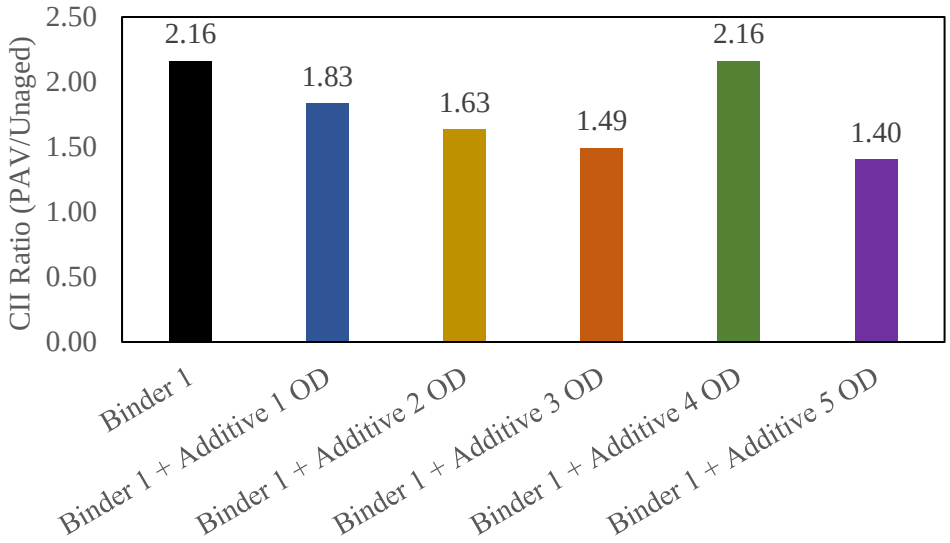

Figure 170. CII ratios for Binder 1

CII ratios for Binder 5 are presented in Figure 171. Smaller CII ratios were observed in this case for all additives except number 3. Aging indices determined through the Glover-Rowe are also consistent with this result.

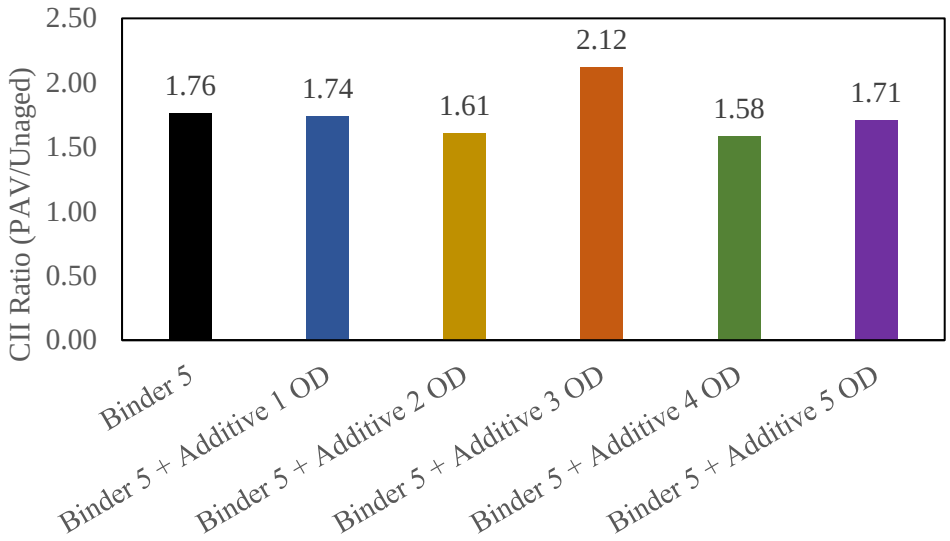

Figure 171. CII ratios for Binder 5

Changes in SARA fractions would lead to changes in rheological properties (J Claine Petersen & Glaser, 2011; Weigel & Stephan, 2017). Therefore, , the effects of CII and asphaltenes content on complex modulus were evaluated. Results presented in Figure 172 and Figure 173 for asphaltenes content showed higher asphaltenes content led to higher stiffness consistent with literature findings (Dehouche et al., 2011; Lesueur, 2009; Mirwald et al., 2020). However, no correlation was observed for Binder 1, and correlations for Binder 5 improved after RTFO plus 60 hours of PAV aging (from R^2=0.39 to in Figure 172 to R^2=0.70 in Figure 173).

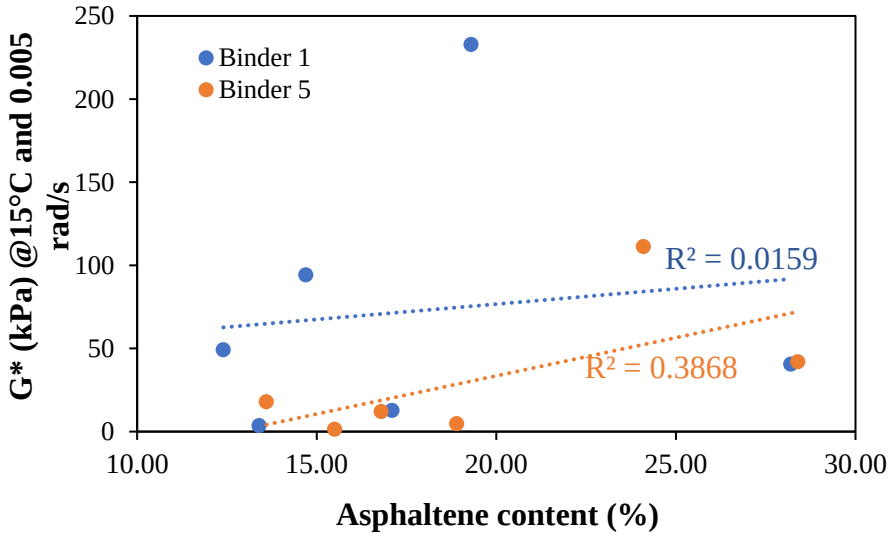

Figure 172. Complex modulus in terms of asphaltene content at the unaged condition

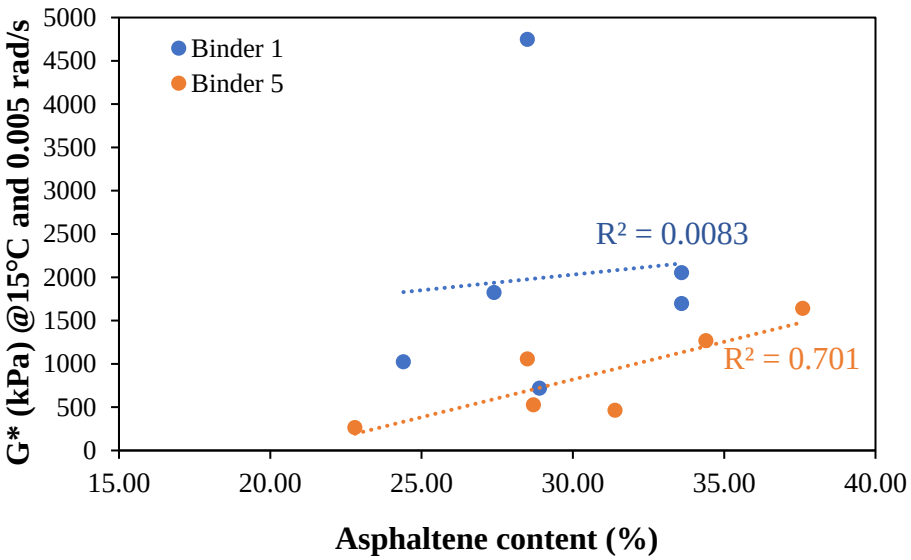

Figure 173. Complex modulus in terms of asphaltene content after RTFO + 60hr PAV

Similar results were obtained for CII indices at both aging conditions, as seen in Figure 174 and Figure 175. Although aging susceptibility has been related to binder dispersion (given by CII), no improvements were observed on this parameter's ability to predict the stiffening effects of aging. Although better correlations were observed for Binder 5, CII did not accurately account for the changes observed in base binder stiffness after aging.

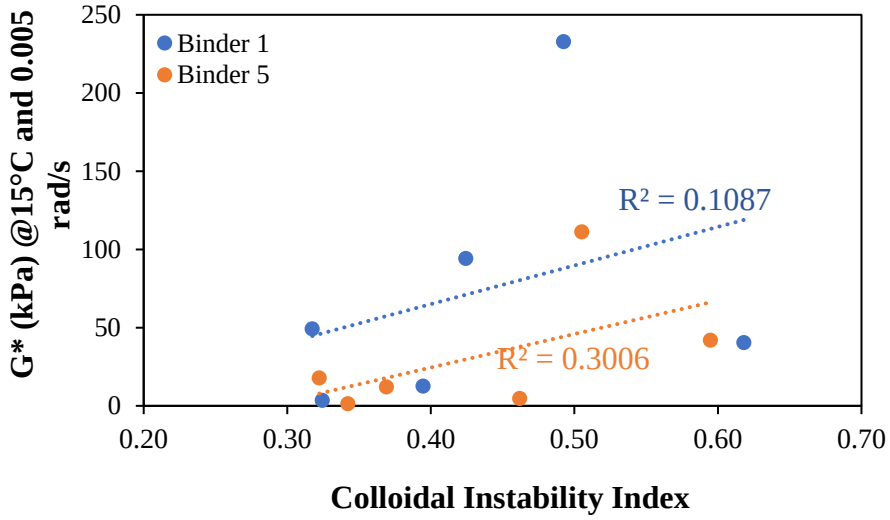

Figure 174. Complex modulus in terms of colloidal instability index at the unaged condition

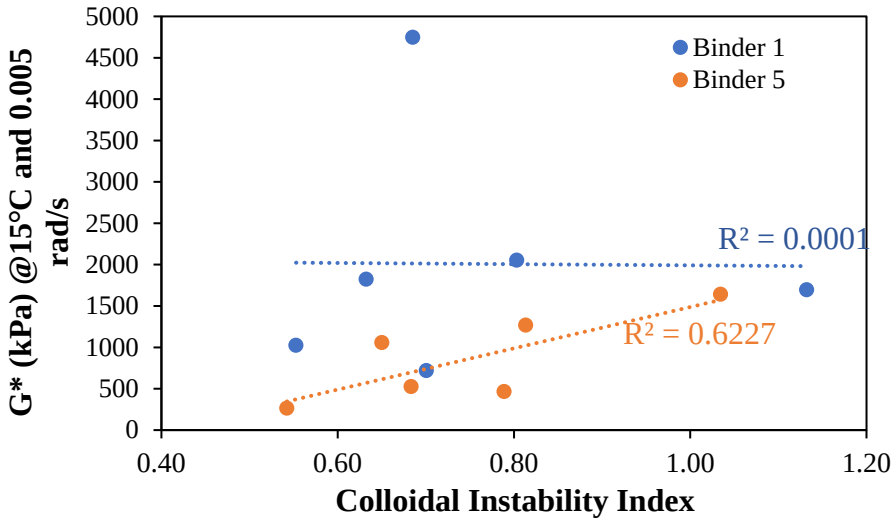

Figure 175. Complex modulus in terms of colloidal instability index after RTFO + 60hr PAV

Overall, SARA fractions showed different levels of interactions between modifiers and each base binder. Binder 1 experienced less variation on its SARA fractions after aging and showed less consistent effects across modifiers. Additive 4 showed the least interaction with all fractions, suggesting improvements in rheology were not given by a restitution of the balance between fractions but potentially by improvements in agglomerations of polar molecules (Lesueur, 2009). Additives 3 and 5 improved aging resistance by potentially mitigating asphaltenes formation. Additives 1 and 2 appeared to improve binder dispersion, as was later shown by CII ratios smaller than the control.

On the other hand, the effects of modification on Binder 5 resulted on consistently greater aromatics and lower resins than the control, suggesting the oxidation of aromatics (and formation of resins) was mitigated (Mirwald et al., 2020). However, improvements in aging resistance were given by Additives 3 and 5, which also mitigated asphaltenes formation. Additive 5, although increased asphaltenes content, improved binder dispersion and therefore its aging susceptibility, as shown by its lower CII ratio.

Although SARA fractions illustrated several working mechanisms for aging resistance, rheological properties were not fully supported by this chemical analysis. One explanation for this difference could be potentially related to the effects that the solvents used for SARA fractions determination may have on additives.

4.3.3 Differential Scanning Calorimetry

Differential Scanning Calorimetry (DSC) was performed on selected samples to determine the glass transition temperatures of base and modified binders after RTFO plus 60 hours of PAV aging. Additionally, T_g results were used for Extended BBR testing, as described in Section 4.2.6.

Glass transition in binders has been explained as the overlap between the transition of the multiple phases present in asphalt and therefore does not occur at a single temperature but over a region. From the DSC results, two T_g temperatures were studied: at the half height [$T_g(H)$] and the glass transition width [$T_g(W)$]. The half-height [$T_g(H)$] has been related to resistance to thermal stresses and low temperature cracking, in many cases providing good correlations with low critical temperatures Tc_s and Tc_m (Elkashef et al., 2020; Memon & Chollar, 1997). In addition, studies have shown that $T_g(H)$ presented better correlation with field performance due to stronger correlations with conditioning times (Bricker & Hesp, 2013), and was therefore selected for extended BBR testing.

$T_g(W)$ is the temperature range between the start of molecular mobility and the end-point, when all molecules have developed molecular motion (Elwardany, King, et al., 2020). Researchers have showed that aging widens the T_g region, as binders become more unstable due to the changes in SARA fractions.

Thus, the effects of additives on $T_g(H)$ and $T_g(W)$ of the base binders were explored. Results for base Binder 1 and modified blends are detailed in TABLE 57, while for Binder 5 and modified blends are detailed in TABLE 58

TABLE 57. Binder 1 Glass Transition Temperatures - RTFO+60hr PAV

	$T_g(H)$ (℃)	$T_g(W)$ (℃)
Binder 1	-17.2	55.2
Binder 1 + Additive 1 OD	-13.9	59.9
Binder 1 + Additive 2 OD	-18.9	64.9
Binder 1 + Additive 3 AD	-20.1	60.8
Binder 1 + Additive 4 OD	-15.6	57.6
Binder 1 + Additive 5 OD	-18.1	57.2

TABLE 58. Binder 5 Glass Transition Temperatures - RTFO+60hr PAV

	$T_g(H)$ (℃)	$T_g(W)$ (℃)
Binder 5	-8.1	77.3
Binder 5 + Additive 1 OD	-5.5	79.3
Binder 5 + Additive 2 AD	-19.6	62.0
Binder 5 + Additive 3 OD	-17.2	55.5
Binder 5 + Additive 4 OD	-17.2	53.0
Binder 5 + Additive 5 OD	-17.0	59.6

Binder 5 presented a $T_g(H)$ of -8.1℃, which is higher than $T_g(H)$ of Binder 1, with -17.1℃ as indicated in TABLE 58 and TABLE 57, respectively, potentially indicating lower thermal cracking resistance. However, rheological measurements showed Binder 5 had better aged properties, and its lower BBR critical temperatures after 60 hours of PAV aging support this conclusion. This highlights the complexity of the glass transition phenomenon and aligns with other researchers' findings where correlations with low critical

temperatures were not as straightforward (Bricker & Hesp, 2013). Nevertheless, the effects of modification on glass transition were still be observed and changes relative to the control binders were successfully evaluated.

Figure 176 compares the $T_g(H)$ for every modified binder with respect to base Binder 1. A reduction in $T_g(H)$ of the control binder was observed for Additives 2, 3, and 5. A shift towards lower temperatures would indicate less embrittlement after aging, potentially increasing the durability of modified binders. Additives 2 and 3 showed greater aromatics content and a reduction in resins, which could potentially favor dispersion of the asphalt phases and thus contribute to a lower $T_g(H)$ as has been found by researchers (Brule, Planche, King, Claudy, & Letoffe, 1990). Conversely, modification with Additive 1 and Additive 4 shifted the $T_g(H)$ of the base binder to warmer temperatures, which would indicate these additives did not improve the brittle behavior of Binder 1 after aging.

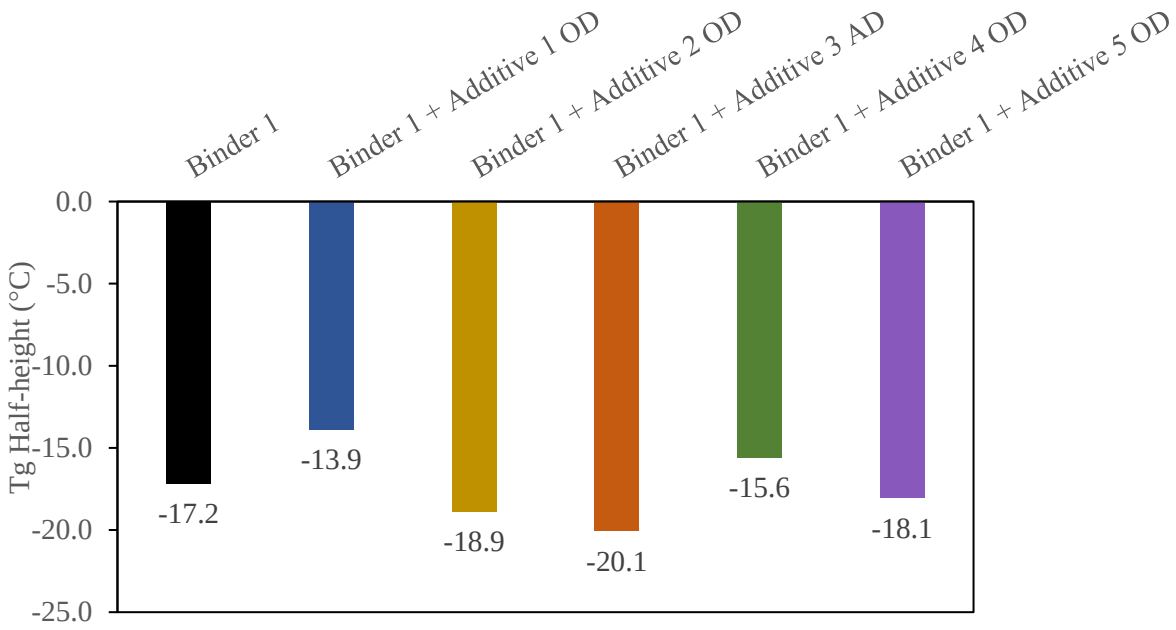

Figure 176. $T_g(H)$ for base Binder 1 and modified blends - RTFO+60hr PAV

$T_g(H)$ results for Binder 5 after aging are shown in Figure 177. Considerable reductions in glass transition temperature were observed for most additives. The effect of rejuvenators present in Additives 3 and 4 can be further observed by lower glass transition temperatures, supporting the effect of rejuvenation found by others (Elkashef et al., 2020; Hassan A. Tabatabaee & Kurth, 2017). Furthermore, the lower $T_g(H)$ obtained after modification with Additive 5 could possibly be explained by the increase in saturates and aromatics introduced by this additive (Brule et al., 1990; Lesueur, 2009).

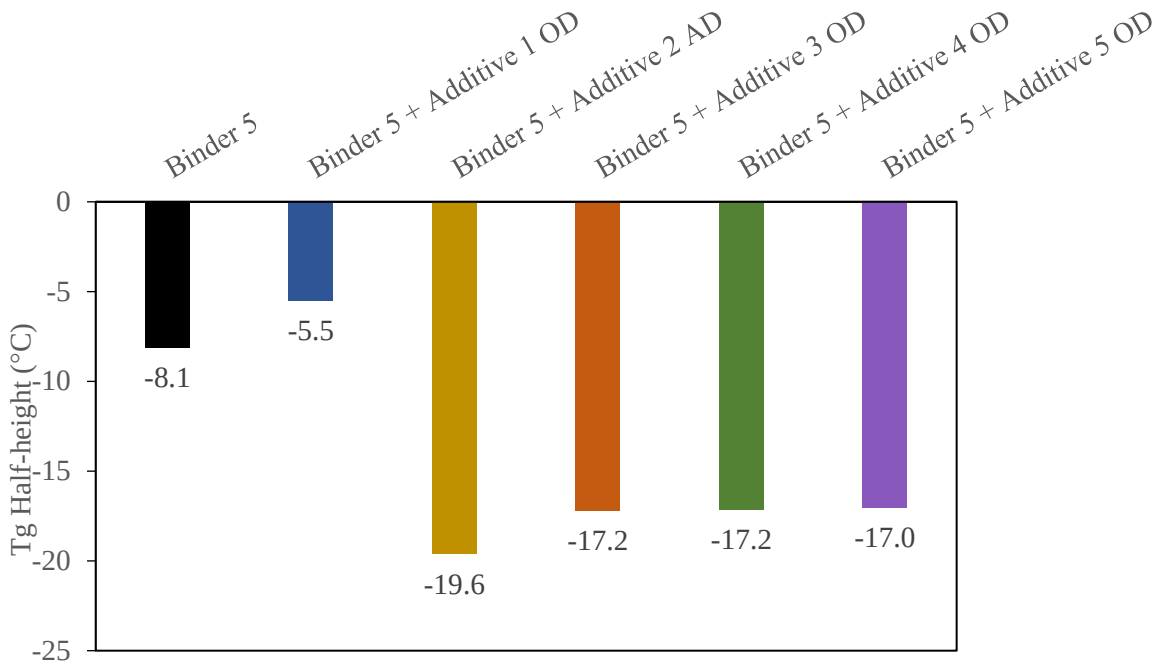

Figure 177. $T_g(H)$ for base Binder 5 and modified blends - RTFO+60hr PAV

The effects of modification on $T_g(W)$ of Binder 1 are shown in Figure 178. Results showed that the modified binders have higher $T_g(W)$ than the base binder, potentially indicating poorer relaxation properties (Brule et al., 1990; Elwardany, King, et al., 2020). However, m-values of base and modified binders did not follow a similar trend, as shown by the lack of correlation between $T_g(W)$ and $T_{c,m}$ in Figure 179.

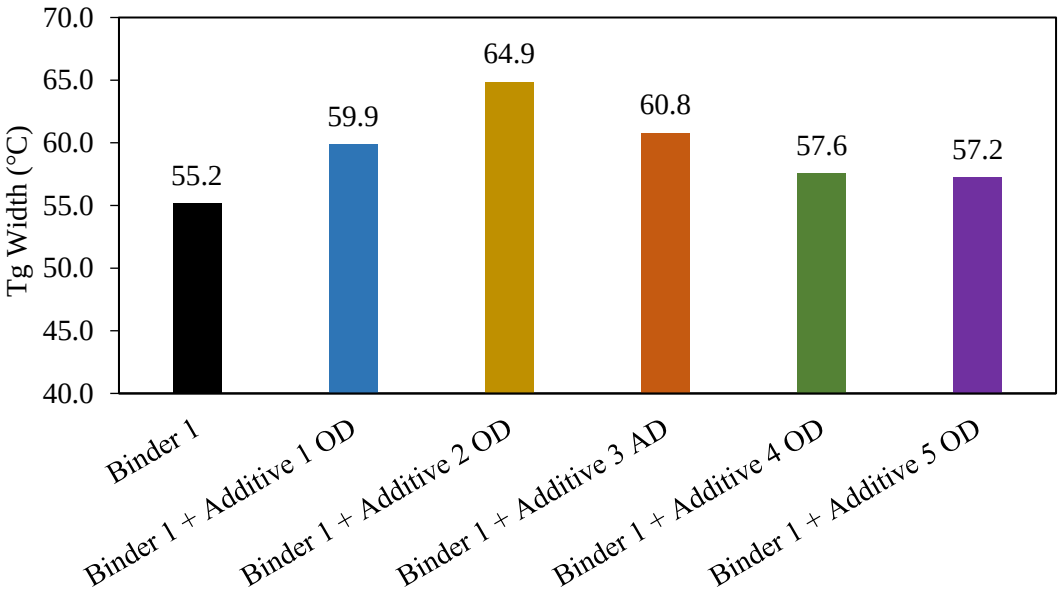

Figure 178. $T_g(W)$ for base Binder 1 and modified blends - RTFO+60hr PAV

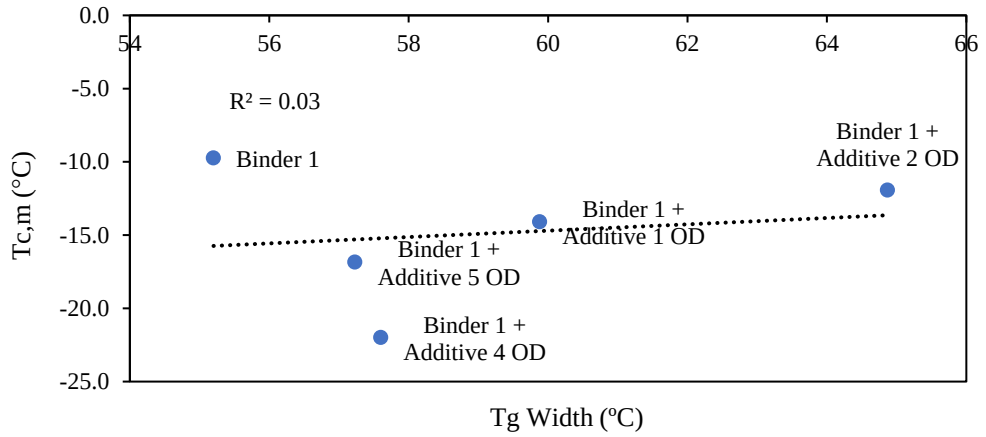

Figure 179. Relationship between $T_g(W)$ and Tc,m for base Binder 1 and modified blends (RTFO + 60hr PAV)

Figure 180 shows the effect of modifiers on $T_g(W)$ of Binder 5. In this case, modification with additives 2, 3, 4, and 5 led to lower values of $T_g(W)$, indicating improved relaxation properties (Brule et al., 1990; Elwardany, King, et al., 2020). Rheological results support this finding, as m-values for base Binder 5 and modified blends followed the same trend. Figure 181 shows high correlations (R^2=0.94) were obtained between $T_g(W)$ and $T_{c,m}$, which contrasts with findings for Binder 1 in Figure 179. However, results should be interpreted with caution due to the limited number of samples evaluated through DSC.

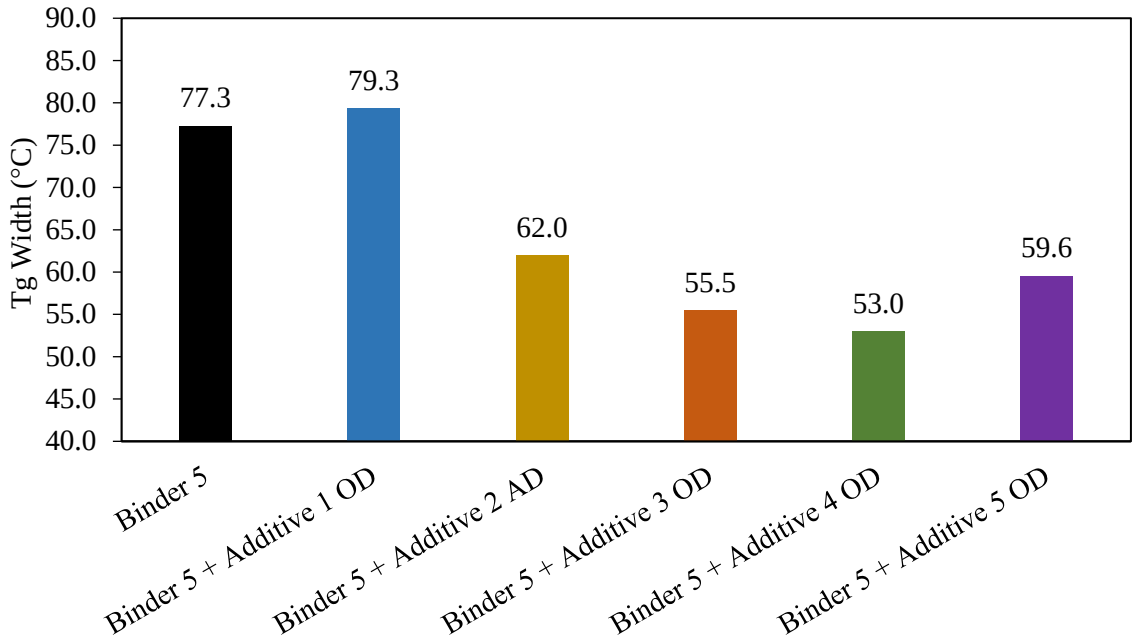

Figure 180. $T_g(W)$ for base Binder 5 and modified blends - RTFO+60hr PAV

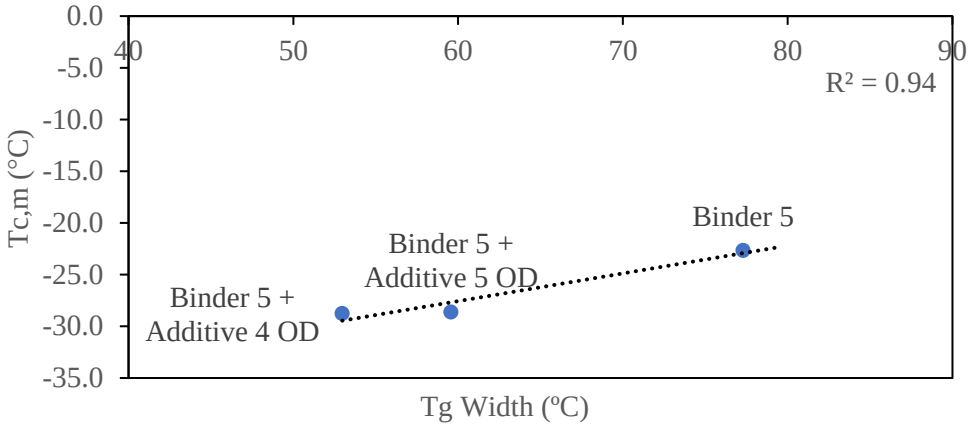

Figure 181. Relationship between $T_g(W)$ and Tc,m for base Binder 5 and modified blends (RTFO + 60hr PAV)

The relationship between $T_g(W)$, ΔT_C and Glover-Rowe parameter of base and modified binders was studied to explore how changes in glass transition related to fatigue cracking resistance and ductility of binders. Better correlations were obtained for Binder 5 than for Binder 1, supporting the base binder dependence observed throughout this work. Figure 182 shows no correlation was observed between ΔT_C and $T_g(W)$ of Binder 1, and similar findings are observed in Figure 183 for the Glover-Rowe parameter.

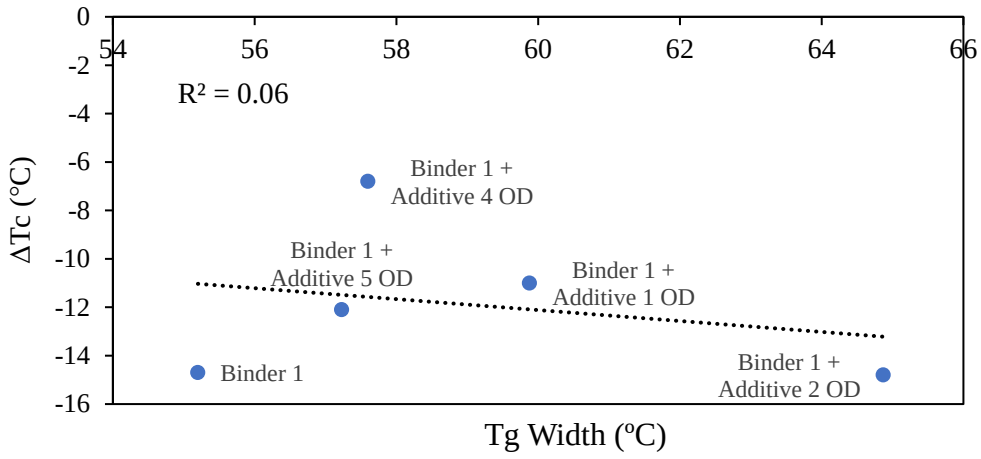

Figure 182. Relationship between $T_g(W)$ and ΔTc for base Binder 1 and modified blends (RTFO + 60hr PAV)

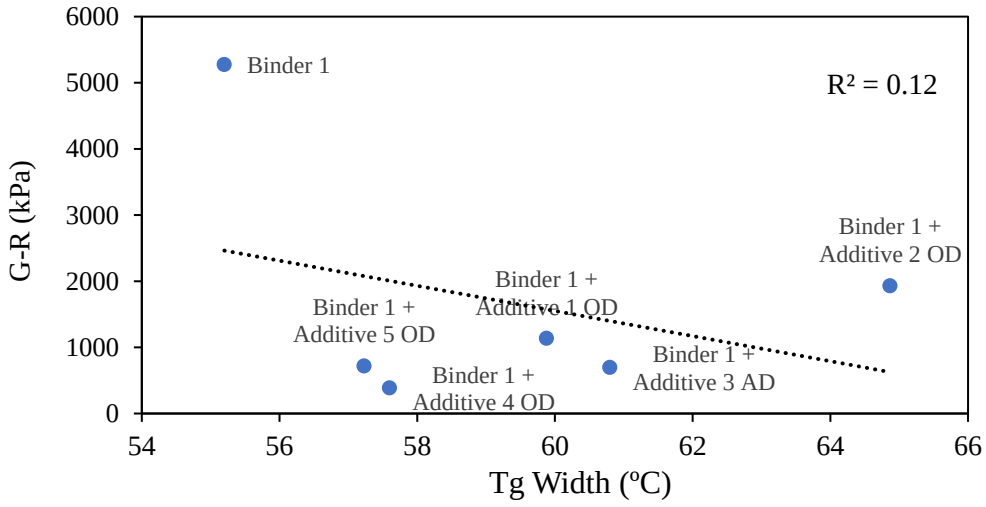

Figure 183. Relationship between $T_g(W)$ and Glover-Rowe parameter for base Binder 1 and modified blends (RTFO + 60hr PAV)

However, results for base Binder 5 and modified blends in Figure 184 showed reductions in $T_g(W)$ after modification improved binder ductility, shown by more positive values of ΔT_C. Additonally, Figure 185 shows higher values of $T_g(W)$, typically indicative of more brittle binders with worse relaxation properties, were also accompanied by higher Glover-Rowe values, indicative of greater fatigue cracking susceptibility.

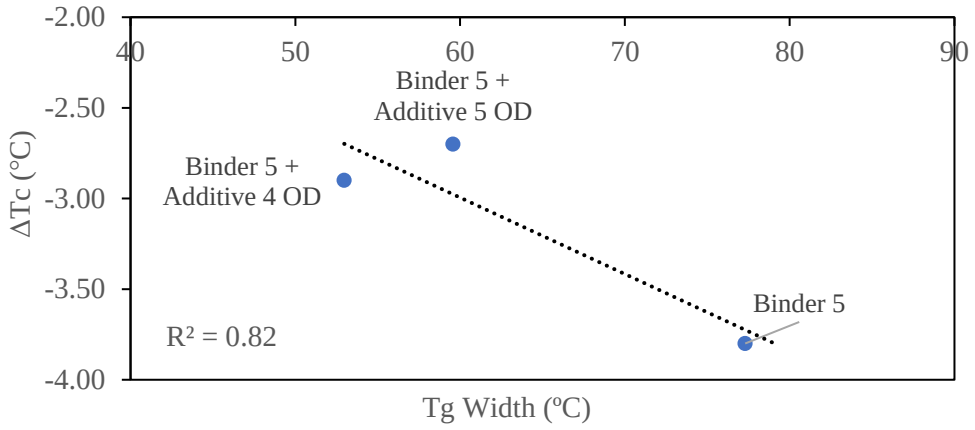

Figure 184. Relationship between $T_g(W)$ and ΔTc for base Binder 5 and modified blends (RTFO + 60hr PAV)

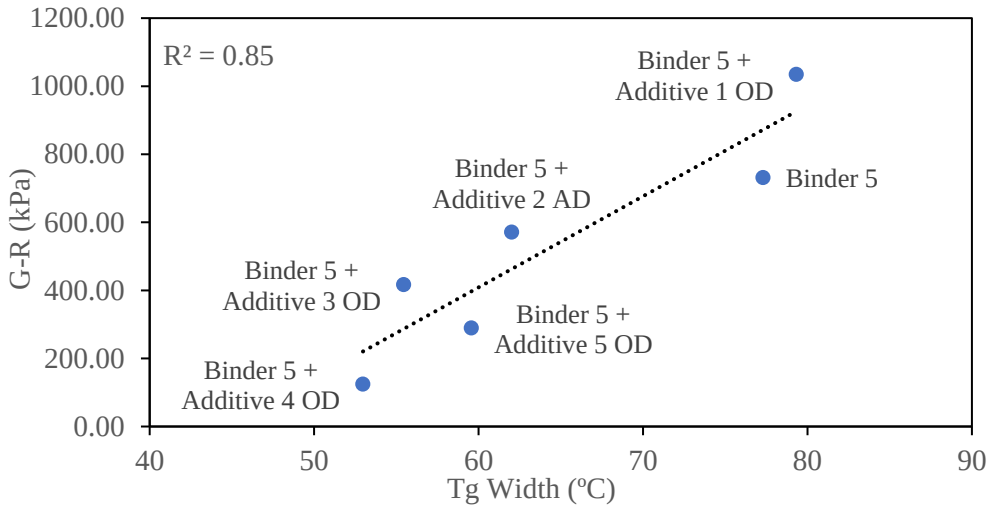

Figure 185. Relationship between $T_g(W)$ and Glover-Rowe parameter for base Binder 5 and modified blends (RTFO + 60hr PAV)

4.3.4 Gel Permeation Chromatography

GPC was performed on modified blends without RAP as well as on the control binders, at the unaged condition and after 60 hours of PAV aging. Molecular size distribution (MSD) before and after aging were evaluated, and relationships with rheology were explored.

Four molecular weights were obtained from the chromatogram:

- M_w: weight-average molecular weight
- M_n: number-average molecular weight
- M_z: z-average molecular weight
- Mp: peak molecular weight

The changes in M_n after 60 hours of PAV aging are shown for both base binders in Figure 186. M_n is usually related to brittleness and flow properties (Isacsson & Zeng, 1997). Results in Figure 186 indicate a smaller increase in M_n for most modified binders when compared against the control. Modification with additive 3, however, showed a greater increase for base Binder 5. In addition, Figure 187 shows higher values of M_n led to reduced strain at peak stress obtained from LAS test, and Figure 188 showed higher M_n values presented more negative (worse) $\triangle T_c$ values. Thus, a smaller increase, or a reduction in M_n as a result of modification would likely improve binder fatigue cracking susceptibility and therefore enhance cracking performance after aging.

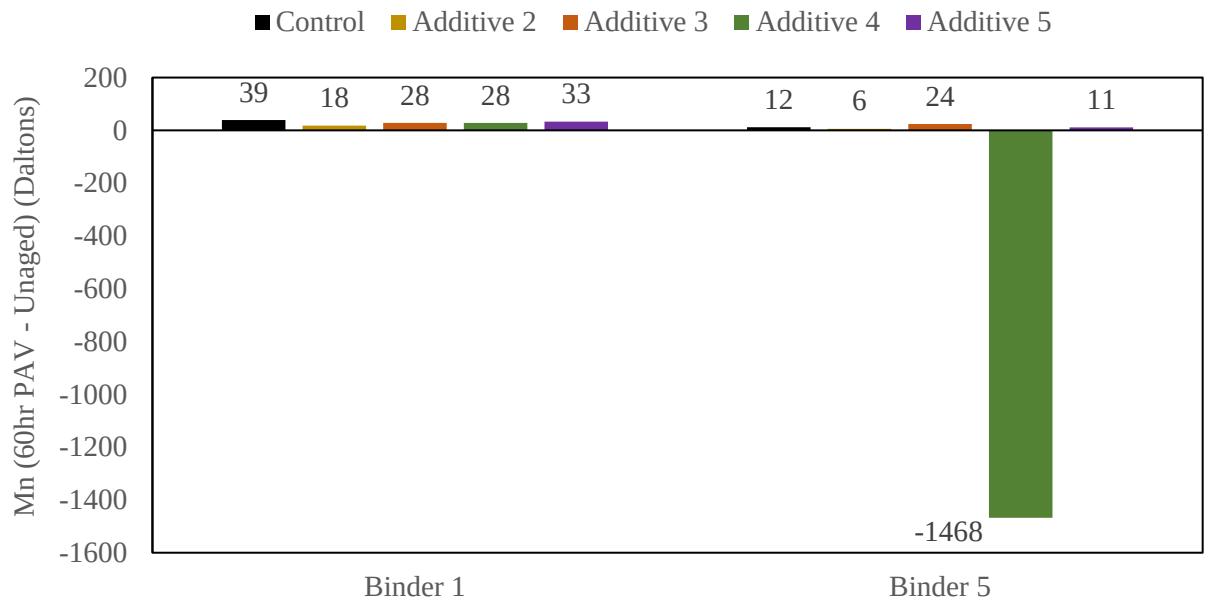

Figure 186. Mn variation for base binder 1 and base binder 5 (60hr PAV - Unaged)

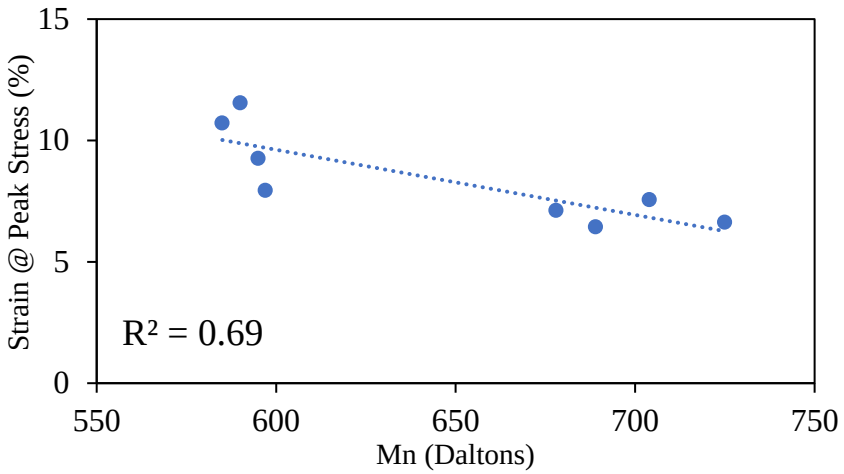

Figure 187. Strain at peak stress and Mn for both base binders and all modified binder blends

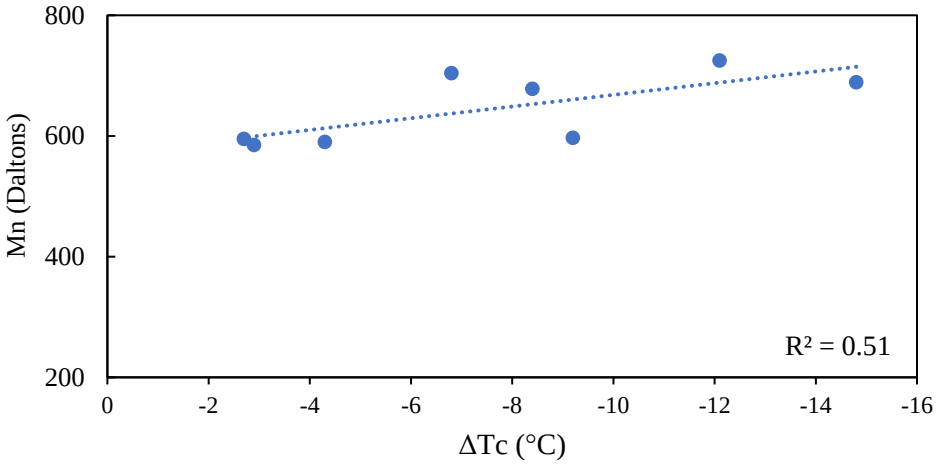

Figure 188. ΔTc and Mn for both base binders and all modified binder blends

CHAPTER 5 - CONCLUSIONS AND RECOMMENDATIONS

This study aimed to determine the effect of five novel technologies on the aging resistance of neat binders and their recycled binder blends. After an initial evaluation, two straight run binders refined from two crude sources were selected as the base binders. These binders showed comparable unaged properties but very different aging behavior. The control materials in this study included the two base binders and their blends with 20% recycled binder extracted from a RAP sample in Alabama. Each of the aging resistant technologies was blended at optimum and alternative dosages with the control materials and their recycled binders for evaluation in this study.

The control materials and modified blends were tested following a comprehensive experimental plan to characterize their rheological and chemical properties before and after aging to evaluate the effectiveness of each aging resistant technology. Prior to testing, base and modified binder samples were laboratory aged following multiple protocols that simulated their aging conditions during production and in service, namely RTFO for short-term aging, RTFO + 20-hour PAV for long-term aging, and RTFO + 60-hour PAV for extended aging. The plan for rheological characterization included Superpave performance grading, MSCR for rutting resistance and elastic response, LAS for intermediate temperature cracking resistance, and temperature-frequency sweeps with master curve analysis to determine the Glover-Rowe parameter for evaluating fatigue cracking resistance and binder ductility. Tests such as the MSCR, LAS and the construction of master curves and evaluation of the Glover-Rowe parameter provided a more accurate characterization of modifiers of various natures, indicating improvements in rheology that may not have been observed through the traditional Superpave PG. Additionally, physical hardening behavior of binders was evaluated through extended BBR testing. Effects of aging on binder chemistry were evaluated through FTIR-ATR spectroscopy, SARA fractions analysis, DSC, and GPC.

Rheological and chemical results showed all the proposed technologies mitigated the effects of aging with respect to the control binders, and therefore improved their aging resistance. The effectiveness of the additives was dependent on the nature of each modifier and base binder type and influenced by the presence of RAP binder.

The key findings from the rheological experiment can be summarized as follows:

Superpave performance grading of the unaged and RTFO + 60-hour PAV aged samples showed improvement in aging resistance of the control binders through lower stiffening rates at high-temperatures, a decrease in the temperature at which the limiting DSR fatigue parameter [$|G^*|\sin(\delta)$] was satisfied, and lower pass/fail low-temperatures, as shown in TABLE 59. Furthermore, ΔT_c parameter results, evaluated through DSR-4mm parallel plate geometry and BBR testing after the aging protocols of RTFO + 20-hour PAV and RTFO + 60-hour of PAV, indicated that the addition of additives 1, 3, 4 and 5 resulted in less negative (better) $\triangle T_c$ values, reducing the block cracking susceptibility of base binders and recycled binder blends.

TABLE 59. Summary of Main Superpave Findings

	Effect at high temperature	Effect at intermediate temperature	Effect at low temperature	
	Lower HT Variation	**Lower IT After RTFO + 60 Hours Pav**	**Lower LT True Grade Variation**	**Higher (More Positive) ΔTc**
Binder 1	Additive 1 OD, AD Additive 2 OD Additive 4 OD	Additive 1 OD, AD Additive 2 OD Additive 3 OD Additive 4 OD Additive 5 OD	Additive 1 OD, AD Additive 2 OD Additive 4 OD	Additive 1 OD, AD Additive 4 OD Additive 5 OD
Binder 5	Additive 3 OD	Additive 3 OD Additive 4 OD Additive 5 OD		
Binder 1 + RAP	Additive 2 OD, AD Additive 4 AD Additive 5 AD	Additive 2 AD Additive 3 OD, AD Additive 4 OD, AD	Additive 2 OD, AD Additive 3 OD, AD Additive 4 OD, AD	Additive 3 OD, AD Additive 4 OD, AD Additive 5 OD, AD
Binder 5 + RAP	Additive 2 OD Additive 3 OD, AD Additive 4 OD, AD Additive 5 OD, AD	Additive 2 OD, AD Additive 3 OD, AD Additive 4 OD, AD Additive 5 OD, AD	Additive 2 OD Additive 4 OD, AD	Additive 4 OD, AD Additive 5 OD

- MSCR results obtained at 64°C after RTFO aging are summarized in TABLE 60. It was observed that the effectiveness of each additive was related to its chemical composition as well as its interaction with the controls and recycled binder blends.

TABLE 60. Summary of Main MSCR Findings

	Improved J_{nr}	Improved Traffic Level	Improved %Recovery
Binder 1	Additive 1 OD, AD Additive 2 OD Additive 3 OD	Additive 2 OD Additive 3 OD	Additive 1 OD, AD Additive 2 OD Additive 3 OD Additive 5 OD
Binder 1 + RAP	Additive 2 OD, AD Additive 3 OD, AD Additive 5 OD, AD	Additive 2 OD, AD Additive 3 OD, AD	Additive 2 OD, AD Additive 3 OD, AD Additive 5 OD, AD
Binder 5	Additive 1 OD, AD Additive 2 OD Additive 3 OD	Additive 1 OD, AD Additive 2 OD Additive 3 OD	Additive 1 OD, AD Additive 2 OD Additive 3 OD Additive 5 OD
Binder 5 + RAP	Additive 2 OD, AD Additive 3 OD, AD Additive 5 OD, AD	Additive 2 OD, AD Additive 3 OD, AD	Additive 2 OD, AD Additive 3 OD, AD Additive 5 OD, AD

- LAS test parameter N_f was influenced by the nature of the additives, where no clear failure in high polymer content binders was observed. Strain at peak stress provided a more accurate comparison across technologies, capturing the benefits of each additive on improving the strain tolerance and ability to relax stresses with respect to the base binders and recycled binder blends. LAS results are summarized in TABLE 61.

TABLE 61. Summary of Main LAS Findings

	Increase In Cycles to Failure (at 5% strain)	Reduction In |B| - Parameter	Increase In Strain Tolerance
Binder 1	Additive 1 AD Additive 2 OD Additive 3 OD Additive 4 OD Additive 5 OD	Additive 1 OD, AD Additive 2 OD Additive 3 OD Additive 4 OD Additive 5 OD	Additive 1 AD Additive 3 OD Additive 4 OD Additive 5 OD
Binder 5	Additive 3 OD Additive 4 OD Additive 5 OD	Additive 4 OD	Additive 3 OD Additive 4 OD Additive 5 OD
Binder 1 + RAP	Additive 2 OD, AD Additive 3 OD, AD Additive 4 OD	Additive 2 OD, AD Additive 3 OD, AD Additive 4 OD, AD Additive 5 OD, AD	Additive 2 OD, AD Additive 3 OD, AD Additive 4 OD, AD Additive 5 OD, AD
Binder 5 + RAP	Additive 2 OD, AD Additive 3 OD, AD Additive 4 AD Additive 5 OD	Additive 3 OD Additive 4 OD, AD Additive 5 OD	Additive 2 OD, AD Additive 3 OD, AD Additive 4 OD, AD Additive 5 OD

- G-R Effectiveness Index results indicated that some technologies were effective in decreasing the stiffness and embrittlement of the controls and recycled binder blends after extended aging TABLE 62.

TABLE 62. Glover-Rowe Effectiveness Index Results

	Decreased Stiffness and Embrittlement
Binder 1	Additive 1 OD, AD Additive 2 OD Additive 3 OD Additive 4 OD Additive 5 OD
Binder 5	Additive 3 OD Additive 4 OD Additive 5 OD
Binder 1 + RAP	Additive 2 OD, AD Additive 3 OD, AD Additive 4 OD, AD Additive 5 OD, AD
Binder 5 + RAP	Additive 2 OD, AD Additive 3 OD, AD Additive 4 OD, AD Additive 5 OD, AD

- Hardening indices calculated from extended BBR results after conditioning and testing of samples at the T_g obtained from DSC measurements showed that all additives improved the physical hardening behavior of Binder 1; while Additives 1 and 3 successfully improved the physical hardening behavior of Binder 5.

Furthermore, the chemical evaluation led to the following key findings:

- FTIR analysis indicated that a reduction in oxygen-containing compounds (i.e., C=O + S=O) was observed on controls and recycled binder blends after modification with the additives (with exception of Additive 2). Two approaches were followed in the analysis: Approach (1) considered the area of C=O between the wavelengths of 1660 and 1753 cm^{-1} and attributed the changes in the entire region to the effect of aging; and approach (2) considered the area of C=O between the wavelengths of 1660 and 1719 cm^{-1} in order to exclude C=O functions present in the composition of some additives. Results showed the C=O bond present in some additives did not overestimate the C=O + S=O area growth of binders due to aging.

- CII ratio calculated as the fraction of the CII of the RTFO + 60-h PAV-aged sample over that of the unaged sample indicated that the additives successfully improved the colloidal stability (which is related to the aggregation or agglomeration of the asphalt fractions) of control binders, with exception of Additive 4 OD when blended with Binder 1 and Additive 3 OD when blended with Binder 5. Aging indices determined through the G-R parameter results are in agreement with this finding. TABLE 63 presents the effect of additives on SARA (saturates, aromatics, resisns, and asphaltenes) fractions of control binders after extended aging.

TABLE 63. Main SARA Fraction Analysis Results

	Binder 1			
	S	**A**	**R**	**A**
Additive 1	**Increased**	Decreased	Decreased	**Increased**
Additive 2	Decreased	**Increased**	Decreased	**Increased**
Additive 3	Decreased	**Increased**	Decreased	Decreased
Additive 4	**Increased**	**Increased**	Decreased	**Increased**
Additive 5	Decreased	**Increased**	**Increased**	Decreased
	Binder 5			
	S	**A**	**R**	**A**
Additive 1	**Increased**	**Increased**	Decreased	**Increased**
Additive 2	Decreased	**Increased**	Decreased	**Increased**
Additive 3	**Increased**	**Increased**	Decreased	**Increased**
Additive 4	**Increased**	**Increased**	Decreased	Decreased
Additive 5	**Increased**	**Increased**	Decreased	**Increased**

- DSC results after RTFO + 60-hour PAV aging showed that Additives 2, 3 and 5 shifted the T_g of Binder 1 towards lower temperatures; while Additives 2, 3, 4 and 5 improved the T_g of Binder 5. Narrower glass transition regions (i.e., lower glass transition widths) were observed for Binder 5, reflecting improvements in relaxation properties of the control. These findings were in agreement with rheological properties evaluated by G-R and ΔTc parameters.

- GPC results showed that the technologies affected the M_n molecular weight, usually related to brittleness and flow properties of control binders. The correlation with strain at peak stress obtained from the LAS rheological test indicated that modified binders with lower M_n presented higher strain tolerance.

The combination of rheological and chemical tests provided an understanding of potential working mechanisms of these technologies. In summary, the five aging resistant technologies improved the aging resistance of the control materials (i.e., base binders and their blends with RAP binder) when the control materials were modified with each technology. Improvement was observed in fatigue resistance, ductility and relaxation properties based on both rheological and chemical test results after the extended aging. If these findings are validated in the ongoing mixture testing program, the aging resistant technologies can be implemented to enhance the cracking resistance and durability of asphalt mixtures, extending the service life of asphalt pavements.

The limitation of the ΔTc parameter to evaluate the resistance to age-related distresses of polymer modified binders is widely recognized and was also observed in this work. Future testing using the Asphalt Binder Cracking Device (ABCD) would better characterize these materials at low temperatures.

In addition, a future line of work could be explored through the chemical characterization of modified binders with RAP binder blends, as additive effectiveness was enhanced (in some cases) in the presence of recycled binder. Therefore, the chemical characterization of these modified binders would provide greater insight into the mechanisms that resulted on those improvements.

Finally, research is currently underway to validate these findings by testing the asphalt mixtures prepared with the base and modified binders. Asphalt Mixture Performance Tester (AMPT) testing is being conducted on lab-mixed, lab-compacted specimens after short-term, long-term oven and ultraviolet aging inside the NCAT Accelerated Weathering System (NAWS) to determine the mixture fatigue cracking performance. Mixture testing results will be used to determine if the aging resistant technologies can help increase the mixture durability and if the improvement can result in life cycle cost savings.

REFERENCES

Airey, G. D. (2003). State of the Art Report on Ageing Test Methods for Bituminous Pavement Materials. *International Journal of Pavement Engineering, 4*(3), 165-176. doi:10.1080/1029843042000198568

Al-Khateeb, G., & Ramadan, K. (2015). Investigation of the effect of rubber on rheological properties of asphalt binders using superpave DSR. *KSCE Journal of Civil Engineering, 19*. doi:10.1007/s12205-012-0629-2

Ameri, M., Reza Seif, M., Abbasi, M., & Khavandi Khiavi, A. (2017). Viscoelastic fatigue resistance of asphalt binders modified with crumb rubber and styrene butadiene polymer. *Petroleum Science and Technology, 35*(1), 30-36.

Anderson, D. A., Christensen, D. W., Bahia, H. U., Dongre, R., Sharma, M., Antle, C. E., & Button, J. (1994). Binder characterization and evaluation, volume 3: Physical characterization. *Strategic Highway Research Program, National Research Council, Washington, DC*.

Anderson, D. A., & Kennedy, T. W. (1993). Development of SHRP binder specification (with discussion). *Journal of the Association of Asphalt Paving Technologists, 62*.

Anderson, D. A., Le Hir, Y. M., Marasteanu, M. O., Planche, J.-P., Martin, D., & Gauthier, G. (2001). Evaluation of fatigue criteria for asphalt binders. *Transportation Research Record, 1766*(1), 48-56.

Anderson, D. A., & Marasteanu, M. O. (1999). Physical hardening of asphalt binders relative to their glass transition temperatures. *Transportation Research Record, 1661*(1), 27-34.

Anderson, R. M., King, G. N., Hanson, D. I., & Blankenship, P. B. (2011). Evaluation of the relationship between asphalt binder properties and non-load related cracking. *Journal of the Association of Asphalt Paving Technologists, 80*.

Andriescu, A., & Hesp, S. A. M. (2009). Time–temperature superposition in rheology and ductile failure of asphalt binders. *International Journal of Pavement Engineering, 10*(4), 229-240. doi:10.1080/10298430802169440

Apeagyei, A. K. (2011). Laboratory evaluation of antioxidants for asphalt binders. *Construction and Building Materials, 25*(1), 47-53.

Apostolidis, P., Liu, X., Erkens, S., & Scarpas, T. (2020). Oxidative aging of epoxy asphalt. *International Journal of Pavement Engineering*, 1-11.

Asgharzadeh, S. M., Tabatabaee, N., Naderi, K., & Partl, M. N. (2015). Evaluation of rheological master curve models for bituminous binders. *Materials and Structures, 48*(1), 393-406.

Aurilio, M., Tavassoti, P., Elwardany, M., & Baaj, H. (2021). Impact of Styrene-Butadiene-Styrene (SBS) content on asphalt Binder's fatigue resistance at various aging levels using Viscoelastic Continuum Damage and fracture mechanics. *Construction and Building Materials, 305*, 124627.

Aurilio, M., Tavassoti, P., Elwardany, M., Baaj, H., & Eng, P. (2020). *Comparing the ability of different tests and rheological indices to evaluate the cracking resistance of polymer modified asphalt binders.* Paper presented at the Proceedings, Canadian Technical Asphalt Association.

Bahia, H. U., Hanson, D., Zeng, M., Zhai, H., Khatri, M., & Anderson, R. (2001). *Characterization of modified asphalt binders in superpave mix design*.

Bahia, H. U., Lyngdal, E., Wisconsin, O., Varma, R., Sweirtz, D., & Teymourpour, P. (2016). *Modified Binder (PG+) Specifications and Quality Control Criteria*: Wisconsin Department of Transportation.

Behnood, A., Shah, A., McDaniel, R. S., Beeson, M., & Olek, J. (2016). High-Temperature Properties of Asphalt Binders: Comparison of Multiple Stress Creep Recovery and Performance Grading Systems. *Transportation Research Record, 2574*(1), 131-143. doi:10.3141/2574-15

Bonaquist, R., Adams, J., & Anderson, D. A. (2021). *Asphalt Binder Aging Methods to Accurately Reflect Mixture Aging*.

Bricker, R. M., & Hesp, S. A. (2013). Modulated differential scanning calorimetry study of physical hardening rates in asphalt cements. In *Airfield and Highway Pavement 2013: Sustainable and Efficient Pavements* (pp. 955-966).

Brule, B., Planche, J., King, G., Claudy, P., & Letoffe, J. (1990). Relationships between characterization of asphalt cements by differential scanning calorimetry and their physical properties. *American Chemical Society, Division of Petroleum Chemistry, Preprints;(United States), 35*(CONF-900802-).

Büchner, J., Wistuba, M. P., Dasek, O., Staschkiewicz, M., Soenen, H., Zofka, A., & Remmler, T. (2020). Interlaboratory study on low temperature asphalt binder testing using Dynamic Shear Rheometer with 4 mm diameter parallel plate geometry. *Road Materials and Pavement Design*, 1-17.

Christensen, D., Mensching, D., Rowe, G., Anderson, R. M., Hanz, A., Reinke, G., & Anderson, D. (2019). Past, present, and future of asphalt binder rheological parameters: Synopsis of 2017 Technical Session 307 at the 96th Annual Meeting of the Transportation Research Board. *Transportation Research Circular*(E-C241).

Cong, P., Tian, Y., Liu, N., & Xu, P. (2016). Investigation of epoxy-resin-modified asphalt binder. *Journal of Applied Polymer Science, 133*(21).

Corbett, L. (1970). *Relationship between composition and physical properties of asphalt and discussion.* Paper presented at the Association of Asphalt Paving Technologists Proc.

D'Angelo, J., Baumgardner, G., Jordan, T., Daranga, C., & Hemsley, M. (2019). *Binder and Mix Performance Testing for Cracking: The Effects of Aging.* Paper presented at the Presentation, 56th Annual Petersen Asphalt Research Conference, Laramie, WY.

Dehouche, N., Kaci, M., Khadija, A., & Mokhtar. (2011). Influence of thermo-oxidative aging on chemical composition and physical properties of polymer modified bitumens. *Construction and Building Materials, 08*. doi:10.1016/j.conbuildmat.2011.06.033

Deme, I., Young FD. (1987). *Ste. Anne Test Road Revisited Twenty Years Later*: Polyscience Publications Inc.

Elkashef, M., Elwardany, M. D., Liang, Y., Jones, D., Harvey, J., Bolton, N. D., & Planche, J.-P. (2020). Effect of using rejuvenators on the chemical, thermal, and rheological properties of asphalt binders. *Energy & Fuels, 34*(2), 2152-2159.

Elkashef, M., Podolsky, J., Williams, R. C., & Cochran, E. W. (2018). Introducing a soybean oil-derived material as a potential rejuvenator of asphalt through rheology, mix characterisation and Fourier Transform Infrared analysis. *Road Materials and Pavement Design, 19*(8), 1750-1770. doi:10.1080/14680629.2017.1345781

Elkashef, M., & Williams, R. C. (2017). Improving fatigue and low temperature performance of 100% RAP mixtures using a soybean-derived rejuvenator. *Construction and Building Materials, 151*, 345-352.

Elwardany, M., King, G., Planche, J.-P., Rodezno, C., Christensen, D., Fertig Iii, R., . . . Bhuiyan, F. H. (2020). Internal Restraint Damage Mechanism for Age-Induced Pavement Surface Distresses: Block Cracking and Raveling. *Asphalt Paving Technology: Association of Asphalt Paving Technologists-Proceedings of the Technical Sessions, 88*.

Elwardany, M., Planche, J.-P., & King, G. (2020). Universal and practical approach to evaluate asphalt binder resistance to thermally-induced surface damage. *Construction and Building Materials, 255*, 119331. doi:https://doi.org/10.1016/j.conbuildmat.2020.119331

Farrar, M., Sui, C., Salmans, S., & Qin, Q. (2015). Determining the low-temperature rheological properties of asphalt binder using a dynamic shear rheometer (DSR). *Report 4FP, 8*, 20.

Federal Highway Administration (FHWA). United States Department of Transportation (2018). Table HM-12: Public Road Length 2017. Miles by type of surface and ownership/Functional System National Summary. In. Highway Statistics 2017: FHWA.

García Mainieri, J. J., Singhvi, P., Ozer, H., Sharma, B. K., & Al-Qadi, I. L. (2021). Fatigue tolerance of aged asphalt binders modified with softeners. *Transportation Research Record, 2675*(11), 1229-1244.

Glover, C., Davison, R., Ghoreishi, S., Jemison, H., & Bullin, J. (1989). Evaluation of Oven Simulation of Hot-Mix Aging by an FT-IR Pellet Procedure and Other Methods. *Transportation Research Record*(1228).

Habbouche, J., Boz, I., Hajj, E. Y., & Morian, N. E. (2021). Influence of aging on rheology-and chemistry-based properties of high polymer-modified asphalt binders. *International Journal of Pavement Engineering*, 1-19.

Habbouche, J., Hajj, E. Y., Sebaaly, P. E., & Piratheepan, M. (2020). A critical review of high polymer-modified asphalt binders and mixtures. *International Journal of Pavement Engineering, 21*(6), 686-702.

Hajj, R., & Bhasin, A. (2018). The search for a measure of fatigue cracking in asphalt binders–a review of different approaches. *International Journal of Pavement Engineering, 19*(3), 205-219.

Hajj, R., Filonzi, A., Rahman, S., & Bhasin, A. (2019). Considerations for using the 4 mm plate geometry in the dynamic shear rheometer for low temperature evaluation of asphalt binders. *Transportation Research Record, 2673*(11), 649-659.

Hao, G., Huang, W., Yuan, J., Tang, N., & Xiao, F. (2017). Effect of aging on chemical and rheological properties of SBS modified asphalt with different compositions. *Construction and Building Materials, 156*, 902-910.

Hasan, M. A., Hasan, M. M., Bairgi, B. K., Mannan, U. A., & Tarefder, R. A. (2019). Utilizing simplified viscoelastic continuum damage model to characterize the fatigue behavior of styrene-butadiene-styrene (SBS) modified binders. *Construction and Building Materials, 200*, 159-169.

Heitzman, M. A. (1992). *State of the practice: Design and construction of asphalt paving materials with crumb-rubber modifier. Final report*. Retrieved from United States: https://www.osti.gov/biblio/7280547

Hesp, S., Genin, S. N., Scafe, D., Shurvell, H., & Subramani, S. K. (2009). Five Year Performance Review of a Northern Ontario Pavement Trial: Validation of Ontario's Double-Edge-Notched Tension (DENT) and Extended Bending Beam Rheometer (BBR) Test Methods. *Proc., Canadian Technical Asphalt Association, 54*, 99-126.

Hintz, C., Velasquez, R., Johnson, C., & Bahia, H. (2011). Modification and Validation of Linear Amplitude Sweep Test for Binder Fatigue Specification. *Transportation Research Record, 2207*(1), 99-106. doi:10.3141/2207-13

Hofko, B., Porot, L., Cannone Falchetto, A., Poulikakos, L., Huber, L., Lu, X., . . . Grothe, H. (2018). FTIR spectral analysis of bituminous binders: reproducibility and impact of ageing temperature. *Materials and Structures, 51*. doi:10.1617/s11527-018-1170-7

Huynh, H. K., Khong, T. D., Malhotra, S. L., & Blanchard, L. P. (1978). Effect of molecular weight and composition on the glass transition temperatures of asphalts. *Analytical Chemistry, 50*(7), 976-979.

Inc, A. (2011). *Rheology Analysis (RHEA) Software User Manual*. Retrieved from Blooming Glen, PA:

Isacsson, U., & Zeng, H. (1997). Relationships between bitumen chemistry and low temperature behaviour of asphalt. *Construction and Building Materials, 11*(2), 83-91.

Kang, Y., Song, M., Pu, L., & Liu, T. (2015). Rheological behaviors of epoxy asphalt binder in comparison of base asphalt binder and SBS modified asphalt binder. *Construction and Building Materials, 76*, 343-350. doi:https://doi.org/10.1016/j.conbuildmat.2014.12.020

Kaseer, F., Martin, A. E., & Arámbula-Mercado, E. (2019). Use of recycling agents in asphalt mixtures with high recycled materials contents in the United States: A literature review. *Construction and Building Materials, 211*, 974-987. doi:https://doi.org/10.1016/j.conbuildmat.2019.03.286

Keyf, S. (2015). The modification of bitumen with reactive ethylene terpolymer, styrene butadiene styrene and variable amounts of ethylene vinyl acetate. *Research on Chemical Intermediates, 41*(3), 1485-1497. doi:10.1007/s11164-013-1287-9

Keyf, S., Ismail, O., Corbacıoglu, B. D., & Ozen, H. (2007). The Modification of Bitumen with Synthetic Reactive Ethylene Terpolymer and Ethylene Terpolymer. *Petroleum Science and Technology, 25*(5), 561-568. doi:10.1080/10916460500294259

Kim, K. W., & Burati Jr, J. L. (1993). Use of GPC chromatograms to characterize aged asphalt cements. *Journal of Materials in Civil Engineering, 5*(1), 41-52.

Kim, Y., Lee, H., & Little, D. (2006). *A Simple Testing Method to Evaluate Fatigue Fracture and Damage Performance of Asphalt Mixtures (With Discussion)*.

King, G., Anderson, R. M., Hanson, D., & Blankenship, P. (2012). Using Black Space Diagrams to Predict Age-Induced Cracking. *7th Rilem International Conference on Cracking in Pavements, Delft, Netherlands, 4*, 453-463. doi:10.1007/978-94-007-4566-7_44

Kluttz, R. (2019). Prepared discussion on relationships between mixture fatigue performance and asphalt binder properties. *Asphalt Paving Technology: Journal of the Association of Asphalt Paving Technologists, 88*, 465-468.

Knotnerus, J. (1972). Bitumen durability-measurement by oxygen absorption. *Industrial & Engineering Chemistry Product Research and Development, 11*(4), 411-422.

Lee, S.-J., Akisetty, C. K., & Amirkhanian, S. N. (2008). The effect of crumb rubber modifier (CRM) on the performance properties of rubberized binders in HMA pavements. *Construction and Building Materials, 22*(7), 1368-1376. doi:https://doi.org/10.1016/j.conbuildmat.2007.04.010

Lesueur, D. (2009). The colloidal structure of bitumen: Consequences on the rheology and on the mechanisms of bitumen modification. *Advances in Colloid and Interface Science, 145*(1), 42-82. doi:https://doi.org/10.1016/j.cis.2008.08.011

Lu, X., & Isacsson, U. (2002). Effect of ageing on bitumen chemistry and rheology. *Construction and Building Materials, 16*(1), 15-22. doi:https://doi.org/10.1016/S0950-0618(01)00033-2

Lu, X., Uhlback, P., & Soenen, H. (2017). Investigation of bitumen low temperature properties using a dynamic shear rheometer with 4 mm parallel plates. *International Journal of Pavement Research and Technology, 10*(1), 15-22.

Marsac, P., Piérard, N., Porot, L., Van den bergh, W., Grenfell, J., Mouillet, V., . . . Hugener, M. (2014). Potential and limits of FTIR methods for reclaimed asphalt characterisation. *Materials and Structures, 47*(8), 1273-1286. doi:10.1617/s11527-014-0248-0

Materials, American Society of Testing and (2017). ASTM D3279: Standard Test Method for n-Heptane Insolubles (Designation IP 143). In. Washington, D.C.

Materials, American Society of Testing and (2018). ASTM D6560 - 17: Standard Test Method for Determination of Asphaltenes (Heptane Insolubles) in Crude Petroleum and Petroleum Products (Designation IP 143). In. Washington, D.C.

Materials, American Society of Testing and (2021). ASTM D8: Standard Terminology Relating to Materials for Roads and Pavements In. PA, United States: ASTM.

Memon, G. M., & Chollar, B. H. (1997). Glass transition measurements of asphalts by DSC. *Journal of thermal analysis, 49*(2), 601-607. doi:10.1007/BF01996742

Mensching, D. J., Rowe, G. M., Daniel, J. S., & Bennert, T. (2015). Exploring low-temperature performance in Black Space. *Road Materials and Pavement Design, 16*(sup2), 230-253. doi:10.1080/14680629.2015.1077015

Miró, R., Martínez, A. H., Moreno-Navarro, F., & del Carmen Rubio-Gámez, M. (2015). Effect of ageing and temperature on the fatigue behaviour of bitumens. *Materials & Design, 86*, 129-137.

Mirwald, J., Werkovits, S., Camargo, I., Maschauer, D., Hofko, B., & Grothe, H. (2020). Understanding bitumen ageing by investigation of its polarity fractions. *Construction and Building Materials, 250*, 118809. doi:https://doi.org/10.1016/j.conbuildmat.2020.118809

Mohammadafzali, M., Ali, H., Musselman, J. A., Sholar, G. A., Kim, S., & Nash, T. (2015). Long-Term Aging of Recycled Asphalt Binders: A Laboratory Evaluation Based on Performance Grade Tests. In *Airfield and Highway Pavements 2015* (pp. 617-627).

Moraes, R., & Bahia, H. U. (2015). Effect of mineral filler on changes in molecular size distribution of asphalts during oxidative ageing. *Road Materials and Pavement Design, 16*(sup2), 55-72.

Moraes, R., & Bahia, H. U. (2018). Developing Simple Binder Indices for Cracking Resistance of Asphalt Binders at Intermediate and Low Temperatures. *Transportation Research Record, 2672*(28), 311-323. doi:10.1177/0361198118792999

Morian, N., Zhu, C., & Hajj, E. Y. (2015). Rheological indexes: Phenomenological aspects of asphalt binder aging evaluations. *Transportation Research Record, 2505*(1), 32-40.

Navarro, F. J., Partal, P., Martínez-Boza, F., Valencia, C., & Gallegos, C. (2002). Rheological characteristics of ground tire rubber-modified bitumens. *Chemical Engineering Journal, 89*(1), 53-61. doi:https://doi.org/10.1016/S1385-8947(02)00023-2

Noureldin, A. S., & Wood, L. E. (1989). Variations in molecular size distribution of virgin and recycled asphalt binders associated with aging. *Transportation Research Record*(1228).

Officials, A. A. o. S. H. a. T. (2016). Standard Method of Test for Determining the Flexural Creep Stiffness of Asphalt Binder Using the Bending Beam Rheometer (BBR). In. Washington, D.C.: AASHTO.

Officials, A. A. o. S. H. a. T. (2020). Determination of Performance Grade of Physically Aged Asphalt Binder Using Extended Bending Beam Rheometer (BBR) Method. In. Washington, D.C: AASHTO.

Officials, A. A. o. S. H. a. T. (2021a). Standard Method of Test for Effect of Air on a Moving Film of Asphalt Binder (Rolling Thin-Film Oven Test): AASHTO T240. In. Washington, D.C AASHTO.

Officials, A. A. o. S. H. a. T. (2021b). Standard Practice for Accelerated Aging of Asphalt Binder Using a Pressurized Aging Vessel (PAV): AASHTO R28. In. Washington, D.C.

Ongel, A., & Hugener, M. (2015). Impact of rejuvenators on aging properties of bitumen. *Construction and Building Materials, 94*, 467-474. doi:https://doi.org/10.1016/j.conbuildmat.2015.07.030

Osmari, P. H., Leite, L. F. M., Aragão, F. T. S., Cravo, M. C. C., Dantas, L. N., & Macedo, T. F. (2019). Cracking resistance evaluation of asphalt binders subjected to different laboratory and field aging conditions. *Road Materials and Pavement Design, 20*(sup2), S663-S677. doi:10.1080/14680629.2019.1618530

Petersen, J. C. (2009). A Review of the Fundamentals of Asphalt Oxidation. Transportation Research Circular E-C140. *Transportation Research Record*.

Petersen, J. C., & Glaser, R. (2011). Asphalt oxidation mechanisms and the role of oxidation products on age hardening revisited. *Road Materials and Pavement Design, 12*(4), 795-819.

Petersen, J. C., Robertson, R.E, Branthaver, J.F., Harnsberger, P.M, Duvall, J.J., Kim, S.S., Anderson, D.A, Christiansen, D.W., Bahia, U.H. . (1994). *SHRP - A-367 Report: Binder Characterization and Evaluation. Volume I*. Retrieved from Washington D.C:

Petersen, J. C., & Strategic Highway Research, P. (1994). *Binder characterization and evaluation. Volume 4, Test methods*. Washington, D.C.: Strategic Highway Research Program, National Research Council.

Pfeiffer, J. P., & Saal, R. (1940). Asphaltic bitumen as colloid system. *The Journal of Physical Chemistry, 44*(2), 139-149.

Qin, Q., Schabron, J. F., Boysen, R. B., & Farrar, M. J. (2014). Field aging effect on chemistry and rheology of asphalt binders and rheological predictions for field aging. *Fuel, 121*, 86-94.

Rad, F. Y., Elwardany, M. D., Castorena, C., & Kim, Y. R. (2018). Evaluation of Chemical and Rheological Aging Indices to Track Oxidative Aging of Asphalt Mixtures. *Transportation Research Record, 2672*(28), 349-358. doi:10.1177/0361198118784138

Ren, R., Han, K., Zhao, P., Shi, J., Zhao, L., Gao, D., . . . Yang, Z. (2019). Identification of asphalt fingerprints based on ATR-FTIR spectroscopy and principal component-linear discriminant analysis. *Construction and Building Materials, 198*, 662-668.

Rios Carreno, L. C. (2021). Effect of Blending Conditions on the Rheological Properties of Asphalt modified by Reactive Ethylene Terpolymer and Polyphosphoric Acid. In.

Rowe, G., King, G., & Anderson, M. (2014). The Influence of Binder Rheology on the Cracking of Asphalt Mixes in Airport and Highway Projects. *Journal of Testing and Evaluation, 42*, 20130245. doi:10.1520/JTE20130245

Rowe, G. M., & Sharrock, M. J. (2016). *Cracking of asphalt pavements and the development of specifications with rheological measurements.* Paper presented at the 6th Eurasphalt & Eurobitume Congress, Prague, Czech Republic.

Ruan, Y., Davison, R., & Glover, C. (2003a). An investigation of asphalt durability: Relationships between ductility and rheological properties for unmodified asphalts. *Petroleum Science and Technology, 21*(1-2), 231-254.

Ruan, Y., Davison, R. R., & Glover, C. J. (2003b). The effect of long-term oxidation on the rheological properties of polymer modified asphalts☆. *Fuel, 82*(14), 1763-1773. doi:https://doi.org/10.1016/S0016-2361(03)00144-3

Safaei, F., & Castorena, C. (2016). Temperature effects of linear amplitude sweep testing and analysis. *Transportation Research Record, 2574*(1), 92-100.

Salim, R., Gundla, A., Underwood, B. S., & Kaloush, K. E. (2019). Effect of MSCR Percent Recovery on Performance of Polymer Modified Asphalt Mixtures. *Transportation Research Record, 2673*(5), 308-319. doi:10.1177/0361198119841283

Santos, F. B., Faxina, A. L., & Soares, S. d. A. (2021). Soy-based rejuvenated asphalt binders: Impact on rheological properties and chemical aging indices. *Construction and Building Materials, 300*, 124220. doi:https://doi.org/10.1016/j.conbuildmat.2021.124220

Sui, C., Farrar, M. J., Harnsberger, P. M., Tuminello, W. H., & Turner, T. F. (2011). New low-temperature performance-grading method: Using 4-mm parallel plates on a dynamic shear rheometer. *Transportation Research Record, 2207*(1), 43-48.

Tabatabaee, H. A. (2012). *Critical Behavior of Asphalt Mixtures Undergoing Glass Transition and Physical Hardening.* (Ph.D.). The University of Wisconsin - Madison, Ann Arbor. Retrieved from ProQuest Dissertations & Theses Global database. (3525987)

Tabatabaee, H. A., & Kurth, T. L. (2017). Analytical investigation of the impact of a novel bio-based recycling agent on the colloidal stability of aged bitumen. *Road Materials and Pavement Design, 18*(sup2), 131-140. doi:10.1080/14680629.2017.1304257

Tabatabaee, H. A., Velasquez, R., & Bahia, H. U. (2012). Predicting low temperature physical hardening in asphalt binders. *Construction and Building Materials, 34*, 162-169.

Tauste, R., Moreno-Navarro, F., Sol-Sánchez, M., & Rubio-Gámez, M. (2018). Understanding the bitumen ageing phenomenon: A review. *Construction and Building Materials, 192*, 593-609.

Technical Advisory Committee, A. I. (2019). *IS-240: Use of the DeltaTc Parameter to Characterize Asphalt Binder Behavior*. Retrieved from

Transportation, Ontario Ministry of. (2011). Test Method LS-308: METHOD OF TEST FOR DETERMINATION OF PERFORMANCE GRADE OF PHYSICALLY AGED ASPHALT CEMENT USING EXTENDED BENDING BEAM RHEOMETER (BBR) METHOD In. Ontario, Canada: Ontario Ministry of Transportation.

Vahidi, S., Mogawer, W. S., & Booshehrian, A. (2014). Effects of GTR and treated GTR on asphalt binder and high-RAP mixtures. *Journal of Materials in Civil Engineering, 26*(4), 721-727.

Wahhab, H. A.-A., Asi, I., Ali, F., & Al-Dubabi, I. (1999). Prediction of asphalt rheological properties using HP-GPC. *Journal of Materials in Civil Engineering, 11*(1), 6-14.

Wang, C., Castorena, C., Zhang, J., & Richard Kim, Y. (2015). Unified failure criterion for asphalt binder under cyclic fatigue loading. *Road Materials and Pavement Design, 16*(sup2), 125-148.

Wang, H., Liu, X., Apostolidis, P., van de Ven, M., Erkens, S., & Skarpas, A. (2020). Effect of laboratory aging on chemistry and rheology of crumb rubber modified bitumen. *Materials and Structures, 53*(2), 26. doi:10.1617/s11527-020-1451-9

Weigel, S., & Stephan, D. (2017). Modelling of rheological and ageing properties of bitumen based on its chemical structure. *Materials and Structures, 50*(1), 1-15.

Wu, S.-p., Pang, L., Mo, L.-t., Chen, Y.-c., & Zhu, G.-j. (2009). Influence of aging on the evolution of structure, morphology and rheology of base and SBS modified bitumen. *Construction and Building Materials, 23*(2), 1005-1010.

Xiao, F., Amirkhanian, S., & Shen, J. (2009). Effects of Various Long-Term Aging Procedures on the Rheological Properties of Laboratory Prepared Rubberized Asphalt Binders. *Journal of Testing and Evaluation - J TEST EVAL, 37*. doi:10.1520/JTE101706

Yin, F., Kaseer, F., Arámbula-Mercado, E., & Epps Martin, A. (2017). Characterising the long-term rejuvenating effectiveness of recycling agents on asphalt blends and mixtures with high RAP and RAS contents. *Road Materials and Pavement Design, 18*(sup4), 273-292. doi:10.1080/14680629.2017.1389074

Youtcheff, J., Gibson, N., Shenoy, A., & Al-Khateeb, G. (2006). *The evaluation of epoxy asphalt and epoxy asphalt mixtures.* Paper presented at the 51st Annual Conference of the Canadian Technical Asphalt Association (CTAA).

Yu, J., Cong, P., & Wu, S. (2009). Laboratory investigation of the properties of asphalt modified with epoxy resin. *Journal of Applied Polymer Science, 113*(6), 3557-3563. doi:https://doi.org/10.1002/app.30324

Yu, X., Zaumanis, M., Dos Santos, S., & Poulikakos, L. D. (2014). Rheological, microscopic, and chemical characterization of the rejuvenating effect on asphalt binders. *Fuel*, *135*, 162-171.

Zhang, H., Xu, G., Chen, X., Wang, R., & Shen, K. (2019). Effect of long-term laboratory aging on rheological properties and cracking resistance of polymer-modified asphalt binders at intermediate and low temperature range. *Construction and Building Materials*, *226*, 767-777.

Zhang, R., Sias, J. E., & Dave, E. V. (2020). Development of new performance indices to evaluate the fatigue properties of asphalt binders with ageing. *Road Materials and Pavement Design*, 1-20.

Zhao, Y., Gu, F., Xu, J., & Jin, J. (2010). Analysis of aging mechanism of SBS polymer modified asphalt based on Fourier transform infrared spectrum. *Journal of Wuhan University of Technology-Mater. Sci. Ed.*, *25*(6), 1047-1052.

Zhou, Z., Gu, X., Dong, Q., Ni, F., & Jiang, Y. (2020). Investigation of the oxidation ageing of RAP asphalt blend binders and mixtures. *International Journal of Pavement Engineering*, 1-17. doi:10.1080/10298436.2020.1763345

Zhu, C. (2015). *Evaluation of Thermal Oxidative Aging Effect on the Rheological Performance of Modified Asphalt Binders.*

APPENDIX 1 - BASE BINDER, RECYCLED BINDER BLENDS AND MODIFIED BINDER MASTER CURVES

Complex modulus and phase angle master curves for neat and modified binders were built at a reference temperature of 15℃. Two aging conditions were evaluated: unaged and RTFO followed by 60 hours of PAV aging, and the effects of modification and aging on binder rheology were observed. Master curve parameters were used to study the aging susceptibility of binders in terms of the Glover-Rowe parameter as detailed in section 4.2.4. This section presents the complete set of master curves and describes the effects of each modifier on the control binders before and after aging.

A. Additive 1

Complex modulus master curves for Additive 1 are shown in Figure 1 through Figure 4, before and after aging. The effects of aging are typically observed on G^* master curves as flattening accompanied by an upward shift, which can be observed for all binders. However, modification with Additive 1 results on less stiffening on Binder 1, shown by the lower complex modulus over the entire frequency range, particularly at high temperatures (or low frequencies). Thus, master curves support improvements in rheological properties of Binder 1 after aging. Modification of Binder 5 resulted in opposite behavior, as stiffer binders at the unaged condition shown by the higher G^* resulted on stiffer binders after aging as well, as master curves from Additive 1 plot above that of the control.

Phase angle master curves at both aging conditions are presented in Figure 5 through Figure 8. A plateau at intermediate temperatures was observed, more pronounced for Binder 5, indicating the effects of polymer modification. This finding is consistent with the nature of Additive 1 which contains thermosetting polymers within its formulation (Cong, Tian, Liu, & Xu, 2016). Improvements in the viscous nature of Binder 1 are observed, shown by the higher phase angles, even after extended aging cycles. Binder 5, on the other hand presents a more elastic behavior at the unaged condition. After aging the presence of the plateau remains, and modified binders present a more brittle behavior than the control, shown by the combination of lower phase angles and higher stiffnesses.

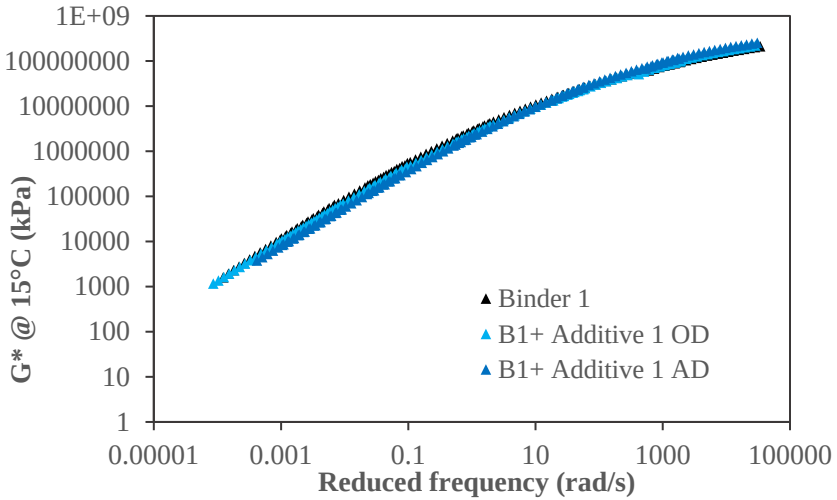

Figure 189. Complex modulus master curves for Additive 1 – Binder 1 Unaged

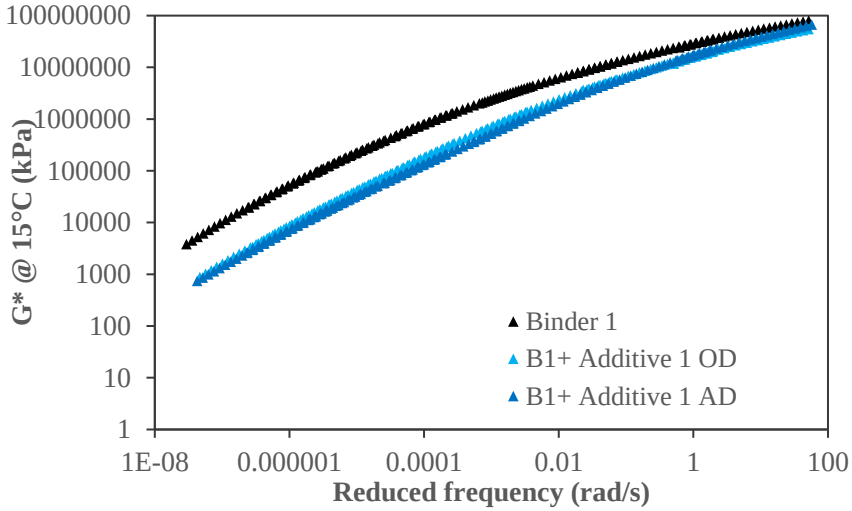

Figure 190. Complex modulus master curves for Additive 1 – Binder 1 RTFO + 60hr PAV

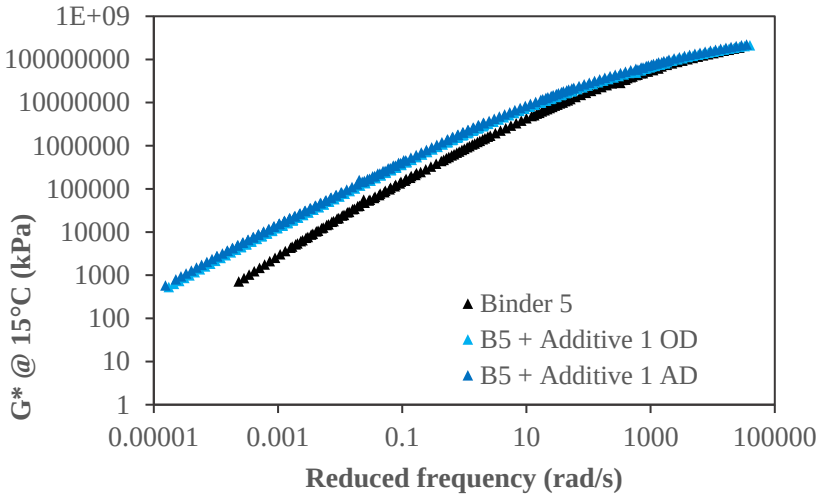

Figure 191. Complex modulus master curves for Additive 1 – Binder 5 Unaged

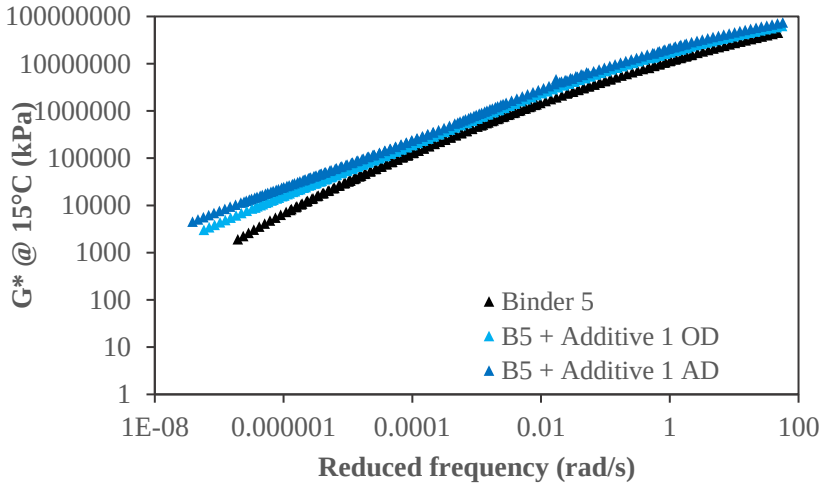

Figure 192. Complex modulus master curves for Additive 1 – Binder 5 RTFO + 60hr PAV

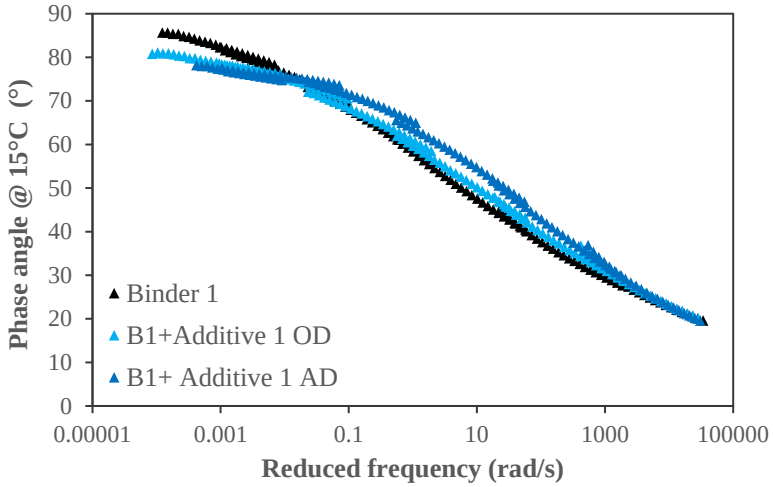

Figure 193. Phase angle master curves for Additive 1 – Binder 1 Unaged

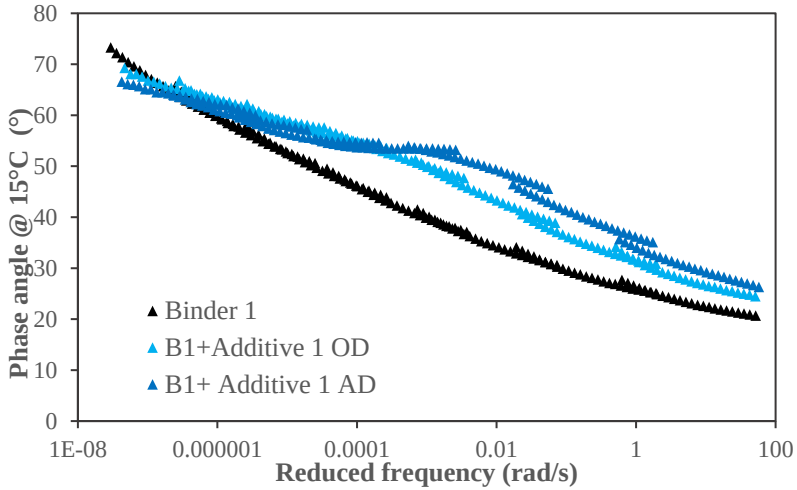

Figure 194. Phase angle master curves for Additive 1 – Binder 1 RTFO + 60hr PAV

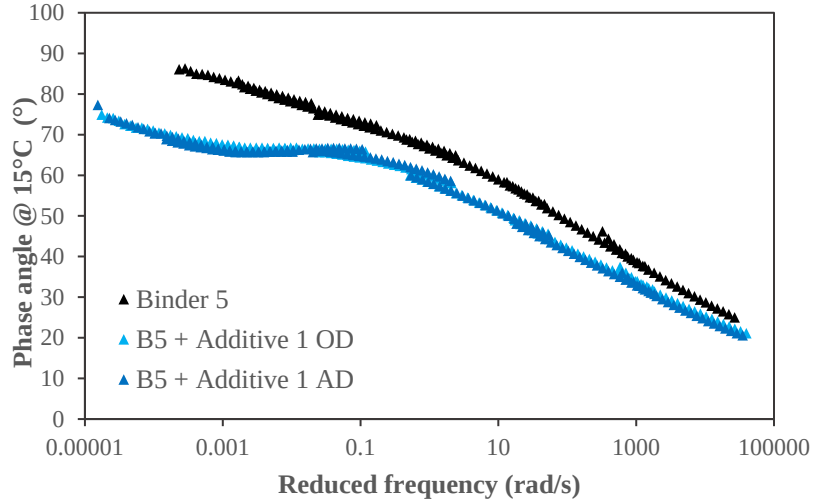

Figure 195. Phase angle master curves for Additive 1 – Binder 5 Unaged

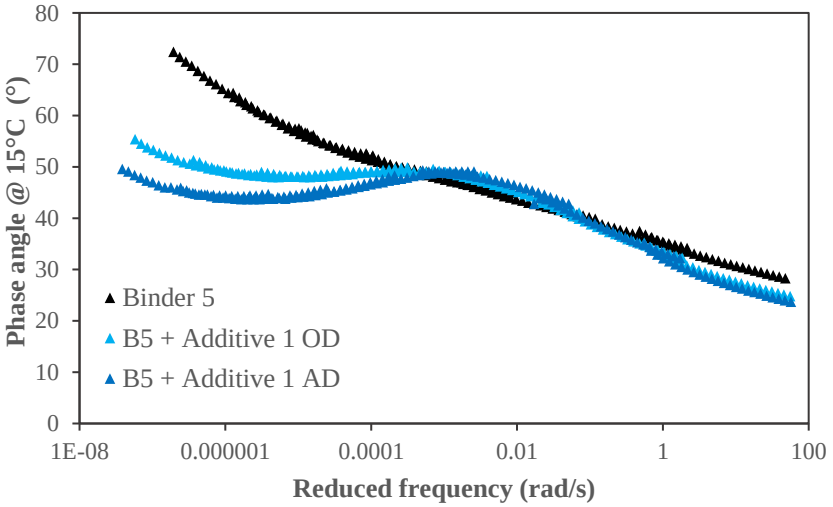

Figure 196. Phase angle master curves for Additive 1 – Binder 5 RTFO + 60 hr PAV

B. Additive 2

Figure 9 through Figure 12 present the complex modulus master curves of unmodified and modified binders with Additive 2. The effects of crumb rubber modification are reflected on the higher G^* values, particularly at high and intermediate temperatures. However, the stiffening caused at the unaged condition does not necessarily result on stiffer binders after aging. Figure 10 shows Additive 2 results on softer binders than Binder 1 after 60 hours of PAV aging, suggesting enhanced aging resistance. The effects on Binder 5 are not as pronounced, as master curves in Figure 12 mostly overlap, thus additive effectiveness at reducing binder stiffness may be lower.

Phase angle master curves in Figure 13 and Figure 15 show the effect of polymer modification on both base binders, given by the intermediate temperature plateau in the master curve. After aging, flatter master curves are observed for both neat and modified binders, as shown in Figure 14 and Figure 16. The plateau region is not as easily identified on aged samples, mostly for Binder 1, which may be indicating some sign of polymer degradation. As a result, Binder 1 exhibits higher phase angles, than the control, indicating better viscous flow properties after aging. Binder 5, however, presents lower phase angles than the control over the entire frequency range, indicative of a more elastic, solid-like binder.

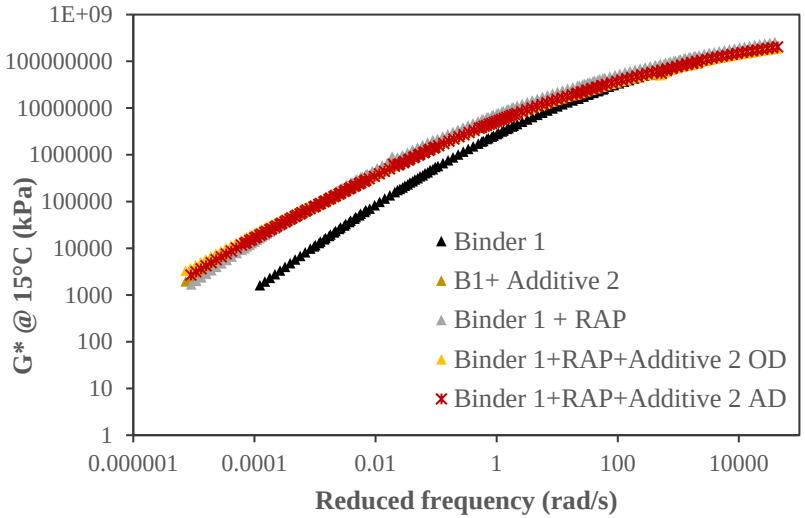

Figure 197. Complex modulus master curves for Additive 2 – Binder 1 Unaged

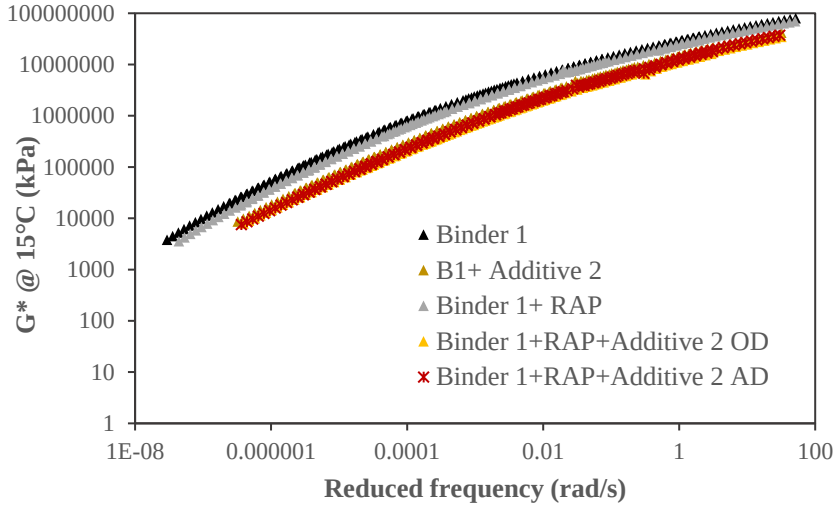

Figure 198. Complex modulus master curves for Additive 2 – Binder 1 RTFO + 60hr PAV

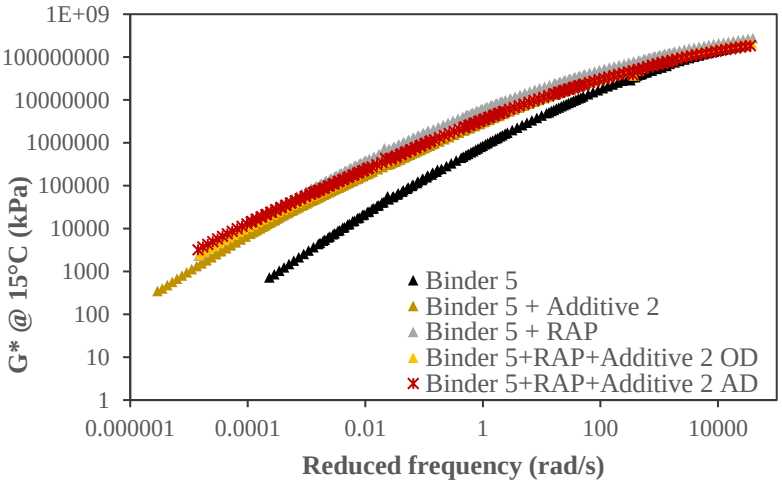

Figure 199. Complex modulus master curves for Additive 2 – Binder 5 Unaged

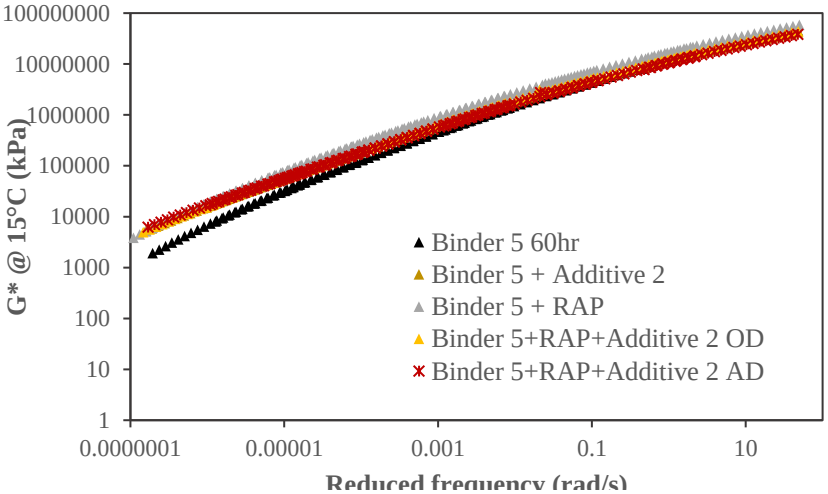

Figure 200. Complex modulus master curves for Additive 2 – Binder 5 RTFO + 60 hr PAV

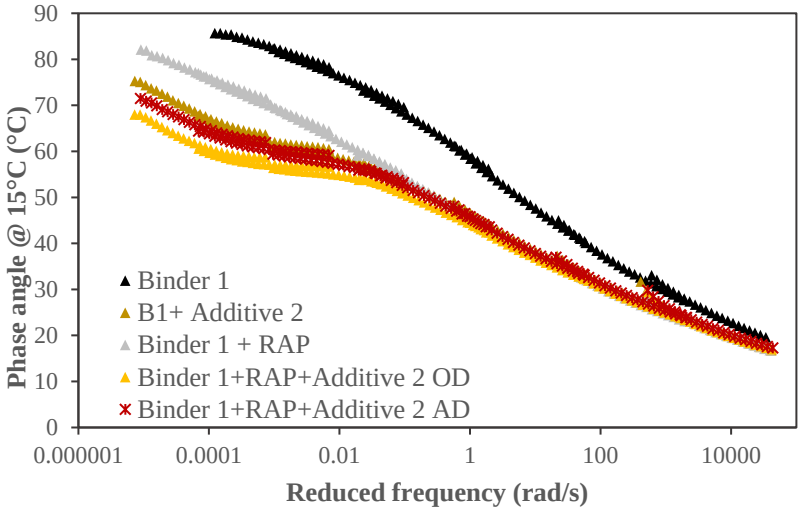

Figure 204. Phase angle master curves for Additive 2 – Binder 1 Unaged

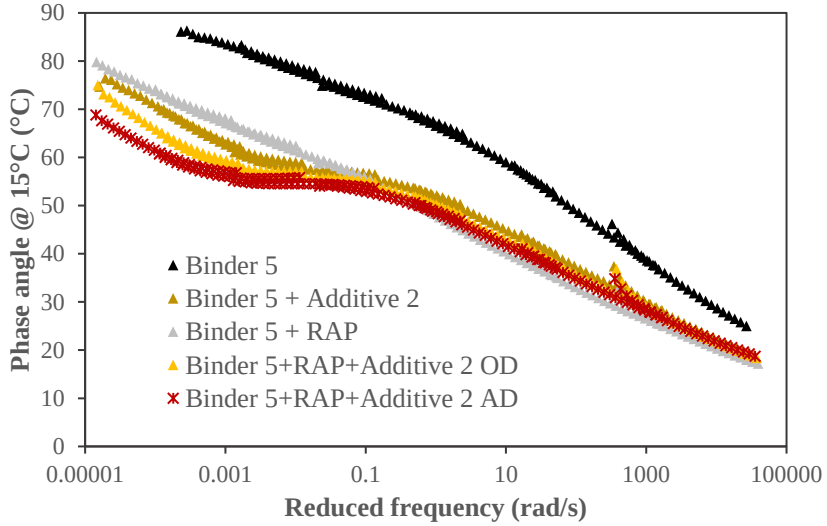

Figure 201. Phase angle master curves for Additive 2 – Binder 5 Unaged

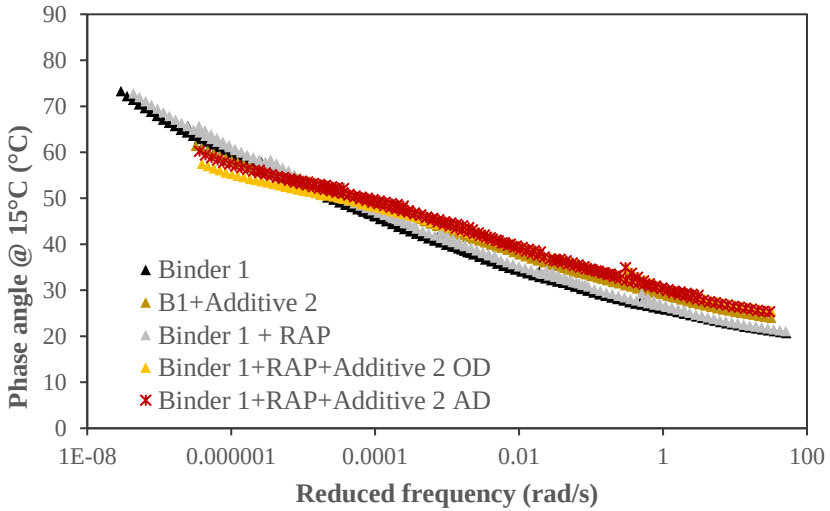

Figure 202. Phase angle master curves for Additive 2 – Binder 1 RTFO + 60hr PAV

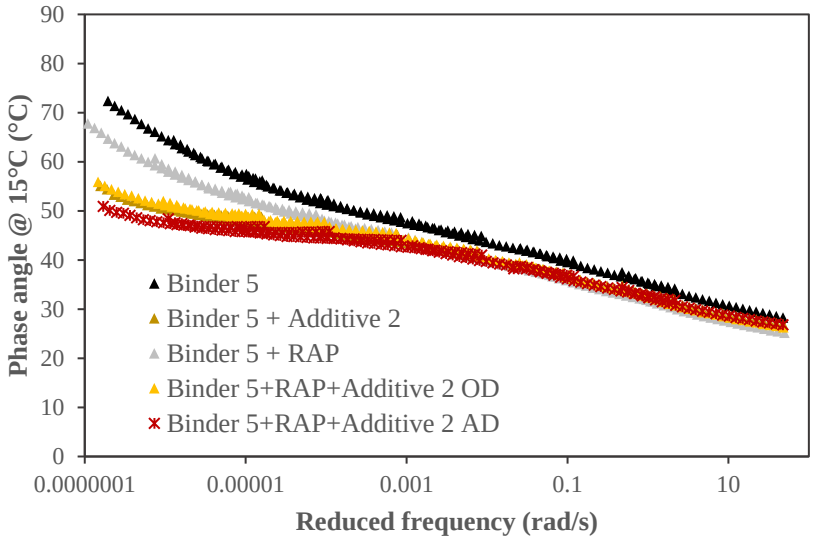

Figure 203. Phase angle master curves for Additive 2 – Binder 5 RTFO + 60hr PAV

C. Additive 3

Figure 17 through Figure 20 present complex modulus master curves for modified binders with Additive 3. Modification caused a shift to lower stiffnesses at higher frequencies (i.e lower temperatures) for both base binders, which may suggest improved resistance to thermal stresses. This observed behavior on master curves would agree with improvements on low PG grade of modified binders found within the rheological evaluation. The reduction in stiffness occurs over a wider frequency range for Binder 5, with RAP blends presenting shifts across the entire measured range and the neat binder displaying slightly stiffer behavior only at the lowest frequencies (i.e higher temperatures). Binder 1, however, showed lower stiffness at the low to intermediate temperature range, and the intersection of the master curves indicate a shift to higher complex modulus as frequency becomes progressively lower. RAP blends with Binder 1 show similar behavior but the intersection of the curves appears to occur at slightly higher temperatures. Additive 3 resulted on a higher PG grade at high temperatures, but complex modulus master curves show lower values across most of the frequency range, which would suggest a softer binder. Therefore, the increase in high PG grade, which indicates improved rutting resistance, is likely driven by reductions in phase angle, as will be observed from Figures 21 through 24.

After aging, G^* master curves in Figure 18 and Figure 20 resulted below the control binders (neat and RAP blends) across most frequencies. Thus, it may be argued that this modifier reduced the stiffening effects of aging of the control binders and therefore improved their aging susceptibility. However, the effects of modification appear more pronounced with Binder 1, where lower stiffnesses are observed until an apparent overlap at the lowest frequencies. This more pronounced shift may be indicative of greater additive effectiveness upon interactions with this binder, which is consistent with other rheological findings.

Phase angle master curves for Additive 3 are shown in Figure 21 through Figure 24. A plateau at intermediate temperatures can be observed, which is indicative of polymer modification. Additionally, there is a reduction in phase angle at lower frequencies (i.e warmer temperatures), which has also been found for these materials (Asgharzadeh et al., 2015). These lower phase angles at higher temperatures reduce the viscous nature of the base binder and provide improvements in rutting resistance (seen for this Additives on the significant reductions in J_{nr}, for example). Additionally, lower stiffnesses at intermediate temperatures accompanied by lower phase angles would indicate improvements in cracking performance of modified binders. The intersecting master curves for both binders show a more viscous behavior at lower temperatures, while increased elastic behavior at high and intermediate temperatures. Therefore, Additive 3 provided enhanced relaxation at low temperatures while improving rutting resistance at high temperatures of neat binders and RAP blends.

After aging, the peak in phase angle slightly flattens, possibly suggesting some polymer degradation with PAV aging. Nevertheless, higher phase angles than the control are still observed at low temperatures, thus showing better relaxation properties, possibly indicating increased durability. Although lower phase angles than the control are observed after aging (at low frequencies), this occurs as a result of modification, as the unaged master curves show as well. Thus, lower phase angles typically resulting from a loss in ductility due to aging may appear misleading in this case. Instead, these results should be paired with the G^* values where lower stiffening may be observed, favoring binder aged properties.

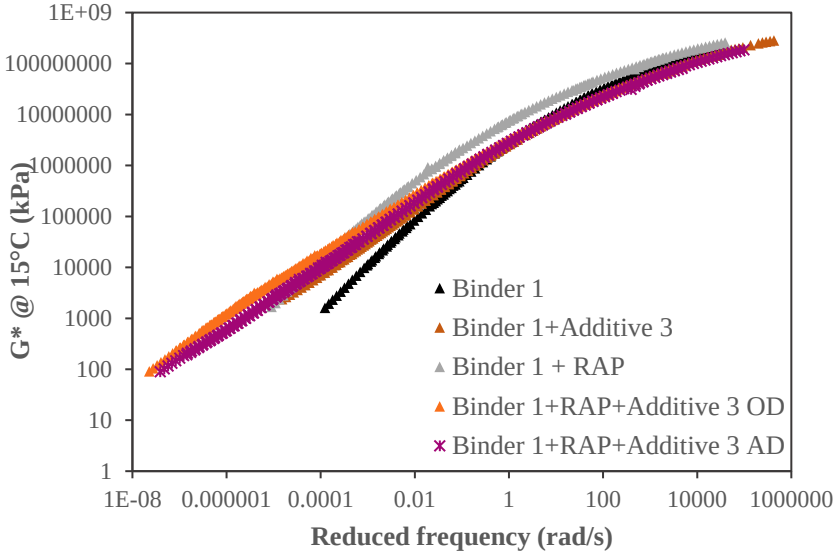

Figure 207. Complex modulus master curves for Additive 3 – Binder 1 Unaged

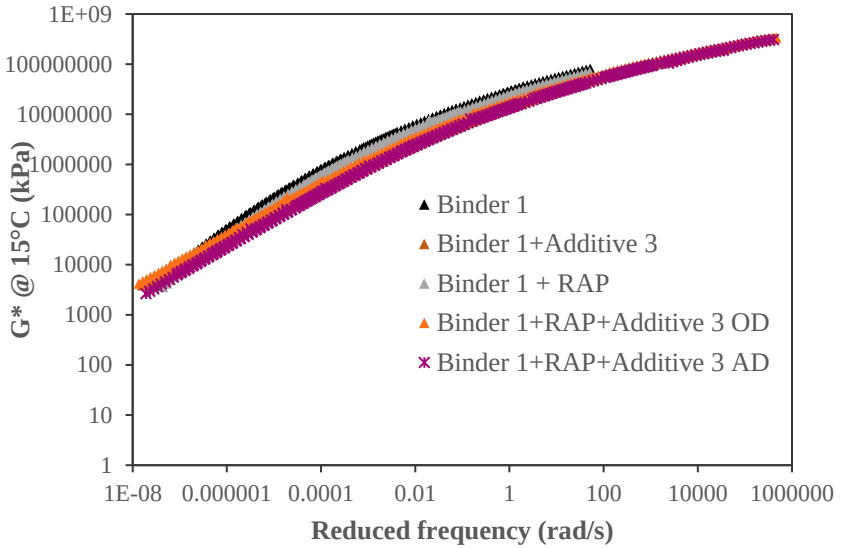

Figure 206. Complex modulus master curves for Additive 3 – Binder 1 RTFO + 60hr PAV

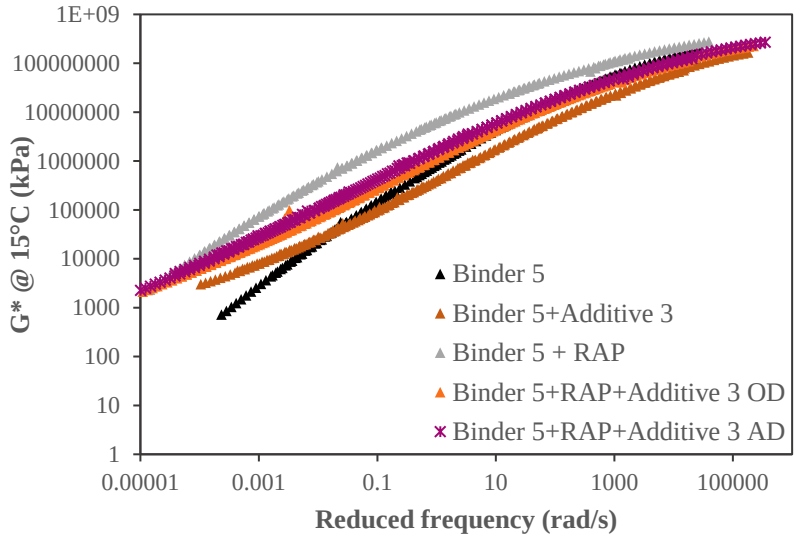

Figure 208. Complex modulus master curves for Additive 3 – Binder 5 Unaged

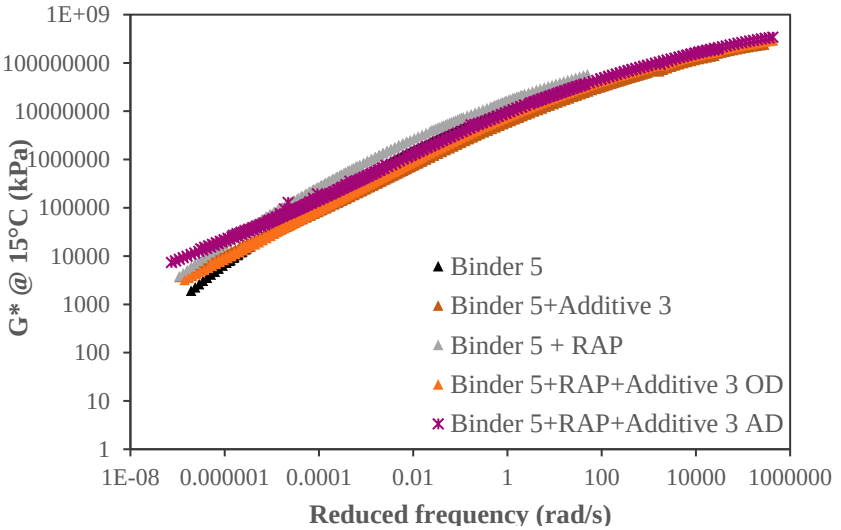

Figure 205. Complex modulus master curves for Additive 3 – Binder 5 RTFO + 60hr PAV

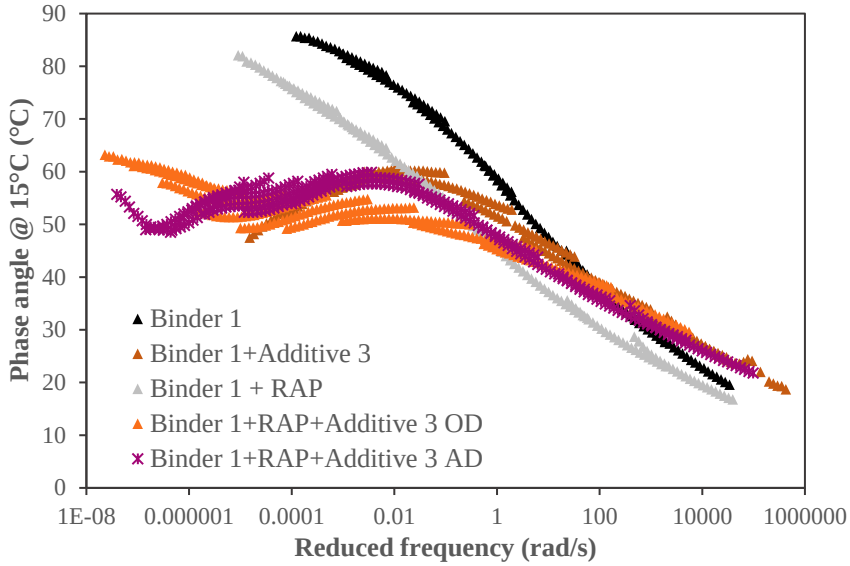

Figure 212. Phase angle master curves for Additive 3 – Binder 1 Unaged

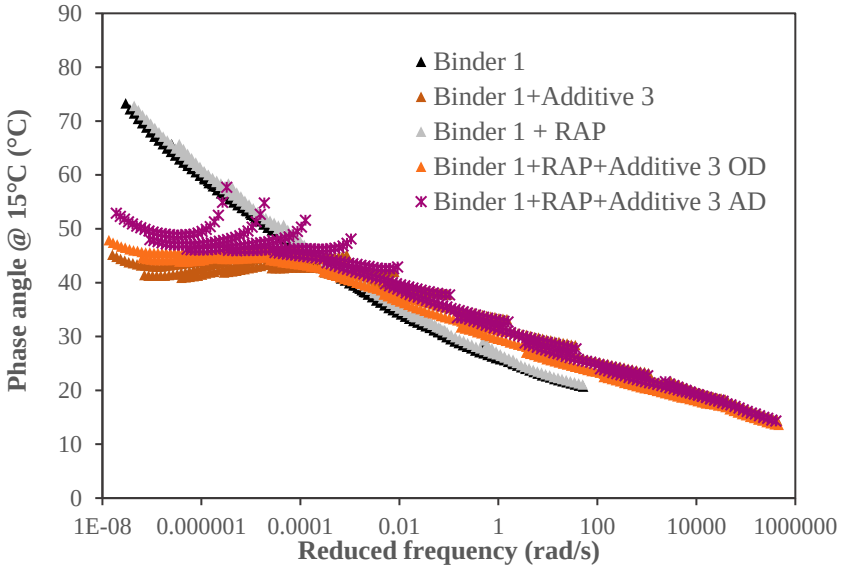

Figure 211. Phase angle master curves for Additive 3 – Binder 1 RTFO + 60hr PAV

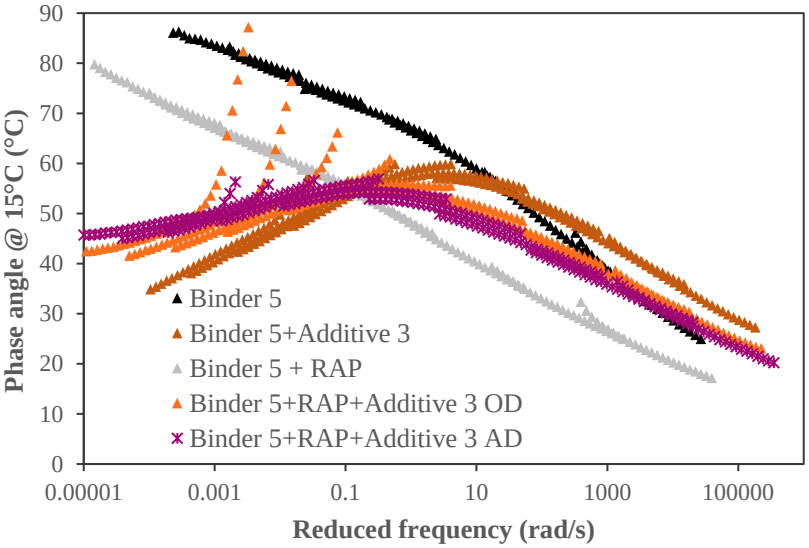

Figure 210. Phase angle master curves for Additive 3 – Binder 5 Unaged

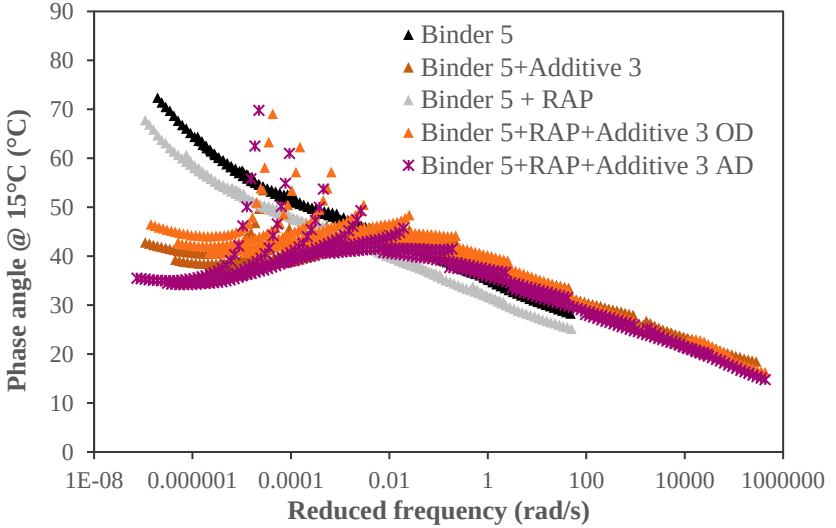

Figure 209. Phase angle master curves for Additive 3 – Binder 5 RTFO + 60hr PAV

D. Additive 4

The effects of Additive 4 on complex modulus of Binders 1 and 5 are presented in Figure 25 through Figure 28, before and after aging. The softening effects of this additive are shown for both base binders by the downward shift of the master curve to lower values of G^*. Although modification results on lower stiffnesses across the entire range of frequencies, they tend to converge at lower temperatures, as expected for most binders (Elkashef & Williams, 2017). Additionally, modified binders present less hardening after aging, as their G^* master curves remain below those of the control binders, both neat and RAP blends.

Additionally, Additive 4 increases the viscous nature of both base binders, as their phase angle master curves are all shifted upwards to higher phase angles, which can be seen in Figure 29 and Figure 31. It should be noted that the shift occurs almost in a parallel manner, therefore the effects of modification impact binder properties across high, intermediate, and low temperatures. Furthermore, Figure 30 and Figure 32 show modified binders have higher phase angles than the control after 60 hours of PAV aging, which suggests enhanced aging resistance of the base binders. The shift towards higher phase angles after aging indicates improvements in relaxation properties at low temperatures and improved cracking resistance at intermediate temperatures. Nevertheless, softening effects may raise concerns regarding high temperature performance at the unaged condition.

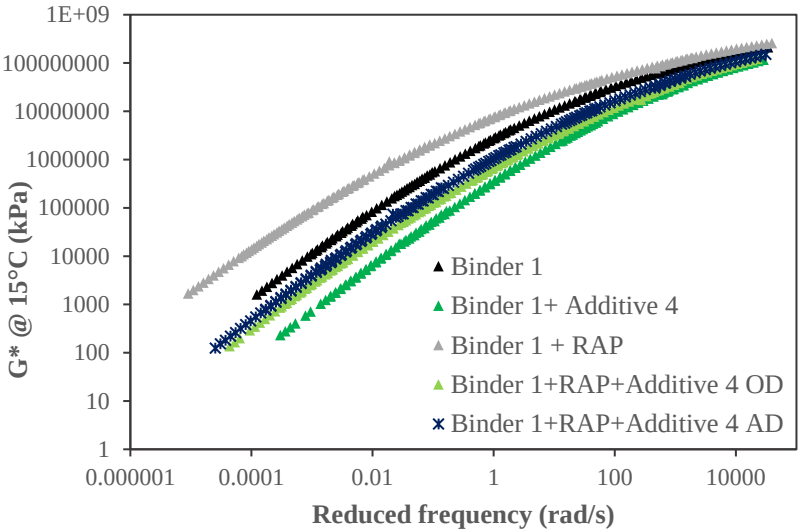

Figure 213. Complex modulus master curves for Additive 4 – Binder 1 Unaged

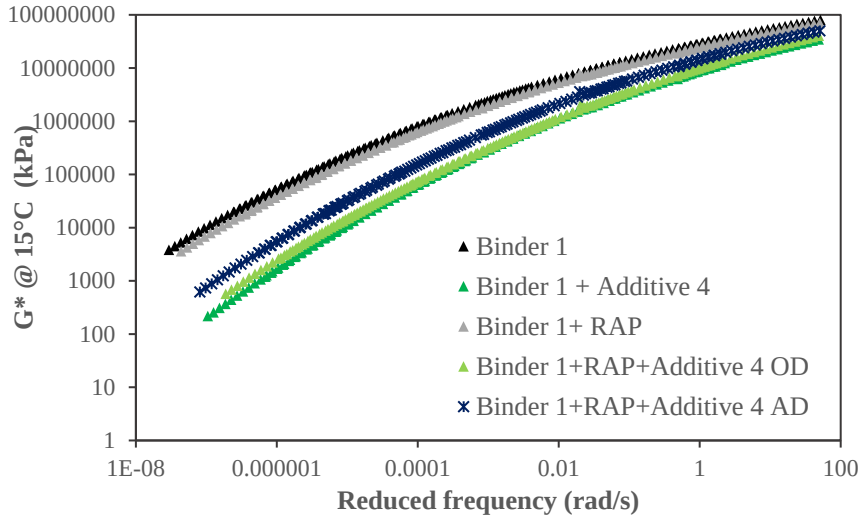

Figure 214. Complex modulus master curves for Additive 4 – Binder 1 RTFO + 60hr PAV

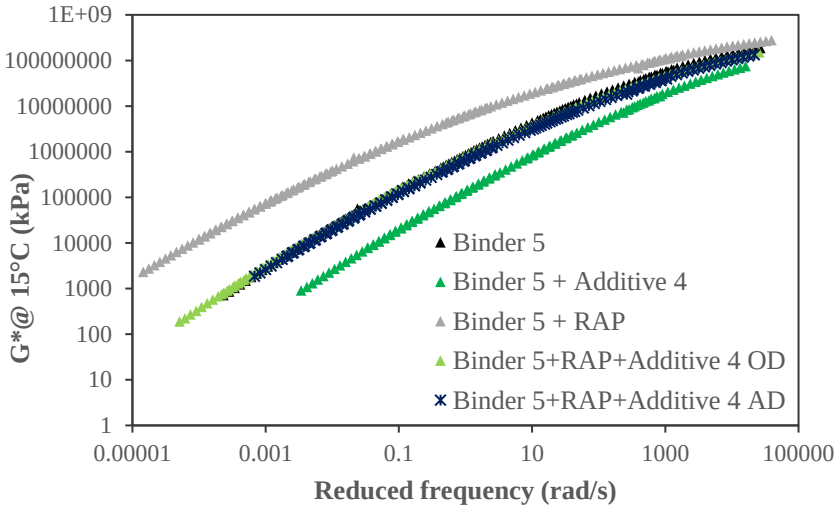

Figure 215. Complex modulus master curves for Additive 3 – Binder 5 Unaged

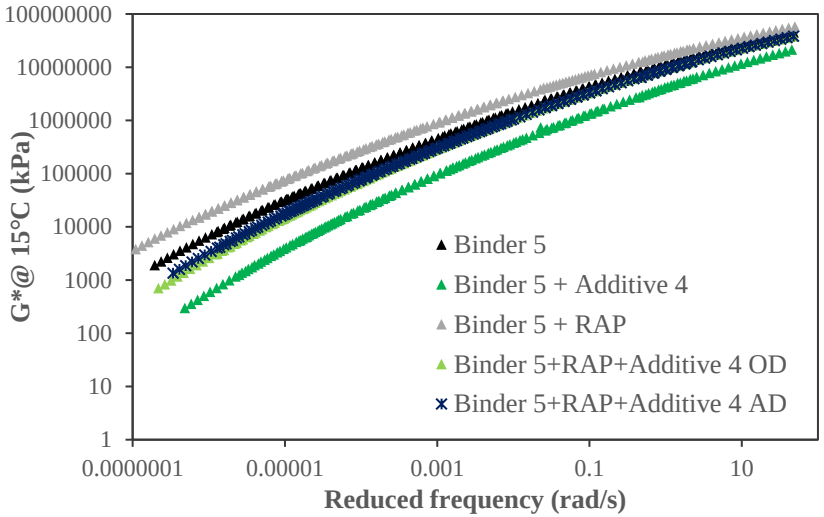

Figure 216. Complex modulus master curves for Additive 3 – Binder 5 RTFO + 60hr PAV

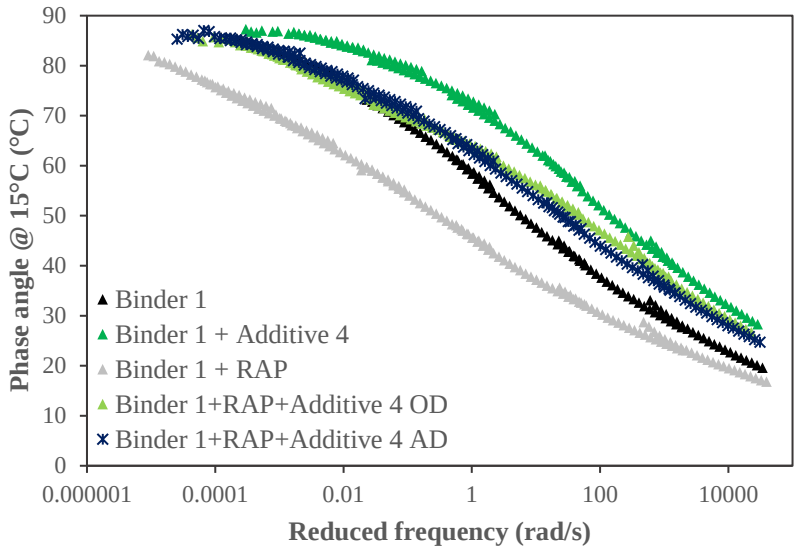

Figure 220. Phase angle master curves for Additive 4 – Binder 1 Unaged

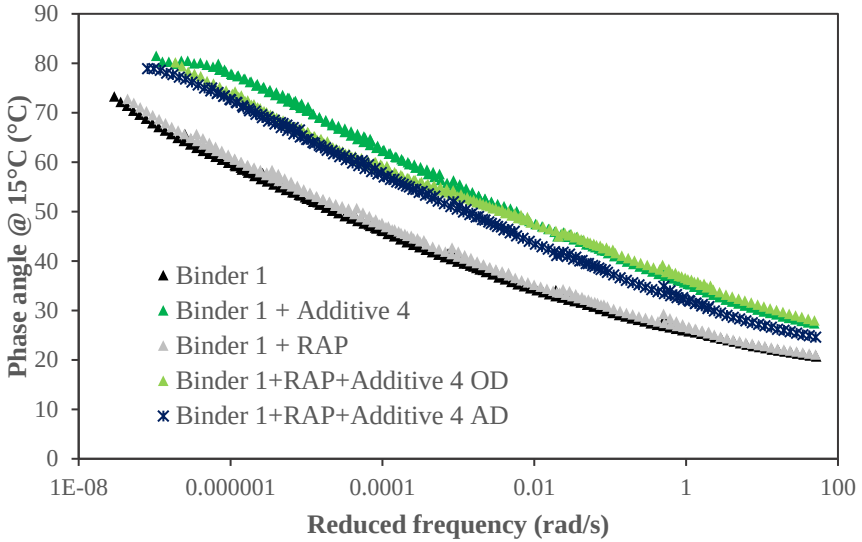

Figure 218. Phase angle master curves for Additive 4 – Binder 1 RTFO + 60hr PAV

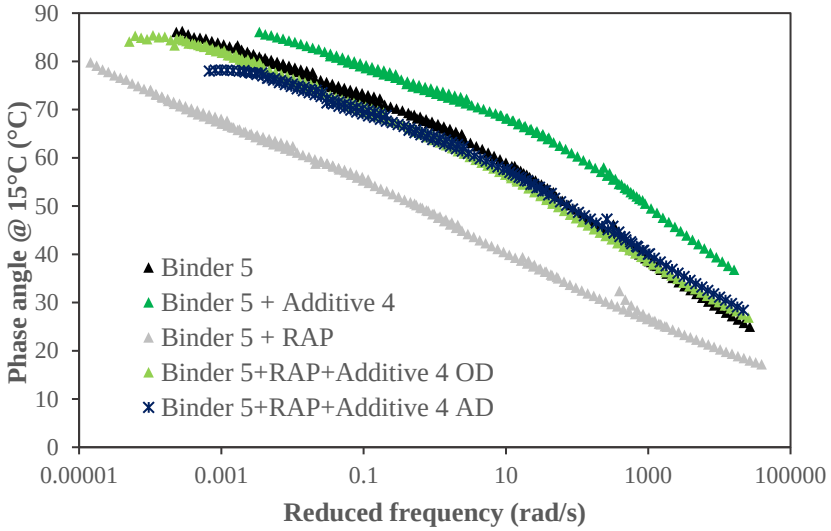

Figure 217. Phase angle master curves for Additive 4 – Binder 5 Unaged

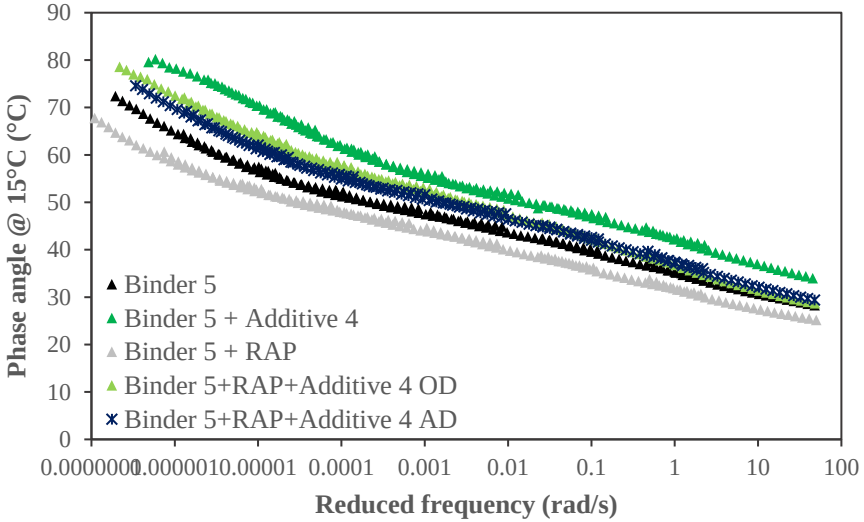

Figure 219. Phase angle master curves for Additive 4 – Binder 5 RTFO + 60hr PAV

E. Additive 5

Complex modulus master curves Figure 33 through Figure 36 indicate Additive 5 reduces stiffness of base binders, particularly at high and intermediate temperatures. Like Additive 4, this modifier results on a softer binder at the unaged condition, which may raise rutting concerns. After extended aging cycles, master curves of modified binders remained below those of the control, thus showing improved aging resistance. Additionally, the offset in G^* between modified and unmodified binders occurs across the entire frequency range in the case of neat binders, while RAP blends appear to converge at low temperatures.

Phase angle master curves are shown in Figure 37 through Figure 40, before and after aging. The previously described reductions in stiffness are accompanied by increased phase angles resulting on a more viscous binder, which confirms the softening effect of the additive. Some degree of polymeric modification can be observed by the plateau in phase angle at intermediate temperatures, more evident for neat binders. More specifically, RAP blends present a more viscous behavior across the complete frequency range, while neat binders show increased elastic behavior than the control at higher temperatures. Changes in additive performance depending on the presence of RAP was observed throughout the rheological evaluation of modified binders, and this provides an example of this behavior. Aging of modified binders results on higher phase angles than the control binders, thus improving the viscous nature of binders, suggesting additive 5 was effective at mitigating the embrittlement of base binders.

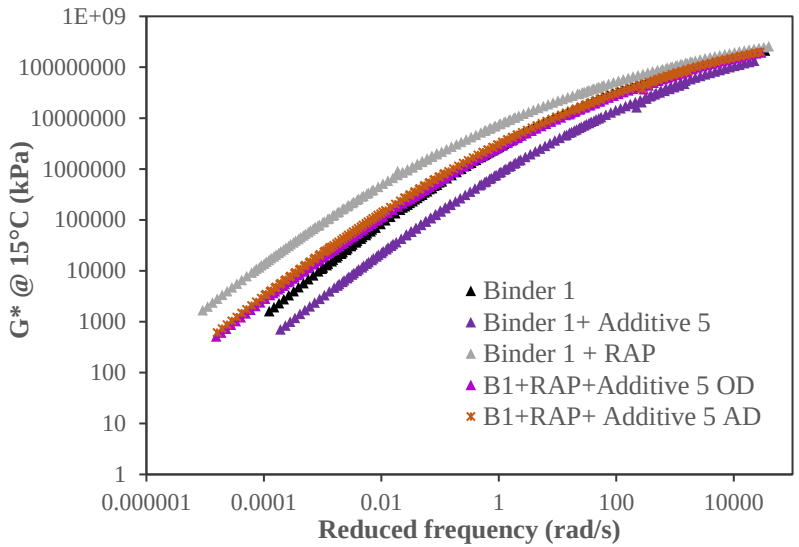

Figure 223. Complex modulus master curves for Additive 5 – Binder 1 Unaged

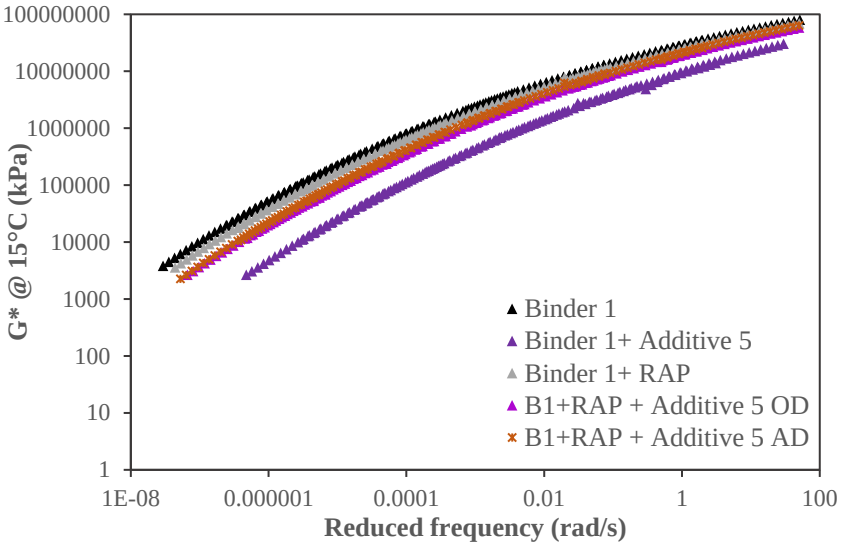

Figure 221. Complex modulus master curves for Additive 5 – Binder 1 RTFO + 60hr PAV

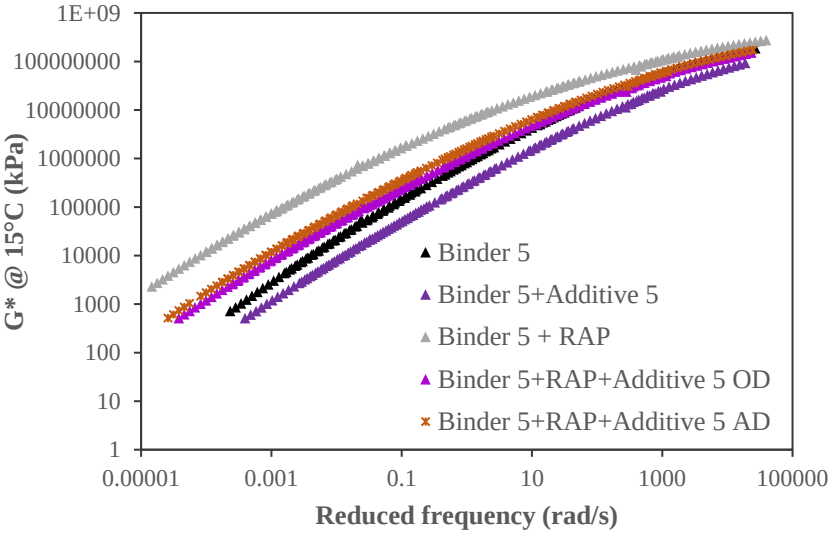

Figure 222. Complex modulus master curves for Additive 5 – Binder 5 Unaged

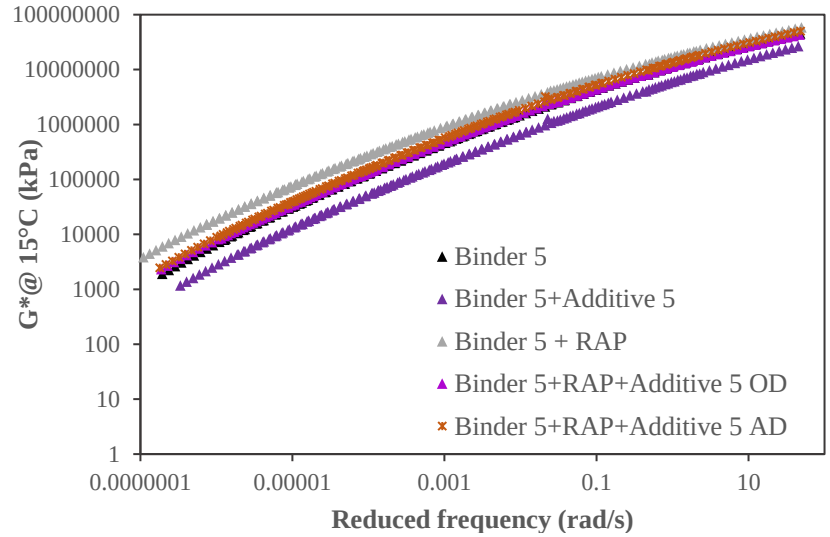

Figure 224. Complex modulus master curves for Additive 5 – Binder 5 RTFO + 60hr PAV

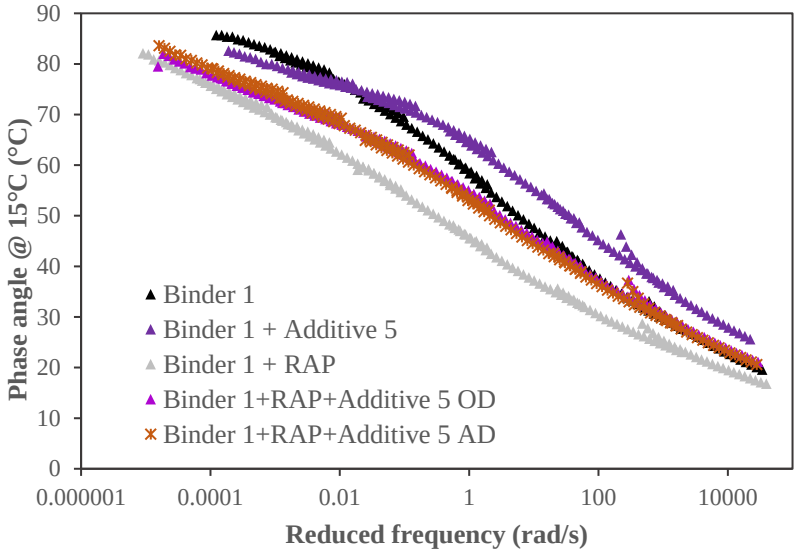

Figure 228. Phase angle master curves for Additive 5 – Binder 1 Unaged

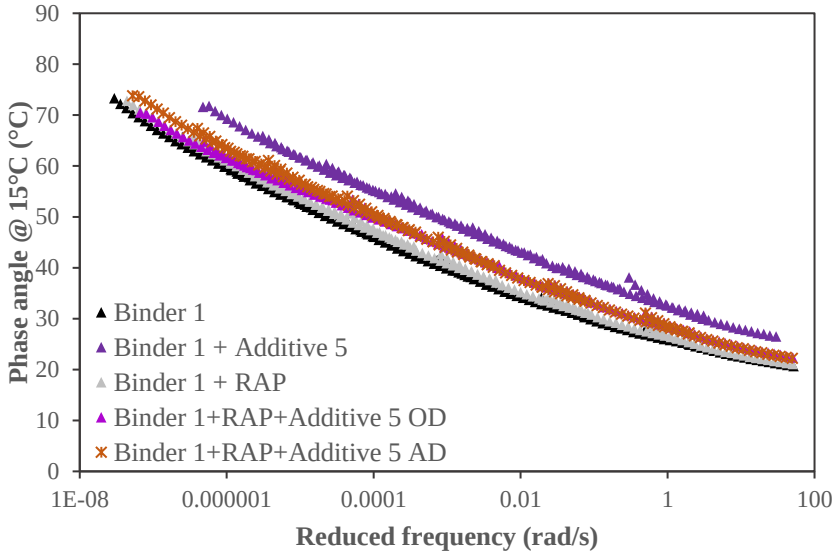

Figure 227. Phase angle master curves for Additive 5 – Binder 1 RTFO + 60hr PAV

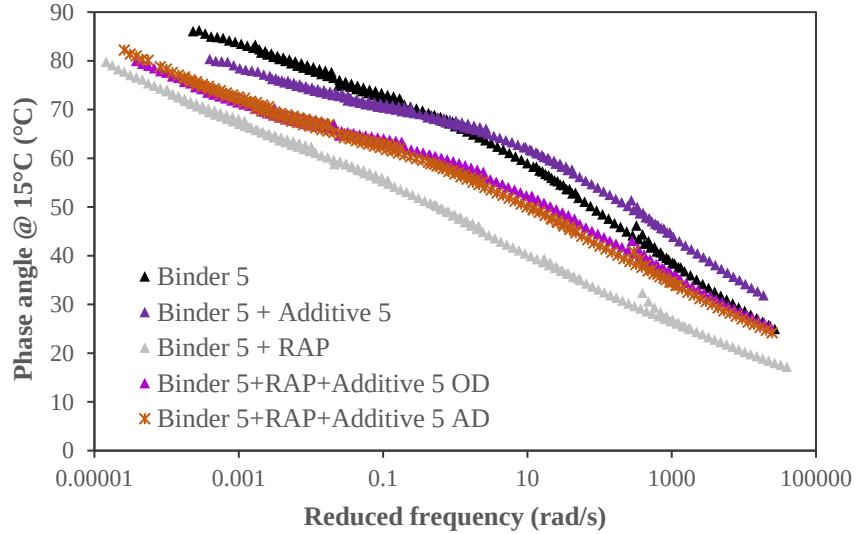

Figure 226. Phase angle master curves for Additive 5 – Binder 5 Unaged

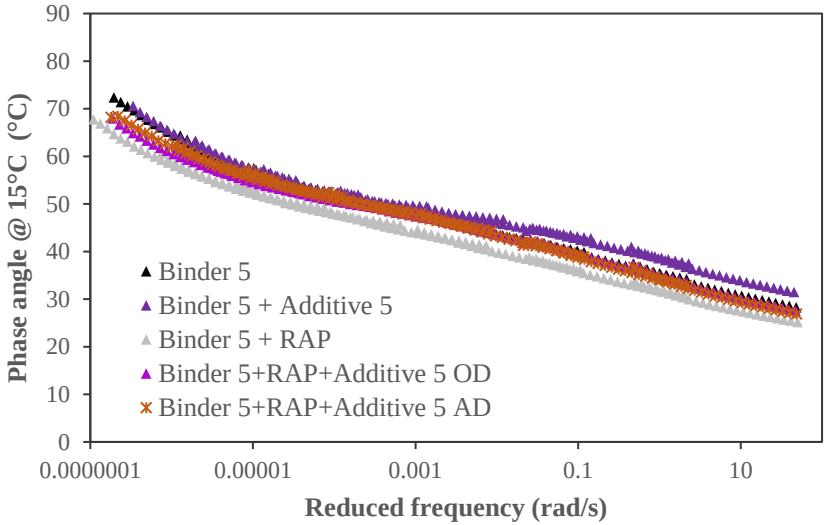

Figure 225. Phase angle master curves for Additive 5 – Binder 5 RTFO + 60hr PAV